

HETEROGENEOUS AND HOMOGENEOUS
EFFECTS IN THE THERMAL
CRACKING OF HYDROCARBONS

by

Christopher Edward Turner, C. Chem., M.R.I.C.

November 1976

A thesis submitted for the
degree of Doctor of Philosophy of the
University of London

Dept. of Chemical Engineering
and Chemical Technology,
Imperial College,
London, S.W.7.

ABSTRACT

The object of this study has been to investigate the heterogeneous and homogeneous effects which are present in the pyrolysis of propane and which influence the gaseous, liquid and solid products.

The experimental parameters which give an indication of the reactions which are occurring are the rate of carbon formation and the conversion of propane to gases and tars. The catalytic influence of the reactor wall on carbon formation and the influence of the reactor wall on the formation of carbon in the gas phase has been studied with an on-line microbalance. The gaseous products and the tars have been determined by gas chromatography. The formation of tars has been monitored with an on-line mass spectrometer.

The carbonisation and carburisation of metal liners in the reactor has been studied by metallography, electron probe microanalysis and x-ray diffraction. Carbon deposits have been examined using spark source mass spectroscopy.

Hydrogen, helium and hydrogen sulphide have been used as diluent gases to help elucidate the course of the surface and gas phase reactions.

The pyrolysis of propane has been shown to be a free radical chain reaction and predictions based on steady-state approximation agree with experiment and show that the disappearance of propane should be first order.

The existence of an induction period which depends on the pressure of the reactants and the temperature, the autocatalytic nature of tar production and the eventual tail-off of rate to a steady value have been shown to be typical of free radical reactions.

The rate of carbon formation on a surface has been found to be dependent upon the chemical nature of that surface and carbon formation on a surface may be affected by the nature of a second surface, physically separated from the first surface by a gap in which gas can react. Iron, stainless steel and nickel have been

shown to exhibit a heterogeneous influence on the rate of carbon deposition, and copper, silica and carbon to act as essentially "third body" materials.

ACKNOWLEDGEMENTS

I should like to thank Prof. D. L. Trimm for his supervision, help and friendship throughout this project.

I also thank the staff of the Department's Electronic Services Group, the Glassblowers, the Engineering Workshop and the Analytical Services Group of Imperial College.

My thanks also go to my colleagues during the past three years for their advice and companionship, and to Alberto La Cava for his assistance with computing methods.

Valuable assistance from the Science Research Council is gratefully acknowledged.

I hope that this thesis will serve as an acknowledgement to the many people who have encouraged me to take advantage of Opportunity.

November, 1976

Christopher E. Turner.

Dept. of Chemical Engineering
and Chemical Technology,
Imperial College,
London, S. W. 7.

CONTENTS

	Page
CHAPTER 1 INTRODUCTION	6
CHAPTER 2 EXPERIMENTAL	43
CHAPTER 3 RESULTS	91
CHAPTER 4 DISCUSSION	209
CONCLUSIONS	252
APPENDIX	257
REFERENCES	262

CHAPTER 1INTRODUCTION

	Page
1. 1. <u>General</u>	7
1. 2. <u>Gas phase reactions</u>	7
1. 3. <u>The formation of carbonaceous material</u>	15
1. 3. 1. Tars	15
1. 3. 2. Pyrolytic carbon	17
1. 3. 3. Gas phase carbon	18
1. 3. 4. Catalytic carbon formation	20
a) The influence of crystal faces	20
b) Formation and growth	21
1. 4. <u>Homogeneous-heterogeneous interaction</u>	27
1. 5. <u>Free radicals in pyrolysis</u>	35
1. 5. 1. Free radical detection	36
1. 5. 2. Molecular beams	37
1. 6. <u>Present work</u>	41

1. 1. General

High temperature pyrolysis of hydrocarbons is a process of considerable industrial importance, forming the basis of the so-called steam cracking (1) and hydrogasification reactions (2). These processes involve the pyrolysis of naphtha or heavier feedstocks, in the presence of steam or of hydrogen, to give light olefins and aromatics, used as petrochemical feedstocks.

The major reactions are free radical in nature (3), occurring in the gas phase. However, surface effects help to determine the overall efficiency of the process, in that the formation of carbonaceous material on a surface inside or immediately after the reactor can lead to reactor blocking. In addition, reactions initiated on a surface may influence the course of reactions occurring in the gas phase (4).

The present studies were aimed at investigating some aspects of these problems. The initial section covers the information available at the start of this project.

The pyrolysis of hydrocarbons in the industrial process of ethylene production has been reviewed by Zdonik (1). Leathard and Purnell (5) discussed paraffin pyrolysis while the pyrolysis of hydrocarbons has been studied by Purnell (6) and Quinn (7)(8).

1. 2. Gas phase reactions

Homogeneous gas phase reactions of stable molecules do not normally proceed at measurable rates unless the reactants are activated by some process of energy absorption. This may be, for example, thermal, photolytic, or radiative activation. Homogeneous gas phase reactions are often initiated by the unimolecular decomposition of one or more of the reactants to form free radicals or atoms. Due to their high reactivity, these undergo a variety of reactions and a complex reaction system is established. The precursors of radicals and atoms are usually molecules with varying amounts of internal activation. The particular mode of internal

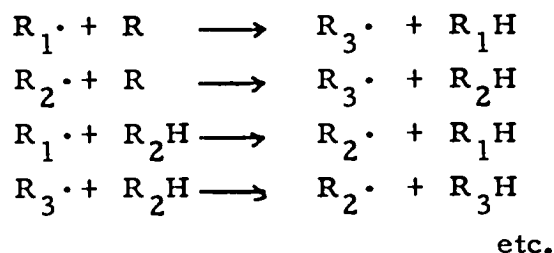
excitation of the molecule depends on the method used to activate the system.

The pyrolysis of hydrocarbons, a thermal reaction, proceeds mainly via vibrationally excited molecules. At the relatively low temperatures required for this process (up to about 1000°C) the population of higher electronic energy levels is insignificant. Vibrationally excited molecules may be deactivated by collisions, or may dissociate to form atoms or free radicals. If radical-radical or radical-molecule reactions occur in the system, the excess energy may result in either vibrational or electronic excitation in the product.

The free radical mechanisms which occur in hydrocarbon pyrolysis, consist of several related stages. The reaction begins as a result of the formation of free radicals or atoms via activation by energy absorption (initiation). The subsequent course of reaction may be considered in general terms. After initiation, usually the splitting of a carbon-carbon or a carbon-hydrogen bond:



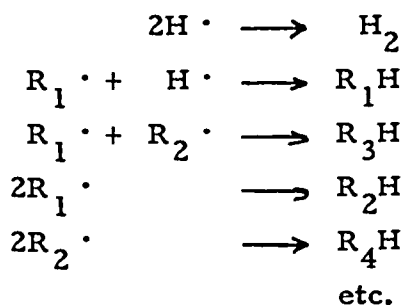
the reaction proceeds by propagation. This is a rapid process and many hydrocarbon species are formed:



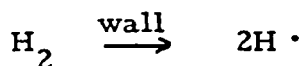
These propagation reactions are all thermodynamically favourable.

During the reaction, inhibition or acceleration can occur as a result of the presence of compounds which combine with free radicals. The formation of a stable compound or a less reactive free radical leads to inhibition, while the formation of a reactive free radical will accelerate the course of the reaction.

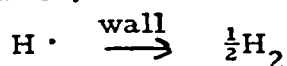
A free radical reaction terminates by the combination of two free radicals to form a stable molecule:



The reactor wall can influence both initiation:



and termination:



The complexity of the overall reactions can be illustrated by considering a specific example, such as the free radical decomposition of propane. Reactions that could occur are listed in Table 1.1. These are deduced from the mechanism of the pyrolysis of hydrocarbons, a system that has been extensively studied.

The pyrolysis of many hydrocarbons and mixtures of hydrocarbons has been studied in detail. Mechanisms which explain the stages of initiation, propagation, and termination, have been proposed. Various gases have been added to the reaction mixtures to study the effect of inhibitors on the free radical reaction. Both product gases from the decomposition of the various hydrocarbons and non-product gases have been found to have an effect on reaction.

In addition to initiation by excitation, products may also lead to initiation. Thus, for example, product ethane was found to be the initiator in the thermal reaction of ethylene at 703-854°C., Taiseki (9). The primary products are hydrogen, ethane, acetylene, propylene, 1-butene and 1,3-butadiene and the secondary products are methane, cyclo-olefins and aromatics. Product butadiene decreased the rates of formation of hydrogen, ethane and butadiene (but not those of methane and propylene) by trapping active hydrogen atoms.

Information on the propagation of free radical reactions can be gained from studying the effects of inhibitors on free radical chain reactions. The inhibition of hydrocarbon decomposition in the temperature range 750-930°C has been studied by Nowak (10).

Table 1.1. Chemical reactions in propane decomposition

Initiation



Propagation reactions

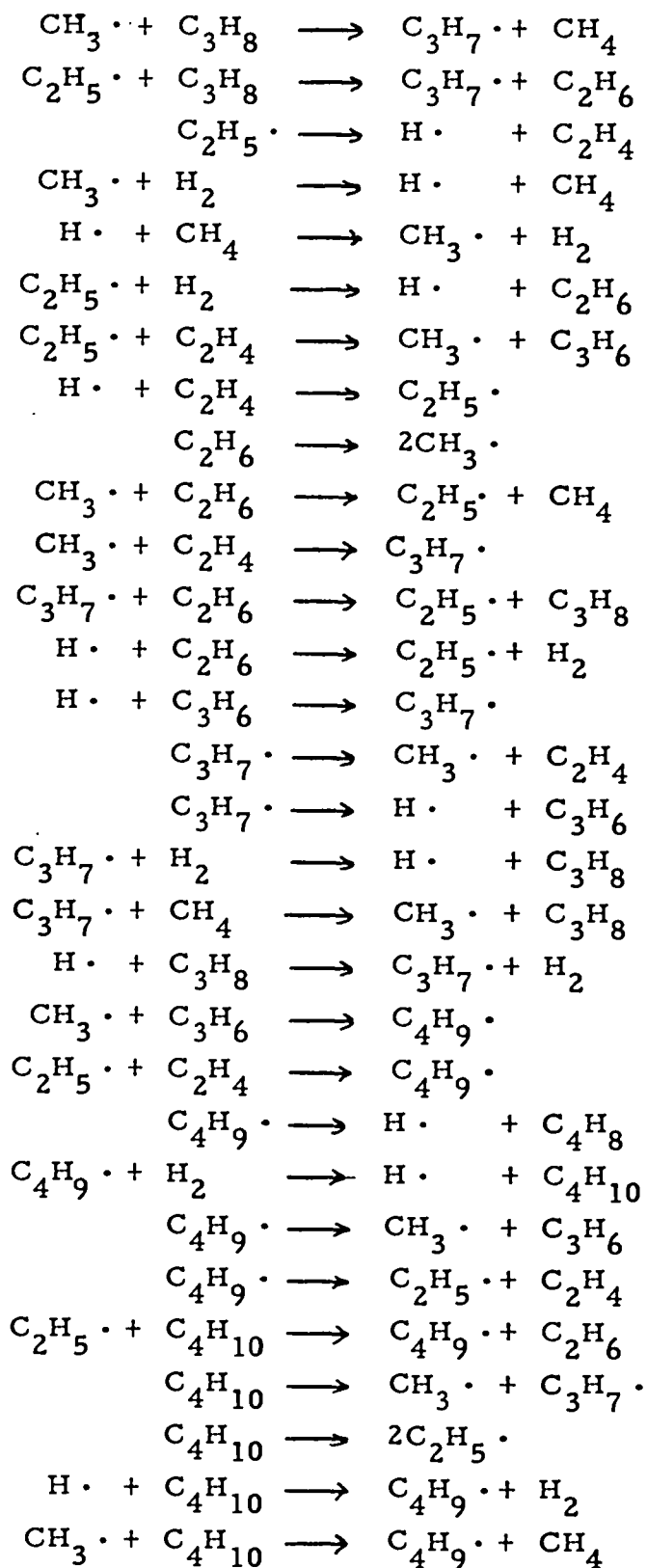
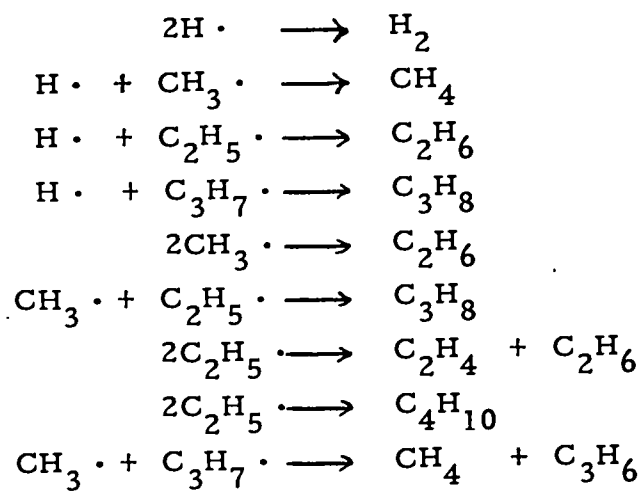


Table 1.1. (continued)

Termination reactions



The thermal decomposition of ethane and propane was strongly inhibited by the addition of propylene but the rate constant of the propylene decomposition was increased by the presence of ethane and propane, the main decomposition products being ethylene and methane. The inhibition effect of propylene results from the removal of hydrogen atoms from the reaction zone by addition to the inhibitor. Chain propagation then continues only through the substantially less reactive methyl radicals. For similar reasons, propylene has an inhibiting action on the cracking of saturated and unsaturated gaseous hydrocarbons and their blends, Ferrara (11). Product formation from hydrocarbon pyrolysis can be greatly influenced by the presence of diluents, which interfere with propagation. In the pyrolysis of propane at 700-950°C. Hirata (12), observed that hydrogen increased the ethylene yield and suppressed the formation of carbon and tar, while it decreased the propylene yield. Water gave the same effects as hydrogen but methane, although increasing the ethylene yield, did not suppress carbon formation.

The addition of sulphur to the pyrolysis reactor also has a significant effect. The pyrolysis of propane has been studied at 830-1180°C by Benson (13), in the presence and absence of hydrogen sulphide. The product distribution is characterised by the decomposition of propane via two routes at roughly equal rates; one route leading to propylene and hydrogen, the other to ethylene and methane or ethane. Propylene is subsequently converted, almost stoichiometrically, to ethylene and acetylene. Hydrogen sulphide accelerates the initial decomposition of propane, thus maintaining high propylene selectivity to high propane conversion.

The course of the propagation reactions can be influenced by some of the highly unsaturated products which are formed. Thus, the distribution of the products from the pyrolysis of nine $C_1 - C_4$ hydrocarbons at 1200°C has been accounted for in terms of the polymerisation of acetylene, produced by the pyrolysis of the hydrocarbons and the addition of CH_2 or CH_3 to some of the acetylene polymers, Friedmann (14). The main products, which

were the same for all the hydrocarbons, were 1,3-cyclopentadiene, benzene, toluene, phenylacetylene, styrene, indene and naphthalene. Twentythree minor products were identified. The presence of acetylene may have a major effect on tar formation (see later).

The key free radical reactions occurring in hydrocarbon pyrolysis can be established by observing the rate of appearance of the molecular gases formed by radical termination. Davies (15) studied ethane cracking between 675-775°C and established the concentration of ethyl and methyl radicals and the rates of key free radical reactions from the rate of appearance of propane and butane. The combination of ethyl radicals to form butane is a major chain termination step, while the combination of methyl and ethyl radicals to form propane is of lesser significance. A long chain free radical mechanism for the pyrolysis of propylene at 555-640°C was proposed by Kallend (16). The main chain termination reaction is the combination of methyl and allyl radicals.

To summarize then, in the pyrolysis of alkanes in the gas phase, molecular processes are generally negligible and chain radical mechanisms are the important reactions. Acceleration and inhibition of the propagation reactions in the pyrolysis of saturated hydrocarbons is complex. The addition of compounds such as hydrogen chloride, hydrogen sulphide, toluene, or olefins, can produce, at the same time, an inhibiting and an accelerating effect, Niclause (17). The overall effect depends on numerous parameters.

The course of the homogeneous gas phase reactions occurring in the pyrolysis of hydrocarbons may also be studied by developing suitable mathematical models. These theoretical considerations are based on the concept that it is possible to suggest a series of chemical reactions and rate equations from which the steady-state concentrations of the gaseous species which participate in the reaction may be derived. Considerable improvements in such models may be obtained by incorporating experimental results which demonstrate which radicals predominate and the type of kinetics

which are present.

The use of well mixed reactors is particularly interesting in connection with experimental measurements of product yields. A batch reactor essentially follows a time sequence, and has to be tapped periodically for analysis. This results in interference in the system and precludes point measurements in the time domain, Garewal (18). Batch reactors are static, mixing is low and almost entirely via diffusion. Large local radical concentrations may occur with practically no reaction occurring in depleted regions such as the reactor wall.

Tubular flow reactors are known to exhibit far from ideal behaviour in many cases, La Cava (19). This is due to diffusional effects or to the lack of temperature or uniformity. In addition, mass and heat balances are represented by differential equations which, when coupled to a kinetic model of free radical reactions, give a set of non-linear stiff differential equations. These are difficult to solve numerically and involve complex and time-consuming computing, Seinfeld (20).

Well mixed reactors, on the other hand, offer a uniformity of concentration and temperature throughout the reactor, Bush (21). Sampling is easy and reproducible, and the appropriate mathematical models can be developed more easily.

The fundamental hypothesis involved in the perfect jet-stirred tank reactor model is that all concentrations and temperatures are uniform inside the system. Short residence times can be used and inaccuracies due to time delay are minimised. As a jet-stirred tank reactor functions at constant concentration, the conservation of mass gives a set of algebraic equations instead of differential equations and the calculation of reaction kinetics is simplified. Mathematical modelling can be applied, in combination with experimental work from a jet-stirred tank reactor, to elucidate unknown free radical mechanisms in pyrolysis.

1. 3. The formation of carbonaceous material

The gas phase decomposition of hydrocarbons is generally considered to proceed via free radical mechanisms. However, these reactions are carried out in a reactor and the interaction of saturated hydrocarbons with metal or silica surfaces may also occur. The initial process, both in the absence and presence of hydrogen, is the loss of hydrogen atoms, with the formation of radicals. In the presence of hydrogen, fission of carbon-carbon bonds occurs and lower molecular weight hydrocarbons are formed. The olefins produced by the free radical process polymerise to form aromatic hydrocarbons and polynuclear aromatic hydrocarbons. These condense or adsorb on the reactor wall to form high molecular weight carbonaceous deposits.

When the reactor wall exerts a heterogeneous effect on the carbon formation, hydrocarbons adsorb on the reactor wall and catalytic reactions occur to form a carbon deposit. This may cause a depletion in some gas phase hydrocarbons and may influence the homogeneous reaction.

Carbon deposits can present a variety of structures ranging from the near amorphous to a highly crystalline graphitic state, depending on the mechanisms by which they are formed. The carbonaceous deposits formed in the pyrolysis of hydrocarbons are:

- a) polynuclear aromatics, referred to as tars
- b) pyrolytic carbon, either soot or wall carbon
- c) catalytic carbon

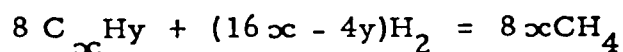
1. 3. 1. Tars

Tar formation during the pyrolysis of acetylene was studied by Berthelot (22). Benzene and aromatic products were observed and a mechanism of synthesis was suggested : hydrocarbon to acetylene to aromatics via a process of acetylene polymerization. However, acetylene is only a minor product in hydrocarbon pyrolysis and for it to play a major role in tar production, a conversion from acetylene

to tars of nearly 100% is necessary.

As a result of this, a second mechanism for tar formation was proposed in which the hydrocarbon could react to a butadiene intermediate and on to aromatics, Fitzer (23). Aromatics and polynuclear hydrocarbons were suggested to be formed via a series of Diels-Alder reactions involving butadiene and alkenes or butadiene and aromatics. Although butadiene is formed from many hydrocarbons under conditions of pyrolysis, it is not likely to be an important intermediate in the synthesis of polynuclear hydrocarbons at high temperatures, where the relative energies for the diene addition and for radical addition suggest that polynuclear hydrocarbon production proceeds via radical and not via molecular addition. However the predominating reactions in the formation of coke from aromatic systems are dehydrogenative dimerisation, trimerisation, etc., Evans (24).

A study of the basic kinetics and mechanism for tar formation during the reaction of hydrocarbons with hydrogen was made by Brooks (25). The simple stoichiometric hydrogasification reaction:

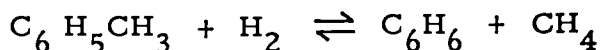


actually involves a complex free radical reaction mechanism. When operating close to the stoichiometric ratio (to maximise the methane content of the product gas) conditions arise where the hydrogen concentration is low. Condensation reactions of hydrocarbons can occur concurrently with breakdown reactions and lead to the formation of aromatic hydrocarbons and carbon. Any attempt to produce pure methane by utilising the stoichiometry of this reaction will thus result in the formation of some aromatic hydrocarbons. The yield of aromatics increases as the hydrocarbon to hydrogen ratio is increased, particularly for cyclic hydrocarbons. The tendency for a hydrocarbon to form aromatics is approximately proportional to the readiness with which olefins are formed initially from pyrolysis. Aromatics are formed by reaction of these unsaturated compounds, the concentrations of which are greatly reduced by the addition of hydrogen.

Aromatic hydrocarbons which are formed under certain reaction conditions can react in several ways.

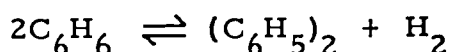
a) Breakdown of the benzene ring to aliphatic hydrocarbons, hydrogen and carbon.

b) Dealkylation of the side chain present on the benzene ring. e. g.



This is potentially reversible.

c) Dimerisation of the aromatic system, with the elimination of hydrogen. e. g.



This is potentially reversible. In the presence of a large excess of hydrogen, the equilibrium will be well over to the left-hand side.

At temperatures above 780°C fission of the benzene ring can occur and large amounts of carbon can be formed. At these temperatures, Brooks (25) used methane formation as an indication of ring fission and observed higher molecular weight compounds from the pyrolysis, including diphenyl, terphenyl, naphthalene, anthracene and fluorene. Ring fission resulted in the production of the active ring building unit (suggested to be the $\text{C}_4\text{H}_3\cdot$ radical) which gave rise to the formation of polynuclear hydrocarbons.

1.3.2. Pyrolytic carbon

Pyrolytic carbons are formed from carbon containing gases at high temperatures, either homogeneously or heterogeneously, giving two distinct types of carbon (gas phase and surface carbon). Gas phase carbon is a microcrystalline form of carbon, produced in spherical particles with crystallites oriented approximately parallel to the surface, Akamatu (26) and Kaye (27). Surface carbons are obtained as films with well ordered crystallites deposited on solid substrates, Cullis (3). This type of carbon is nearer to graphite than gas phase carbon, having larger crystallites,

higher density and lower interlayer spacings. The formation of both types of carbon is largely determined by the conditions of pyrolysis rather than by the structure of the starting gas, Cullis (3) and both can be produced concurrently under certain conditions of temperature and pressure, Conroy (28), Diefendorf (29), and Cullis (30). It has been stated by Cullis (3), that there is no single mechanism for carbon formation and that the reactions may involve many different radicals.

1. 3. 3. Gas phase carbon

In contrast to the variety of surface carbons which may be formed, one type of carbon is formed in the gas phase. It is a very light fluffy mass of carbon having a very large surface area and porosity, Cullis (3). Gas phase carbons have greater interlayer spacings and smaller crystallite dimensions than surface carbons and the temperature of formation has little effect on the interlayer spacings and crystallite dimensions of the gas phase carbon. The individual constituent particles of gas phase carbon are roughly spherical in shape and are linked together into networks of chain-like structures. The chemical structure of the pyrolysed hydrocarbon has little effect on the structure of the gas phase carbon and the carbons formed have similar properties, which suggests formation via a common mechanism.

The concentration and size of the gas phase carbon particles is controlled by the processes of nucleation, coagulation and growth. Several theories of carbon formation, which are actually qualitative chemical models, have been developed, both for nucleation and for growth. An explanation of nucleation is that the nuclei are formed by condensation of drops of polynuclear aromatic hydrocarbons produced in the reaction. The initial hydrocarbon reacts by a gas phase reaction to produce polynuclear aromatic hydrocarbons, the partial pressure of which increases with reaction time until supersaturation is high enough to induce condensation droplet formation. The formation of liquid nuclei

eliminates the supersaturation, and the formation of additional liquid nuclei is no longer possible. The polynuclear aromatic hydrocarbons which continue to be formed maintain the growth of the nuclei and the liquid droplets are pyrolysed into gas phase carbon, Lahaye (68).

Studies of the pyrolysis of aromatic hydrocarbon and argon mixtures in a shock tube has thrown light on the initial formation of gas phase polynuclear aromatic species from which soot is ultimately formed, Graham (69). Initially, soot is formed directly from gas phase intermediates and its formation is not preceded by the sudden nucleation and coagulation of droplets of liquid polynuclear aromatic species, in contradiction to the theory of Lahaye (68). Graham (69) suggests that the intermediates of the initial formation of soot are present in the gas phase and are not present in the condensed phase. Soot is formed at a nearly constant rate from the onset of its formation to the end of the flow, where the conversion of intermediates into soot is still not complete.

Following nucleation, Lahaye (68) suggests that growth of the droplets occurs by condensation of polynuclear aromatics followed by pyrolysis to give soot. Graham (69) proposes that some growth may occur from the polynuclear aromatics in the gas phase and that further growth occurs by the aggregation of soot particles.

Nuclei grow very rapidly once they are formed in the gas phase, and it is likely that a species more complicated than the inlet gas molecule is required to produce carbon growth. The molecule responsible may well be polyunsaturated hydrocarbons formed by polymerization and dehydrogenation, growth occurring by decomposition on the nuclei surface. Ring formation within the particles, accompanied by loss of hydrogen, leads to the formation of carbon.

It has been suggested by Thomas (31) that gas phase carbon is an aggregate of large polybenzenoid free radicals and that the intermediates and nuclei are highly conjugated free radicals that undergo Diels-Alder additions with smaller unsaturated species. There is no fundamental conflict between this theory and the

polyunsaturate-polyacetylenic theory.

1. 3. 4. Catalytic carbon formation

In heterogeneous pyrolysis, all substrates can be considered to have some catalytic activity, since the surface process appears to be the controlling factor in producing laminar carbons. However, deposits formed on some metallic substrates at much lower temperatures leads to these substrates being considered as catalysts, in comparison with "inert" surfaces such as graphite, silica and porcelain. Nickel, cobalt and iron have been found to be most effective substrates and have been the subject of many studies, Akamatu (32), Banerjee (33), Karu (34), Robertson (35), Tamai (36)(37), Presland (38), Blau (39), Moayeri (40), Renshaw (41), Lobo (42), Saito (43), Tomita (44), Derbyshire (45), Figueiredo (46). Certain metals, especially iron, cobalt and nickel, exhibit high catalytic activity for carbon formation. They not only accelerate the rate of carbon formation but also influence the structure of the carbons formed.

Most of the earlier literature on the subject was devoted to the study of carbon deposition from carbon monoxide on iron, and has been reviewed by Renshaw (41). More recently, interest in avoiding carbon deposition on reactor walls and heat exchangers has directed more attention to the study of carbon formation from hydrocarbons on metals.

1. 3. 4. a. The influence of crystal faces

The catalytic activity of the substrate has been shown to depend on the crystal faces presented to the gas phase, Gwathmey (48). Different faces show different activities and only certain ones may be stable in a particular reaction environment, in that the surface will re-arrange to expose these faces. It may well be that reaction will preferentially take place at those places where the crystal lattice is rearranging or growing, Wagner (49). In the study

of carbon deposition from ethylene over single crystal nickel, Gwathmey (48), noted that visible deposits were not formed until the surface had begun to rearrange, and he suggested that the carbon deposition was controlled by the rearrangement pattern of the crystal faces.

The annealing and pyrolysing atmospheres can also influence changes in crystal orientation, Gwathmey (48), Tamai (36), Tomita (44), Maoyeri (50), and different faces are stable in different environments. It may be that the principal effect of pretreatment is to produce a particular crystalline rearrangement. If this is similar to the stable orientation produced during pyrolysis it will assist the catalytic action of the metal; if it is different, the surface will rearrange during pyrolysis and the catalytic action will be retarded, at least initially. This may explain effects such as the induction period observed in many surface reactions.

1. 3. 4. b. Formation and growth

A summary of the literature on catalytic carbon formation reveals several common features in a large number of different systems:

- a) Rates of deposition remain constant for extended periods of time, Tomita (44), Lobo (51), Nishiyama (52), Walker (53).
- b) The inclusion of metal in carbon deposits has been reported for deposition from hydrocarbons, Rostrup-Nielsen (54), Baird (55), Robertson (35), Baker (56), Tesner (57), Tomita (44), Lobo (51), Nishiyama (52), as well as in the case of carbon monoxide disproportionation, Hofer (58), Ruston (59), Renshaw (47), Walker (53).
- c) The presence of carbides has been reported under similar circumstances, Lobo (42), Derbyshire (45), Ruston (59), Renshaw (41), Tamai (36).
- d) A maximum rate of carbon formation has been observed at temperatures in the region 550-600°C,

Derbyshire (45), Tesner (57), Renshaw (47), Lobo (60), Walker (53), Haas (61) and approximately zero order kinetics have been determined for the low temperature region, Derbyshire (45), Lafitau (62), Lobo (63), Walker (53).

e) Hydrogen has been generally found to increase the rates of deposition, Tesner (57), Lobo (63), Nishiyama (52), Walker (53), Haas (61).

f) The rate determining step has been associated with a solid-state diffusion mechanism by many researchers, both at low temperatures ($< 350^{\circ}\text{C}$) where carbides are the final solid products, Cimino (64), Escoubes (65), Nagakura (66), and at higher temperatures ($\approx 350\text{-}550^{\circ}\text{C}$) where carbon is formed, Baker (67), Lafitau (62), Lobo (63), Nishiyama (52), Haas (61).

These observations suggest that a general mechanism for carbon formation must apply under a variety of circumstances.

Substrate metal has been found in some carbon deposits, Kehrer (70), Cunningham (71), Robertson (72), Lobo (42), Tomita (44), and it has been proposed that the metal diffuses through the carbon to the outer graphite layers where it continues to catalyse the reaction, Tamai (36)(37), Baird (73), until the metal content is too dilute.

Baker (56)(74) studied pyrolysis over nickel and iron films evaporated onto silica and graphite substrates. In both cases, the metal nucleated into particles on heating and graphite platelets were observed to grow from the edges of larger particles which had lost their mobility. A mechanism by which crystallites of nickel were transported on the surface of the growing graphite crystals was suggested by Lobo (42). The process is analagous to that described by Baker (56) for the growth of carbon fibres. The hydrocarbon decomposes on the upper surface of the nickel and carbon atoms diffuse through the crystallite to "active growth" regions (which may be carbides) to form graphite.

The majority of carbon fibres formed over iron, nickel and cobalt exhibit distinct similarities. They are long and thin,

sometimes up to 7 microns in length and 0.1 microns wide, and have a hollow tubular core. The fibre tip contains a particle of metal or metal carbide whose size appears related to the fibre and core diameters. Metal or metal carbide particles are also found distributed in the hollow core along the fibre length, Walker (53), Ruston (59), Tesner (57), Renshaw (41), Robertson (35), Baird (73), Baker (56), Rostrup-Nielsen (54). Their structure is turbostratic, with a preferred orientation of the basal planes parallel to the fibre axis, Robertson (35), Baird (55)(73).

Baker (56) studied the growth of fibres from the pyrolysis of acetylene on sintered nickel films and proposed a mechanism by which mobile nickel particles act as growth centres. Carbon is taken into solution and diffuses along a thermal gradient to be precipitated at the rear of the particle, which thus continually moves forward at the head of the growing fibre. The growth curves showed a falling rate, indicative of gradual poisoning. After 10-15 seconds, the nickel particles lost their mobility and growth ceased, when the particles were found to be encapsulated within a layer of carbon. Growth could be regenerated by heating in hydrogen or oxygen.

Filaments formed on iron surfaces have been reported to form branched structures, Walker (53), Ruston (59), while only single filaments have been found on nickel. Ruston (59), in studying the decomposition of carbon monoxide over iron, proposed that the head particle in the filaments was the carbide Fe_7C_3 and that growth originated from small crystals of this carbide. Filament growth was propagated by surface or bulk diffusion through the particle. Disintegration of the particles during growth left a trail of smaller particles, some of which initiated branching. Renshaw (41) suggested that the filaments originated from platelets of Fe_2C and were formed by the graphitisation of Fe_2C whiskers almost immediately after they began to grow.

The non-fibrous deposits, other than laminar graphite, found in these systems have been described as "polycrystalline", "nodular" and "flocculent amorphous". Their common feature is their lack of orientation with the substrate and usually their crystallite size

is small. Non-oriented graphite is formed together with laminar graphite at high rates of carbon deposition, Blau (39), Baird (73). It has been suggested that the carbon originates from gas phase polymerization, Baker (56), or that the initial laminar layer is unable to cover the substrate completely before less ordered deposits begin to grow, Blau (39). This indicates a condition where the rate of deposition is greater than the rate of the surface re-arrangement process. The kinetic studies by Tamai (36)(37), Lafitau (62), and Tomita (44), do not differentiate between the two microstructures and it is assumed that the deposits usually comprise a mixture of both. Tamai (36) studied the pyrolysis of several hydrocarbon gases over iron and nickel substrates at surface temperatures of 870-1030°C. Deposition rates on iron from methane and ethane were temperature and pressure dependent and were attributed to some degree of gas phase reaction. The deposition rates from ethylene over iron were practically independent of temperature and pressure. In all cases the reaction rate decreased with time and, with ethylene, this was a very pronounced effect. The results over nickel were similar to the iron-ethylene system and it was suggested that a surface process was the rate controlling step. Generally, deposition rates on iron were about five times faster than on nickel, as also found by Baird (73).

Lafitau (62) studied the pyrolysis of hydrogen-methane mixtures over nickel foils at about 1000°C and found that the kinetic data could be explained in terms of a diffusion limited reaction in either the gaseous or solid phase, depending on the conditions. The reaction rate decreased with increasing deposit weight, which suggests a fall in catalytic activity as the substrate becomes coated with the deposit. The formation of crystalline graphite over nickel, cobalt and iron substrates was studied by Derbyshire (45), and a diffusion-precipitation process was considered operative in the pyrolytic systems. Some gas phase reaction of the light hydrocarbons was observed.

A mechanism for carbon formation on nickel foils was proposed by Lobo (42). The adsorption of olefins on the surface is followed by dehydrogenation and hydrogenolysis reactions to produce

carbon atoms; these then migrate through the nickel to active growth regions. Disruption of the nickel takes place and crystallites, detached from the surface, are carried with the growing carbon and catalyse further production of carbon. Induction periods, observed under certain conditions, can be accounted for in terms of the nucleation of a new solid phase presenting an initial energy barrier. The rate determining step at low temperatures is the diffusion of carbon through the nickel.

The incorporation of atomically dispersed metal in carbon layers was confirmed by oxidation studies, Baird (55). The metal atoms or small clusters of atoms that diffuse into the carbon result in catalytic activity for carbon growth. Carbon formation from benzene on copper-nickel alloys was studied by Nishiyama (52). Preferential nucleation at grain boundaries was suggested to explain the presence of metal grains in the carbon deposits. Nucleation on the surface was suggested to be responsible for encapsulation of the metal and inhibition of further deposition. The observed enhancement of deposition by hydrogen was ascribed to the elimination of carbon nuclei at the surface, preventing encapsulation.

The catalytic influence of sheets of chromium, copper, zinc, iron and nickel on the rate of coke formation and on the pyrolytic gas composition, was studied by Starshov (75). The minimum coke formation was observed with chromium, the maximum with nickel and iron. In the quartz reactor, the gas composition changed very little during the experiment but in the chromium lined reactor, the sum of the ethylene and propylene concentrations increased with time.

The effects of diluent gases on carbon deposition from hydrocarbons on metal surfaces has been the subject of several studies. The diluent gases may influence either the metal surface, or the gas phase reaction, or both. Hydrogen was considered to act on the gas phase reactions, Tamai (37) and accelerated the deposition on iron. Helium retarded the deposition on iron and neither hydrogen nor helium affected the rates of deposition on nickel. The dilution of propane with nitrogen increased the rate of formation of carbon, at 1040°C in a quartz tube, Milosavljevic (76) with the addition of 7.4%

nitrogen to the propane increasing the rate by 34%. Larger amounts of nitrogen caused much smaller relative increases of the carbon formation rate.

A study by Anisonyan (77), on carbon formation observed during the pyrolysis of methane in a quartz reactor, indicated a gas phase influence of hydrogen. When conversion was low, or when hydrogen was used as a diluent, only a trace of aromatic hydrocarbons was observed. At high conversions, the primary products were aromatic hydrocarbons, which though slowly formed, underwent rapid dehydropolycondensation on the reactor surface to yield carbon.

Carbon formation from propylene on nickel is autocatalytic, showing an acceleration in rate until a steady-state is reached; this lasts for a long period, Figueiredo (46). For heavy deposits, this can be followed by a drop in the rate. Induction periods are observed under certain conditions, but disappear if hydrogen is added to the system. Although the initial stages are dependent on the type of pre-treatment given to the catalyst, steady-state rates are little affected. The rates of carbon formation on nickel foils are proportional to the geometric area of the foil.

The catalytic nature of the decomposition of propylene over nickel has been established by using nickel foils previously poisoned, Figueiredo (46). Poisoning was achieved by vaporizing about 1 cm.³ of ethanethiol in the reactor. No carbon deposition occurred over the sulphur poisoned foils. Carbon deposition did not occur over activated carbon and graphite rod samples. However, fast deposition of carbon was observed over samples of carbon collected from previously used nickel foils. Nickel particles were found in the carbon deposits and acted as active sites for further carbon formation. The rates of carbon deposition observed were of the same order of magnitude as the rates observed for nickel foils.

The observed features of the process of carbon formation on nickel foils can again be explained with the following model:

- (i) Adsorption of the reactants on the surface.
- (ii) Surface reaction, leading to adsorbed carbon species.

(iii) Diffusion of carbon through the nickel crystallites and precipitation of graphite at the grain boundaries, lifting up the crystallites, which will subsequently be carried on top of the growing carbon, thus ensuring constant rates of deposition.

At low temperatures (below 550°C), diffusion of carbon in nickel is assumed to be rate determining, while in the range from 550 - 650°C surface reaction seems to be controlling. At temperatures above 650°C , carbon formation in the gas phase becomes important.

Nucleation of the carbon may occur on the external surface or at grain boundaries, the latter being energetically more favourable. Growth of surface nuclei cannot lift metal particles out of the substrate; instead it would result in the encapsulation of the active surface, inhibiting further deposition. The presence of hydrogen may prevent this type of nucleation by keeping the surface clean of such encapsulating species. Nucleation at grain boundaries would then be enhanced and the growth of carbon there could push metal grains out of the substrate. Hydrogen enhances grain boundary grooving, Moayeri (50), which may account for the elimination of induction periods.

1.4. Homogeneous-heterogeneous interaction

In many gas phase reactions which are considered to be essentially homogeneous, interference of the reactor wall cannot be disregarded. One of the most important industrial examples is the thermal cracking of hydrocarbons. Several techniques have been reported in the literature to elucidate and eliminate the specific effects of the reactor wall, e. g. changing the surface to volume ratio of the reactor, pre-treatment of the reactor wall by oxygen, acids and sulphur compounds, or changing the wall material, Crynes (78). Gold reactors, which are expected to have no or a very low activity on thermal cracking, have been used, Slotboom (4).

During investigations on the thermal hydrocracking of polyaromatic compounds, Penninger (79)(80), observed several effects

of the reactor age on conversion and selectivity, and temperature history, which were attributed to a participation of the reactor wall. Experiments with a stainless steel reactor revealed considerable changes in conversion and product distribution during the first period of operation. Subsequently, a steady-state system was established. The rate constants of the reactions were approximately half of the original values, while changes in the cracking selectivity were not observed. After the steady-state in conversion and selectivity had been established (after the primary ageing phase), participation of the reactor wall in the hydrocracking reactions remained. A reactor "temperature history" effect was identified. A steady conversion level at a new temperature was only established after a certain operation time at that temperature. The conversion increased if the previous temperature was lower than the new temperature; the conversion decreased if the previous temperature was higher. These results demonstrate that the reactor wall remains active in the thermal hydrocracking after the primary ageing stage of the wall has passed. The steady conversion at a particular temperature is independent of the previous temperature cycle; hence, the adaptation of the surface condition is apparently a reversible process. The presence of a hydrocarbon is essential; hydrogen alone does not cause surface adaptation.

Slotboom (4) demonstrated the continuous participation of the reactor wall in thermal hydrocracking, with the ageing effects of a gold-plated reactor. A completely different tendency from that of the stainless steel reactor was observed. With an increase in ageing time an increase in conversion occurred. The gold reactor experienced a slow process of activation which tended to the steady-state obtained with the stainless steel reactor. The conversion and product selectivity were essentially the same in the aged gold reactor and in the aged stainless steel reactor.

Thermal hydrocracking was found to proceed only in the presence of an active reactor wall; the absence of such a surface resulted in zero or very low reaction rates. With the gold-plated reactor, the formation of some products was highly sensitive to the

ageing conditions, whilst other products were independent of this factor. The formation of the products which were independent of the ageing was considered as predominantly homogeneous. The formation of the products which were highly sensitive to the ageing conditions of the gold reactor had been shown to proceed via a chain reaction, Penninger (79). This reaction did not proceed at all, or only at a very low rate, in the unaged gold reactor. Thus the chain reactions are developed only in the presence of an "active" reactor wall, and the surface area is not critical in the range of surface to volume ratios examined.

Thus, the initiation and termination reactions, i. e. the formation and removal of hydrogen atoms, are heterogeneous, and are both dependent on the size and nature of the surface to the same extent. Thus, the surface of the reactor has no effect on the steady-state concentration of the hydrogen atoms but remains essential for their formation.

Cramers (81) found that, in the thermal cracking of hydrocarbons in stainless steel reactors, excessive coke formation occurred, which resulted in a strong decrease of both the conversion rate and the product selectivity. In a gold reactor, coke formation was much slower but resulted in an increase of the conversion rate which paralleled the amount of coke present on the gold surface. The pyrolytic coke activated hydrocarbon cracking reactions and this was attributed to the presence of free radicals which were detected by electron spin resonance spectroscopy, Holbrook (82).

The pyrolysis of propane was investigated in stainless steel, low carbon steel and nickel tubular reactors, which were treated with sulphur containing compounds and oxygen and hydrogen, to elucidate the role of the surface, Crynes (78). Metal oxide surfaces in the reactor were effective in promoting secondary reactions of propane and ethylene at 700°C . with propane conversion increasing. The metal oxide on the reactor surface was reduced by hydrogen contact and the oxides were converted to a relatively durable and passive metal sulphide layer by contact with sulphur containing compounds.

Heterogeneous effects can play a major role in determining the products and rates of reaction in the pyrolysis of some paraffins. These effects depend on the condition and nature of the reactor surface. A comparative critical survey of the literature has been published by Leathard and Purnell (5), which shows that in no instance is there complete agreement on the data. The evidence indicates that, in the absence of oxygen, and with reaction vessel surfaces that are stable and not coated with carbonaceous material, the pyrolysis of propane, n-butane, isopentane and neopentane is essentially homogeneous at the normal temperatures and pressures of paraffin studies. If the surface to volume ratio was increased sufficiently, then some heterogeneous contribution to the overall rate would probably be introduced.

There is general agreement that the pyrolysis of ethane and isobutane is markedly heterogeneous in almost all circumstances. However, Quinn (8) found that the initial rate of methane formation from ethane was independent of the surface to volume ratio for a variety of surface treatments. As primary methane arises from the chain initiation step, this work showed that carbon-carbon bond scission in ethane is homogeneous above 550°C.

Leathard and Purnell (5) considered that carbon conditioning of the reactor was necessary to achieve reproducible heterogeneous behaviour. This was supported by the observation of Gordon (83) that results were irreproducible when a quartz vessel was first put into the furnace, but that reproducibility improved considerably after continued use.

A correlation was noted by Leathard and Purnell (5), between the extent of hydrogen production and the degree of heterogeneity observed. Hydrogen is a dominant product of both ethane and isobutane pyrolysis, but is a comparatively minor product of n-butane and isopentane pyrolysis and a trivial product with neopentane. The marked heterogeneity associated with ethane and isobutane pyrolysis is a result of the important role played by hydrogen atoms in chain propagation and the relative ease of their diffusion to and removal at the wall. Marshall (84) showed that the observed increase in overall

order of ethane pyrolysis at low pressure can be accounted for by a first order wall termination reaction of hydrogen atoms. Lin (85) confirmed experimentally that the heterogeneous termination did not produce n-butane, but commented that Marshall (84) had overstated the effect of heterogeneity by ignoring the pressure dependence of the carbon-carbon bond rupture in ethane.

Purnell (86) has also produced a hypothesis for the wall effects in paraffin pyrolysis. In untreated vessels in the absence of traces of oxygen, the pyrolysis is essentially homogeneous unless there is sufficiently significant hydrogen atom participation in chain propagation such that their removal at the wall constitutes an important chain termination process. However, this hypothesis leads to the expectation that propane pyrolysis should be classed among the heterogeneous reactions, since hydrogen amounts to about 25% of the total products.

This apparent discrepancy was resolved by Leathard and Purnell (5) who reached conclusions by excluding from consideration all work where carbon conditioned vessels were used (it has been shown that carbon coatings are reactive) and results obtained where the presence of oxygen or other impurities were suspected. Based on these restrictions, it was assumed that the only significant heterogeneous process was the removal of hydrogen atoms at the wall. This effect only becomes apparent if hydrogen is an important product. Hence, heterogeneity is most important at low temperatures and at low pressures, since diffusion to the wall is then easier.

The presence of wall effects in homogeneous reactions have been identified by changing the surface to volume ratio in the reacting system. If no change in the reaction rates were observed, it was assumed that the reaction was homogeneous. However, this over-simplified criteria has been shown to fail under certain conditions. Slotboom (4) found that changing the surface to volume ratio from 3.1 to 13.3 cm^{-1} did not produce a change in the conversion rate and product selectivity. Similar observations were made with a static reactor when the surface to volume ratio was changed from 1.5 to 6.5 cm^{-1} . These experimental observations could have been taken

as proof of no participation of the surface in the reaction. However, a "temperature history" effect was observed that was attributed to surface conditioning. These results demonstrate that conclusions from surface to volume changes must be made with caution. Surface to volume changes producing changes in homogeneous rates can be taken as evidence of surface participation. However, no change with surface to volume changes cannot be taken as proof of no participation of the surfaces.

The influence of the contact time and the surface to volume ratio in the reaction zone on pyrolytic carbon formation, was investigated during methane pyrolysis in a flow system, Makarov (87), between 815-1100°C. An assumption of the possibility of transition of the reaction centres from the gas phase to the surface was made to interpret the dependence of the experimental rates of pyrolytic carbon formation on the surface to volume ratio. The kinetic model proposed, postulated that the reaction proceeded on the surface and in the gas phase. The reaction was initiated by the active intermediates (active centres) such as radicals. Growth of carbon occurred by the addition reaction of hydrocarbon molecules to the active centre. The addition reactions were accompanied by dehydrogenation, ring formation and other reactions associated with changes in the electronic structure of molecules. The active centres generated in the gas phase were partly captured by the surface. Conditions which allowed the simultaneous conversion both in the gas phase and on the surface were named as the conditions of homo-heterogeneous pyrolysis. The surface reaction was initiated by the centres both generated by methane decomposition and captured by the wall. The radical termination stages were the formation of highly carbonized products : soot in the gas phase and pyrolytic carbon on the surface.

During heterogeneous conversion, all stages of the reaction proceed on the surface. The reaction rate is proportional to the surface area, and pyrolytic carbon is the only carbonaceous product of the reaction. During homo-heterogeneous conversion, individual or total stages of the reaction proceed simultaneously, both according to homogeneous and heterogeneous mechanisms.

The rate of pyrolytic carbon formation increased with an increase of the contact time. The lower the surface to volume ratio, the higher the increase of rate. Confirmation of the radical transition from the gas phase to the surface was demonstrated by an increase of the rate of growth of carbon layers on the surface when the surface to volume ratio was diminished. The rate of formation of active centres in the volume unit was approximately 10^4 larger than that on the surface unit. Therefore, the surface will influence the reaction rate when the surface to volume ratio is not less than 10^3 cm^{-1} . At surface to volume ratios greater than 10^4 cm^{-1} , the reaction is heterogeneous during all stages.

As the surface to volume ratio of the reactor is diminished, the influence of homogeneous reaction is increased. At surface to volume ratios of less than 10^3 cm^{-1} , the homogeneous mechanism of the active centres formation begins to prevail. In the transient period of homo-heterogeneous reaction, the influence of the surface to volume ratio on the rate of pyrolytic carbon formation, changes with increasing contact time. At short times of reaction, the rate of pyrolytic carbon formation was proportional to the surface to volume ratio.

Heterogeneous-Homogeneous effects have been found to be of importance under industrial conditions. A study of the hydrogenation of oils to gaseous hydrocarbons, Thompson (2), showed that carbon can be produced in three distinct ways: catalytically by contact with the reactor, by build-up on surfaces already covered with carbon and in free space with the appearance of soot in the outlet gas. Carbon can arise from the decomposition of hydrocarbons at catalytically active surfaces and those containing nickel were found to be the most active. Usually, there was direct evidence from the corrosion and pitting of the surface that the metal had participated. Carbon was also observed to form on a surface already covered with carbon. This was particularly likely to form if the underlying surface was inert or of low activity. This "wall carbon" was thought to result from the decomposition of hydrocarbons by a chain mechanism that is favoured by the surface having insufficient

activity to break the chain by the hydrogenation of unsaturated compounds. "Space carbon" was produced in the gas phase and was responsible for soot being present in the outlet gas. It was thought to arise from a similar chain mechanism to wall carbon, but was distinguished from it by two complementary observations. There was no evidence of carbon being dislodged from the wall to give soot in the gas. Occasionally, soot was present in the gas without any accumulation on the wall. Secondly, wall carbon can form whilst the gas remained clean.

The reactor for these experiments was constructed from 18/8 chrome/nickel steel. Other materials of construction were studied in an attempt to limit carbon formation and the corrosion and pitting of the surface. Copper alloys containing nickel were inactive towards hydrocarbon gases individually, but became very active for the decomposition of ethane if carbon monoxide was present or if the reactor had previously been exposed to carbon monoxide. The reactor was also plated with copper and difficulty in initiating the reaction was experienced. This indicated that the surface was important in starting the reaction. When the reaction started it proceeded normally, with only traces of carbon in the outlet gas. However, the reactor walls were covered with a very large deposit of carbon, most of which was sooty, but underneath it a hard skin of carbon was found adjacent to the metal surface. The sooty carbon could not have been produced in contact with the metal and then diffused through the hard skin of carbon that covered the metal. It was thought that two types of carbon were involved, one deposited on the metal, the other on the carbon covered surface. Analysis of the sooty deposit showed that it was not pure carbon, but contained complex hydrocarbons, indicating that it may have been formed by the cyclisation of intermediate unsaturates.

It was found that traces of sulphur compounds prevented both the catalytic formation of carbon in contact with materials such as nickel steels and the associated pitting. Traces of sulphur compounds, supplemented by the presence of steam in the hydrogenating gas, stopped the formation of soot. The sulphur compounds were

required in higher concentration, 100 ppm. in the distillate, to avoid a slow build-up of carbon on the reactor walls. Preliminary sulphiding of the reactor surface did not prevent catalytic activity giving carbon formation. The catalytic activity was re-generated as soon as the supply of sulphur was stopped, and soot appeared again in the gas. When steam was also present, 10 ppm. by weight of sulphur in the distillate supply was sufficient to avoid soot formation. When the sulphur concentration was reduced below 2 ppm., soot appeared in the outlet gas and the temperature fell. By indicating that carbon formation was endothermic, this showed that it arose mainly by the decomposition of hydrocarbons, and not by the decomposition of carbon monoxide, which is exothermic.

The literature which has been referred to in the above sections, indicates that the important parameters in hydrocarbon pyrolysis are:

- (i) the nature of the kinetics of the free radical reactions
- (ii) homogeneous and heterogeneous interactions
- (iii) routes for carbon formation

These parameters can be clarified by devising suitable experimental systems capable of demonstrating the consequences of each parameter and the inter-relation between them. Hydrocarbon pyrolysis proceeds by free radical mechanisms; initiation, propagation and termination. Heterogeneous interactions of the reactor surface can occur in the initiation and termination stages. Carbon formation occurs via intermediates which are susceptible to heterogeneous interactions and when a heterogeneous surface is present, the rate of carbon formation is influenced by the catalytic nature of the surface.

1.5. Free radicals in pyrolysis

A complicated relationship exists between gas phase free radical reactions and those reactions that occur at the reactor wall. The free radical reactions proceed in the gas phase, although some interaction with the reactor wall occurs. The general kinetics can be explained without involving the wall. Hydrocarbon decomposition

occurs both by the process of hydrogen abstraction and carbon-carbon bond cleavage. Combination processes between free radicals and molecules, and pairs of free radicals, give rise to heavier molecular weight species. Such associations quickly result in the production of aromatic and polynuclear aromatic compounds, which are carbonaceous in nature. As a result the elucidation of the mechanism of the formation of carbonaceous materials can be greatly aided by experimental determination of the free radical species which are present in the gas phase.

1. 5. 1. Free radical detection

Traditional methods of investigating gas phase reactions involve the analysis of reaction mixtures for stable products by, for example, gas chromatography. On the basis of these results, a reaction scheme is then proposed to account for the observed overall kinetics and product distribution. However, the large variety of radicals present in such systems means that many reaction schemes could account for the overall kinetics and uncertainties about the prevailing mechanisms may remain. The chemical reactions in such systems are chiefly those involving free radicals and atoms. The identification of these species in a reacting environment would remove many of the uncertainties arising from stable product analysis and allow more definitive reaction schemes to be established.

Due to their high reactivity, the free radical concentration at atmospheric pressure is usually small. Radical-radical reactions occur very rapidly with zero activation energy and little steric hinderance. The rate constants associated with these reactions are usually of the order of 10^{13} mole. cm.⁻³ sec.⁻¹, or close to the frequency for molecular collisions. Radical-molecule reactions proceed more slowly but still have high reaction rates.

There are two main pre-requisites for the observation of free radicals in a reacting system. Firstly, they must be removed from the reacting system and transferred to a detector without loss or modification and with minimum disturbance to the system under

observation. Methods of preventing free radicals from reacting involve either their isolation, or to place them in a very low temperature environment. Collisional isolation either entails rapid expansion of the sample into a vacuum or operation with low pressure reactors. Secondly, the detector must be capable of distinguishing the radicals from a large excess of structurally similar molecules. For the full description of a system, the detection and estimation of both stable and unstable species is desirable. A technique that is capable of detecting both stable molecules and free radicals is mass spectrometry.

1. 5. 2. Molecular beams

Many free radicals have been detected by mass spectrometry. The method offers an effective means of analysing reacting systems and is sensitive and non-discriminating. The analysis of both stable and unstable species may be achieved. Since mass spectrometers operate at low pressures (typically 10^{-6} torr) a means of transferring a sample from the reacting system (which may be at pressures up to one atmosphere) to the ion source of the mass spectrometer, without loss of reactive species, is required. It is important that any radicals detected are derived from the reaction under investigation and are not the result of radical-radical or radical-molecule reactions after sampling, or of reactions having occurred on a surface. The required pressure reduction and means of transport can be achieved by a molecular beam sampling system.

The first element of any molecular beam apparatus is an orifice at which the initial pressure reduction from the sampling zone occurs. The conditions at the orifice determine the subsequent treatment of the sample and also determine the intensity, velocity distribution and composition of the final working beam. Source conditions also determine the integrity of the sample with respect to the nature of the reactive species that are finally detected. A convenient method of describing source conditions is in terms of the Knudsen number.

The Knudsen number.

For a gas contained in a vessel, two limiting cases may be encountered. Firstly, the mean free path of the gas, λ , is much smaller than the dimensions of the vessel. In this situation, the properties of the gas are determined by inter-molecular collisions and the gas is said to be in the continuum regime. The second limiting situation is when λ is much larger than the dimensions of the vessel. The gas properties are then determined by gas molecules colliding with the walls of the container and the gas is in the free molecular flow regime. These extreme conditions, and also intermediate situations, are expressed by reference to the Knudsen number, defined as the ratio of the mean free path of the gas to the characteristic dimension of the vessel.

$$Kn = \frac{\lambda}{d}$$

The continuum regime pertains to the situation when $Kn < 10^{-1}$, and the free molecular flow regime when $Kn > 10$. The intermediate values, when $10 > Kn > 10^{-1}$, is the transition regime. The conditions existing at a sampling orifice may be described in terms of a Knudsen number, where the characteristic dimension, d , is the diameter of that orifice.

Effusive sources

Historically, molecular beam systems have been constructed such that $Kn > 10$, i. e. effusive systems. The gas being sampled is separated from the rest of the apparatus by a pinhole leak, Fig. 1.1. Molecules effuse through the hole into a low vacuum chamber, where intermolecular collisions virtually cease. A collimator behind the leak may be used to define a working beam. A major disadvantage of this system for the sampling of reactive systems is that the molecules constituting the beam will have suffered many collisions with the material of the pinhole and any reactive species detected may have been modified at the surface. Thus, the sample is no longer representative of the homogeneous gas phase. This limitation was recognised by Eltenton (88) in his pioneering work, but lack of pumps with sufficiently large pumping speeds prevented the use of larger

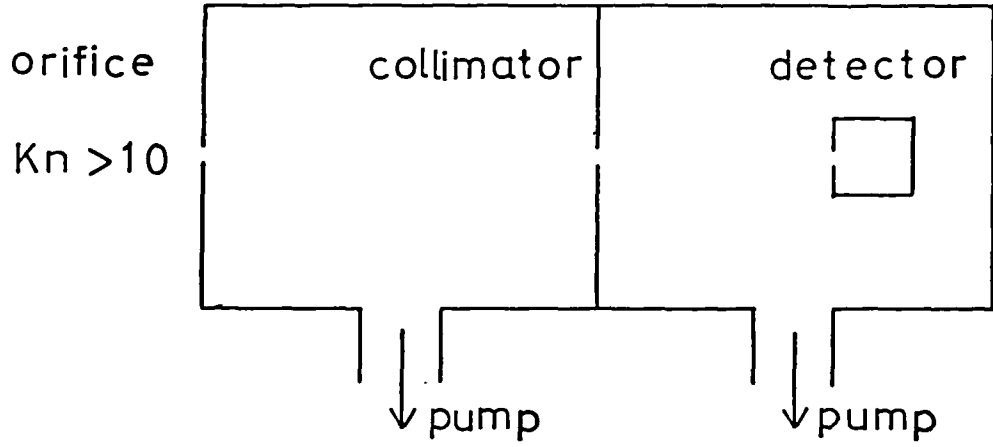


Fig. 1.1. Effusive source

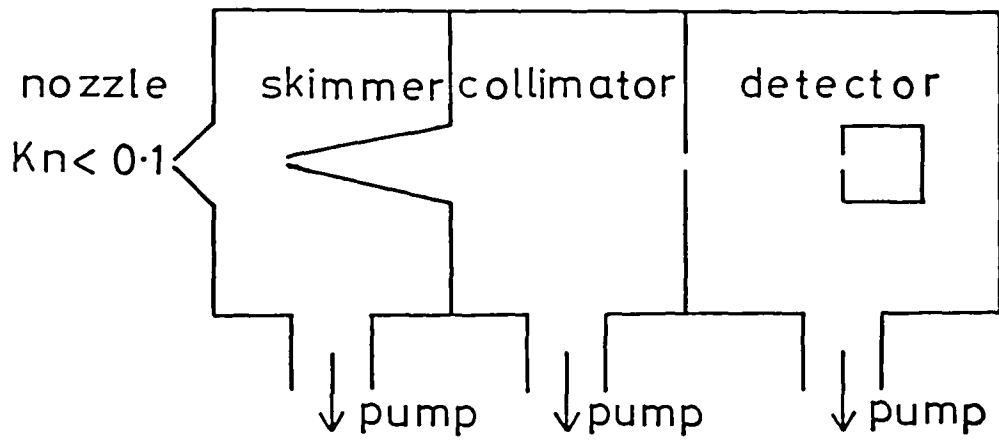


Fig. 1.2. Nozzle source

orifices at that time. The classic text dealing with effusive molecular beams is that of Ramsey (89).

Continuum sources

In 1951, Kantrowitz and Grey (90) suggested that the use of a supersonic nozzle source, instead of a conventional slit or circular orifice, followed by a skimmer to extract a working beam (Fig. 1. 2.) would produce a beam of greater intensity than a conventional effusive system. A gain in intensity due to the pre-collimation effect of such a nozzle was predicted. A further gain in intensity was predicted due to the increased rate of effusion, the final beam intensity being about 75 times that of a conventional effusive source sampling at similar pressures. Another advantage derived from such a system is the much narrower velocity distribution compared to an effusive source. The design and construction of the skimmer requires special attention, so that it causes minimal interference when immersed in the supersonic gas flow.

A system based on these ideas, operating in the continuum regime ($Kn < 10^{-1}$), offers many advantages in the sampling of reacting systems and subsequent analysis for reactive species. Firstly, the sample is not contaminated by boundary layer reactions. It is representative, with respect to the nature of the reactive species, of the bulk reaction mixture. Secondly, the increased beam intensity gives greater sensitivity. This is an important consideration when the species under observation may be in very small concentrations. Thirdly, the rapid expansion of the gas behind the sampling nozzle causes the flow to evolve from the continuum regime in the nozzle, into free molecular flow within a short distance downstream. The reactive species are effectively isolated and no loss by intermolecular collisions is possible.

A major disadvantage of such a system is the difficulty in obtaining quantitative data, due to mass separation effects. Very careful calibration is required to make quantitative measurements, even when sampling for stable components of a system. The problem is even more difficult when quantitative measurements of reactive

species are required.

Many workers have followed the ideas of Kantrowitz and Grey (90), and built systems capable of producing supersonic beams and operating in the continuum regime. Zapata (91) succeeded in producing a supersonic beam having an intensity less than that predicted. This was attributed to attenuation at the skimmer. Lack of sufficient pumping capacity in the chamber behind the skimmer precluded the use of a skimmer large enough to reduce the skimmer interference. The lip radius of the skimmer was a critical parameter in the production of a supersonic beam. A lip radius of 0.02 mm. produced only a sonic beam and therefore caused considerable interference with the gas flow behind the nozzle. A lip radius of 0.01mm produced a supersonic beam of increased intensity.

Several groups of workers later constructed nozzle source molecular beam systems whose performance approached theoretical predictions (92-96). Deckers and Fenn (92) measured beam intensities as a function of the nozzle-skimmer separation and Scott and Drewry (96) measured radial intensity profiles. They found that at a particular value of the ratio of the nozzle-skimmer separation to the nozzle diameter, the beam width was minimised and the intensity maximised. This is indicative that a position of "best skim" exists, where skimmer interference is at a minimum. Milne and Greene (97) constructed a nozzle source molecular beam coupled to a mass spectrometer as detector. They investigated the mass separation effect and found it to be proportional to molecular weight. From a mixture of two gases of different molecular weights, the beam becomes enriched in the heavier species.

1.6. Present work

Methods of experimentation, measurement and analysis have been devised to elucidate the homogeneous and heterogeneous effects and their interactions occurring in hydrocarbon pyrolysis. The gaseous molecular products and the liquid aromatic and polyaromatic compounds have been determined by gas liquid chromatography. The

catalytic influence of the reactor wall on carbon formation has been studied with an on-line microbalance and the influence of the reactor wall on the formation of carbon in the gas phase has been studied by lining the reactor with various metals. The influence of various metals on the product distribution of polynuclear hydrocarbons can be measured with an on-line mass spectrometer. The various free radicals which are present in the gas phase processes can be identified by use of the molecular beam sampling mass spectrometer.

CHAPTER 2

EXPERIMENTAL

		Page
2. 1.	<u>Introduction</u>	45
2. 2.	<u>Apparatus</u>	46.
2. 2. 1.	The reactor	46
2. 2. 2.	The furnace, temperature control and measurement	49
2. 2. 3.	The gas inlet system	52
2. 2. 4.	The microbalance	56
2. 3.	<u>Analysis of gases</u>	58
2. 3. 1.	Flame ionisation detector chromatograph	59
2. 3. 2.	Microkatharometer detector chromatograph	62
2. 4.	<u>Analysis of liquids</u>	63
2. 5.	<u>Analysis of solids</u>	63
2. 5. 1.	Electron probe micro-analysis	63
2. 5. 2.	Spark source mass spectroscopy	64
2. 5. 3.	Metallography	65
2. 5. 4.	X-ray diffraction	66
2. 6.	<u>Procedure</u>	66
2. 6. 1.	Carbon deposition measurements and the analysis of gases	66
2. 6. 2.	Analysis of aromatic and polyaromatic compounds	69
2. 7.	<u>The molecular beam mass spectrometer system</u>	70
2. 7. 1.	The reactor	70
2. 7. 2.	The molecular beam system	73
	a) The nozzle beam system	73
	b) The vacuum system	80

	Page
2.7.3. The mass spectrometer	84
2.7.4. Signal processing	87
2.7.5. Procedure	88

2.1. Introduction

Experiments were devised with the objective of defining the factors which influence the rate of carbon formation during propane pyrolysis. The hydrocarbon products were analysed by gas chromatography and the rate of carbon formation measured using an on-line microbalance. A jet-stirred reactor was used to ensure uniform gas composition and temperature inside the reactor.

2.2. Apparatus

The reaction system consisted of a jet-stirred reactor and associated microbalance, furnace and temperature controller, feed system for the gases and an on-line gas chromatograph. The system is shown in Fig. 2.1. The sample disc, on which the carbon deposition was measured, was suspended inside the heated reactor, from one arm of the microbalance. The reactant gases were introduced into the reactor and the hydrocarbon products analysed with the on-line flame ionisation detector (F.I.D.) gas chromatograph. A separate microkatharometer detector gas chromatograph was installed later.

2.2.1. The Reactor

The jet-stirred reactor was made of silica and based on the design by Bush (21); it is shown diagrammatically in Fig. 2.2. The jet is a smooth continuous taper with a hole of 0.8 mm. diameter. The mixing process occurring inside the reactor can be considered as three continuous mechanisms.

- a) The bulk transport of unreacted material from the inlet to other parts of the reactor.
- b) The first stage of dispersal of this material into its immediate surroundings accomplished by turbulent dispersion.
- c) The final mixing on the molecular scale accomplished by molecular diffusion.

These processes apply not only to fresh feed but to any other species differentiated from its surroundings by temperature or composition. This results in uniformity of temperature and composition inside the reactor.

The reactor volume was 57.5 mls. and the jet inlet was constructed from capillary tubing to limit pre-decomposition

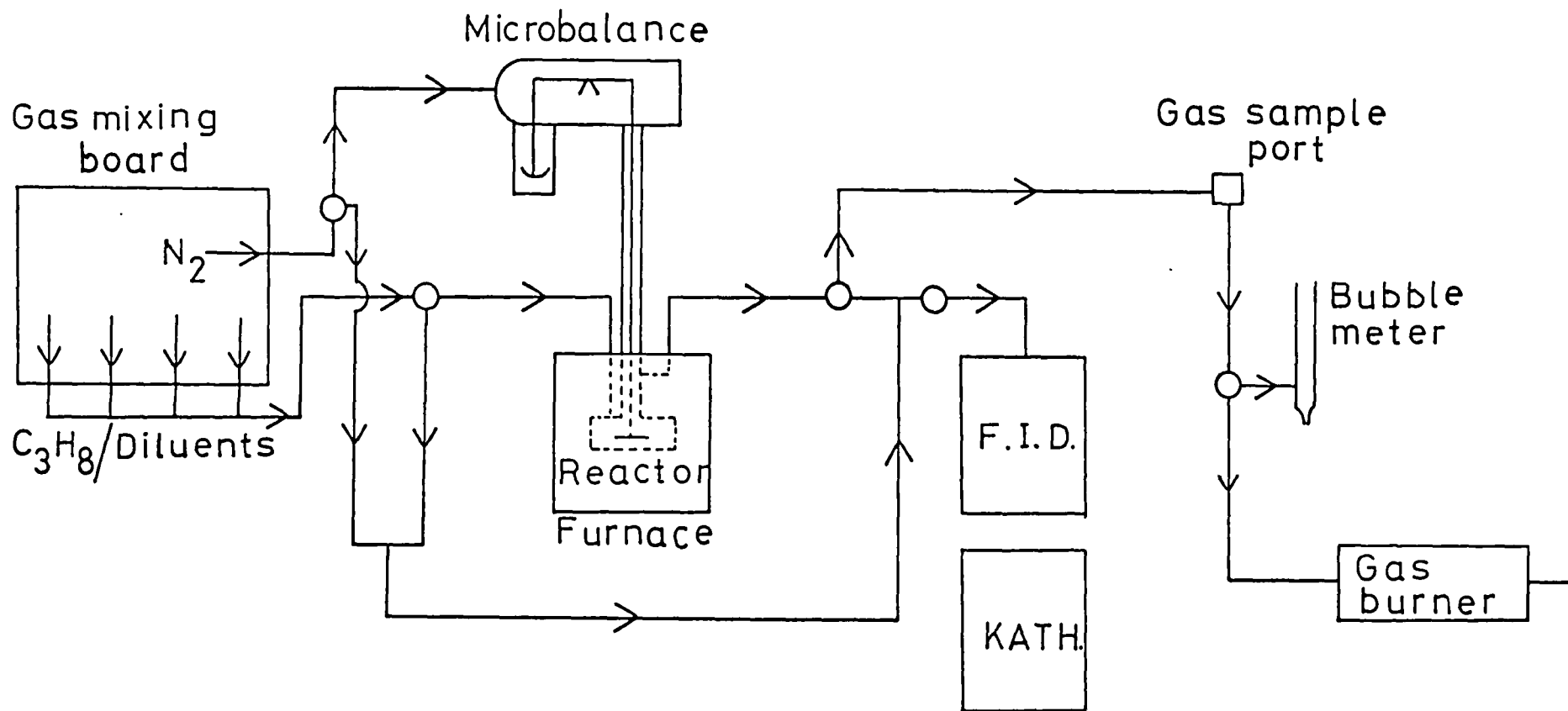


Fig. 2.1. The experimental system

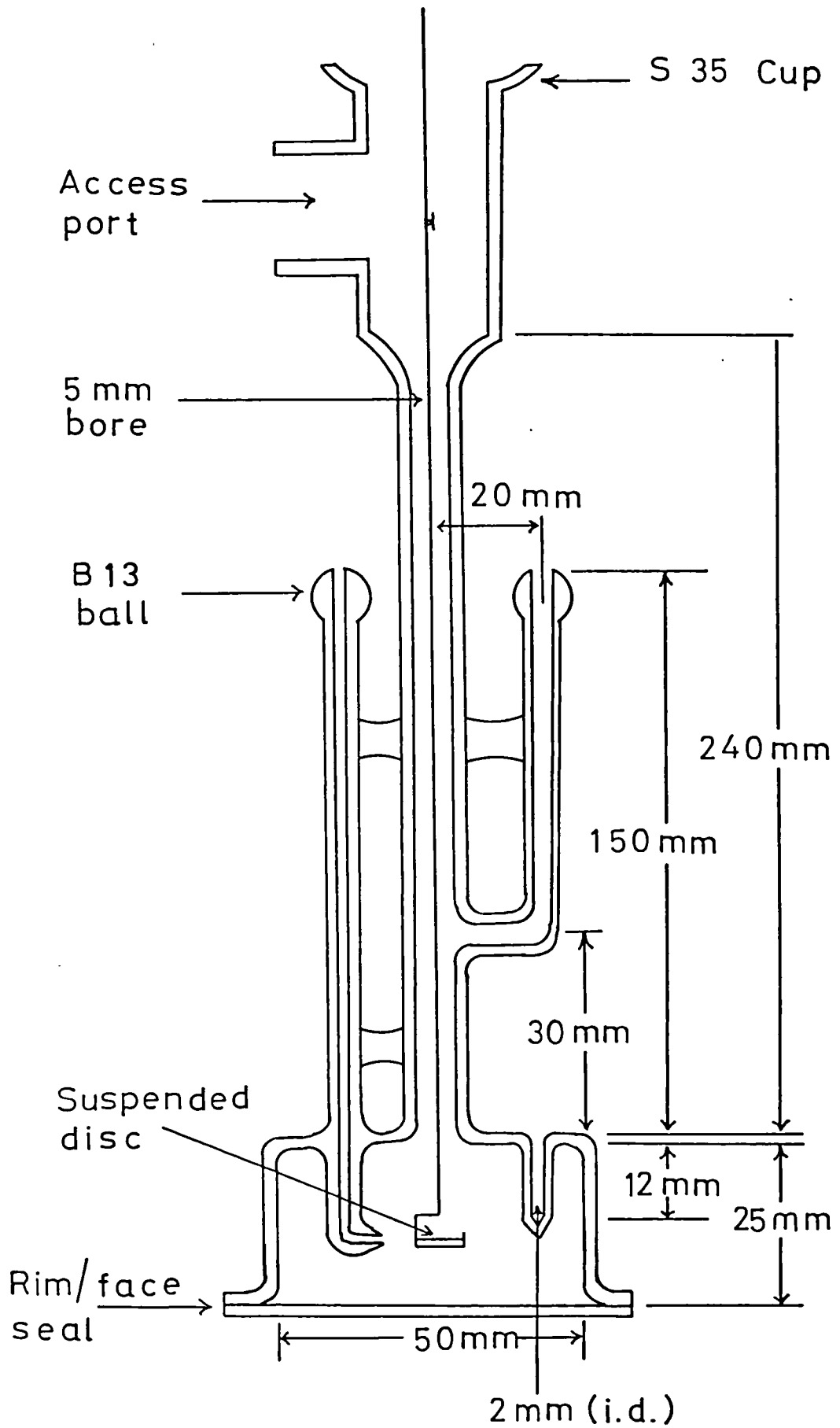


Fig. 2.2. The microbalance reactor

of the reactant gas. An important aspect of the design of the reactor is provision for easy insertion of metal foil liners inside the reactor. This is most conveniently done by being able to part the upper and lower parts of the reactor. However, the two parts had to be clamped together as the reactor was heated to temperatures greater than 750°C . A metal clamp with a sprung tightening mechanism outside the furnace hot zone was used and is shown in Fig. 2.3. The springs compensate for the thermal expansion of the metal clamp.

The reactor was fitted with a Quickfit cup socket and clamped to the microbalance case ball joint with a sprung clip. This ball and cup joint enabled movement of the reactor relative to the microbalance case, to ensure that the microbalance suspension holding the disc did not touch the reactor wall. The side port, enabling access to hook the silica suspension fibre over the glass fibre hook, was closed with a rubber bung.

2.2.2. The Furnace, Temperature Control and Measurement

The furnace heating element of 35 ohms resistance, (Nichrome 5 wire, British Driver Harris), was coiled into a spiral of 7 mm. internal diameter and then coiled around a silica tube of internal diameter 4" and length 4". This was positioned inside an insulating jacket of aluminous porcelain. An insulating case of fire-clay sheets was built around the furnace tube assembly and the space between the insulating jacket and the fire-clay sheet case filled with Kaowool insulating material (Morgan Ceramic Fibres). The construction of the furnace is shown in Fig. 2.4.

The furnace was heated and controlled at temperature with a temperature controller (Eurotherm International 070 Series). Measurement of the furnace temperature was made with a chromel/alumel thermocouple which was connected to the temperature controller. The chromel and alumel wires (British Driver Harris) were sheathed in silica tubing. The measurement of the temperature inside the reactor was made with a second chromel/alumel

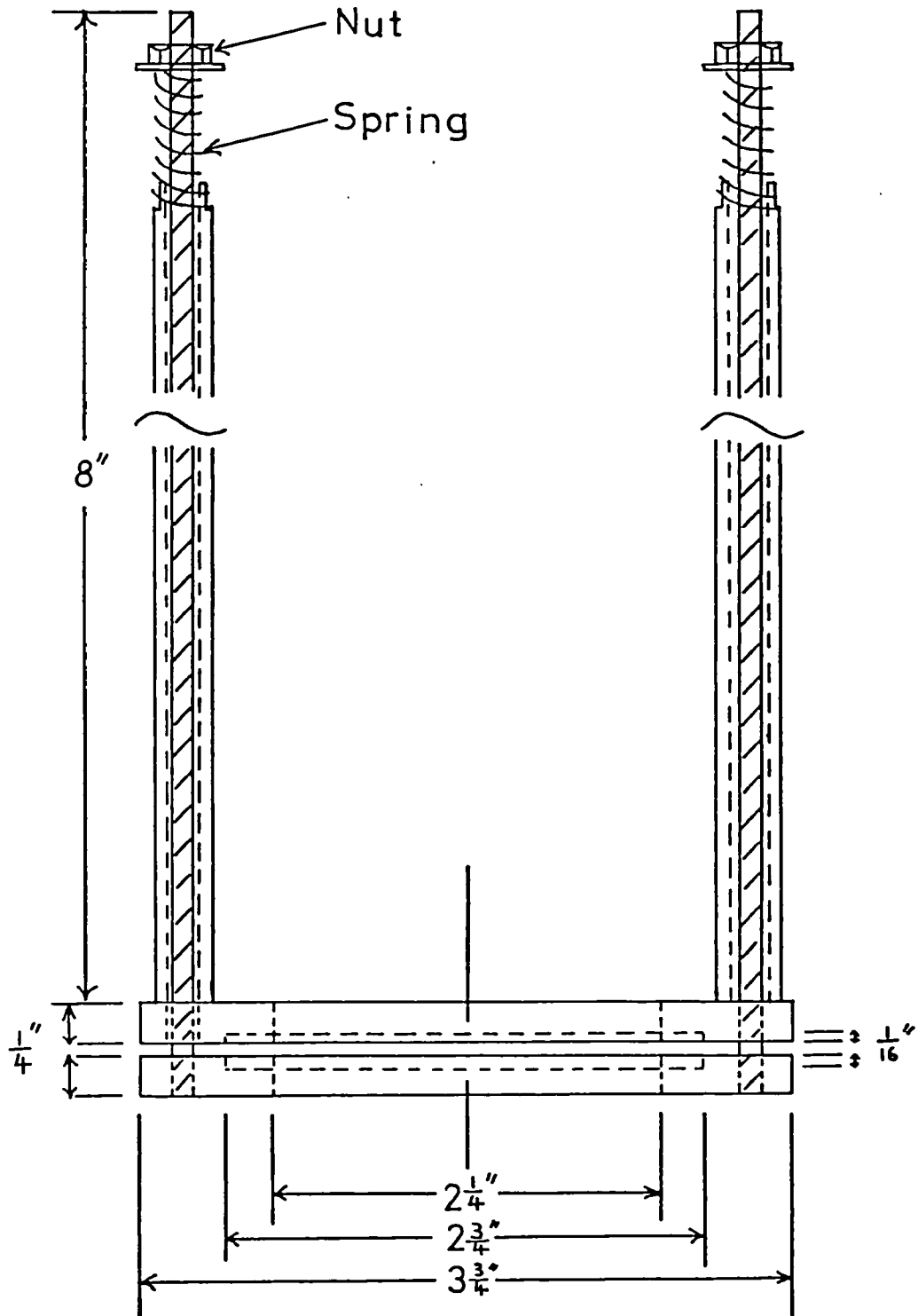


Fig. 2.3. Metal clamp for the microbalance reactor

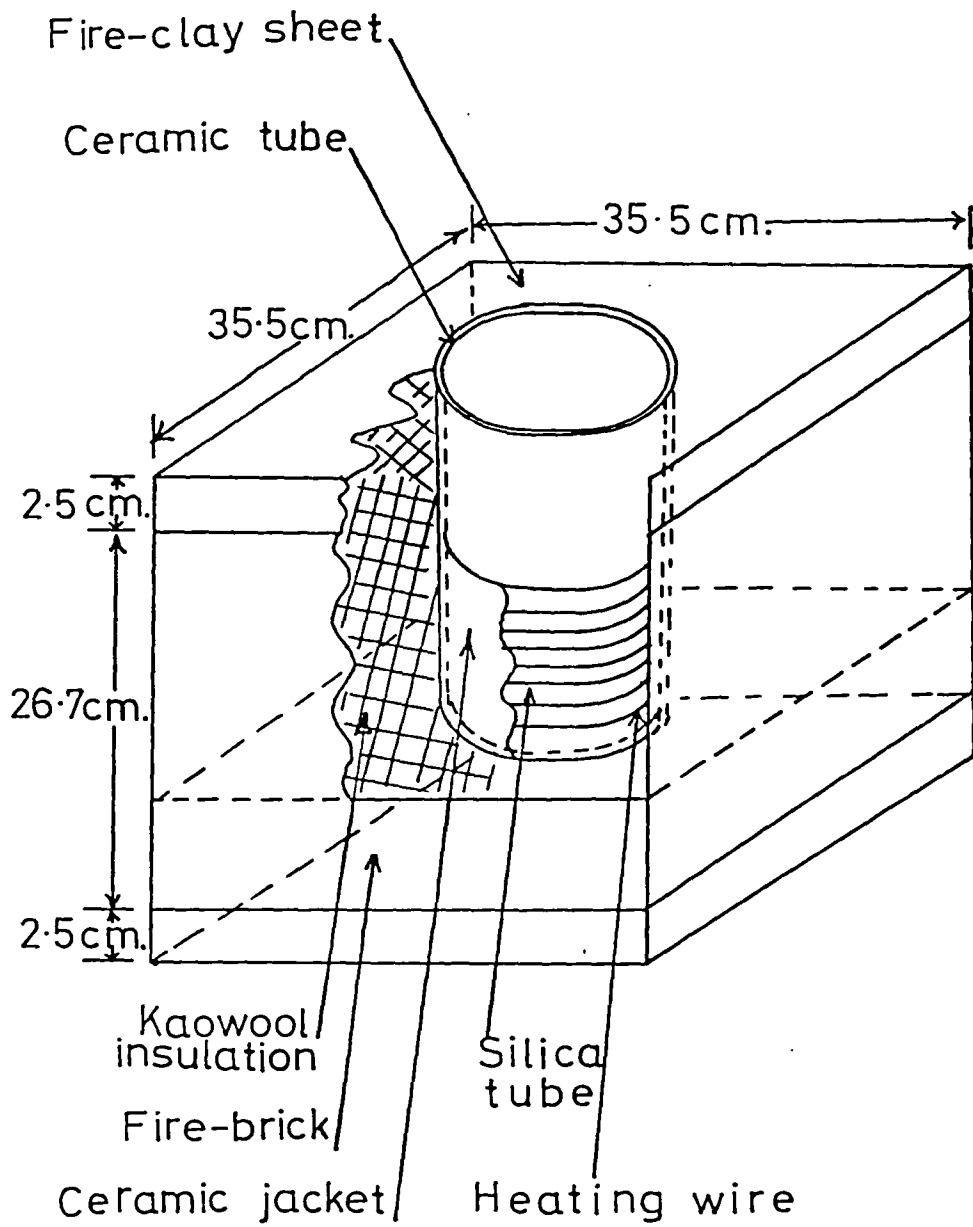


Fig. 2.4. The microbalance reactor furnace

thermocouple, connected to a potentiometer (Croydon Precision Instruments type P. 6.). The furnace was controlled to a constant temperature with a thermocouple positioned outside the reactor, so that any temperature change that occurred inside the reactor during propane pyrolysis would not cause the furnace temperature to alter. The chromel/alumel thermocouples were calibrated against a commercial chromel/alumel thermocouple (British Insulated Callender's Cables). The indicated temperatures at 825°C were found to be within 2°C , the smallest marked division on the potentiometer scale.

The temperature profile of the furnace is shown in Fig. 2.5. The temperature was controlled at 810°C by the furnace thermocouple positioned 8 cms. above the floor of the reactor. This is the distance that the jet in the jet-stirred reactor is above the furnace floor. The furnace temperature at various distances above the furnace floor was measured with a commercial chromel/alumel thermocouple.

The top of the furnace tube was insulated against heat loss with Kaowool bulk fibre.

2. 2. 3. The Gas Inlet System

Gases were supplied to the reactor from cylinders (British Oxygen Company and Air Products), through two-stage pressure regulators. The flow rates, at constant pressures indicated by mercury manometers, were measured with rotameters (G. E. C. Elliott), calibrated with soap bubble-meters. The gas flow rates were controlled with fine control needle valves (Hoke International). The individual gas streams were combined in a glass manifold and passed through a glass mixing column, which also served as a flame trap, into the reactor. The gas inlet system is shown in Fig. 2.6.

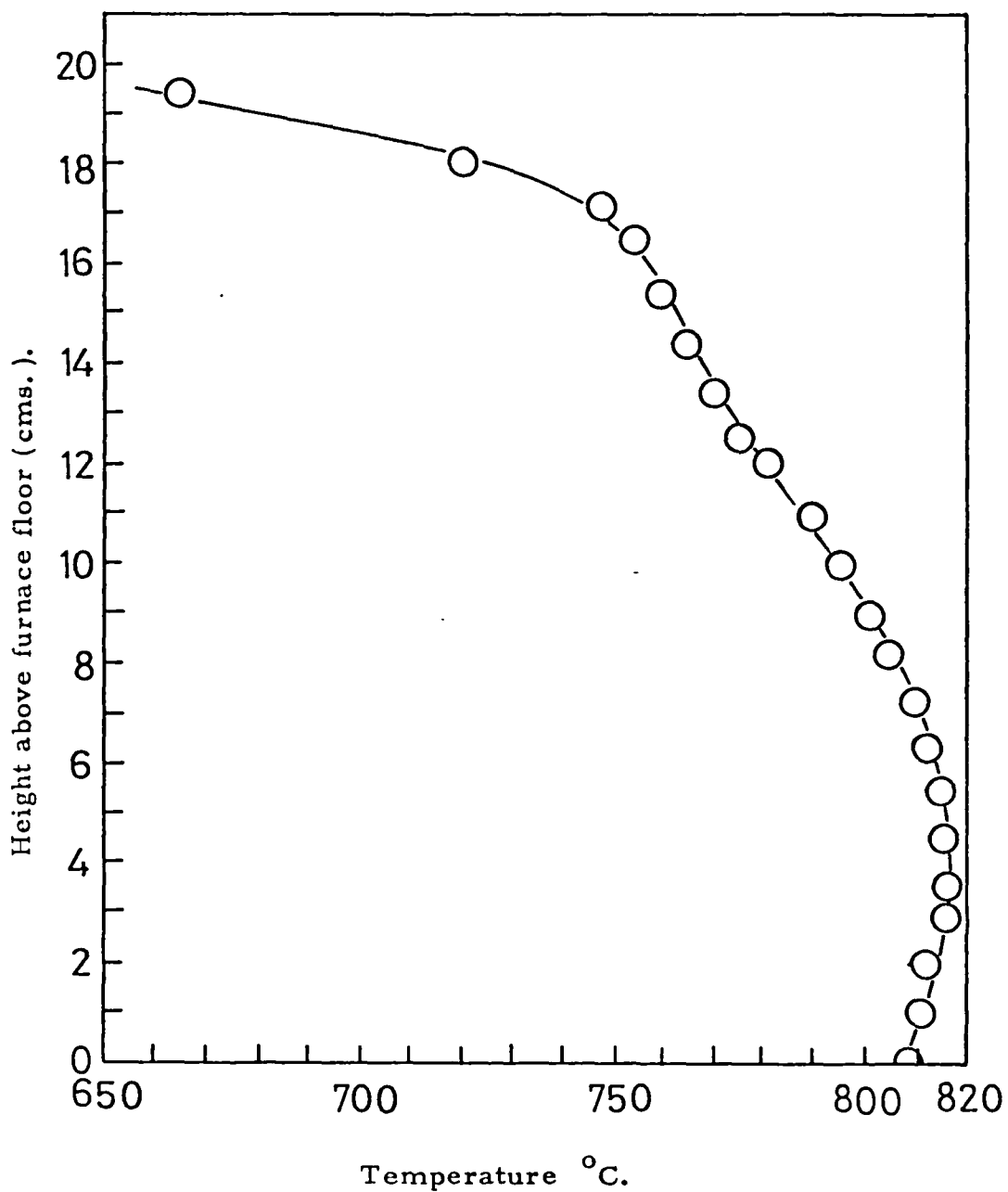


Fig. 2.5. Temperature profile of microbalance reactor furnace (controlled at 810°C. with a thermocouple 8 cms. above the furnace floor).

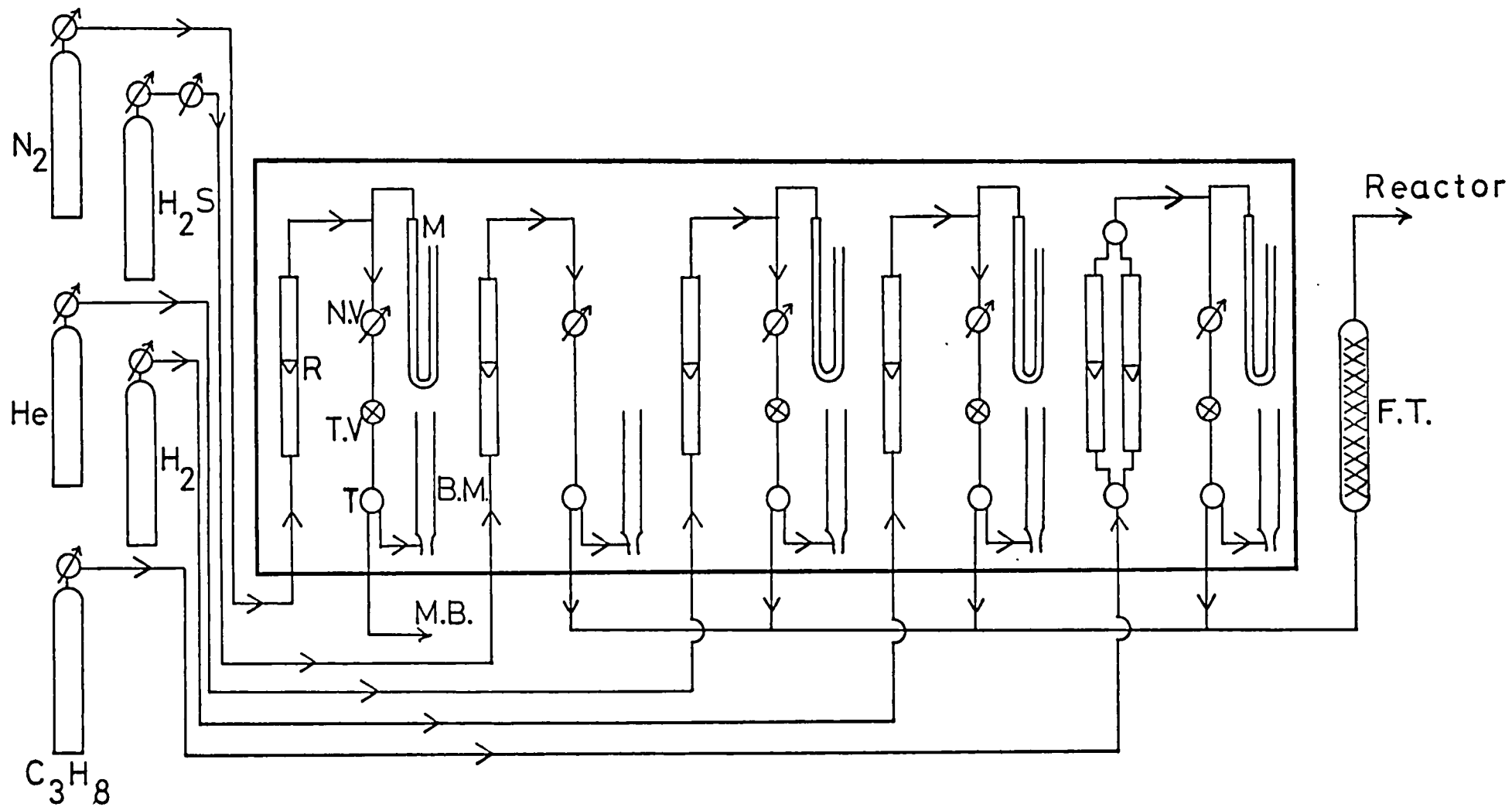


Fig. 2.6. The gas inlet system

Key to Fig. 2.6. The gas inlet system

R	=	Rotameter
N. V.	=	Needle valve
T. V.	=	Toggle valve
T	=	Tap (double oblique).
M	=	Manometer (mercury).
B. M.	=	Bubble meter (soap).
M. B.	=	Microbalance
F. T.	=	Flame trap (glass ball).

2.2.4. The Microbalance

A C. I. Electronics Mark I microbalance was used. The remote balance head was joined to a brass end-plate and fitted inside a glass balance head case having two S 35 ball joints. These enabled the connection of a chamber for the counterweight (left) and the reactor with the sample disc suspension (right). The brass end-plate was clamped to the glass balance head and sealed in position with black wax. The electrical connections from the balance head to the control cabinet were made through the brass end-plate. The control cabinet allowed a choice of five scales ranging from 0 - 100 micrograms to 0 - 10 milligrams. The maximum electrical tare was 5 milligrams. The output signal from the control cabinet passed through a "matching box" to a potentiometric recorder (Leeds and Northrup) and was recorded directly as a function of time. The "matching box" provided facilities for expanding the range of the balance, within the scales already described, and for damping the signal.

The sample foil and counterweight were suspended from the balance arms by glass fibres with hooks at each end. The silica suspension fibre, diameter 0.5 mm., joined to the suspension cradle, was hooked over the glass fibre hanging from the sample side of the microbalance beam, and suspended the disc horizontally inside the reactor. The suspension cradle allowed free access of the reactant gases to both faces of the sample disc. The sample suspension system is shown in Fig. 2.7. The height of the suspended disc, relative to the jet, was varied by using glass fibres of various lengths.

To prevent product gases passing up the reactor stem and entering the balance head, nitrogen was introduced into the balance head glass case through a side arm. This nitrogen flowed through the balance case and down the reactor stem. The flow rate, at constant pressure indicated by a mercury manometer, was measured on a rotameter calibrated with a soap bubble-meter. The nitrogen flow was adjusted with a fine control needle valve to balance

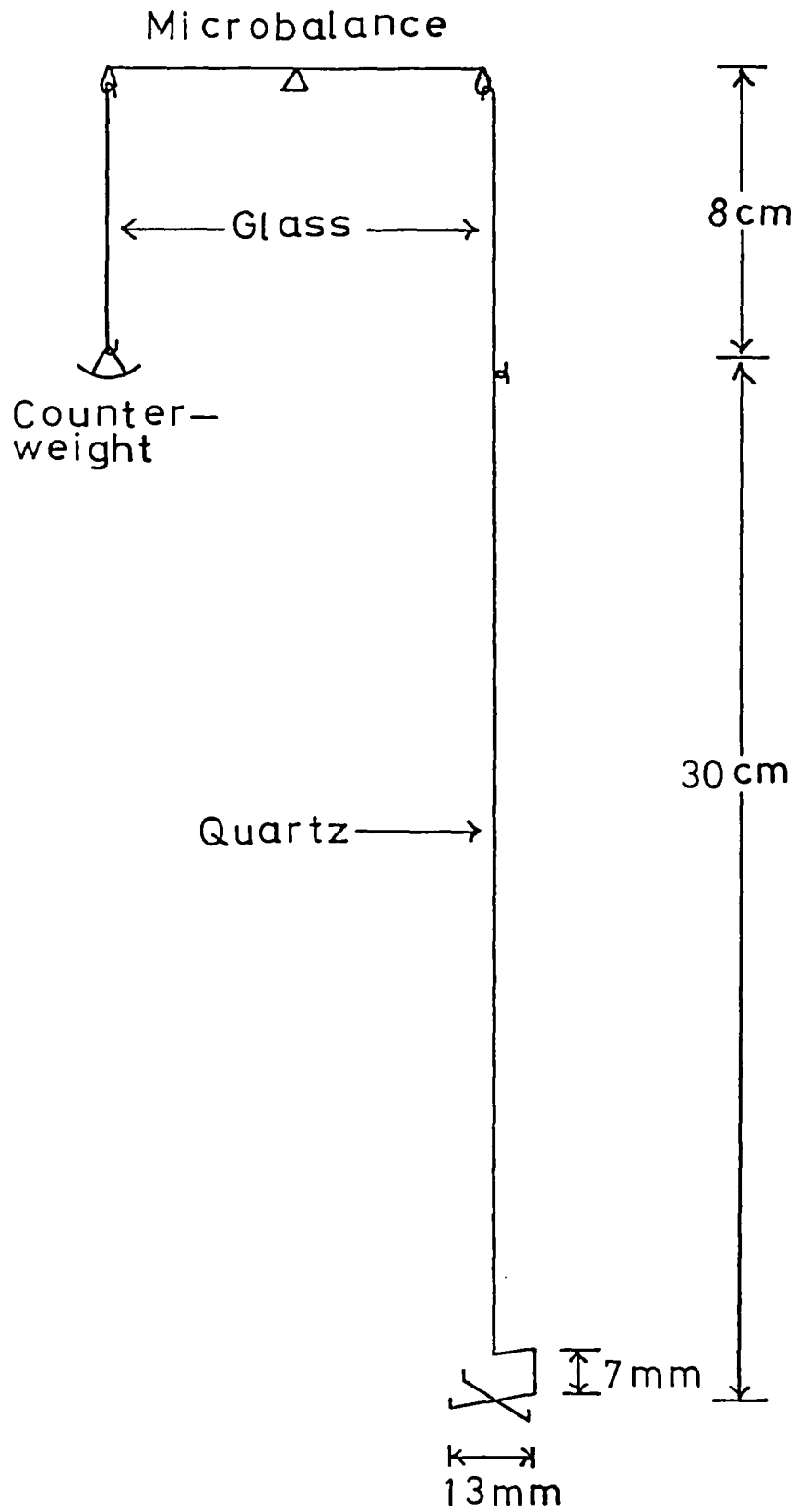


Fig. 2. 7. Sample suspension system

the upward flow of the product gases in the reactor stem. The nitrogen flow was then increased slightly so that all the product gases passed through the reactor outlet, (with the nitrogen), none entering the reactor stem.

The balance head was insulated from the heat of the furnace by lagging the outside of the glass case with Kaowool bulk insulating fibre. This lagging also served to insulate the photocells in the balance head from the variable level of luminosity in the room.

2.3. Analysis of Gases

The sample of product gases injected by the gas sample valve into the gas chromatograph, includes species not detected by the flame ionisation detector (F. I. D.), or not eluted by the column. i. e.

- a) Nitrogen
- b) Hydrocarbons heavier than C_3
- c) Hydrogen

a) Nitrogen

This is a constant flowing purge from the microbalance case, the flow rate of which is measured.

b) Heavy hydrocarbons have been analysed using a temperature programmed chromatograph.

c) Hydrogen

This is not detected by an F. I. D. , but an indication of the amount is obtained by measuring the reactor outlet flow rate and deducting the nitrogen contribution. This volume expansion of product hydrocarbons, derived from a known flow rate of propane, is rationalised to a volume of propane by applying the chromatographic response factors. The difference in integrator counts obtained is due to the hydrogen and the hydrocarbons heavier than C_3 .

Samples of the reactor outlet gas stream were analysed

with a katharometer to determine the nitrogen and hydrogen concentrations. The results of the measured hydrogen concentration were in good agreement with the values obtained by the difference method. However, it was considered advisable to be able to measure the hydrogen concentration directly, so a microkatharometer was installed.

2. 3. 1. Flame Ionisation Detector Chromatograph

A Pye 104 series flame ionisation detector (F. I. D.) and amplifier was used for the measurement of the hydrocarbon products. The F. I. D. detector was used because of its high sensitivity and stability. The gas sample was injected onto the column using a Pye 104 series gas sample valve fitted with a 1 ml. sample loop. An 8ft. x $\frac{1}{8}$ in. stainless steel column was packed with activated alumina type H, 100 - 120 mesh (Perkin-Elmer). The separation was made isothermally at 115⁰ C using nitrogen as the carrier gas at a flow rate of 18 mls/min. The response signal from the eluted components was recorded on a Vitatron linear integrating recorder.

The product gases from the reactor were found to contain a small percentage of polyaromatic compounds, referred to as tars. These blocked the gas ports of the gas sample valve, and attempts to remove the tars from the product stream were unsuccessful. A cotton-wool fitter quickly became saturated and blocked the product stream and a water-cooled condenser failed to condense the tars. However, a glass trap cooled to solid carbon dioxide temperature did condense most of the tars, but this was unsuitable as propane and propylene, gases which were required to be analysed, were also partially condensed. To avoid this problem, a heated by-pass system to the gas sampling valve was constructed. The product stream from the reactor was passed through a glass "T"-piece and through the by-pass tube, to a waste disposal line to be burnt in the flame of a bunsen burner. When it was required to take a gas sample through the gas sample valve, the product stream was diverted down the

other arm of the "T"-piece. The product stream passing through the sample valve was re-combined into the by-pass tube and hence to the waste disposal line. The product stream was diverted to the sample valve by partially closing a grease-free tap (Youngs) on the by-pass line. The by-pass system and gas sample valve were heated at 170°C with two heating cables controlled by variacs (Gallenkamp). Chromel/alumel thermocouples were constructed and positioned at various points to monitor the temperature. The temperature stability was very good and did not vary by more than 10°C from the 170°C set temperature at any point of the by-pass line and gas sample valve. No blocking of the gas sample valve ports was experienced with this heated system.

The ratios of the F. I. D. detector flame gases, hydrogen and air, were adjusted and set to give the maximum sensitivity to the eluted hydrocarbons. The hydrocarbons detected by the chromatograph were methane, ethane, ethylene, propane, propylene and acetylene. The linearity of response for each hydrocarbon was checked and found to be good over the range of sample injections used. Known mixtures of each of the hydrocarbons in turn were made using propane as a diluent. This was done by using the gas inlet board, and the mixture was introduced into the chromatograph using the gas sampling valve. Response factors for the hydrocarbons, relative to propane, were determined and compared to the theoretical factors. Good agreement was found. The response factors are listed in Table 2.1. A standard hydrocarbon gas mixture (British Oxygen Company) was analysed, using the determined response factors and found to give good agreement with the specified composition.

A by-pass line from the reactor and microbalance head gas inlets was connected to the F. I. D. gas sampling system. This enabled the measurement of the propane composition in the propane and nitrogen mixture, by reference to the response obtained from pure propane. Hence, allowance for the nitrogen component in the gas product stream could be made and the hydrocarbon products related to the response obtained from an equivalent volume of propane.

A soap bubble-meter was connected to a by-pass line,

Table 2.1. Hydrocarbon Response Factors (F.I.D.)

Hydrocarbon	Theoretical response factors for rationalising to propane ref. (98).	Determined response factors
Methane	3.01	3.36
Ethane	1.50	1.60
Ethylene	1.50	1.50
Propane	1.00	1.00
Propylene	1.00	0.95

The theoretical response factors were applied to the gas chromatography results.

just prior to the gas product stream burner. This enabled the measurement of the gas product flow rate.

2. 3. 2. Microkatharometer Detector Chromatograph

Initial results indicated that it was desirable to measure the hydrogen concentration in the gas product stream. An indication of this was obtained from the mass balance "remainder" value of the hydrocarbons detected by the F.I.D. Subsequently, a micro-katharometer detector gas chromatograph was assembled and used to measure the production of hydrogen and, in later experiments, of methane. A Taylor-Servomex microkatharometer MK 158 was used. It was not installed on-line, thus ensuring that no disruption of the existing on-line microbalance and F.I.D. occurred. 1 ml. samples of the product gas stream were taken from an injection port on the gas delivery line to the burner. Separation of the product hydrogen from the nitrogen purging through the microbalance case was made using a stainless steel column, 2 metres x $\frac{1}{4}$ in. O.D. , packed with silica gel, 80 - 100 mesh (Perkin-Elmer). The separation was made isothermally at room temperature using argon as the carrier gas at a flow rate of 19 mls/min. Argon was used to avoid the peak inversions of eluted hydrogen, which occur in the helium carrier gas system. The katharometer was controlled with a Solartron power supply unit at 3.5 volts and 0.2 amps. The signal from the katharometer was attenuated using a unit built by the Electronics Workshop of Imperial College, and recorded on the Vitatron linear integrating recorder. A switch was installed to permit either the signal from the F.I.D. or the katharometer to be recorded.

The katharometer was calibrated for hydrogen and nitrogen and found to give a linear response over the concentration range occurring in the propane pyrolysis. During later experimental determinations, it was found possible to measure the methane component in the product gases, using the katharometer. Calibration for methane also gave a linear response over the required range.

2.4. Analysis of Liquids

The aromatic and polyaromatic compounds formed from propane pyrolysis, are referred to as tars. The rate of tar production was measured by trapping the tars present in the reactor outlet gas stream and weighing the trap. The trapped tars were dissolved in chloroform and analysed using a Pye G. C. D. temperature programmable F. I. D. chromatograph. The components of the tar solution were separated on a 2.5 metre glass column of internal diameter 2 mm. , packed with 3% OV - 1 on Gas Chrom Q, 80 - 100 mesh (Phase Separations). A second column was used as a reference column when temperature programming. The detector was heated to 320°C and the injector to 350°C. The oven initial temperature on injection of the sample was 40°C, which was held for 2 mins. The temperature was then increased at a rate of 8°C/min. to 300°C. The response from the amplifier was recorded on a Vitatron linear integrating recorder. A solution of known aromatic and polyaromatic compounds was analysed under the same conditions, for comparison with the tar sample.

2.5. Analysis of Solids

A nickel disc and the associated deposit obtained from an experiment with 1% hydrogen sulphide (v/v) in the propane feed, were analysed : the disc by electron probe micro-analysis and the deposit by spark source mass spectroscopy. Iron and stainless steel foil liners and the associated deposits obtained from propane pyrolysis, were analysed : the metal liners by metallography and the deposits by X-ray diffraction. The samples were analysed by the Analytical Services Laboratory of Imperial College.

2.5.1. Electron Probe Micro-Analysis (EPMA).

When a beam of monoenergetic electrons is directed onto a target element they are slowed down, the energy loss resulting in

the production of primary X-rays, whose energy spectrum is continuous and possesses only one maximum. The electron's primary X-rays can also knock out inner shell electrons and the resulting spectrum is superimposed on the continuous one. The intensity of the emission spectrum is so great that if a beam of electrons is collimated to a cross-sectional area of $1\mu\text{m}$ and directed at a sample, characteristic X-rays are emitted and as little as 10^{-14} g. of an element can be detected with an accuracy of 1 - 2%. The beam only penetrates to a depth of 1 - $2\mu\text{m}$ so the element must be present at a level of about 1%. Generally it is a disadvantage to have an analysis of a small area of the surface because it is unrepresentative of the whole. However, for this reason, the technique has become of great importance in the study of solids where variations in the nature of the surface are of the utmost importance i. e. catalysis, ceramics, metals. It is possible to show the presence of inclusions, and the examination of a cross-section reveals concentration gradients of elements in a sample.

The carbon deposited nickel foil and a portion of unused nickel foil as a control, were mounted edge-ways in plastic and ground and polished. They were carbon coated for probe examination. Photographs of the back-scattered electron image (BEI) were taken of the control and used foils, to show the surface disruption that had occurred on the used foil. X-ray photographs were taken to show the nickel and sulphur distributions in the used foil.

2. 5. 2. Spark Source Mass Spectroscopy (SSMS)

With a spark source mass spectrometer, inorganic impurities can be quantitatively determined in graphite, alloys, semi-conductors and similar materials without prior separation and without interference from the bulk of the material or matrix. Ionization is achieved by a vacuum spark, this having approximately the same ionization efficiency for all elements. The intensity of the response for a given element is proportional to its concentration, when the natural isotopic abundance pattern is taken into account.

The limits of detection are in the range 0.001 - 0.1 ppm. After ionization the ions are separated according to their masses by a magnetic field. Ions that pass through the exit slit impinge on a photographic plate.

Portions of the deposits were taken and mixed with spectroscopic grade graphite and pressed into rods for sparking. The sample rods were sparked and mass spectra (range $M = 7 - 250$) were taken, starting from a 30 nC (nano coulomb) exposure, then 10 - 3 - 2 - 1 0.0003 - 0.0001 nC. A blank of pure graphite was run under similar conditions. After development, the plates were examined and the elements found estimated for the quantity present by assuming that "just visible" at 1 nC is equivalent to 1 ppma (parts per million atomic, i. e. number of atoms in 1 million atoms), for a pure (100%) isotope. Factors were applied to allow for the dilution of the sample and for the isotopic proportions. The nano coulomb (nC) is the unit of charge of the spark.

2.5.3. Metallography and Microscopic Examination

The foil samples were cut and mounted in plastic to enable examination of the foil edge, then ground and polished. The samples were then etched to distinguish the metallic phases present.

(i) Irons. These were etched in 2 - 3% nitric acid in ethanol (nital) for 15 - 20 secs. , then examined, carbon coated and checked on the micro-probe and finally re-polished and etched in boiling alkaline picrate and re-examined.

(ii) Stainless steel. This was not attacked by nital and so was etched in 10% hydrochloric acid in ethanol. After carbon coating and micro-probe examination this was also re-polished and then etched in alkaline ferricyanide (Murakami's reagent) and re-examined.

Control samples from unused iron and stainless steel foil sheets were prepared and examined using the same techniques as for the carbon deposited foils.

2.5.4. X-ray Diffraction

The wavelengths of X-rays are of the same order of magnitude as interatomic distances in crystals and are thus diffracted by crystals. Diffractions occur in accordance with Braggs' Law, which relates the wavelength of the incident radiation, the interatomic spacing in each plane, and the angle of diffraction. In the powder diffraction technique, the powdered sample is placed in the centre of a circle of photographic film and irradiated with a beam of monochromatic X-rays. The diffracted beam comes out of the sample in the directions allowed by Braggs' Law and darkens the film giving a pattern of lines which are characteristic of the crystalline phases present in the sample. Comprehensive reference files of the diffraction patterns of many materials are available so that the method can be used for qualitative identification.

Samples of the carbon deposits were removed from the foils and examined using the powder diffraction technique with copper radiation and a nickel filter.

2.6. Procedure

The reactor outlet system allowed either the gaseous or the liquid products from the propane pyrolysis to be analysed. The gaseous products were analysed using the F.I.D. and the microkatharometer gas chromatographs. The liquid products were trapped and then dissolved in chloroform and analysed using the temperature programmable gas chromatograph. Typical experimental procedures are described below.

2.6.1. Carbon Deposition Measurements and the Analysis of Gases

The product gases were analysed simultaneously with the measurement of the rate of carbon deposition.

The disc to be used for the measurement of the rate of carbon deposition was positioned on the suspension cradle and hung from the sample arm of the microbalance at the position relative to

the jet which was found to give no interference with the mixing of the gases inside the reactor. The surface area of the silica discs (Heraeus Quartz Fused Products) was 2.64 sq. cms. The surface area of the metal foil discs (Goodfellow Metals) was 2.2 sq. cms. The specifications of the polycrystalline foil sheets, from which the discs were cut, are listed in Table 2.2. The sides and base of the reactor were lined with metal foil. These liners were also cut from the foil sheets. The area of the liner surface exposed to the reactant gases was 58sq. cms. The reactor socket was clamped to the microbalance head glass case and nitrogen, at a flow rate of 250 mls. /min. , was purged through the balance head case, down the reactor stem to the reactor outlet. This flow was maintained throughout the propane pyrolysis to prevent product gases from entering the microbalance head case and damaging the balance mechanism. The weight indicated by the microbalance was susceptible to any fluctuations in the nitrogen flow. Hence, it was critical to keep the nitrogen purge at a constant flow rate.

The reactor was heated to temperature whilst nitrogen purged through the microbalance case and helium through the reactor jet. When the furnace temperature was steady, the disc was reduced in hydrogen.

Measurements of the rate of carbon deposition at various inlet residence times were made using two experimental methods.

- a) Deposition when the inlet residence time is increased from 2.0 secs. to 7.5 secs.
- b) Deposition when the inlet residence time is decreased from 7.5 secs. to 2.0 secs. , followed by deposition at 2.0 secs. at various temperatures.

Measurements were also made at 2.0 secs. inlet residence time at various temperatures, without previously depositing carbon at longer residence times.

The hydrocarbon components of the product gas stream were analysed using the on-line F.I.D. The hydrogen component was analysed using the microkatharometer. It was also possible to analyse for methane using the microkatharometer. Hence, the

Table 2.2. Specifications of the Metal Foils

Metal	Purity %	Thickness (mm)
Copper	99.9%	0.125 mm
Nickel	99.0%	0.125 mm
Iron	99.0%	0.125 mm
Stainless Steel	Grade EN58E Cr 17 - 19% Ni 9 - 11% C <0.07%	0.125 mm

facility to analyse for methane using both the F. I. D. and the microkatharometer, gave a direct correlation between the results of the two techniques.

The microbalance was sensitive to the pressure change caused by operating the Pye gas sampling valve to inject a sample onto the column. However, as soon as this process was completed, the microbalance returned to the correct reading and hence, this interruption was of no consequence.

After the experimental measurements were completed, the reactor was flushed with helium and the carbon deposits burnt off by passing compressed air into the reactor. However, if the disc or liner were to be analysed, the reactor was cooled over-night whilst passing helium through the jet and nitrogen through the microbalance head case. The liner and disc were removed from the cold reactor the following morning.

2.6.2. Analysis of Aromatic and Polyaromatic Compounds

A glass trap was loosely packed with glass wool and weighed together with the short length of delivery line from the reactor. The delivery line was connected to the reactor outlet with a Quickfit S 13 cup-joint. The trap was cooled in liquid nitrogen and the propane pyrolysis started. The product gases were passed into the trap. After 30 mins. an appreciable deposit was observed in the inlet tube to the trap and the trap itself. No tars were observed after the trap. The liquid nitrogen dewar flask was removed and the trap was very slowly warmed whilst passing helium through to remove those hydrocarbons which are gases at room temperature. The trap and delivery tube from the reactor outlet were weighed and the deposition rate of tars calculated. The trapped tars were dissolved in chloroform and analysed using a Pye G. C. D. temperature programmable F. I. D. chromatograph.

2.7. The molecular beam mass spectrometer system

Analysis of the gas phase species present in the pyrolysis of hydrocarbons was made using the nozzle source molecular beam mass spectrometer system designed and constructed by Tristram (99). This system was capable of sampling reactive systems up to pressures of 500 torr. The existing quadrupole mass spectrometer was replaced with a quadrupole mass spectrometer capable of much greater sensitivity and stability in operation. Additional components were added to the existing vacuum equipment and the whole was re-wired in a series of safety circuits permitting continuous pumping and fail-safe shut-down. A quartz jet-stirred reactor was made and positioned so that the nozzle sampled the gaseous species generated in the pyrolysis of propane. The design of the apparatus may be considered in four parts: the reactor, the molecular beam system, the mass spectrometer detector and the subsequent signal processing.

2.7.1. The reactor

The reactor of 80 cm.³ volume was constructed from quartz components supplied by Heraeus Quartz Fused Products, and is shown in Fig. 2.8. The jets of 0.6 mm. bore have a smooth continuous taper. The reactor was designed to give uniformity of temperature and composition inside the reactor. The jet assembly inlet was constructed from capillary tubing to limit pre-decomposition of the reactant gas. The inlet gases were introduced through a glass tap connected to a B10 socket which fits onto the reactor inlet B10 cone. The outlet gas stream passed through a glass tube starting with a B10 socket which fits onto the reactor outlet and a double oblique glass tap: one arm to vent to the atmosphere, the other arm to connect to the reactor pump vacuum line. Measurement of the reactor pressure was made using a capsule dial gauge, 760-0 torr (Edwards) which was connected across the reactor vacuum

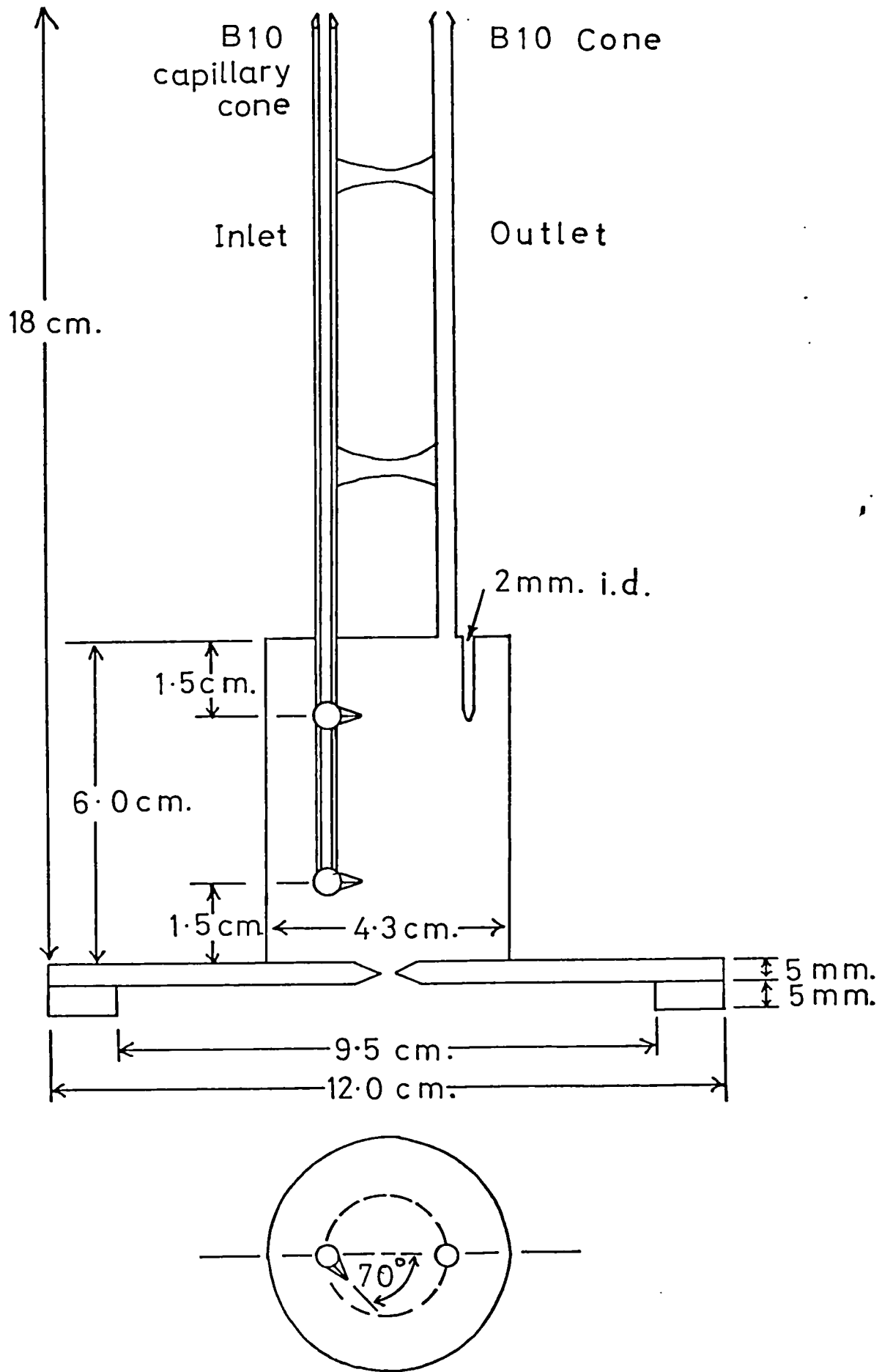


Fig. 2.8. The mass spectrometer reactor

line. The calibration of the capsule dial gauge was checked with a mercury manometer and found to be correct. The base-plate of the reactor was recessed on each side so that the nozzle cone protruded by 1-2 mm. into the reactor. This ensured that the sampling point was inside the reactor. A vacuum seal was maintained between the reactor and the nozzle flange with a Viton "O" ring, held in place with a stainless steel ring, the internal surface of which located over screw heads of the nozzle-skimmer assembly. This prevented the "O" ring being distorted when the reactor was pumped to draw the reactor down onto the "O" ring. The reactor was clamped to the nozzle flange with eight screw clamps having feet cut from a $\frac{1}{2}$ " diameter P. T. F. E. rod. The clamps screwed into tapped holes in the nozzle flange and the feet were screwed down onto the reactor to hold it down on the "O" ring.

In use, the jet-stirred reactor was first clamped to the nozzle flange. Gases were supplied to the reactor as described in section 2.2.3. The reactor was heated with a furnace of 35 ohms resistance constructed from a ceramic tube (Anderman and Co.) of dimensions i.d. 6.5 cm. and o.d. 7.5 cm. and length 10 cm., heated by Nichrome 5 wire (British Driver Harris Co. Ltd.), insulated with Kaowool (Morgan Ceramic Fibres Ltd.) and asbestos rope. The heating wire was held in place with alumina cement. The furnace was heated and controlled at temperature as described in section 2.2.2. The controlling thermocouple was positioned outside of the reactor, midway between the two jets. The furnace tube ends were insulated against heat loss with Kaowool bulk fibre. The reactor was heated to temperature whilst nitrogen passed through the jets. When the furnace temperature was steady, the reactant gas mixture was introduced.

2.7.2. The molecular beam system

The two major design considerations for the construction of the nozzle beam system are the selection of the vacuum pumps and the nozzle-skimmer configuration. The design of the system which Tristram (99) showed was capable of sampling reactive transient species is outlined, followed by a description of the modifications made to the vacuum system to permit continuous pumping and fail-safe shut-down.

2.7.2.a. The nozzle beam system

The basic design of the system is shown schematically in Fig. 2.9. and a detailed drawing in Fig. 2.10. The sampling nozzle, a 90° converging cone, was constructed in stainless steel, Fig. 2.11. The cone has an orifice of 0.25 mm. diameter, permitting sampling of systems in the pressure range 5-500 torr. The angle of the cone is a compromise between the necessity to minimise interference of the cone with the flowing gas on the sample side, and the opposing requirement for maximising the pumping speed on the low vacuum side. The inside angle must be as large as possible to maximise the pumping speed behind the orifice. A vacuum seal between the cone and the nozzle-skimmer assembly was made with a P. T. F. E. "O" ring.

The skimmer, a 55° converging cone, was constructed in brass, Fig. 2.12. The skimmer has an orifice of 0.25 mm. diameter. Earlier attempts to construct the skimmer from stainless steel were unsuccessful since a sharp lip to the orifice could not be produced. Hence, the skimmer was made from brass, a material more suited to the machining techniques available. The outside cone angle was 55° and the inside angle 45° . This ensured that the shock became attached to the skimmer lip and did not "stand off" as a detached bow shockwave. A vacuum seal between the skimmer and its base plate was made with a P. T. F. E. "O" ring.

The nozzle and skimmer, the two beam forming elements,

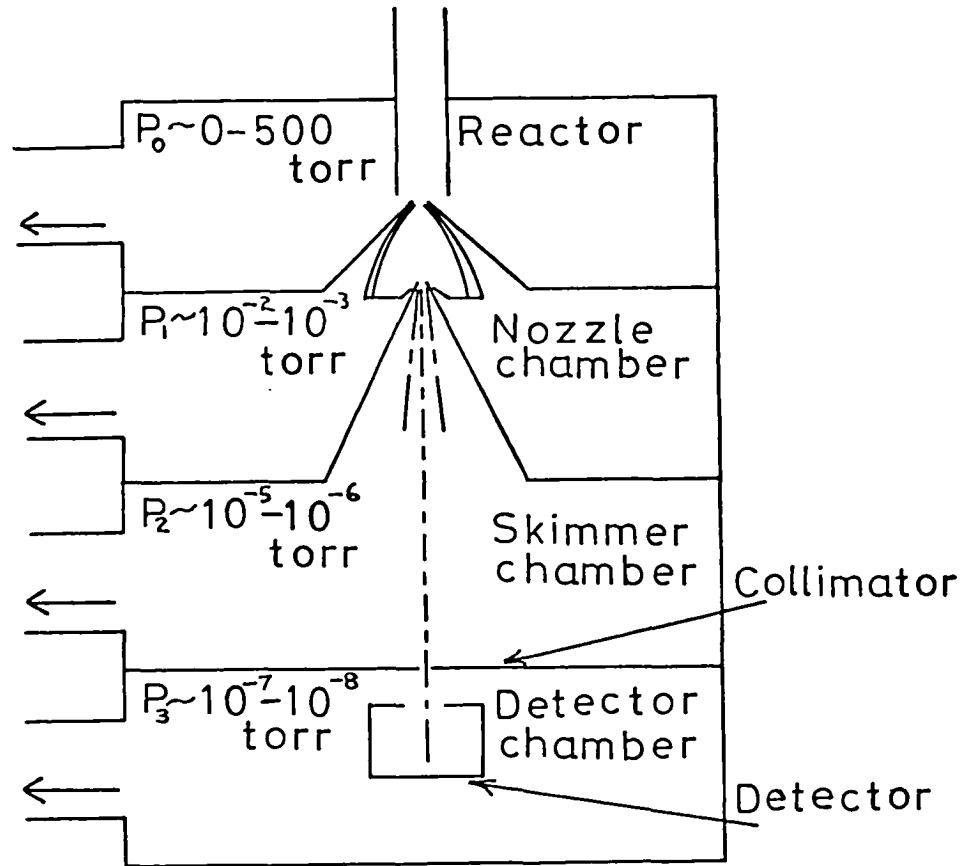


Fig. 2.9. Nozzle source molecular beam apparatus: schematic

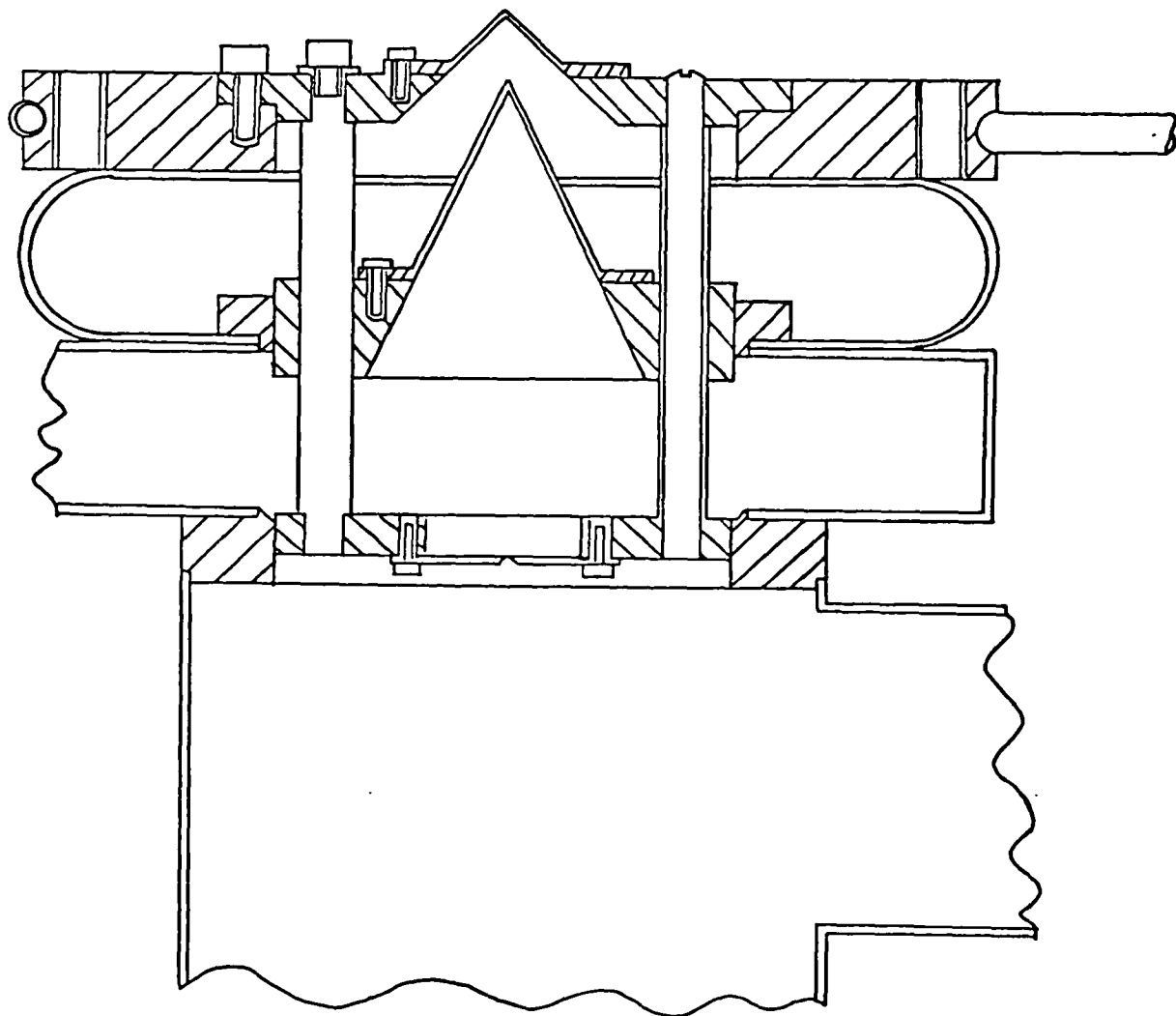


Fig. 2.10. Nozzle source molecular beam apparatus:
section

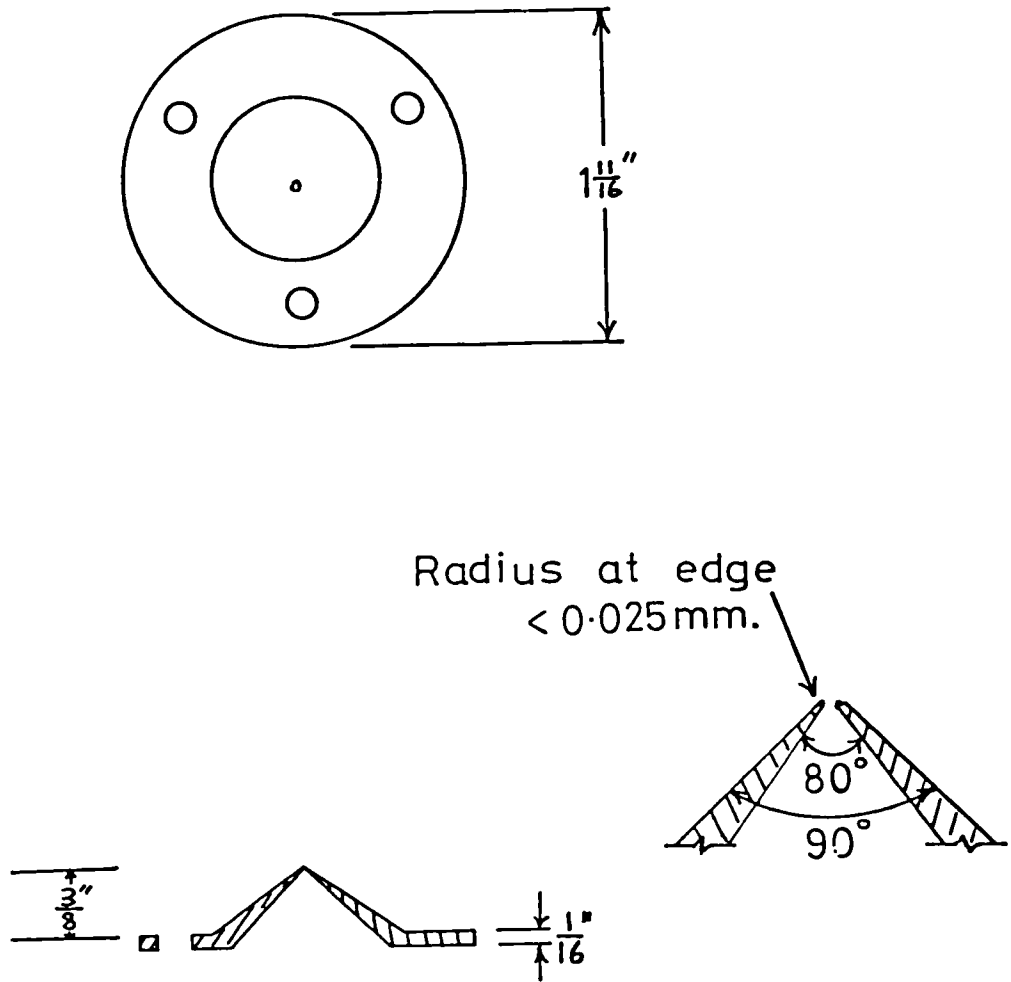


Fig. 2.11. The sampling nozzle

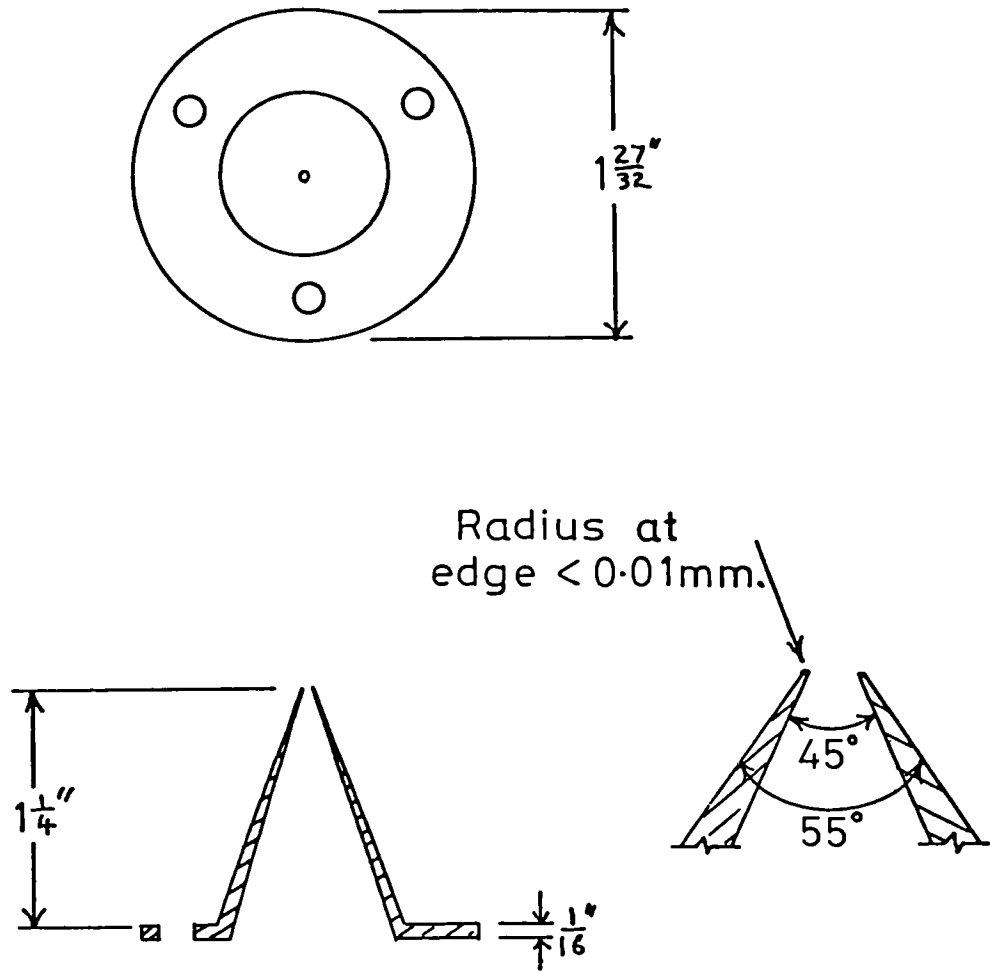


Fig. 2.12. The skimmer

were mounted in the nozzle-skimmer assembly, Fig. 2.13. The nozzle-skimmer assembly and the main vacuum chamber were constructed in stainless steel. This assembly can be completely removed from the mounting flange, permitting accurate adjustment of the nozzle-skimmer separation and exact alignment of the two orifices using an optical bench and a small neon laser, Fig. 2.14. Tristram (99) used a nozzle-skimmer separation of $\omega^c/d_o = 100$ where d_o is the diameter of the sampling orifice (0.25 mm.) and ω^c is the nozzle-skimmer separation (25 mm.). The alignment is probably not critical for the extraction of a working beam, but when sampling reactive systems it is necessary to skim from that point of the free jet expansion that has least boundary layer contamination, namely the portion nearest the centre. The source conditions conducive to the sampling of reactive species, namely continuum flow through the nozzle, result in the gas expanding into the region of the low pressure side of the nozzle in the form of a free jet. As the gas expands through the orifice, axial collisions effectively cease. The flow behind the nozzle is isentropic and supersonic and the central portion of the expansion is unaffected by wall reactions in the nozzle.

The central portion of the expansion is transferred to the ion source of the mass spectrometer by inserting a skimmer into the gas stream. A collision free beam is extracted without loss of any reactive species present. An object immersed in a supersonic gas stream causes shock formation in the gas. The position of this shock in relation to the skimmer apex influences the flow through the skimmer orifice and hence the beam intensity. At small values of the nozzle-skimmer separation, the gas is still in the continuum regime and the skimmer swallows the shock, resulting in a large molecular flux through the skimmer orifice. At larger values of the nozzle-skimmer separation, the density has decreased and the skimmer can no longer swallow the shock. The beam intensity is reduced due to the formation of a bow shock wave in front of the skimmer. Under these conditions, the skimmer is sampling from a gas in post-shock conditions where the gas

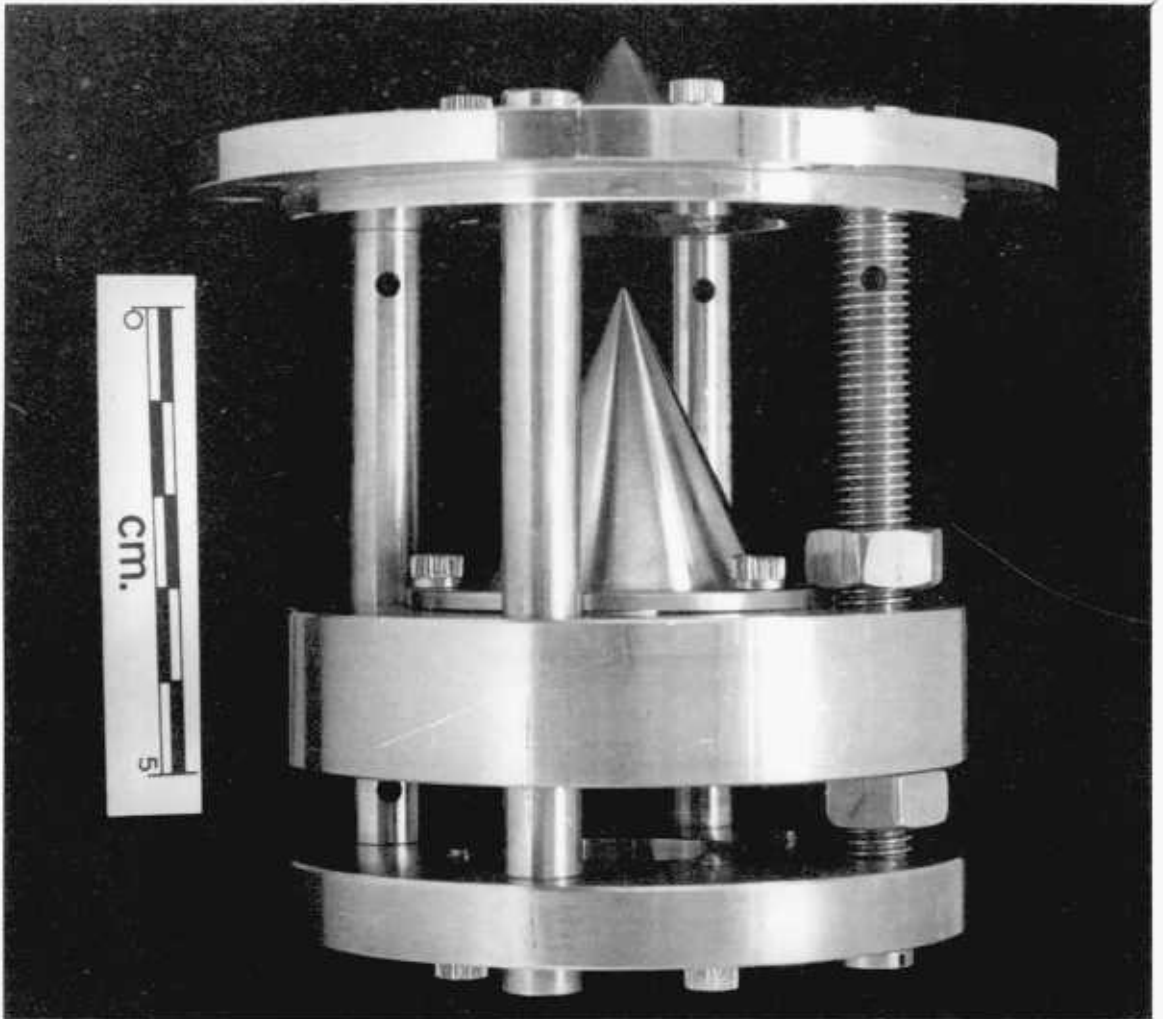


Fig. 2.13. The nozzle-skimmer assembly.

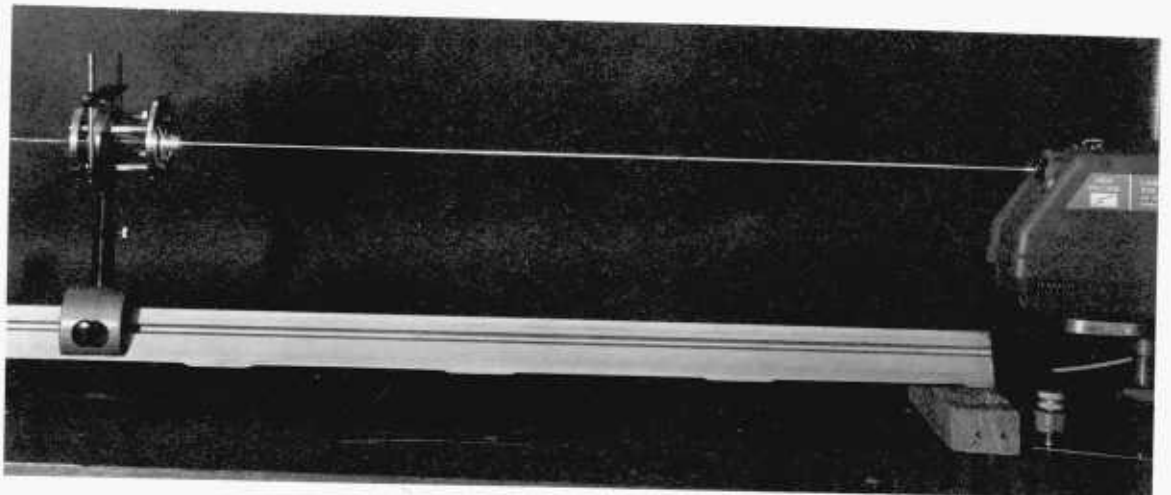


Fig. 2.14. Nozzle-skimmer alignment.

molecules have undergone many collisions. This loss by intermolecular reactions must be avoided when sampling reactive species. As the nozzle-skimmer separation is increased further, the beam intensity reaches a maximum, corresponding to minimum skimmer interference and optimum beam formation. The shock becomes attached to the skimmer and the central portion of the expansion passes through the skimmer without experiencing shock conditions. This is the optimum condition for sampling and detecting reactive species. Further increases in the nozzle-skimmer separation cause a reduction in the beam intensity due to the decreasing density of the nozzle expansion. The skimmer can only function correctly when the shock becomes attached to the skimmer lip. This places constraints on the shape of the cone. The lip radius must be small (≤ 0.01 mm.) and the external angle 60° or less, to avoid the formation of a detached shock.

2.7.2. b. The vacuum system

The rotary and diffusion pumps used in the system had pumping speeds sufficient to produce a free jet expansion of the reactive gaseous species. The pressures obtained in each stage are shown in Fig. 2.9. The reactor was pumped with an Edwards ES 50 rotary pump and the gas flow through the pump controlled with an Edwards $\frac{1}{2}$ " valve. The pressure in the reactor was measured with a capsule gauge. The nozzle chamber was pumped with an Edwards 9B4 vapour booster pump backed by an Edwards ISC 450B rotary pump. The vapour booster pump was connected to the first stage of the molecular beam by a stainless steel manifold. The pumping speed delivered to the nozzle chamber could be controlled by a six inch butterfly valve.

The second stage pump, an Edwards EO6 oil diffusion pump, was connected to the skimmer chamber by a stainless steel manifold and six inch butterfly valve and was backed by an Edwards ES 330 rotary pump. The final stage pump, an Edwards EO4 oil

diffusion pump was separated from the detector chamber by a pneumatically operated four inch butterfly valve and was backed by an Edwards ES150 rotary pump. This system allowed all the pumps to be independently isolated and is shown in Fig. 2.15. The backing pressure of each diffusion pump was measured by Edwards Pirani gauges. High vacuum measurements were made by two Mullard ionisation gauges, one situated in the skimmer chamber, the other in the detector chamber. The pressure of the detector chamber was also monitored with an Edwards Penning gauge.

Although some safety features had been incorporated by Tristram (99), these were insufficient to permit continuous pumping or to produce fail-safe shut-down. Additional valves and relay systems were incorporated and the whole apparatus was re-wired in a series of safety circuits, shown in Appendices 1.1., 1.2., 1.3. Each of the pumping stages was protected against a rotary pump failure by using a rotary pump rotation detector (Imperial College Electronics Services) coupled to a magnetic valve (Edwards) and a solenoid operated air admittance valve (Edwards). Failure of a rotary pump would result in the closure of the magnetic valve between the diffusion pump and the rotary pump, the admittance of air to the rotary pump and the switching off of the diffusion pump heater. Each of the cooling water lines to the diffusion pumps were protected by thermal sensors which disconnected the heaters of the diffusion pumps if the temperature of the cooling water rose above the recommended temperature.

A safety circuit, operated by an over-pressure trip on the ionisation gauge in the detector chamber, was used to switch off the quadrupole mass spectrometer if the pressure in the detector chamber rose above a pre-set value. The four inch pneumatically operated butterfly valve separating the EO4 diffusion pump and the mass spectrometer and the thermo-electric (Peltier) water-cooled baffle above the EO4 diffusion pump, were also connected to this trip: the valve to close and the power to the baffle to be disconnected. The magnetic valves and rotary pumps were controlled by latching relays.

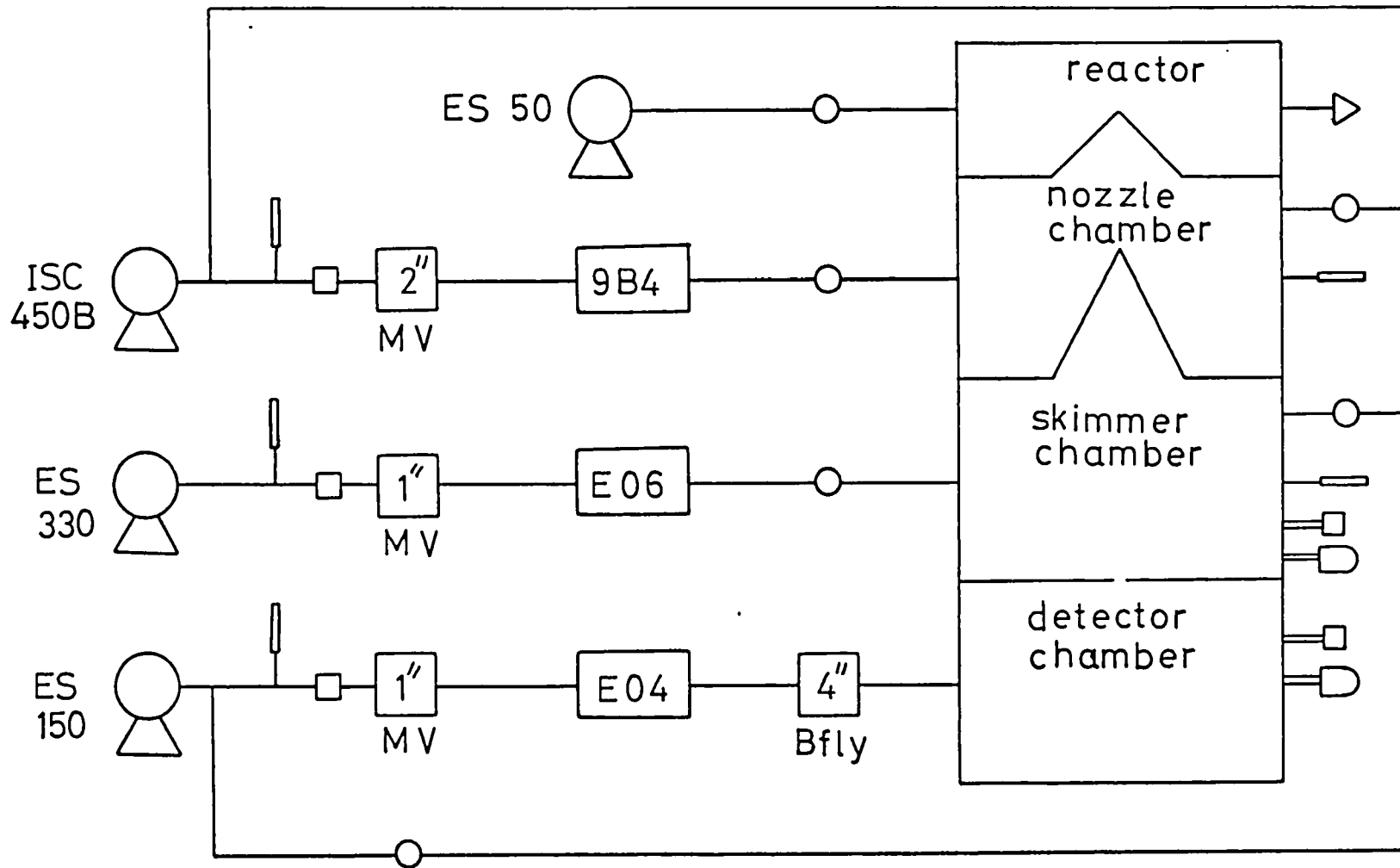
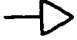







Fig. 2.15. The vacuum system

Key to Fig. 2.15.The vacuum system

	Capsule dial gauge
	Pirani gauge
	Penning gauge
	Ionisation gauge
	Manual valve
	Air admittance valve
MV	Magnetic valve
Bfly	Butterfly valve.

Hence, if the power supply was discontinued and later re-connected, the apparatus would fail-safe and not re-start. The rotary pump relays were also coupled to the diffusion pump heaters so preventing heating of the diffusion pump oil when the rotary pump was not pumping.

A vacuum chamber to accommodate the new mass spectrometer was supplied by Spectrum Scientific Ltd. A foreline trap (Edwards) was incorporated between the EO4 diffusion pump and the rotary backing pump to prevent rotary pump oil vapour passing into the detector chamber.

2.7.3. The mass spectrometer

A mass spectrometer consists of three basic units : an ion source, a mass analyser and an ion detector, all of which operate in a vacuum of 10^{-6} - 10^{-8} torr. Ions, produced in the ion source, usually by electron impact, are transmitted into the mass analyser where they are separated according to their mass to charge ratio. The quadrupole mass filter consists of four rods, located in a square array and held accurately in position to keep them mutually parallel. When a pure radio frequency signal is applied to spatially opposite rods, so that one pair is 180° out of phase with the other pair, ions injected into the centre of the structure are transmitted to the other end. Mass selection is possible by the application of suitable d. c. voltages to the rod pairs. Ions of a given mass to charge ratio are transmitted through the mass filter axially, whilst ions of different mass to charge ratios are placed on unstable orbits and are lost by striking one of the rods. A continuous mass scan is obtained by ramping the d. c. voltages and controlling the r. f. amplitude. The mass resolution of a quadrupole analyser is variable and the separation between adjacent peaks at the high mass end of the scale is the same as that in the low mass region. After the mass filter, the ions pass into an electron multiplier, in which the ion current is amplified about 10^5 times and converted into an output voltage for display on an oscilloscope or chart recorder.

Ionisation of the gas stream is carried out by accelerating the electrons emitted from a heated filament to about 70 eV. At this high energy, the target molecule is fragmented into a number of ions, which give a compound its characteristic cracking pattern. The cracking patterns of hydrocarbons at 70 eV contain peaks at mass to charge ratios corresponding to hydrocarbon radicals. Consequently, the signal due to the radical is swamped. However, radicals may be selectively detected by operating the ion source at a sufficiently low electron energy at which the electrons do not cause dissociative ionisation. The ionisation potentials for hydrocarbon radicals are less than the appearance potentials for the interfering ions. This selectivity may only be achieved at the expense of sensitivity.

The mass spectrometer used by Tristram (99) was a Finnigan Miniquad 200 quadrupole. This was chosen as a medium performance low cost instrument, capable of analysing ions up to a mass to charge ratio of 200. However, the ion source was not designed for molecular beam detection. The filament wire was spot welded onto two metal supports. Consequently, there was no provision for accommodating the thermal expansion of the wire that occurred under normal operating conditions. As a result of this thermal expansion, the filament became bent and moved away from the optimum position for ionising the beam molecules. Each time the filament was switched on, it tended to move to a different position.

The free radical concentrations generated by Tristram (99), using a microwave discharge in hydrocarbons, were estimated as being about 10^3 greater than those which are likely to be present in the pyrolysis of hydrocarbons. The sensitivity of the Finnigan instrument is insufficient to detect free radical concentrations at this lower level. Because of this insufficient sensitivity and the unsuitable ion source, the Finnigan instrument was replaced by an Extranuclear Laboratories quadrupole, supplied by Spectrum Scientific Ltd.

The various units of this modular quadrupole system

were chosen to meet the performance necessary for the detection of free radicals present in the pyrolysis of hydrocarbons. The molecular beam model axial ionizer is designed specifically for ionizing, with the highest efficiency, molecular beams. The beam enters on the geometrical axis of the ionizer and quadrupole. While in the ionizing region, the beam passes along the axis of a cylindrical grid which accelerates electrons towards the axis from four filaments which form a square surrounding the grid. The molecular beam ionizer is very precisely aligned to the axis of the quadrupole, causing minimum interference with the beam passage and allowing high efficiency of ionization and ion extraction. The quadrupole mass filter is a precision-made assembly consisting of four parallel rods of circular cross-section, housed in a solidly constructed outer case. The choice of a quadrupole mass filter depends on three constraints:

- (i) Increasing the pole diameter increases the sensitivity by the square of the pole diameter.
- (ii) Decreasing the pole diameter increases the mass range, for a given radio frequency of operation used to drive the mass filter.
- (iii) Increasing the pole length increases the resolution and the capability of handling ions of higher energies.

In most applications, optimal performance (resolution and sensitivity) is achieved with the quadrupole having the largest pole diameter and the highest operating frequency, consistent with the mass range to be covered. A quadrupole mass filter having poles of diameter 1.90 cm. and length 22 cm. and two radio frequency heads of frequencies 3.0 MHz and 1.5 MHz were chosen. The head of 3.0 MHz gives the maximum possible sensitivity up to 60 atomic mass units (a. m. u.) and the 1.5 MHz head gives slightly lower sensitivity up to 300 a. m. u. These combinations were chosen to permit the detection of free radicals of up to 60 a. m. u. under the conditions of maximum sensitivity and the detection of polynuclear aromatic molecules up to 300 a. m. u.

A sweep generator was built by Imperial College Electronics Services, the circuit diagram is shown in Appendix 1.4. This supplies a d. c. ramp to the mass spectrometer and either a single mass scan or continuous mass scanning of the spectrum is possible. A range of sweep times are available, permitting display of the mass spectrum on either an oscilloscope or a chart recorder.

A Channeltron electron multiplier was chosen to multiply the resulting ion current. This is a unit which is little affected by frequent opening of the detector vacuum chamber to atmospheric pressure. The electron multiplier was offset from the line of sight path of the quadrupole to avoid noise generated by x-rays produced in the mass filter and to enable an optical axial alignment of the ionizer and mass filter with the nozzle-skimmer assembly. The quadrupole assembly was mounted vertically beneath the nozzle-skimmer assembly. A 6" vacuum chamber to accommodate the quadrupole assembly was supplied by Spectrum Scientific Ltd. The port which had accommodated the Finnigan quadrupole horizontally beneath the nozzle-skimmer assembly was closed with a blank flange.

2.7.4. Signal processing

The signals obtained from the resulting mass spectra of molecular species can be displayed either on an oscilloscope or on a chart recorder. At the low electron energies used for the detection of free radicals, the electron flux is considerably reduced. The probability of ionisation is reduced and, as a result, the sensitivity drops by a factor of about $10^2 - 10^3$. When operating at low signal levels, a sophisticated system of signal processing to extract the desired information is essential.

Background molecules in the ion source can interfere with the detection of free radicals by mass spectrometry. Signals are produced at mass numbers which give the maximum interference with the beam molecules. To discriminate against these background

molecules (and consequently increase the sensitivity of the instrument) Tristram (99) modulated the beam by means of a piezo-electric chopper, imparting an a. c. component to the beam signal. The beam was modulated in the skimmer chamber, directly behind the skimmer. Two methods of utilising the a. c. character of the beam signal were installed, namely, phase sensitive detection and pulse counting.

2.7.5. Procedure

A description of the installation of the Extranuclear Laboratories quadrupole mass spectrometer is given, followed by a description of the operation of the vacuum system and the reactor.

The Finnigan quadrupole assembly and the EO4 diffusion pump beneath the detector chamber were removed. The new vacuum chamber, having a 6" diameter U. H. V. rotatable flange at the lower end, compatible with the Extranuclear Laboratories quadrupole assembly U. H. V. rotatable flange, was mounted beneath the detector chamber. The EO4 diffusion pump with the pneumatically operated butterfly valve and the Peltier baffle was bolted to the side elbow of the new vacuum chamber. The vacuum connections and cooling water supply were then connected to the diffusion pump. The quadrupole assembly was carefully raised up inside the vacuum chamber and the two rotatable flanges loosely bolted together. The mirror assembly and the viewing port window (used in the optical alignment of the quadrupole assembly with the molecular beam) were removed from the detector chamber and mounted on ports on the vacuum chamber, beneath the electron multiplier level. The piezo-electric chopper was removed. The ports on the skimmer and detector chamber which were now open were closed with blank flanges. A small halogen lamp was positioned directly above the nozzle orifice and the quadrupole assembly was rotated on its flange until the reflection of the light source was visible through the viewing window on the mirror assembly. The quadrupole flange bolts were tightened and a check made to ensure

that the light source reflection was still visible. Thus, the quadrupole mass filter and the ionizer were aligned with the geometric axis of the molecular beam.

Polyphenyl ether fluid (Santovac 5) was used in the three vapour diffusion pumps. The oil in each rotary pump was also fresh.

During the start up procedure, the whole system is roughed to about 10^2 torr by means of the rotary pumps and then evacuated to low pressures with the diffusion pumps. When the system is closed down, the molecular beam chambers and detector chamber are flooded with dry inert gas (argon).

a) Start up procedure

(i) Clamp the reactor to the nozzle flange and pump with the ES 50 rotary pump.

(ii) Switch on the ES 150, ES 330 and ISC 450 B rotary pumps and depress the respective latching relays to activate the pumps. This also closes the solenoid operated air admittance valves.

(iii) Depress the magnetic valve latching relays to open the magnetic valves.

(iv) Manually open the hand valve on the foreline trap.

(v) Open the six inch butterfly valves and the four inch pneumatically operated butterfly valve, (protect override on).

(vi) When the pressure has fallen to between 10^{-1} - 10^{-2} torr, indicated by the Pirani gauges, switch on the 9B4 vapour booster pump and the EO6 and EO4 diffusion pumps.

(vii) When the pressure in the detector chamber has fallen to about 10^{-6} torr, indicated by the Penning gauge, the ionisation gauges may be activated.

(viii) Switch on the thermo-electric (Peltier) water cooled baffle.

(ix) When the pressure in the detector chamber has fallen to about 10^{-7} torr, switch the ionisation gauge

trip switch to the operate position (protect override off) and switch on the mass spectrometer.

b) Shut down procedure

(i) Switch off the mass spectrometer

(ii) Switch off the ionization gauge trip switch (protect override on).

(iii) Switch off the Peltier baffle, the ionisation gauges and then the diffusion pumps.

(iv) When the diffusion pump fluids have cooled, close the six inch butterfly valves, the four inch pneumatically operated butterfly valve (protect override off) and the manual valve on the foreline trap.

(v) Switch off the rotary pumps. This also closes the magnetic valves and opens the solenoid operated air admittance valves.

(vi) Close the reactor tap on the reactor vacuum line, switch off the reactor pump and let air into the pump.

(vii) Bleed dry argon through the air admittance valves into the detector vacuum chamber.

CHAPTER 3RESULTS

	Page
3. 1. <u>Initial investigation of propane pyrolysis</u>	93
3. 2. <u>Carbon deposition on suspended discs</u>	94
3. 2. 1. Carbon deposition measurements	94
3. 2. 2. Gas analysis	97
3. 3. <u>The influence of a metal liner on carbon deposition</u>	98
3. 3. 1. Carbon deposition measurements	98
3. 3. 2. Gas analysis	100
3. 4. <u>The influence of hydrogen and helium as diluent gases</u>	102
3. 4. 1. Carbon deposition measurements	103
a) Hydrogen dilution	103
b) Helium dilution	103
3. 4. 2. Gas analysis	104
a) Hydrogen dilution	104
b) Helium dilution	104
3. 5. <u>The influence of hydrogen sulphide</u>	105
3. 5. 1. Pre-sulphided discs	105
3. 5. 2. 1% hydrogen sulphide (v/v) in the propane feed	107
3. 5. 3. Analysis of a nickel disc and carbon deposit	110
a) Electron probe micro-analysis	111
b) Spark source mass spectroscopy	113
3. 6. <u>The temperature at which carbon deposition starts</u>	115
3. 7. <u>Tars from propane pyrolysis</u>	117
3. 7. 1. The rate of tar production	117

3.7.2.	Analysis of tars	117
3.7.3.	Hydrogen and carbon balances	119
3.7.4.	Calculation of the tar concentrations	119
3.7.5.	A consideration of tar production	128
3.7.6.	Mass spectrometric measurement of tar production	128
3.8.	<u>Carbonisation and carburisation of metal liners</u>	132
3.8.1.	Examination of metal liners from the jet-stirred reactor	133
3.8.2.	Metallography and microscopic examination	133
3.8.3.	Microprobe examination	135
3.8.4.	X-ray diffraction	135
3.9.	<u>Graphs 3.1. - 3.72.</u>	136

3.1. Initial investigation of propane pyrolysis

A preliminary investigation of the pyrolysis of propane in the jet-stirred reactor was made to characterise the performance of the system under non-catalytic conditions. The relationships between the reactor temperature and hydrocarbon products and the rate of carbon formation inside the reactor, were studied. The position of a suspended disc relative to the position of the jet was investigated with respect to carbon formation.

The initial experiments were aimed at verifying that the presence of a sample disc did not interfere with the mixing of gases inside the reactor. If the reactor is well mixed, the rate of carbon formation is theoretically independent of the position of the sample disc.

Carbon deposition was measured using a silica disc of 12 mm. diameter and 1.0 mm. thickness. (Heraeus Quartz Fused Products). The surface area was 2.64 sq. cms. A silica disc was used in preference to a metal disc, to ensure the absence of a catalytic surface inside the silica reactor. The disc was positioned on the silica suspension cradle. The surface area of that part of the suspension cradle that was subject to carbon deposition was 1.44 sq. cms. This surface area had been minimised by constructing the suspension cradle from silica fibres of diameter 0.5 mm.

The results of the study of the position of the sample disc relative to the jet are shown in graph 3.1 and graph 3.2. Two temperatures (850°C and 840°C) and two inlet residence times (τ), (2.0 and 2.3 secs.) were used.

To check that the presence of a suspended silica disc inside the reactor did not alter the gas mixing inside the reactor, the product gases from the reactor, at various temperatures, without a suspended disc, were analysed.

The F. I. D. system was used for the separation and measurement of the hydrocarbon components of the product gases. The hydrocarbon products from propane pyrolysis over the temperature range 775°C - 850°C at 2.0 secs. inlet residence time, were analysed.

The initial aim was to investigate the system and to ensure that the gas chromatographic separation worked. Hence, at this stage, no relative response factors for the eluted hydrocarbons were calculated. In subsequent experiments involving a suspended silica disc, no significant change in the product distribution was observed. The gas product distribution as a function of the reactor temperature was re-investigated when the microkatharometer had been installed. The hydrocarbon response factors were applied and the results including the hydrogen concentration, are shown in graph 3.3.

3.2. Carbon deposition on suspended discs.

The discs used for this study were suspended at the position relative to the jet which has been found to give no interference with the mixing of the gases inside the reactor. Discs of silica, copper, nickel, iron and stainless steel were used. The silica discs of 12 mm. diameter and 1.0 mm. thickness (Heraeus Quartz Fused Products), had a surface area of 2.64 sq. cms. The metal discs were cut from foil sheets of thickness 0.125 mm. (Goodfellow Metals) and had an area of 2.2 sq. cms.

3.2.1. Carbon deposition measurements

Graphs 3.4. - 3.8. show the rate of carbon deposition on the disc as a function of the inlet residence time at 810°C. Graphs 3.4. and 3.5. (silica and copper discs) show no significant difference in deposition rate at 2 secs. inlet residence time on the clean disc, relative to the rate of deposition that occurs on a carbon covered disc. Graph 3.6. (nickel) shows an increased rate of deposition at 2.0 and 2.3 secs. (points A and B). The disc then exhibits a steady rate of deposition consistent with carbon being deposited on a carbon covered disc. Graph 3.7. (iron) shows a very high initial rate of carbon deposition at 2 secs. (point C). When the disc has been covered in carbon the rate observed is that of carbon being

deposited on carbon and is referred to as the "carbon on carbon" rate. Graph 3. 8. (stainless steel) shows the initial high rate of deposition observed on a clean disc (point A), falling (points B and C), to zero (point D). Point D corresponds to a total deposition of 1.5 mg. on the disc. The dotted line is that obtained from results for silica, copper, nickel and iron discs. and is considered as the "carbon on carbon" deposition system. Points E and F deviate from this line.

The results of changing the inlet residence time from long to short, show similar results. Graph 3. 4. (silica) shows a deposition rate that increases whilst the disc is being covered in carbon at 7.5 secs. (points D and E). The rates then observed are those of carbon being deposited on carbon. Graph 3. 5. (copper) shows the same trend (points F and G). Graph 3. 6. (nickel) shows the rates of carbon deposition on a carbon covered disc. Graph 3. 7. (iron) shows a very high initial rate of carbon deposition at 5 secs. (point H). Point I is the deposition rate on the partially carbon covered disc. The rates at shorter inlet residence times are those of carbon being deposited on a carbon covered disc. Graph 3. 8. (stainless steel) shows the rate of deposition falling from a high rate (point G), to a lower rate (points H and I). Subsequent points show a higher rate of deposition than the "carbon on carbon" rate.

The period during which the rate of deposition was found to be dependent on the disc material ceased when between 1.5 and 2.0 mgs. of carbon had been deposited.

Graph 3. 9. (iron disc, 810°C) shows the very high rates of deposition observed when the disc was not encapsulated with carbon and the disc surface remained active. The disc was found to have distorted. This is the only time that encapsulation with carbon was not observed.

Graph 3. 10. shows the rate of carbon deposition on the disc as a function of the reactor temperature. The results of runs 51, 54, 55 and 56 were obtained using discs which had been carbon covered during a previous part of the run. The inlet residence time was fixed at 2 secs. and the reactor temperature was increased. Runs 48 and 50

were made using discs which had not previously been carbon covered. The inlet residence time was fixed at 2 secs. and the reactor temperature was increased. Each of the single measurement points were made on a clean silica disc.

Graph 3.11. is a psuedo-Arrhenius plot of the results shown on Graph 3.10. Carbon deposition does not occur at a significant rate when the reactor temperature is less than 817°C . The line in Graph 3.11. was calculated by the method of least squares, neglecting those points at temperatures below 817°C , and runs 48 and 50. The psuedo-activation energy was 134.5 kcal/mole.

Graph 3.12. (stainless steel) shows the rate of carbon deposition on the disc as a function of the reactor temperature at $\tau = 2.0$ secs. The disc used had been previously used in a study of decreasing inlet residence time to 2 secs. and had a carbon deposit of 4 mg. The rates obtained differed from the previously determined "carbon on carbon" rates (dotted line).

Graph 3.13. is a psuedo-Arrhenius plot of the results shown on Graph 3.12. Previous results indicated that carbon deposition does not occur at a significant rate when the reactor temperature is less than 817°C . Hence point A may be ignored. The psuedo-activation energy was 189.5 kcal/mole. The previously determined "carbon on carbon" value was 134.5 kcal/mole. (dotted line).

The rate of carbon deposition on an iron disc at 765°C with a reactor inlet residence time of 2.0 secs., was measured. The reactor temperature was set to 765°C , 40°C . below the temperature required to observe the "carbon on carbon" deposition system. Graph 3.14. (run 76) is a plot of the rate of deposition ($\mu\text{g}/\text{min}/\text{cm}^2$.) against the time since the beginning of the experiment. Initially, a very high rate of deposition was observed, which decreased until 6 mins. after the start. At 3 mins. the rate was observed to be $127 \mu\text{g}/\text{min}/\text{cm}^2$, and at 6 mins. $33.6 \mu\text{g}/\text{min}/\text{cm}^2$. The disc remained active and was therefore not encapsulated with carbon. A total of 5.5 mg. of carbon were deposited. Previous results showed that discs are normally encapsulated with carbon at this inlet residence time (2.0 secs.) and 40°C higher temperature (i. e. 805°C), after 1.5. - 2.0 mg. of carbon have been deposited. No significant deposit was

observed on the silica reactor walls, but tars were observed in the reactor outlet.

Graph 3. 15. shows the effect of the nature of the sample collection disc on the rate of carbon deposition, as a function of the time since the start of the reaction. Measurements were made at 810°C and 2.0 secs. inlet residence time. At the start of a reaction, the metal surfaces are carbon-free and the rates of carbon deposition observed are those associated with the "clean" metal surface. As the reaction progresses the rates of deposition observed tend to the "carbon on carbon" rate.

3. 2. 2. Gas analysis

Graphs 3. 16. -3. 20. show the gas analysis of the products (% v/v) as a function of the inlet residence time at 810°C. The product distribution is very similar for each of the disc materials used. The major products are methane and ethylene. No difference in product distribution was detected when the rate of carbon deposition on the disc was subject to the type of disc material, prior to the disc becoming carbon covered. The results of run 53 (iron disc) in which a very high rate of carbon deposition occurred on an active iron disc are very similar to those runs in which the iron disc was encapsulated by carbon.

Graphs 3. 21. -3. 25. show the gas analysis of the products (% v/v) as a function of the reactor temperature at $\tau = 2.0$ secs. Again, the product distribution is very similar for each of the disc materials used.

The figures for the "remainder" hydrogen were calculated as outlined in section 2. 3. The "remainder" figure represents the hydrogen and hydrocarbons heavier than C_3 . Samples of the product gases were analysed using a katharometer and the hydrogen concentration was in good agreement with the "remainder" hydrogen estimation. The results of the hydrogen concentration in the product gas stream for silica, copper, nickel and iron suspended discs were obtained by the "remainder" method. The experiments with stainless

steel suspended discs were made after the installation of the microkatharometer. Hence, the hydrogen concentration was measured directly.

3. 3. The influence of a metal liner on carbon deposition

The effect of various metal liners on carbon deposition and gas composition was studied. Foil liners of copper, nickel, iron and stainless steel were used to investigate the effect of a large surface area of metal on carbon deposition. Any observed alteration in the behaviour of the system, relative to the unlined silica reactor, was due to the presence of the metal.

Carbon deposition was measured using a copper (collector) disc and thus avoided the "ageing" effects of a silica disc. The catalytic activity of copper was previously found to be very similar to silica and both to be slightly less active for the generation of carbon than carbon itself.

For comparison with the metal foil liner results, the results of carbon deposition on a copper disc in an unlined reactor were studied. These may be considered to be generated by a silica "Liner" in the reactor.

The hydrocarbon products were analysed by gas chromatography using the F. I. D. system. The microkatharometer was used to measure the production of hydrogen and, in later runs, of methane.

3. 3. 1. Carbon deposition measurements

Graphs 3. 26. -3. 31. show the rate of carbon deposition on a copper (collector) disc as a function of the inlet residence time at 810°C. Graph 3. 26. is of results using a copper disc in an unlined reactor. Graphs 3. 26. and 3. 27. (silica and copper liners) show no significant difference in deposition rate at 2 secs. inlet residence time on a clean disc with generation of carbon from a clean liner, relative to the rate of deposition that occurs on a carbon covered

disc generated by a carbon covered liner (Point A on both graphs). Graph 3. 28.(nickel liner) shows an increased rate of deposition at 2 secs. (Point B). A steady rate of deposition consistent with generation from a carbon covered liner is then observed. Graph 3. 29. (iron liner) shows a still higher initial rate of deposition (Point C) at 2 secs. , and then exhibits the "carbon on carbon" rate. Graph 3. 30. (stainless steel liner) shows that on increasing the inlet residence time, the high initial rate (Point A) falls to the low rate (Point B) and subsequent points show a lower rate of deposition than the "carbon on carbon" rate (dotted line). Points C and D fall far below this line.

The results of changing the inlet residence time from long to short, show similar results. Graph 3. 26. (silica liner) shows a deposition rate that increases whilst the disc and reactor are being carbon covered (Points B and C) at 7.5 secs. Graph 3. 27. (copper liner) also shows this trend. Graph 3. 28.(nickel liner) shows the initial higher rates of deposition (Points E and F) at 5 secs. Graph 3. 29. (iron liner) indicates that the liner quickly became encapsulated with carbon during the period prior to a steady rate of carbon deposition. Point G is below the "carbon on carbon" rate of point H. If the iron surface was active and not encapsulated with carbon, it is expected that point G would be above the "carbon on carbon" rate. Graph 3. 30. (stainless steel) shows that when the inlet residence time is decreased, the rate of deposition falls from a rate close to the "carbon on carbon" rate (Point E) to a lower rate (Points F and G). Subsequent points show a lower rate of deposition than the "carbon on carbon" dotted line.

In one experiment it was evident that iron was not encapsulated with carbon, although the conditions were the same as for other experiments. The results for this system are shown in Graph 3. 31. The deposition rates at 5 secs. were in the sequence A, B, C. The inlet residence time was then changed and the deposition rate remained constant. After point D the reactor outlet blocked. There was no reason apparent as to why the liner was not encapsulated with carbon. The results for suspended discs in an unlined reactor (section 3. 2. 1.) show that the period during which the rate of deposition is dependent

on the disc material, ceases when between 1.5 and 2.0 mgs. of carbon have been deposited. The results for the metal foil liners with a suspended copper collector disc show that the period during which the rate of deposition is dependent on the liner material, ceases when between 0.2 and 0.3 mg. of carbon have been deposited on the copper collector disc.

/ Graph 3.32. shows the rate of carbon deposition on the suspended carbon covered copper collector disc, as a function of the reactor temperature at $\tau = 2.0$ secs. for carbon covered silica, copper, nickel and iron liners. The dotted line is that obtained from the results of the experiments using an unlined reactor and suspended carbon covered discs of silica, copper, nickel and iron. Graph 3.33. is a psuedo-Arrhenius plot of the results shown on Graph 3.32. The dotted line is that which was obtained by the method of least squares for the carbon covered suspended discs and gave a psuedo-activation energy of 134.5 kcal/mole. Good agreement is shown between the points from the liner experiments and the dotted lines of the results from the unlined reactor experiments.

Graph 3.34. shows the effect of the nature of the reactor wall lining material on the rate of carbon deposition on a copper (collector) disc, as a function of the time since the start of the reaction. Measurements were made at 810°C and 2.0 secs. inlet residence time. At the start of a reaction, the rates of carbon deposition observed are those associated with the "clean" metal surface. The gradual change in the rates of carbon deposition to the "carbon on carbon" rate indicates that the nature of the liner (generator) surface is affecting the rate of carbon formation on the suspended disc.

3.3.2. Gas analysis

Graphs 3.35. -3.39. show the gas analysis of the products (% v/v) as a function of the inlet residence time at 810°C for silica, copper, nickel, iron and stainless steel liners. The product distribution is very similar for each of the liner materials used.

On graphs 3. 37. (nickel liner) and 3. 38. (iron liner), analysis of the product gas stream was made at 6, 18 and 33 mins. after the start of the reaction i. e. Graph 3. 37., run 61 at 2 secs. inlet residence time, run 62 at 5 secs. Graph 3. 38., run 63 at 2 secs. and run 66 at 5 secs. The analysis made after 6 mins. reaction time was during the period when the rate of carbon deposition was subject to the liner material. The analysis at 18 and 33 mins. was during the "carbon on carbon" period. No significant difference in composition was detected.

Graph 3. 40. shows the gas analysis of the products (% v/v) as a function of the reactor temperature at $\tau = 2.0$ secs. These results were obtained from carbon covered systems. Again the product distribution is very similar for each of the liner materials used.

No difference in the hydrocarbon distribution was observed when an increased rate of carbon deposition occurred due to the presence of a metal foil liner. However, calculations indicate that such a change need not be observed. Thus, for example, a significant change in the carbon deposition rate (i. e. $10 \mu\text{g}/\text{min}/\text{cm}^2$) on the reactor surface of 80 sq. cms. results in the deposition of an extra 0.8 mg/min. carbon. If this carbon was converted to methane (the hydrocarbon with least carbon per mole), 1.5 mls/min. methane would be produced. Now, for an inlet residence time of 5 secs., a propane flow rate of 183 mls/min. is required. Reaction results in a two-times volume expansion, with methane as 45% v/v of the products, i. e. the reaction produces 165 mls/min. methane. An increase of 1.5 mls/min. in a flow of 165 mls/min. is below the detection level of the on-line gas chromatograph to be considered significant and would not be observed.

Graph 3. 41. shows the gas analysis results when an iron liner at 810°C , generated a very high rate of carbon formation and was not encapsulated by carbon. (The carbon deposition results are shown on Graph 3. 31.). The lines on Graph 3. 41. are those from the results of the gas analysis obtained from the silica, copper, nickel, iron and stainless steel liners. (Graphs 3. 35. -3. 39). The results

from the non-encapsulated iron liner show the propane and ethylene concentrations to be significantly lower. This is consistent with a much higher than usual rate of carbon deposition.

During the measurement of the rate of carbon deposition as a function of the inlet residence time, the furnace temperature was constant. However, due to the endothermic nature of the reaction which causes a temperature change when changing the inlet residence time, the experiments at short inlet residence times were at 804°C and those at longer inlet residence times at 814°C. The results of Graph 3.3. show the change in product distribution (% v/v) as a function of the reactor temperature. The propane concentration falls by 3% v/v between 804°C and 814°C. When the product distribution is considered as a function of the inlet residence time, the propane concentration falls by 9% v/v between 2 secs. and 7.5 secs. These complementary effects should be considered together.

When the methane present in the product gas stream was determined using both the F. I. D. and the microkatharometer, the results obtained from the two detectors were in good agreement.

3.4. The influence of hydrogen and helium as diluent gases

The propane feed was diluted with hydrogen (a product gas), and helium (an inert gas). Carbon deposition was measured on iron discs (active), and copper discs (low activity). Hydrocarbon products were analysed by gas chromatography using the F. I. D. The microkatharometer was used to measure the production of hydrogen and methane.

The pyrolysis of the diluted propane was studied at 806°C with an inlet residence time of 3.0 secs. The propane concentration was progressively increased from 10 - 100% (v/v), followed by measurement again at 10% (v/v). This enabled the rate of carbon deposition from a 10% (v/v) propane mixture observed on a "clean" metal disc, to be compared to the rate observed on a disc with a carbon deposit present. At these conditions, undiluted propane gives

a low rate of carbon deposition ($\leq 4 \mu\text{g}/\text{min}/\text{cm}^2$), when no catalytic activity is influencing the generation of carbon.

3. 4. 1. Carbon deposition measurements

a) Hydrogen dilution

Graph 3. 42. shows the rate of carbon deposition as a function of the propane concentration (% v/v in hydrogen). For an iron disc (run 68) the initial high rate of deposition continued (points A, B, C). When the propane concentration was increased to 22% v/v high rates were observed (point D). Point E was measured after 2.3 mg. had been deposited on the disc. This is normally considered as a point in the "carbon on carbon" deposition system, but is not so in this hydrogen dilution. As the propane concentration was progressively increased, the rate of deposition fell until an increase to a steady rate of deposition occurred. Point F was obtained by returning to 10% propane, after completing the sequence of progressive concentration increases. The rate is not as high as the initial rates (points A, B, C) obtained for this concentration and indicates that the disc is not as active. The "carbon on carbon" rate of deposition ($\leq 4 \mu\text{g}/\text{min}/\text{cm}^2$ at this inlet residence time and temperature) was not observed, indicating that the iron disc was not encapsulated with carbon.

The copper disc (run 69) showed no initial activity and the rate gradually increased to the "carbon on carbon" rate as the propane concentration was increased. Point G was obtained by returning to 10% propane after completing the sequence of progressive concentration increases. The rate of deposition corresponds to the zero rate initially observed.

b) Helium dilution

Graph 3. 43. shows the rate of carbon deposition as a function of the propane concentration (% v/v in helium). For an iron

disc (run 70) the initial high rate of deposition (point H) continued until 0.5 mg. of carbon had been deposited. The rate gradually fell to point I, obtained after 1.0 mg. had been deposited. As the propane concentration was progressively increased, the rate of deposition remained constant at the "carbon on carbon" rate. The zero rate (point J) was obtained by returning to 10% propane after completing the sequence of progressive concentration increases.

The copper disc (run 71) showed no initial activity (point K) and the rate gradually increased to the "carbon on carbon" rate as the propane concentration was increased. The zero rate (point L) was obtained by returning to 10% propane after completing the sequence of progressive concentration increases.

3.4.2. Gas analysis

a) Hydrogen dilution

Graph 3.44. shows the gas analysis of the products (% v/v) as a function of the propane concentration (% v/v in hydrogen) in the presence of an iron disc. Graph 3.45. is for a copper disc. Both graphs are very similar, again showing no difference in product distribution when the rate of carbon deposition is influenced by high initial metal activity at individual dilutions. (However, any such difference may not be observed). The figures for the production of hydrogen were estimated by using the inlet hydrogen flow rate. When less than 37% propane is present in the inlet mixture, hydrogen is consumed and the methane and ethane concentrations increase.

b) Helium dilution

Graph 3.46. shows the gas analysis of the products (% v/v) as a function of the propane concentration (% v/v in helium) in the presence of an iron disc. Graph 3.47. is for a copper disc. Both graphs are very similar, and also very similar to the product distribution obtained for undiluted propane at 806°C with an inlet

residence time of 3 secs. No difference in product distribution was observed when the rate of carbon deposition was influenced by the high initial activity of an iron disc (Graph 3.46., A and B sequences at 10% propane).

3.5. The influence of hydrogen sulphide

Hydrogen sulphide was used to study the effect of sulphur on the activity of the metal foils for carbon deposition. Iron, stainless steel, nickel and copper discs were pre-sulphided to investigate the effect of sulphur on the initial activity for carbon deposition, the rate of which was determined. Iron, stainless steel, nickel, copper and silica discs were subject to a propane feed containing 1% (v/v) hydrogen sulphide. The rate of carbon deposition was determined, the hydrogen sulphide turned off and the rate of deposition continuously measured. This showed if any change in the activity of the disc was reversible when the hydrogen sulphide flow was discontinued.

Carbon deposition results indicate that a carbon covered suspended disc starts to deposit carbon from propane at 805°C at 2.0 secs. inlet residence time. The sulphiding experiments were made at these conditions to enable comparison with carbon covered discs as well as "clean" discs.

3.5.1. Pre-sulphided discs

The sulphiding experiments were made at 805°C and 2.0 secs. inlet residence time. The discs were heated to temperature and reduced with hydrogen. Hydrogen sulphide was then introduced into the reactor and the weight of the disc increased. The sulphiding was discontinued after 43 mg. had been deposited on the disc. This weight was deposited on the first disc and subsequently used for the other pre-sulphiding experiments. The nickel, iron and stainless steel discs were 65 - 70% sulphided, but only 33 mg. deposited on the copper disc. This was sufficient to fully sulphide the copper to

copper (1) sulphide. After the discs were pre-sulphided, propane was introduced into the reactor at a flow rate to give an inlet residence time of 2.0 secs. The rate of carbon deposition on the disc was measured using the microbalance.

a) Iron disc Graph 3.48. Run 81

The initial rate of deposition observed on the pre-sulphided disc was $8.52 \mu\text{g}/\text{min}/\text{cm}^2$. This is significantly less than the rate of $20 \mu\text{g}/\text{min}/\text{cm}^2$ for a "clean" iron disc. The rate of deposition on the pre-sulphided disc quickly fell to the "carbon on carbon" rate of $2 - 3 \mu\text{g}/\text{min}/\text{cm}^2$. This was observed after 0.4 mg. of carbon had been deposited. A "clean" iron disc does not exhibit this "carbon on carbon" rate until 1.5 - 2.0 mg. of carbon are deposited.

b) Nickel disc Graph 3.49. Run 83

A constant rate of deposition, equivalent to the "carbon on carbon" rate, was observed throughout the experiment. A "clean" nickel disc exhibits a higher initial rate ($4 - 5 \mu\text{g}/\text{min}/\text{cm}^2$).

c) Stainless steel disc Graph 3.50. Run 86

The rate of uptake of sulphur was slower than that for the iron and nickel discs. The initial rate of carbon deposition ($7 \mu\text{g}/\text{min}/\text{cm}^2$) was lower than that for a "clean" stainless steel disc ($13 \mu\text{g}/\text{min}/\text{cm}^2$). The pre-sulphided disc exhibited the "carbon on carbon" rate of deposition after 1.7 mg. of carbon were deposited. A "clean" stainless steel disc did not exhibit the "carbon on carbon" rate. A significantly higher rate was observed.

d) Copper disc Graph 3.51. Run 88

The rate of uptake of sulphur was slower than that for the stainless steel disc. The sulphur uptake ceased after a weight increase

of 33 mg. For the previous disc (iron, nickel and stainless steel), a saturation point was not reached and 43 mg. were rapidly deposited from the hydrogen sulphide.

The initial rate of carbon deposition ($10 \mu\text{g}/\text{min}/\text{cm}^2$) on the pre-sulphided copper disc, was significantly higher than that for a "clean" copper disc, which exhibits a rate equivalent to the "carbon on carbon" rate ($2 - 3 \mu\text{g}/\text{min}/\text{cm}^2$). At the completion of the pre-sulphided copper disc experiment, a total of 2.7 mg. of carbon had been deposited and the "carbon on carbon" rate was not observed.

3.5.2. 1% Hydrogen sulphide (v/v) in the propane feed

Experimental measurements were made at 805°C and 2.0 secs. inlet residence time to enable comparison with previous results. The discs were heated to temperature and reduced with hydrogen. The propane feed, containing 1% hydrogen sulphide (v/v) was then introduced into the reactor. The rate of carbon deposition was measured for two hours, after which time the hydrogen sulphide was turned off. The rate of deposition was continuously measured for at least a further two hours with the propane only gas feed entering the reactor.

a) Iron disc Graph 3.52. Run 82

Initially, a zero rate of deposition was observed. After 14 mins., a rate equivalent to the "carbon on carbon" rate was observed. A "clean" iron disc exhibits an initial rate of $20 \mu\text{g}/\text{min}/\text{cm}^2$. After 2 hrs. the hydrogen sulphide was turned off and the propane left flowing. 0.5 mg. of carbon had been deposited on the disc. After 3 hrs. 23 mins. (1.3 mg. of carbon deposited) the rate of carbon deposition increased very rapidly. When the experiment was discontinued, a total of 4.9 mg. of carbon had been deposited. The outlet flow was measured both with and without the hydrogen sulphide flowing. The volume expansion from the inlet flow was

1.9 and consistent with previous results. As no change in the outlet flow was detected, any change in the composition that occurred, would not be detected by the gas chromatograph as it is below the detection level to be considered a significant change.

b) Nickel disc Run 84

A very fast rate of deposition was observed, too fast to measure on the microbalance. When the microbalance maximum tare had been used (5 mg.), the hydrogen sulphide in the propane feed was turned off, (after 1 - 2 mins.). Counter-weights were added and the very fast rate of deposition was observed to continue from the propane only feed. The propane was turned off and the reactor purged with helium for 35 mins. to ensure that all traces of hydrogen sulphide were removed from the gas lines. More counter-weights were added and the propane feed was re-introduced. The very fast rate of deposition continued. The propane was turned off and the reactor was purged with hydrogen for 3 hrs. During the hydrogen purge, 16.75 mg. weight were lost. The propane only feed was re-introduced into the reactor and the very fast rate of deposition continued. The experiment was discontinued and the reactor was cooled overnight whilst purging with helium.

On examination, the disc was found to be in the centre of a "layered" carbon deposit. The disc had been lifted off the base of the suspension cross by the carbon deposited. The disc and the carbon deposit were weighed:

disc (unused)	0.1091 g
disc (used) weight lost	0.0131 g
carbon deposit	0.2868 g

The carbon deposit of 0.2868 g. was deposited from propane which flowed through the reactor for 22 mins. i. e. a rate of deposition of 13.0 mg/min. on a nickel disc of surface area 2.2. sq. cm. No significant carbon deposit was found on the walls of the silica reactor.

Samples were sent for analysis by the Analytical Services Laboratory of Imperial College to determine if a nickel transport mechanism through the "growing" carbon deposit had occurred. The results of this analysis are reported in section 3.5.3.

c) Stainless steel disc Graph 3.53. Run 85

Initially, a rate of deposition of $6 \mu\text{g}/\text{min}/\text{cm}^2$ was observed, compared to that for a "clean" stainless steel disc of $13 \mu\text{g}/\text{min}/\text{cm}^2$. When the hydrogen sulphide flow was discontinued, a rate equivalent to the "carbon on carbon" rate was observed. At this point, 1.2 mg. of carbon had been deposited on the disc. When the experiment was discontinued, a total of 2.1 mg. of carbon had been deposited and the "carbon on carbon" rate of deposition had been observed for 4 hrs. Previous results showed that a "clean" stainless steel disc did not exhibit the "carbon on carbon" rate. A significantly higher rate was observed.

The outlet flow was measured both with and without the hydrogen sulphide flowing. The volume expansion from the inlet flow was 1.9 and consistent with previous results. As no change in the outlet flow was detected, any change in the composition that occurred, would not be detected by the gas chromatograph as it is below the detection level to be considered a significant change.

d) Copper disc Graph 3.54. Run 87

The initial rate of carbon deposition ($4.3 \mu\text{g}/\text{min}/\text{cm}^2$) was significantly higher than that for a "clean" copper disc, which exhibited a rate equivalent to the "carbon on carbon" rate ($2 - 3 \mu\text{g}/\text{min}/\text{cm}^2$). After 2 hrs. the hydrogen sulphide was turned off: 1.2 mg. of carbon had been deposited on the disc. When the experiment was discontinued, the rate of deposition was still a little above the "carbon on carbon" rate and a total of 2.4 mg. of carbon had been deposited on the disc.

e) Silica disc Graph 3. 55. Run 89

The initial rate of carbon deposition ($0.8 \mu\text{g}/\text{min}/\text{cm}^2$) was consistent with previous results for a "clean" silica disc, (rate less than $1 \mu\text{g}/\text{min}/\text{cm}^2$). After 2 hrs. the hydrogen sulphide was turned off: 0.4 mg. of carbon had been deposited on the disc. The rate of deposition remained below the "carbon on carbon" rate, ($2 - 3 \mu\text{g}/\text{min}/\text{cm}^2$). When the experiment was discontinued a total of 0.8 mg. of carbon had been deposited on the disc.

3. 5. 3. Analysis of a nickel disc and carbon deposit

A very high rate of carbon deposition occurred on a nickel disc from a propane feed containing 1% hydrogen sulphide (v/v). The very high rate of carbon deposition continued from the propane only gas feed after the 1% hydrogen sulphide component had been discontinued.

Deposition was made on a nickel foil disc of area 2.2 sq. cms. , heated at 805°C and suspended in the jet-stirred reactor. The inlet residence time of the propane feed containing 1% hydrogen sulphide (v/v), was 2.0 secs. (Run 84).

Samples were sent for analysis by the Analytical Services Laboratory of Imperial College to determine if a nickel transport mechanism through the "growing" carbon deposit had occurred.

- (i) Used nickel foil. To determine the presence of sulphur and carbon on the surface and sulphur through the foil
- (ii) Deposit adjacent to the foil
- (iii) Deposit away from the foil

To determine the presence of nickel sulphide and the nickel and sulphur contents of each.

The foil was analysed by electron probe micro-analysis and the deposit by spark source mass spectroscopy.

a) Electron probe micro-analysis.

Visual examination showed the used foil to have a surface layer approximately 3 microns thick. No surface layer was visible on the control sample. The surface of the used foil was very pitted as compared to the control, but no cracks or intergranular penetration were visible. The thickness of the used foil was estimated to have been reduced by 5 microns from both faces, by reference to the thickness of the unused foil. The nickel discs were cut from foil sheets 0.125 mm. thick.

EPMA did not detect sulphur near or at the sample surface, but some nickel was detected in the surface layer as small, ill-defined particles. A few tiny sulphur containing inclusions were found in the nickel foil: none were detected in the control foil. The "probe" shows the pitted surface of the sample, but again, no other defects, (photographs 3.1.). Sulphur was not detected in the surface layer (under 0.2 - 0.4%). The limit of detection for carbon in a metal matrix is 5%.

Photographs (3.1.).

(i) Control nickel foil. Back-scattered electron image (B. E. I.). Magnification x1200. Shows edge of control nickel foil. (white zone).

(ii) Used nickel foil. B. E. I. Magnification x 1200. Shows pitted edge of foil (white zone). Two metal zones (white) are apparent away from the foil surface. The actual distance away from the foil surface has been increased by the mounting technique, but these zones are considered to be located in the surface layer, (carbon layer).

(iii) X-ray nickel ($K\alpha$). (The same region of the used foil as photograph (ii)). Magnification x 1200. The surface disruption is apparent and the presence of nickel in the surface layer is confirmed. The "banding" of the nickel x-ray spots is due to spectrometer de-focussing.

PHOTOGRAPHS 3.1.

(i) Control nickel foil.

B.E.I.



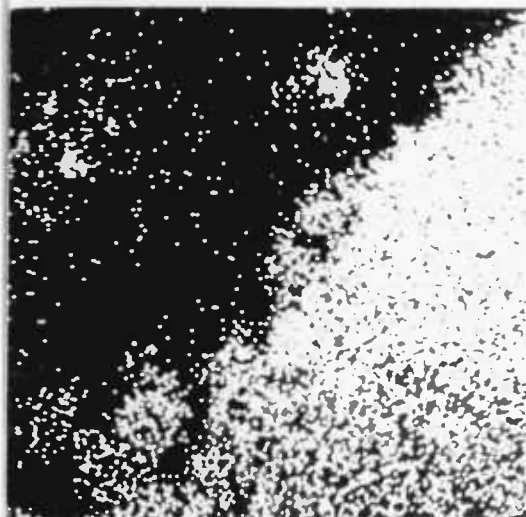
(ii) Used nickel foil.

B.E.I.



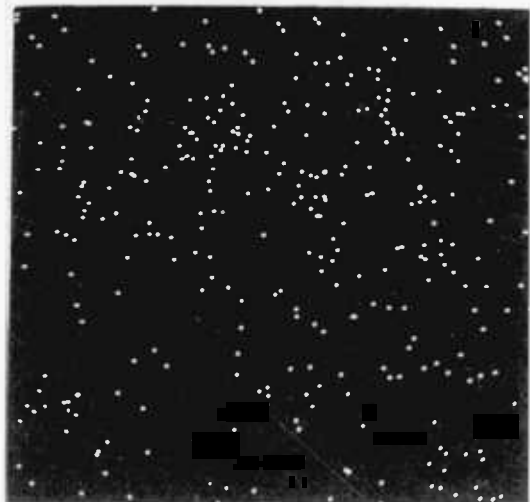
(iii) Used nickel foil.

X-ray nickel.



(iv) Used nickel foil.

X-ray sulphur.



(iv) X-ray sulphur ($K\alpha$). (The same region of the used foil as photographs (ii) and (iii). Magnification $\times 1200$. All the sulphur x-ray spots are considered to be due to the background.

b) Spark source mass spectroscopy.

The reported results are quoted in Table 3.1.

Both nickel and sulphur are present in both samples, nickel fairly strongly in both and sulphur strongly in (b), the deposit away from the nickel disc. The other elements detected are considered to be of little significance.

The amounts of nickel and sulphur detected are too low to reveal the presence of nickel sulphide by x-ray diffraction.

Table 3.1. Spark source mass spectroscopy

Sample (a) Deposit adjacent to the nickel disc.

Sample (b) Deposit away from the nickel disc.

Z	Element	(a)	(b)	
29	Cu	0.3	15	(all ppma. atoms per million atoms).
28	Ni	300	300	
27	Co	6	20	
26	Fe	20	20	
25	Mn	20	60	
20	Ca	2	2	
19	K	6	6	
16	S	20	200	
15	P	20	60	
14	Si	20	20	
13	Al	20	60	
11	Na	50	50	

3.6. The temperature at which carbon deposition starts

To confirm the order of activity for carbon deposition previously found, the temperatures at which carbon deposition started on iron, stainless steel, nickel, copper and silica suspended discs, were measured. Comparison was made with the system of carbon being deposited on a carbon covered disc, referred to as the "carbon on carbon" system.

Metal discs having an area of 2.2 sq. cms. were cut from foil sheets 0.125 mm. thick. The silica disc of area 2.64 cms. , had been conditioned in previous experiments. Each disc was reduced with hydrogen at 500°C, prior to the start of the experiment. The inlet residence time for the propane was fixed at 2.0 secs.

Propane conversion increases with increasing temperature. This increase in volume expansion causes the suspended disc to become more buoyant and to register as a decrease in apparent weight on the microbalance. It is not possible to increase the reactor temperature whilst propane is flowing, and to measure an increase in disc weight due to carbon deposition, at the same time. The reactor temperature must be increased by small increments (10 - 20°C), and microbalance measurements recorded for at least 12 mins. at each temperature setting, so as to determine whether an actual increase in weight is occurring. For these experiments, the reactor temperature was increased, in increments, from 400°C. The results are quoted in Table 3.2.

Table 3.2. The temperature at which carbon deposition starts

Disc Material	Temp °C. deposition started	Rate observed ($\mu\text{g}/\text{min}/\text{cm}^2$)
Iron	590	4.36
Stainless steel	650	2.84
Nickel	802	11.36
Copper	805	3.13
Silica	805	2.0
"Carbon on carbon"	805	2-3 (from previous results).

Inlet residence time 2.0 secs.

3.7. Tars from propane pyrolysis

The aromatic and polyaromatic compounds formed from propane pyrolysis, are referred to as tars. The rate of tar production was measured by trapping the tars present in the reactor outlet gas stream and weighing the trap. The tars were then dissolved in chloroform and analysed by a temperature programmable F. I. D. gas chromatograph.

3.7.1. The rate of tar production

The propane was pyrolysed at 800°C with an inlet residence time of 4.92 secs. No foil liner was present. These conditions were the same as for run 59(3) for which the carbon and hydrogen balance had been calculated from the gas chromatography results. Run 59 was with a copper suspended disc and a copper foil liner and the hydrogen concentration in the product gas stream was measured with the microkatharometer. This system of pyrolysis is considered to be in the absence of a catalytically active surface. Copper was used for comparison in preference to a silica disc system, as the hydrogen concentrations found in the earlier silica results were implied by balance and were not determined with the microkatharometer.

The trap and tube used in the measurement of the production of tars had increased in weight by 1.2 gms. after 30 mins. i. e. a rate of 40 mg/min. This agrees with the figures obtained in the carbon balance calculations, (section 3.7.3.).

3.7.2. Analysis of tars

The results from the analysis of solutions of known aromatic and polyaromatic compounds, were compared with those from the tar sample. Many of the components of the tar sample were identified and are listed in Table 3.3. An indication of the abundance of each of the components of the tar sample is also given.

Table 3.3. Analysis of tars

Retention time	Component	Abundance
2 mins.	benzene	main component
3.5	toluene	minor
6	ethyl benzene	minor
10	diethyl benzene	trace
13	naphthalene	major
15.5	methylnaphthalene	trace
17	diphenyl	trace
18	dimethyl naphthalene	minor
18.5	acenaphthene	trace
20	fluorene	trace
22	methyl fluorene	trace
23	anthracene/phenanthrene	minor
24.5	unknown	trace
25.5	unknown	trace
26.5	fluoranthene	trace
27	pyrene	minor
30.5	unknown	trace
31.5	chrysene	minor
34.5	unknown	trace
38	unknown	trace

3. 7. 3. Hydrogen and carbon balances

Calculations based on the conversion of propane were made to check the hydrogen value obtained with the microkatharometer and the carbon figure obtained from the trapped tars experiment.

a) Hydrogen balance

Calculations were made for run 59 (3), (5) and (7). The measured hydrogen figures were 16.9%, 17.0% and 15.7% respectively. The hydrogen balance figures were 18.5%, 12.8% and 14.7%. These show fair agreement.

b) Carbon balance

Calculations for run 59 (3), (5) and (7) gave a loss of carbon of 39.9, 33.7 and 40.0 mg/min. A deposition rate of $10\mu\text{g}/\text{min}/\text{cm}^2$ measured on the microbalance, corresponds to a deposition rate of 0.8 mg/min. on the reactor walls. The difference is the carbon lost as tar. These figures agree with the measured rate of tar production, 40 mg/min. , (section 3. 7. 1.)

3. 7. 4. Calculation of the tar concentrations

The amount and concentration of tars produced in the pyrolysis of propane were calculated with a computer. The values were obtained using the carbon mass balance information obtained from the gas chromatography results and the gas flow rate measurements. 149 sets of data were analysed.

The amounts of tars produced were expressed as mg. of carbon/min. and the concentration in mole % as anthracene, a component indicated by the gas chromatography analysis of the tars. Two methods of quoting the results were used.

(i) The figures for the amounts of tars produced include the carbon deposited inside the reactor and that deposited on the suspended disc.

(ii) The figures for the amounts of tars produced do not include the carbon deposited inside the reactor and that deposited on the suspended disc. In this case, for the calculation of the tar

amounts and concentrations, the rate of carbon deposited per unit area inside the reactor was assumed to be equal to the rate of deposition on the disc.

The amount of carbon in the tars is always much larger than that deposited inside the reactor. The results are quoted in Table 3.4. The experiment run number is defined by a four figure number. The first and second digits designate the run number, the third and fourth digits designate the sub-section of the run.

The disc and reactor wall materials used in the experiments tabulated in Table 3.4. are listed in Table 3.5.

Table 3.4.

Tar concentrations

(i) The figures for the amounts of tars produced include the carbon deposited inside the reactor and that deposited on the suspended disc.

(ii) The figures for the amounts of tars produced do not include the carbon deposited inside the reactor and that deposited on the suspended disc.

Run	Methane % v/v	Ethane % v/v	Ethylene % v/v	Propane % v/v	Propylene % v/v	Temp. °C.	τ sec.	Flow in mls/ min.	Flow out mls/ min.	C. deposited on disc 2 $\mu\text{g}/\text{min}/\text{cm}^2$	(i)		(ii)	
											Tar mg. carbon/ min.	Tar moles % as anthracene	Tar mg. carbon/ min.	Tar moles % as anthracene
4701	34.30	3.18	27.76	13.08	5.89	798	2.0	457	850	7.58	37.35	0.59	36.74	0.58
4702	35.14	3.27	28.04	13.00	5.79	797	2.0	457	850	4.55	32.61	0.51	32.24	0.51
4703	34.86	3.27	27.94	12.90	5.61	797	2.0	457	850	3.03	38.62	0.61	38.38	0.60
4801	36.37	3.16	29.02	10.58	5.86	810	2.0	457	850	5.40	47.09	0.74	46.65	0.73
4802	36.93	3.26	29.58	10.42	5.58	809	2.0	457	850	5.40	48.64	0.76	48.20	0.76
4803	37.77	3.26	29.77	10.42	5.94	808	2.0	457	850	5.40	38.16	0.60	37.73	0.59
4804	37.77	3.26	29.77	10.60	5.67	808	2.0	457	850	6.63	39.39	0.62	38.86	0.61
4805	38.97	3.22	29.23	8.27	5.24	818	2.0	457	850	8.52	76.90	1.21	76.22	1.20
4806	40.37	3.11	28.68	6.12	3.93	829	2.0	457	850	15.15	123.80	1.94	122.58	1.92
4807	41.09	2.64	27.82	4.73	3.45	838	2.0	457	850	21.78	158.17	2.48	156.42	2.45
5001	34.52	3.01	27.09	9.41	4.61	809	2.0	457	900	4.07	74.97	1.11	74.64	1.11
5002	36.50	3.01	27.94	8.37	4.52	818	2.0	457	900	5.21	73.57	1.09	73.15	1.08
5003	38.48	2.73	27.66	6.02	3.67	829	2.0	457	900	8.52	115.70	1.71	115.01	1.70
5004	39.07	2.52	26.54	4.67	3.46	838	2.0	457	924	15.61	132.60	1.91	131.35	1.90
5101	43.86	2.71	22.70	3.71	2.71	814	6.2	147	295	23.70	56.16	2.54	54.27	2.45
5102	44.36	3.19	25.10	5.44	3.45	813	5.0	183	347	18.77	56.87	2.19	55.36	2.13
5103	43.03	3.23	25.00	5.47	3.23	812	4.5	203	401	15.44	56.43	1.88	55.20	1.84
5104	42.16	3.21	26.00	6.65	3.68	811	4.0	229	440	11.55	57.88	1.75	56.96	1.73
5105	41.49	3.33	27.90	7.70	4.02	810	3.5	261	489	7.01	55.02	1.50	54.46	1.49
5106	40.54	3.26	27.60	8.80	5.65	808	3.0	305	565	4.92	49.43	1.17	49.03	1.16

Table 3.4. (continued)

Run	Methane % v/v	Ethane % v/v	Ethylene % v/v	Propane % v/v	Propylene % v/v	Temp. °C.	τ sec.	Flow in ml/min.	Flow out ml/min.	C. deposited on disc $\mu\text{g}/\text{min}/\text{cm}^2$	(i)		(ii)	
											Tar, mg carbon/ min.	Tar moles % as anthracene	Tar, mg carbon/ min.	Tar moles % as anthracene
5107	37.87	3.25	28.50	10.66	5.79	806	2.5	366	695	1.90	27.03	0.52	26.88	0.52
5108	36.50	3.33	28.80	11.84	5.97	803	2.0	457	876	0.34	10.86	0.17	10.83	0.16
5109	36.98	3.32	29.00	10.54	5.07	810	2.0	457	796	1.80	101.41	1.70	101.27	1.69
5110	36.65	3.29	28.40	7.34	3.67	818	2.0	457	827	4.63	136.07	2.19	135.70	2.19
5111	39.33	3.08	27.70	5.58	3.27	830	2.0	457	849	10.42	154.80	2.43	153.97	2.42
5112	41.06	2.60	27.70	5.10	3.27	838	2.0	457	849	14.68	157.84	2.48	156.67	2.46
5201	48.57	3.78	25.39	4.17	3.39	818	6.2	147	296	81.40	30.74	1.38	24.22	1.09
5202	48.18	3.52	25.00	3.39	3.26	818	6.2	147	296	46.40	37.74	1.70	34.03	1.53
5203	46.61	3.39	24.48	2.87	2.47	814	6.2	147	296	43.30	48.53	2.19	45.06	2.03
5301	33.70	3.24	27.50	15.00	7.22	803	2.0	457	803	41.70	38.25	0.64	34.92	0.58
5302	35.48	3.41	29.03	12.81	6.36	803	2.02	452	812	41.70	39.68	0.65	36.34	0.60
5303	35.93	3.28	27.75	10.21	5.68	805	2.54	360	688	75.70	41.69	0.81	35.64	0.69
5304	39.70	3.55	28.02	9.04	5.28	808	3.04	301	572	108.00	36.95	0.86	28.32	0.66
5305	41.59	3.43	27.87	7.40	4.29	810	3.57	256	482	133.00	51.82	1.43	41.18	1.14
5306	43.02	3.35	28.04	7.04	4.02	811	4.01	228	432	152.00	44.77	1.38	32.61	1.01
5307	44.32	3.36	27.03	5.80	3.94	811	4.55	201	388	167.00	43.82	1.51	30.46	1.05
5308	45.94	3.27	26.18	5.33	3.64	811	5.10	179	350	186.00	40.62	1.55	25.74	0.98
5401	47.75	3.65	23.60	3.51	3.23	815	7.5	121	247	24.10	32.39	1.75	30.46	1.64
5402	45.24	3.34	23.78	3.73	2.96	814	6.2	147	298	19.30	45.37	2.03	43.83	1.96
5403	43.27	3.16	25.61	5.26	3.86	813	5.0	183	374	14.20	37.28	1.33	36.15	1.29
5404	42.39	3.07	25.57	5.57	4.55	811	4.5	203	400	11.05	47.59	1.58	46.71	1.56
5405	43.11	3.28	27.46	7.11	4.60	811	4.0	229	445	9.94	34.93	1.05	34.14	1.02
5406	40.53	3.68	26.84	7.58	4.95	809	3.5	261	500	4.89	46.69	1.25	46.30	1.23
5407	41.20	3.70	29.70	9.60	5.10	806	3.0	305	583	3.95	12.12	0.35	14.81	0.34
5408	38.75	3.37	29.71	11.44	5.87	803	2.5	366	678	0.79	18.54	0.36	18.47	0.36
5409	36.70	3.39	29.45	13.76	6.42	801	2.0	457	826	0.00	13.53	0.22	13.53	0.22
5410	37.45	3.45	29.45	11.91	6.09	806	2.0	457	846	0.00	21.77	0.34	21.77	0.34

Table 3.4. (continued)

Run	Methane % v/v	Ethane % v/v	Ethylene % v/v	Propane % v/v	Propylene % v/v	Temp. °C.	γ sec.	Flow in mls/ min.	Flow out mls/ min.	C. deposited on disc $\mu\text{g}/\text{min}/\text{cm}^2$	(i)		(ii)	
											Tar mg, carbon/ min.	Tar moles % as anthracene	Tar mg carbon min.	Tar moles % as anthracene
5411	39.56	3.45	30.22	10.25	5.99	811	2.0	457	856	1.26	20.82	0.32	20.72	0.32
5412	41.82	3.16	30.08	6.50	4.34	828	2.0	457	876	12.70	73.58	1.12	72.57	1.11
5413	40.20	2.89	27.82	7.32	4.34	838	2.0	457	876	21.30	93.38	1.42	91.68	1.40
5501	47.67	3.39	23.62	3.25	2.97	816	7.5	121	248	26.10	34.55	1.86	32.46	1.75
5502	46.49	3.51	24.03	4.03	3.25	815	6.2	147	296	23.67	40.53	1.83	38.64	1.74
5503	44.76	3.57	26.07	5.71	3.81	813	5.0	183	365	16.10	34.81	1.27	33.52	1.22
5504	42.63	3.31	25.71	6.40	4.00	812	4.43	206	402	13.73	47.06	1.56	45.96	1.52
5505	42.26	3.21	26.77	6.75	3.76	811	4.0	229	440	9.94	52.75	1.59	51.95	1.57
5506	41.19	3.40	27.39	7.43	4.35	810	3.5	261	495	6.82	53.20	1.43	52.66	1.41
5507	38.92	3.21	27.68	8.63	4.51	808	3.0	305	589	3.88	48.03	1.09	47.72	1.08
5508	37.94	3.09	28.12	10.72	5.22	806	2.5	366	680	0.95	48.40	0.95	48.32	0.95
5509	35.60	3.12	27.80	12.29	5.60	802	2.0	457	821	0.00	69.83	1.13	69.83	1.13
5510	36.80	3.11	27.85	9.77	4.57	814	2.0	457	841	1.89	95.85	1.52	95.70	1.52
5511	37.35	3.11	28.68	9.13	4.38	817	2.0	457	841	4.26	97.11	1.54	96.77	1.53
5512	39.56	2.72	28.58	4.17	3.36	837	2.0	457	871	10.51	152.33	2.33	151.49	2.32
5513	38.00	2.73	28.82	6.18	3.91	825	2.0	457	861	6.63	128.49	1.99	127.96	1.98
5601	43.88	3.18	25.06	5.18	3.53	816	5.0	183	375	23.90	39.97	1.42	38.06	1.35
5602	42.87	3.31	25.54	6.16	3.65	814	4.5	203	406	12.60	43.47	1.43	42.47	1.40
5603	42.87	3.31	26.41	6.30	3.87	814	4.10	228	440	11.50	55.33	1.62	52.41	1.59
5604	40.11	3.17	26.67	6.46	4.13	813	3.48	264	500	7.58	71.87	1.92	71.26	1.90
5605	40.00	3.20	28.40	8.00	4.80	811	3.0	305	601	3.41	34.26	0.76	33.98	0.75
5606	37.60	3.08	28.56	8.85	4.62	810	2.5	366	688	1.23	67.44	1.31	67.34	1.31
5607	35.05	3.12	28.53	10.09	5.32	802	2.0	457	831	0.00	90.81	1.46	90.81	1.46
5608	34.89	3.20	27.40	8.95	5.11	806	2.0	457	841	1.33	111.49	1.77	111.38	1.77
5609	38.00	3.07	29.15	7.13	4.69	817	2.0	457	893	2.27	74.74	1.12	74.55	1.11
5610	38.81	2.89	27.89	5.51	4.15	832	2.0	457	893	6.91	115.63	1.73	115.08	1.72
5611	38.64	2.62	27.06	5.43	3.26	836	2.02	452	882	9.85	140.16	2.12	139.37	2.11
5701	32.96	2.97	26.65	13.46	5.76	803	2.0	457	821	0.40	75.33	1.22	75.30	1.22

Table 3.4. (continued)

Run	Methane % v/v	Ethane % v/v	Ethylene % v/v	Propane % v/v	Propylene % v/v	Temp. °C.	τ sec.	Flow in mls/ min.	Flow out mls/ min.	C. deposited on disc ² $\mu\text{g}/\text{min}/\text{cm}$	(i)		(ii)	
											Tar mg. carbon/ min.	Tar moles % as anthracene	Tar mg. carbon/ min.	Tar moles % as anthracene
5702	35.05	2.91	26.99	10.49	5.53	803	2.5	366	688	0.47	61.47	1.19	61.43	1.19
5703	37.26	2.94	26.09	8.83	4.16	805	3.0	305	589	3.16	66.42	1.50	66.17	1.50
5704	39.25	3.10	25.56	7.70	4.28	807	3.5	261	500	5.52	64.50	1.72	64.06	1.71
5705	40.34	3.24	25.36	6.82	4.13	809	4.01	228	440	7.10	59.06	1.79	58.49	1.77
5706	40.35	3.12	24.97	6.36	3.70	810	4.5	203	402	8.68	53.35	1.77	52.66	1.75
5707	41.55	3.21	24.88	5.71	3.69	810	5.0	183	372	12.23	43.13	1.55	42.15	1.51
5708	42.60	2.73	22.21	3.64	2.99	812	6.2	147	303	18.15	53.83	2.37	52.37	2.30
5709	43.12	2.98	20.85	2.70	2.89	813	7.55	120	254	26.04	46.49	2.44	44.41	2.33
5801	33.43	3.15	28.33	13.61	6.76	804	2.0	457	803	20.27	56.92	0.95	55.30	0.92
5802	33.70	3.15	27.96	12.87	6.20	802	2.0	457	803	2.18	75.72	1.26	75.54	1.25
5803	37.02	3.27	27.98	10.58	5.29	803	2.5	366	688	2.84	45.92	0.89	45.69	0.89
5804	38.59	3.43	27.17	8.48	4.65	806	3.0	305	578	5.68	59.20	1.37	58.74	1.36
5805	40.21	3.10	26.31	7.70	4.39	808	3.55	258	486	10.42	62.36	1.71	61.52	1.69
5806	42.78	3.33	27.22	6.78	4.00	810	4.0	229	436	12.78	49.84	1.52	48.82	1.49
5807	42.97	3.00	25.58	5.53	3.57	810	4.54	201	395	15.15	53.36	1.80	52.15	1.76
5808	43.23	2.87	25.39	5.39	3.35	811	5.06	180	356	16.38	49.02	1.84	47.71	1.79
5809	46.01	3.14	24.58	3.27	3.01	812	6.2	147	293	22.40	47.42	2.16	45.62	2.08
5810	49.78	3.17	24.60	2.88	2.73	813	7.5	121	242	27.65	36.08	1.99	33.87	1.87
5901	45.73	3.20	22.67	3.33	3.20	813	7.5	121	250	27.46	37.67	2.01	35.47	1.89
5902	45.31	3.21	23.70	4.20	3.21	813	6.2	147	303	25.19	39.23	1.73	37.22	1.64
5903	43.91	3.33	25.40	5.17	3.33	811	4.92	186	378	16.86	41.99	1.49	40.65	1.44
5904	42.01	3.24	25.70	5.92	3.46	811	4.54	201	409	11.65	42.49	1.39	41.56	1.35
5905	42.31	3.30	27.03	6.81	4.07	810	4.0	229	456	8.71	36.73	1.07	36.04	1.05
5906	40.62	3.51	26.91	7.53	4.43	808	3.5	261	510	5.49	44.21	1.16	43.77	1.14
5907	38.04	3.14	27.25	9.22	4.90	806	2.96	309	601	2.27	42.04	0.93	41.86	0.93
5908	35.42	2.99	27.20	10.56	5.61	804	2.5	366	702	0.00	45.49	0.86	45.49	0.86
5909	35.47	3.38	28.70	14.63	6.31	800	2.0	457	841	0.00	2.56	0.04	2.56	0.04

Table 3.4. (continued)

Run	Methane % v/v	Ethane % v/v	Ethylene % v/v	Propane % v/v	Propylene % v/v	Temp. °C.	τ sec.	Flow in mls/ min.	Flow out mls/ min.	C. deposited on disc $\mu\text{g}/\text{min}/\text{cm}^2$	(i)		(ii)	
											Tar mg. carbon/ min.	Tar moles % as anthracene	Tar mg. carbon/ min.	Tar moles % as anthracene
5910	37.86	3.06	28.60	8.36	4.50	820	2.04	448	893	4.73	51.38	0.77	50.99	0.76
5911	38.67	2.88	27.52	6.56	4.05	830	2.08	440	897	10.42	76.17	1.13	75.33	1.12
5912	39.29	2.58	26.40	4.98	3.64	839	2.08	440	893	19.60	118.15	1.76	116.58	1.74
6001	34.81	3.24	27.78	11.67	5.37	803	2.0	457	838	1.26	70.17	1.12	70.07	1.11
6002	36.91	3.29	28.70	10.05	4.73	805	2.5	366	685	1.62	55.26	1.08	55.13	1.07
6003	39.38	3.52	28.40	8.36	4.33	807	3.0	305	583	3.79	48.88	1.12	48.58	1.11
6004	40.93	3.59	27.43	6.96	3.59	810	3.52	260	501	6.82	56.53	1.50	55.98	1.49
6005	43.16	3.59	27.13	6.39	3.59	811	4.0	229	431	7.20	57.37	1.76	56.79	1.76
6006	41.75	3.30	26.17	5.57	3.41	811	4.5	203	388	9.09	60.94	2.09	60.21	2.07
6007	42.05	3.11	24.73	4.66	3.11	813	5.1	179	350	12.51	60.71	2.31	59.71	2.27
6008	44.62	3.15	23.62	3.67	2.89	814	6.2	147	281	19.88	58.84	2.79	57.25	2.72
6009	48.06	3.33	23.75	3.19	2.92	815	7.5	121	246	26.73	35.58	1.93	33.44	1.81
6101	36.26	3.27	28.88	13.08	6.54	801	2.0	457	831	0.00	24.75	0.40	24.75	0.40
6102	38.65	3.29	28.41	10.82	5.51	806	2.54	360	674	0.00	33.19	0.66	33.19	0.66
6103	39.34	3.42	27.97	10.06	5.23	807	3.0	305	568	2.84	39.85	0.94	39.62	0.93
6104	40.64	3.40	27.77	8.30	4.15	808	3.5	261	485	4.17	54.84	1.51	54.50	1.50
6105	44.33	3.74	27.39	7.37	4.07	810	4.0	229	436	6.82	38.89	1.19	38.34	1.17
6106	43.88	3.18	26.71	6.24	3.88	811	4.5	203	382	9.47	51.97	1.81	51.21	1.79
6107	47.10	3.41	27.65	5.56	3.79	812	5.0	183	347	12.69	38.91	1.50	37.89	1.46
6108	47.25	3.49	25.37	4.43	3.09	814	6.2	147	281	19.79	44.25	2.10	42.67	2.02
6109	49.50	3.43	25.18	3.58	3.00	815	7.5	121	241	27.94	31.18	1.72	28.94	1.60
6201	44.15	3.22	25.42	5.25	3.58	816	5.0	183	350	21.00	54.23	2.07	52.55	2.00
6202	42.97	3.37	27.06	6.97	4.07	811	4.4	208	382	12.00	54.01	1.89	53.05	1.85
6203	42.30	3.35	27.34	7.25	4.13	809	4.0	229	431	9.47	49.80	1.54	49.04	1.52
6204	40.00	3.19	27.13	8.51	4.26	807	3.5	261	501	6.63	46.51	1.24	45.98	1.22
5205	38.21	3.23	27.52	9.88	5.14	805	3.0	305	583	3.69	38.01	0.87	37.72	0.86
6206	36.10	3.33	27.43	11.62	5.90	802	2.5	366	685	2.56	37.09	0.72	36.89	0.72

Table 3.4. (continued)

Run	Methane % v/v	Ethane % v/v	Ethylene % v/v	Propane % v/v	Propylene % v/v	Temp. °C.	τ sec	Flow in mls/ min.	Flow out mls/ min.	C. deposited on disc ₂ $\mu\text{g}/\text{min}/\text{cm}^2$	(i)		(ii)	
											Tar mg, carbon/ min.	Tar moles % as anthracene	Tar mg, carbon/ min.	Tar moles % as anthracene
6207	34.01	3.40	27.48	15.07	6.34	797	2.0	457	830	0.00	23.03	0.37	23.03	0.37
6208	38.55	3.09	28.55	8.91	4.82	822	2.0	457	850	10.40	83.19	1.30	82.35	1.29
6209	39.49	2.90	27.90	7.70	4.17	829	2.04	448	860	11.10	90.17	1.40	89.29	1.38
6301	34.13	3.41	28.51	13.84	6.67	799	2.0	457	838	0.00	18.42	0.29	18.42	0.29
6302	36.91	3.38	28.12	9.86	4.73	805	2.54	360	685	3.31	51.30	1.00	51.04	0.99
6303	37.68	3.43	27.88	9.39	4.85	806	3.0	305	583	2.75	43.48	0.99	43.26	0.99
6304	40.42	3.39	27.62	8.04	4.44	806	3.46	265	501	3.03	50.44	1.34	50.20	1.34
6305	42.34	3.41	27.13	7.04	4.20	809	4.02	227	431	6.06	58.15	1.49	47.67	1.47
6306	42.24	3.42	26.71	6.28	3.65	809	4.38	209	388	7.20	60.90	2.09	60.32	2.07
6307	43.59	3.59	26.11	4.81	3.59	811	5.04	181	350	10.89	50.52	1.92	49.64	1.89
6308	45.32	3.51	24.42	4.29	3.64	813	6.2	147	281	17.52	48.11	2.28	46.70	2.22
6309	48.49	3.45	24.89	4.03	2.88	814	7.5	121	246	24.62	28.53	1.55	26.56	1.44
6601	46.22	3.29	26.34	5.49	3.90	813	5.0	183	350	15.15	43.49	1.66	42.28	1.61
6602	44.94	3.45	27.13	6.32	3.91	813	4.38	209	380	12.78	57.40	2.01	56.38	1.98
6603	42.78	3.26	26.28	6.95	4.34	812	3.94	232	431	11.36	59.44	1.84	58.53	1.81
6604	42.55	3.62	27.66	7.87	4.04	810	3.5	261	501	7.48	41.44	1.10	40.84	1.09
6605	40.04	2.96	26.92	8.38	4.04	808	3.0	305	583	3.60	62.09	1.42	61.80	1.41
6606	36.64	3.28	27.74	10.50	4.64	805	2.5	366	685	1.26	59.40	1.16	59.30	1.15
6607	34.41	3.15	27.30	12.61	5.41	800	2.0	457	838	0.00	63.88	1.02	63.88	1.02
6608	36.80	3.20	28.13	9.41	5.21	820	2.0	457	850	0.00	81.82	1.28	81.82	1.28

Table 3.5. Disc and reactor wall materials

Experiment	Disc	Reactor wall
47	nickel	silica
48	copper	silica
50	nickel	silica
51	nickel	silica
52	iron	silica
53	iron	silica
54	silica	silica
55	copper	silica
56	iron	silica
57	silica	silica
58	iron	silica
59	copper	copper
60	copper	copper
61	copper	nickel
62	copper	nickel
63	copper	iron
66	copper	iron

3.7.5. A consideration of tar production

The values of the tar concentration as moles % anthracene were those obtained in section 3.7.4. (ii). The data are liable to an accumulation of errors from the gas composition and gas flow rate measurements.

Graphs 3.56.- 3.62 show the effect of the inlet residence time on the production of aromatics at 810°C . The line on each of these graphs is drawn in the same position and although many of the points are scattered about the line, a general trend is observed : the production of aromatics increases with increasing inlet residence time. The presence of different metals as reactor liners has no significant effect on the production of aromatics. The influence of a "clean" liner appears to be similar to a carbon covered liner. Those materials which are active for carbon deposition (nickel and iron), exhibit the same behaviour for aromatic production as those materials which are non-active for carbon deposition (copper and silica).

Graphs 3.63. and 3.64. show the effect of temperature on the production of aromatics at $\tau = 2.0$ secs. Small differences between the experimental runs may account for the series of different lines. However, a general trend is observed : the production of aromatics increases with increasing temperature.

3.7.6. Mass spectrometric measurement of tar production

As discussed in the introduction, the mass spectrometer system was developed to give fast sampling and to allow the identification of free radicals. The system was designed to give fast sampling, via the molecular beam, from a reactor into which various metal surfaces could be placed. As a result of the time needed to bring the apparatus on-line, it was not possible to use this apparatus to its full extent. The design of the reactor, figure 2.8. , was outlined in section 2.7.1. Two earlier reactors were made to a different design, the jet-stirred chamber of these reactors being constructed from a quartz D45 cone

and socket. These reactors were designed to permit the jet assembly (mounted on the socket), to be parted from the base assembly (joined to the cone), enabling the insertion of metal foil liners. Difficulties were encountered with these reactors, in that the base plate was found to crack, and separation of the cone and socket joint after reaction was almost impossible. As a result, the modified reactor shown in figure 2.8. was developed, and, due to lack of time, a programme of runs was carried out based on the obtainable objectives using that reactor.

To avoid base plate cracking, experiments at a range of increasing temperatures were carried out. In all, the experiments covered the following reaction conditions:

Reactor temperature	= 600, 650, 700, 750, 800°C
Reactor pressure	= 200, 300, 400 torr
Inlet residence time	= 0.6, 0.8, 1.0, 1.5, 2.0, 2.5, 3.0 sec.

Operating the reactor at 750°C, with a reactor pressure of 400 torr and an inlet residence time of 2.23 sec., a complete analysis of the tars was carried out up to 290 atomic mass units (a. m. u.). The settings on the mass spectrometer were as follows, (Table 3.6.).

The groups of aromatic and polynuclear aromatic compounds observed, together with their abundance relative to benzene (see later), are given in Table 3.7., together with an assignment of possible molecular peaks present. No account was taken of possible cracking products.

Semiquantitative analysis of the results was carried out using the peak height a. m. u. = 78 (benzene) as an indicator. Benzene was found to be the major product amongst the tars from the pyrolysis, but the signal is expected to be proportional to benzene and to cracking products from other hydrocarbons. Time did not allow the distinction of the components.

The peak at a. m. u. 78 was found to be a reliable indicator of the production of tars in general. In selected cases, a full analysis of the tars showed a general tendency for the amount to increase or

Table 3.6. Mass spectrometer settings

Mass range to 290 a. m. u. Detector chamber pressure 5×10^{-7} torr

Electron multiplier voltage 2.75 kV (3 is unit max.)

Sensitivity 2V

Time constant 1 ms

Input resistor 10^7

Zero offset. Off.

Log-linear switch. Linear.

Scope time constant. High.

Function switch. Sweep.

Level. Low.

Resolution. 3 - 75

Δ M. 0.

High calibration. 3 - 84 Calibrated so that the mass meter and
low mass dial must be multiplied by 2
to give the actual mass reading.

Filament amps. + 3.5

Filament volts + 5.8

Electron energy. eV. +70.0

Emmision. mA. + 2.0 (5 is unit max.)

Ion energy +11.0

Extractor - 5.8

Lens 1 -82.0

Lens 2 - 0.2

Lens 3 -66.6

Table 3.7. Mass spectrometer analysis

<u>Group (a. m. u.)</u>	<u>Abundance</u>	<u>Assignment</u>	
78	100	Benzene.	78. 12
90	40	Toluene	92. 15
105	22	Dimethyl benzene	106. 17
		Ethyl benzene	106. 17
continuous up to 128	18	Substituted benzenes	
130	60	Naphthalene	128. 19
135	20	Diethyl benzene	134. 22
		Butyl benzene	134. 22
145	45	Methylnaphthalene	142. 20
continuous up to 180	8	Diphenyl	154. 21
		Dipropyl benzene	162. 23
		Substituted naphthalenes	
		Fluorene	166. 23
180	40	Anthracene and phenanthrene	178. 24
205	10	Pyrene and fluoranthene	202. 26
230	7	Chrysene	228. 30
250	5	Perylene	252. 35
280	5	Picene	278. 36

decrease as peak a. m. u. 78.

The effect of increasing inlet residence time on the "benzene" peak is shown for all five temperatures in graph 3.65. During these runs, the reactor pressure was held at 200 torr. At short inlet residence times (< 1 sec.) and low temperatures (600°C), no aromatic species could be detected.

Similar trends were observed when the reactor pressure was held at 300 torr (graph 3.66) and 400 torr (graph 3.67). An increase in reactor temperature and inlet residence time led to increased tar production. These results agree with the observations made on the basis of carbon balances (section 3.7.5.) where tar production was found to increase with inlet residence time and temperature.

Although quantitative analysis is difficult between these runs, a general trend of increasing tar with increasing pressure could also be distinguished. As a result, experiments designed to elucidate this trend were carried out. Increasing the reactor pressure was found to increase the tar production at all temperatures (graphs 3.68 - 3.72).

It was possible to estimate the sensitivity of the instrument in several ways. No quantitative measurements were made but approximate estimations gave the sensitivity of the instrument to benzene and picene. The tar formation calculations (section 3.7.4.) show that at 800°C and 2.5 secs. inlet residence time, tars are produced at a rate of approximately 40 mg. carbon/min. Allowing for the difference in reactor pressure, the peak height of benzene from the mass spectrometer (100 units) is equivalent to 6 mg. carbon/min., and that of picene (5 units) is equivalent to 0.3 mg. carbon/min. This is equivalent to 0.08 moles/min. of benzene and 0.001 moles/min. of picene.

3.8. Carbonisation and carburisation of metal liners

The carbon deposits on iron and stainless steel liners, and the foils, were examined by metallography, electron probe micro-analysis and X-ray diffraction by the Analytical Services Laboratory of Imperial College to ascertain whether the transport of metal into the carbon and carbon into the metal had occurred.

3. 8. 1. Examination of metal liners from the jet-stirred reactor

The liners and their deposits, were those obtained from experiments previously outlined.

Run 64. Iron liner (generating surface) with a copper (collector) disc. The inlet residence time was reduced from 5 secs. by 0.5 sec. intervals. The iron surface remained active and was not encapsulated with carbon.

Run 66. Iron liner (generator) with a copper (collector) disc. The inlet residence time was reduced. The liner quickly became encapsulated with carbon.

Run 75. Stainless steel liner (generator) with a copper (collector) disc. The inlet residence time was reduced. The rate of deposition observed on the copper collector disc, was less than the "carbon on carbon" rate. Previous results had shown that a stainless steel collector disc exhibited a deposition rate which was higher than the "carbon on carbon" rate. These results indicated that stainless steel has a high affinity for carbon. In the stainless steel liner system, less carbon is available for collection on the suspended copper disc than in the "carbon on carbon" system.

3. 8. 2. Metallography and microscopic examination

a) Control samples (unused foil)

(i) Iron

This showed a structure of squashed ferrite (α - iron) grains with an even dispersion of pearlite nodules (lamellar structure of alternate layers of α -iron and cementite, Fe_3C). (Pearlite is much stronger than ferrite alone). The pearlite appears to be associated with some free nodular cementite. The abundance of the pearlite constituent indicates an overall carbon content of about 0.04% by weight. The overall structure indicates a history of subcritical annealing (below $727^{\circ}C$) for stress relief during rolling, followed by full annealing above $727^{\circ}C$ after rolling.

(ii) Stainless steel EN58E

Supplier's (Goodfellow Metals) listed composition :

C < 0.07%; Cr 17-19%; Ni 9-11%. The structure is that normally expected for EN58E stainless steel sheet material. Due to the very low carbon content, 0.07% by weight, the carbides, very finely divided, would not be obtrusive at the magnification available (up to x 1000 diameters).

b) Carbon deposited foils

(i) Iron. Run 64. Active (not encapsulated)

The sample showed fairly large grains (25-50 μm) which were mainly lamellar pearlite (fairly coarse), with interspersed white material, presumably ferrite. The picrate confirmed the carbide (cementite) in the pearlite and also that the white material remained white and was therefore ferrite and not pearlite. Visual estimation showed about 80-90% pearlite, or about 0.75-0.80% carbon. The structure extended throughout the thickness, including the carbon face.

(ii) Iron. Run 66. Carbon encapsulated

The central band was similar to that of the previous sample (run 64), mainly pearlite, but the carbon face in many places had a white layer about 20-30 μm wide. The white layer contained fine black lines surrounding small areas. As it was uncertain what this material was, the picrate etch was carried out and this showed that the small white areas were coloured and hence cementite, while the white areas around them remained white and were ferrite. The carbide in the pearlite also showed up as dark areas.

(iii) Stainless steel. Run 75

The hydrochloric acid/ethanol etch showed a pattern of grain boundaries throughout, but at the carbon face an additional darkening and etching of the grains to a depth of about 20-30 μm . The central grains remained white. Re-polishing and etching with cold Murakami's reagent showed up fairly heavy grain boundaries

containing small black particles. There was no visible difference between the carbon face and the foil centre in this case.

3. 8. 3. Microprobe examination

(i) Iron foils. Run 64 and 66:

A qualitative examination showed that nickel and chromium were "absent" (under 0.25%), but a little manganese (0.3-0.5%) was present throughout both samples.

Traces for iron were run across the width of the sample and of the carbon layer. These showed a fairly even trace across the metal and a peak slightly separated in the carbon layer. These peaks were too narrow relative to the x-ray resolution of about $5\mu\text{m}$. to quantify, but clearly show the presence of iron in the carbon layer.

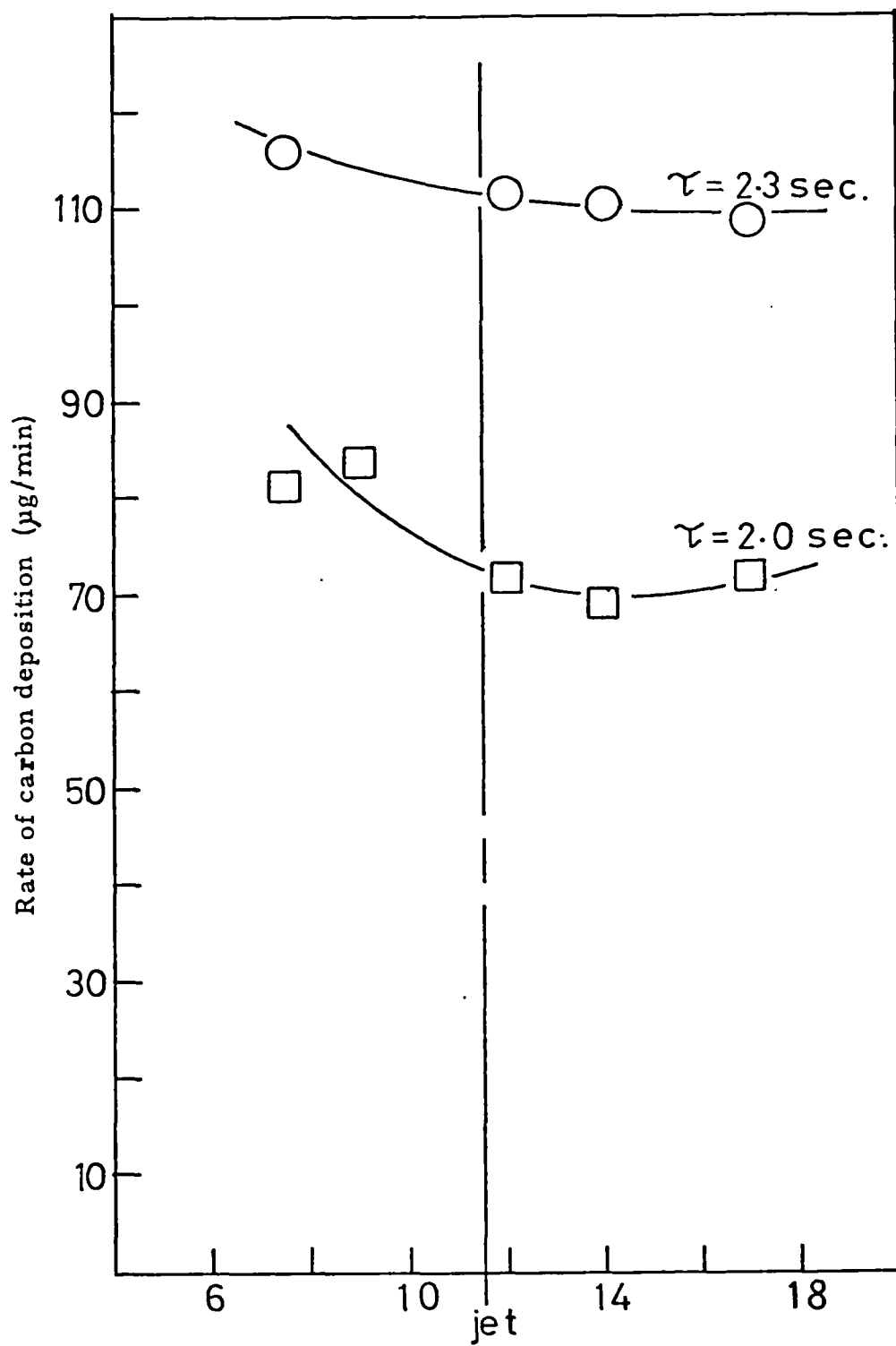
(ii) Stainless steel. Run 75

Traces were run for iron/chromium and then for nickel/chromium. These were a little variable (but insufficiently so to relate reliably to structure), but show a fairly constant iron and chromium content throughout, but an appreciable fall in nickel. No peak for metals was detected in the carbon layer : it should be noted, however, that x-ray diffraction showed the presence of an iron-carbon phase in the carbon deposit.

3. 8. 4. X-ray diffraction

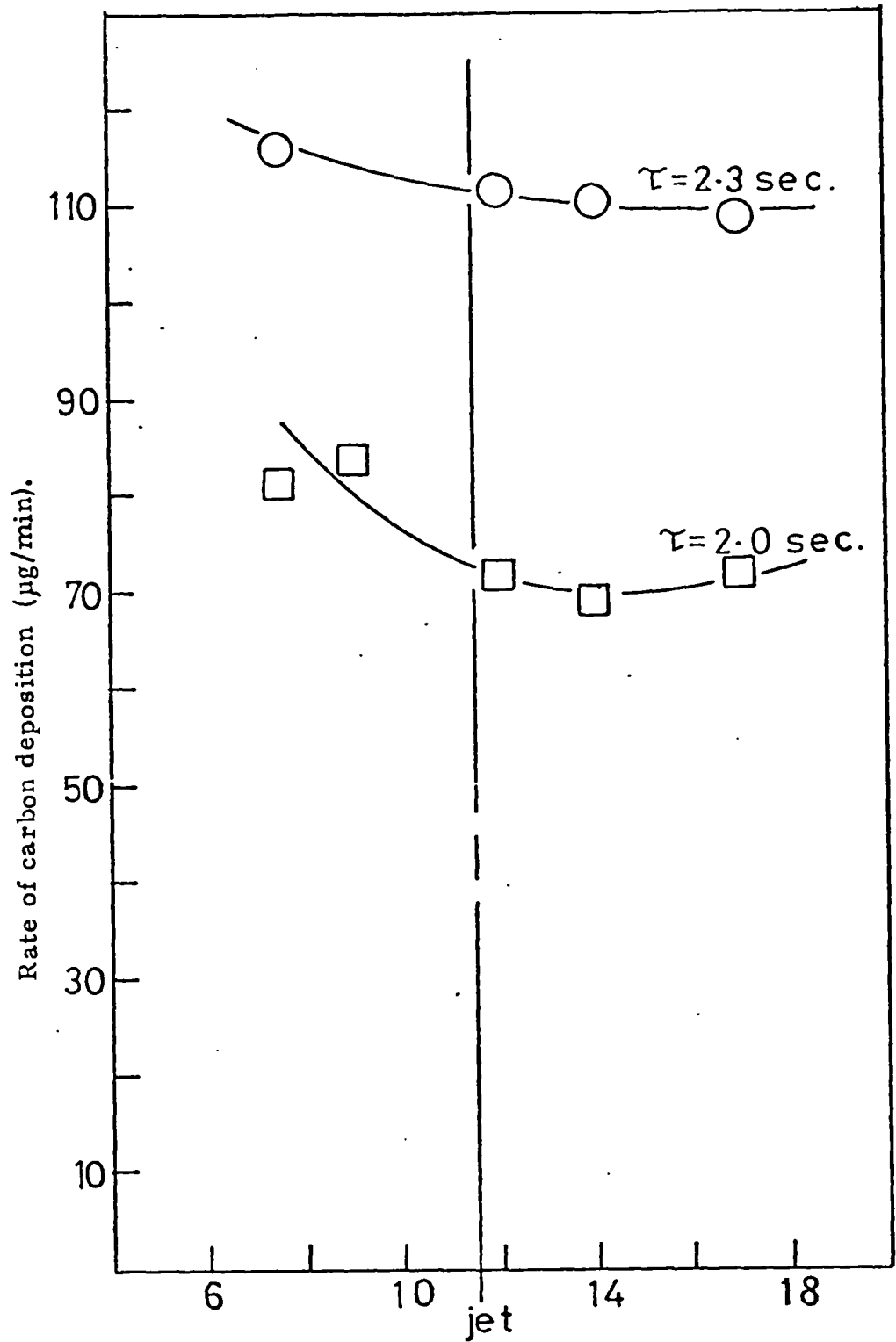
All three samples gave diffractions attributed to graphitic elemental carbon and also an iron-carbon system, showing that iron had diffused into the carbon layer.

3.9 Graphs 3.1 - 3.72



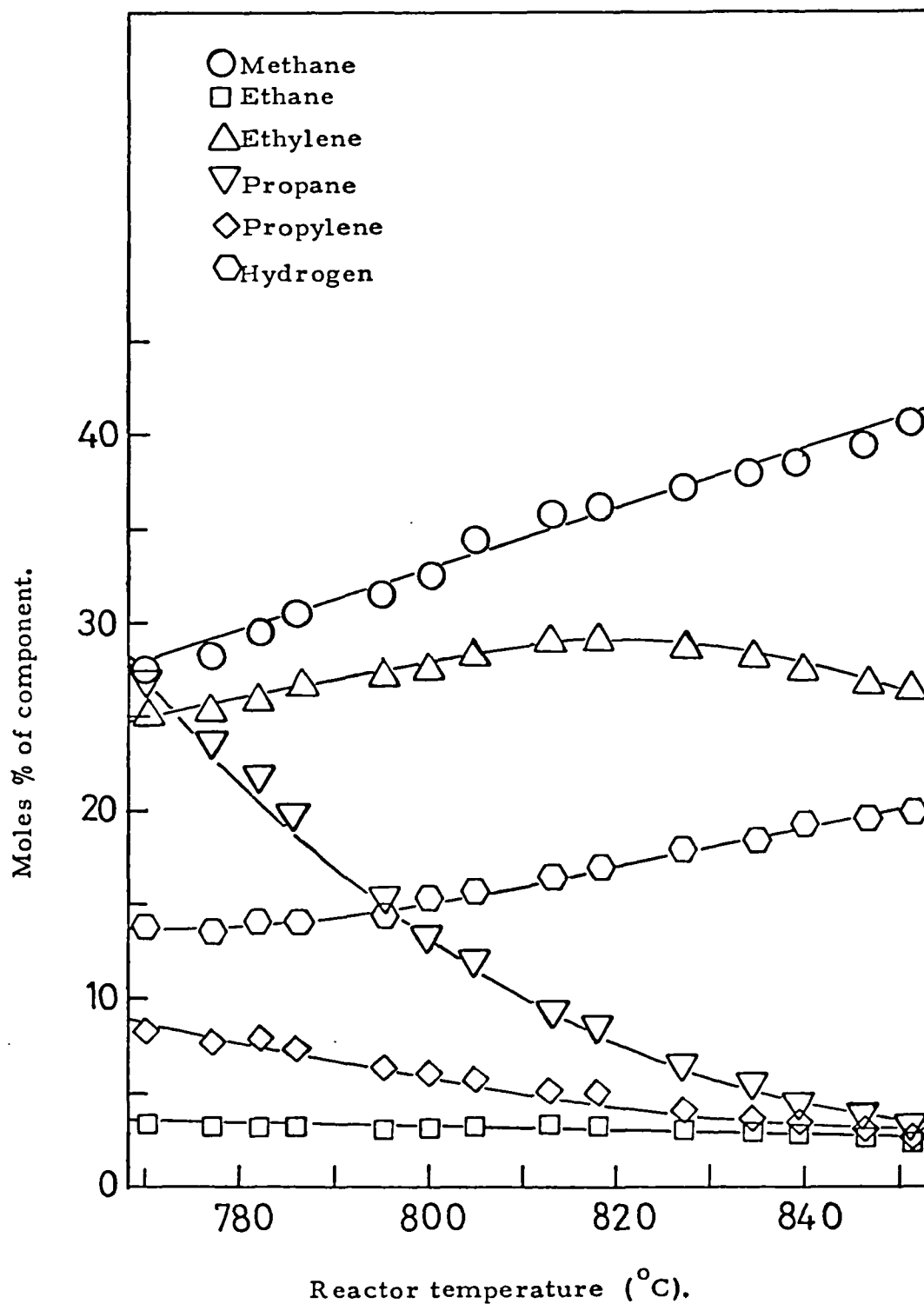
Distance of disc below top of reactor (mm)

Graph 3. 1. 850°C.

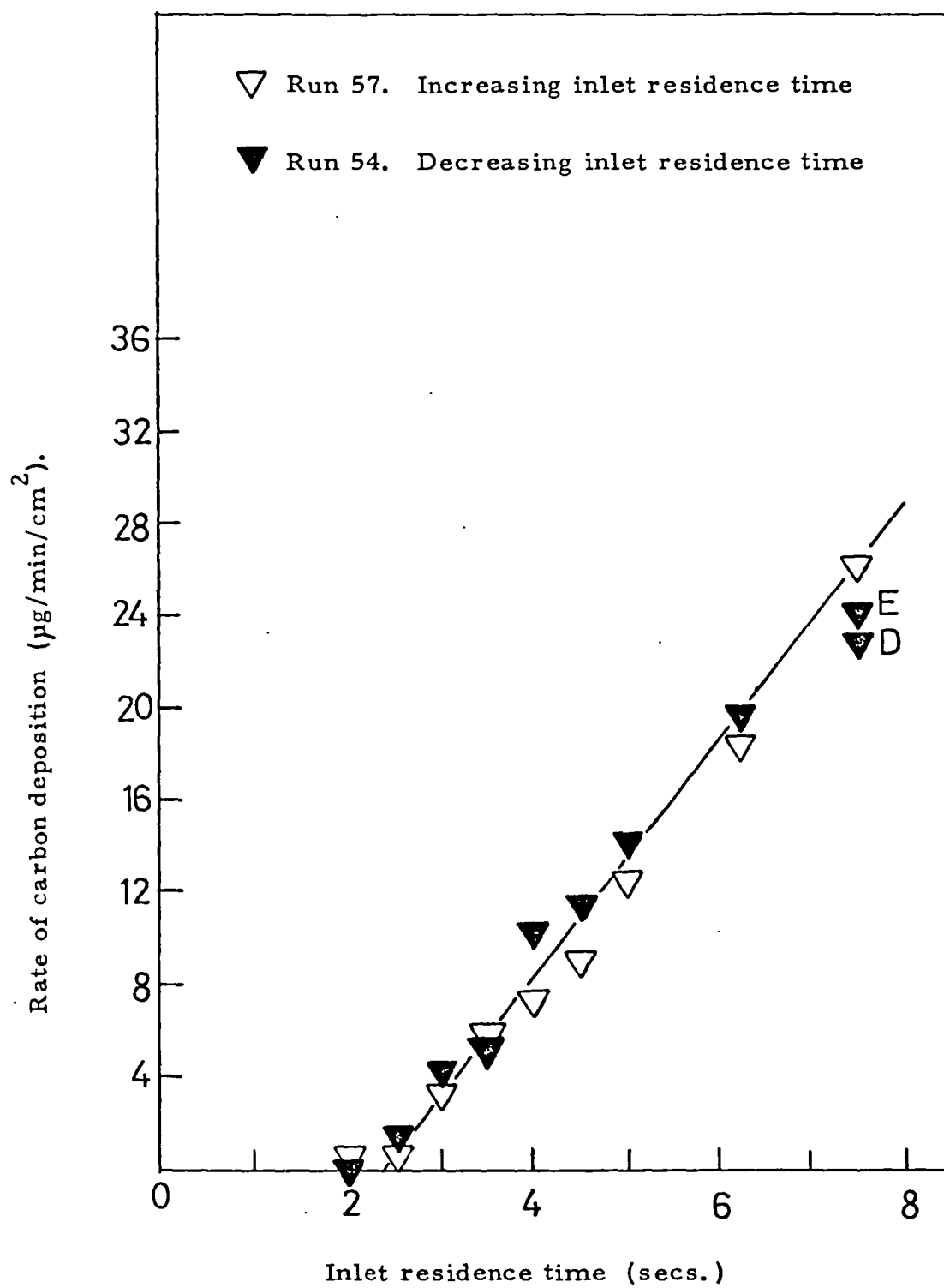


Distance of disc below top of reactor (mm).

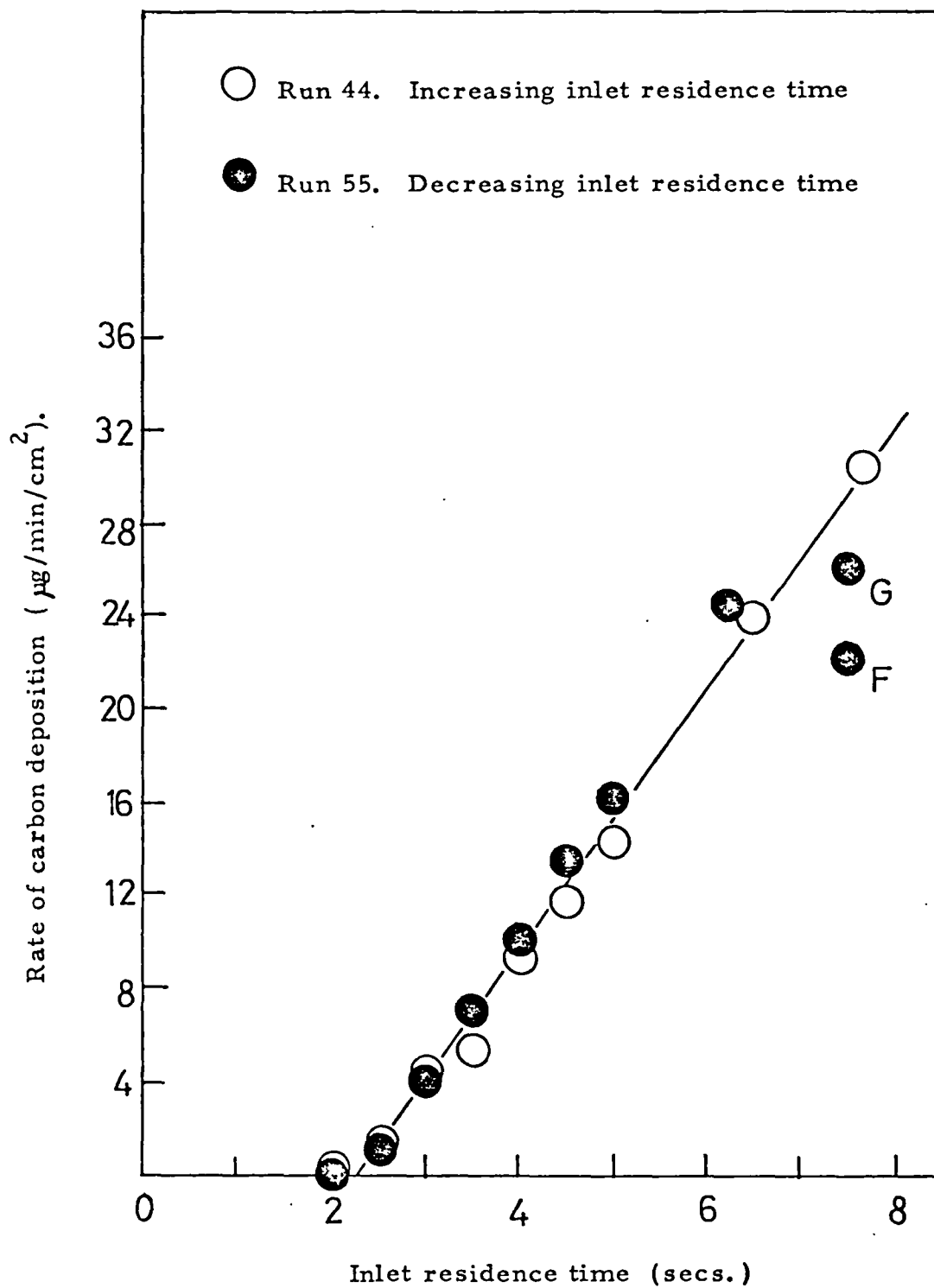
Graph 3.2. 840°C.



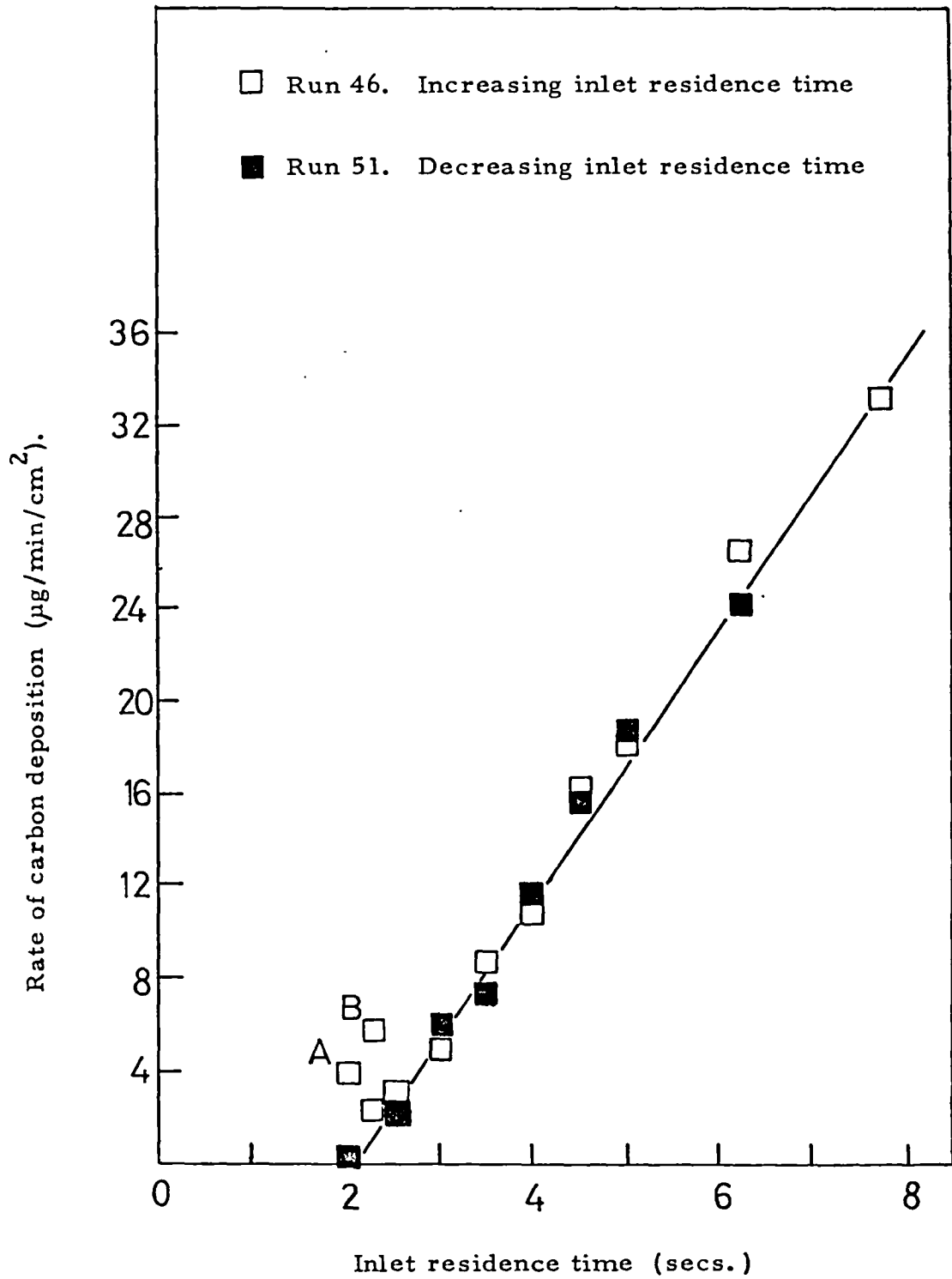
Graph 3.3. Inlet residence time = 2.0 secs.



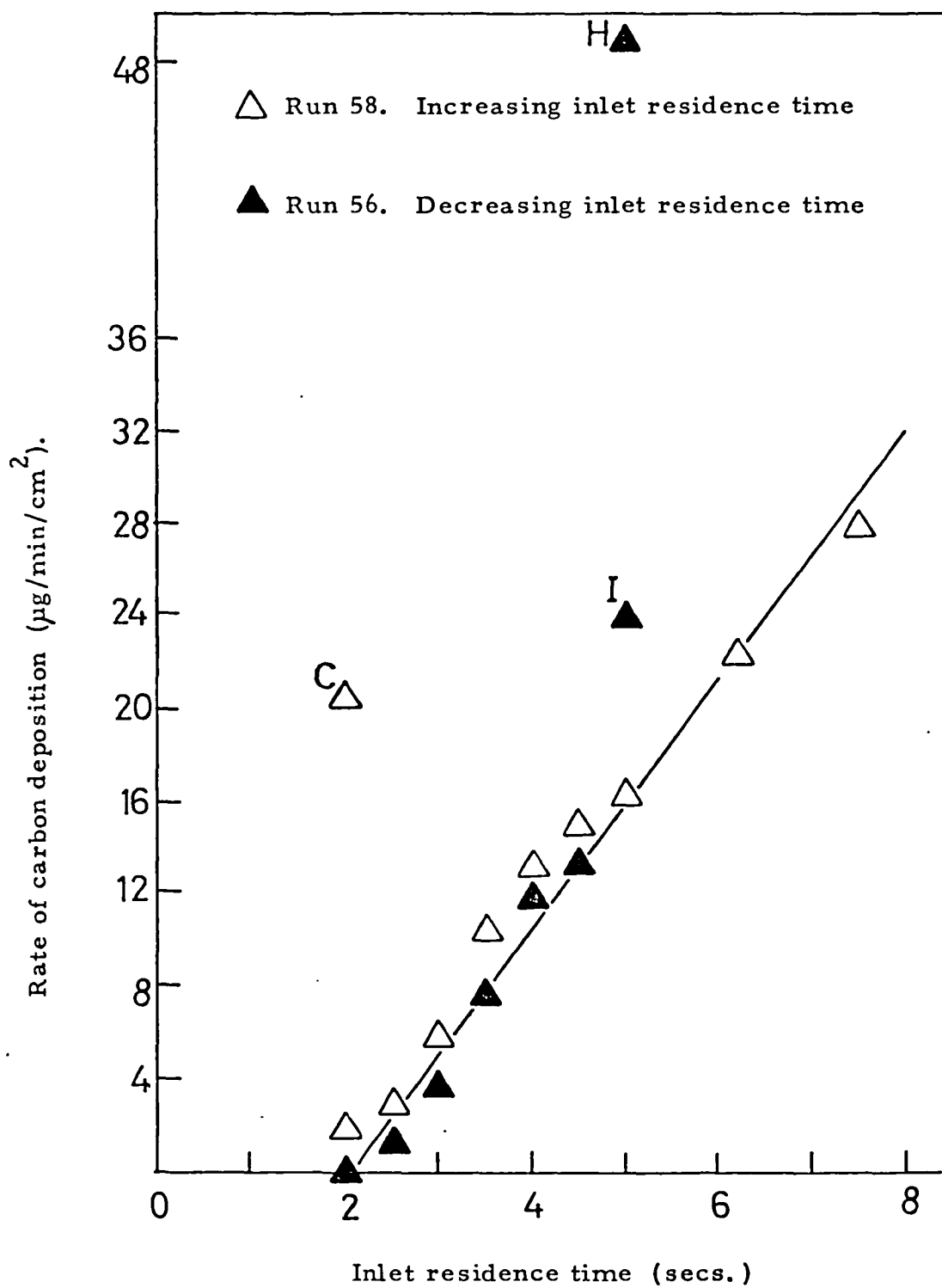
Graph 3.4. Silica disc 810°C .



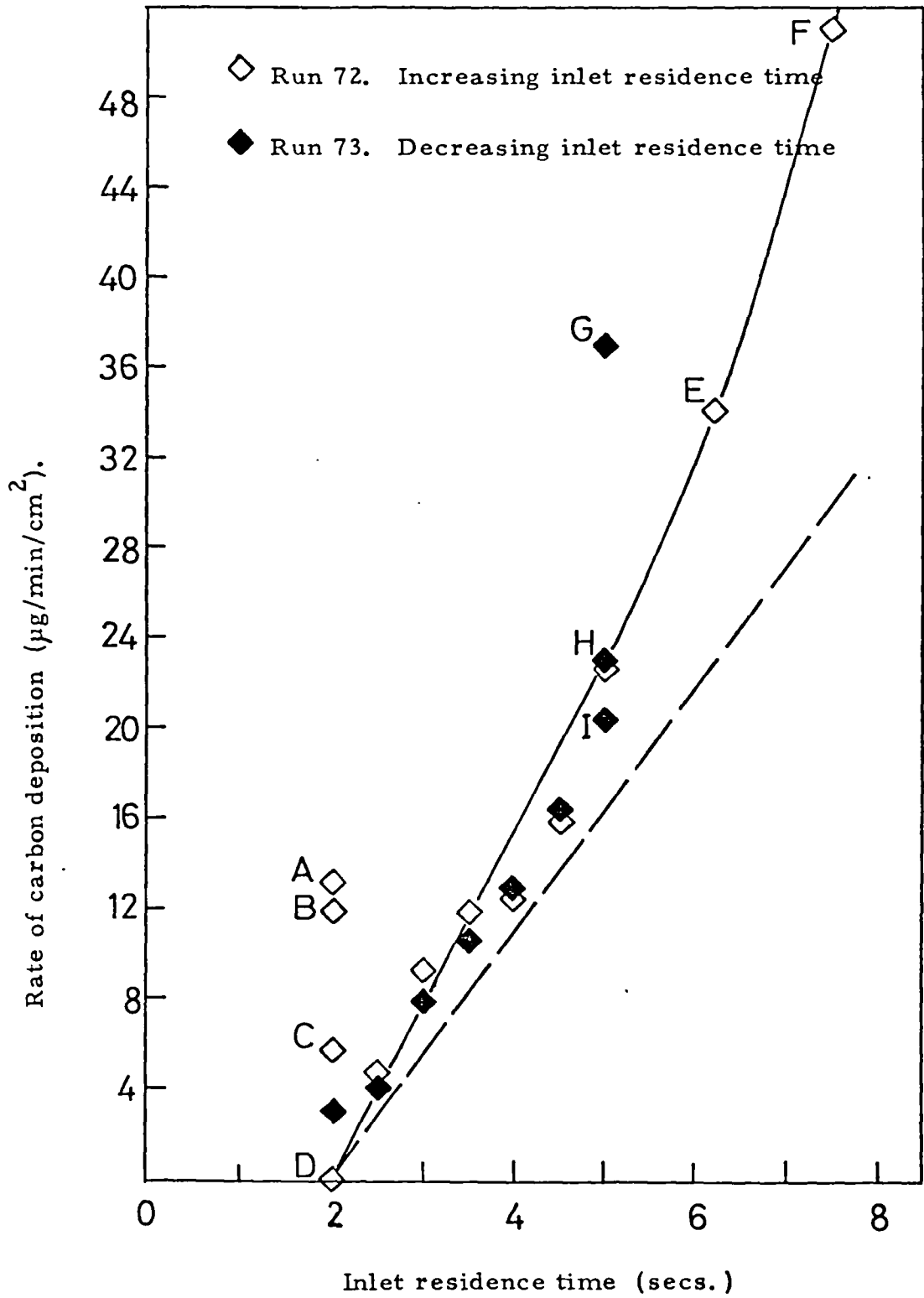
Graph 3.5. Copper disc 810°C .



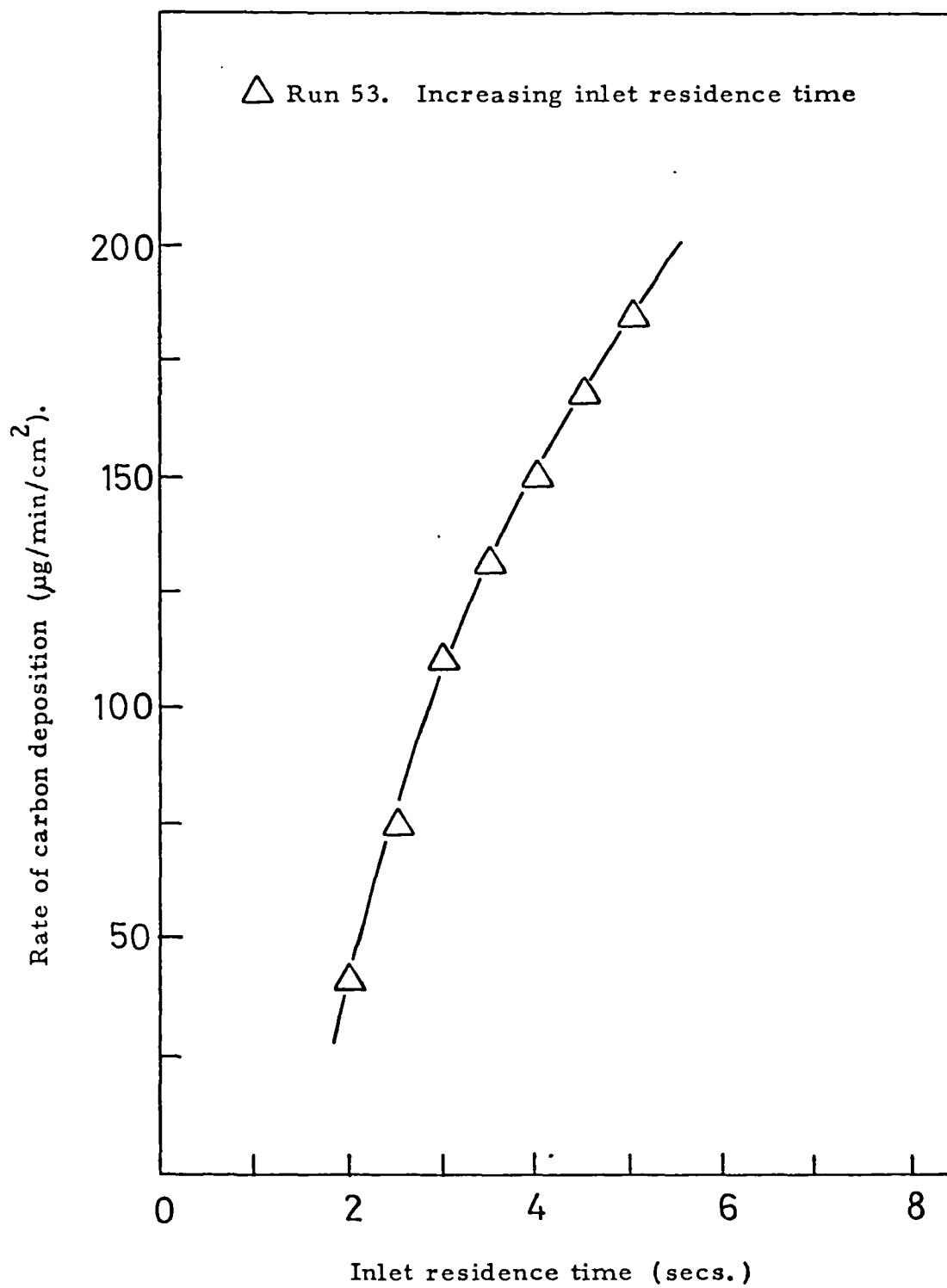
Graph 3.6. Nickel disc 810°C .



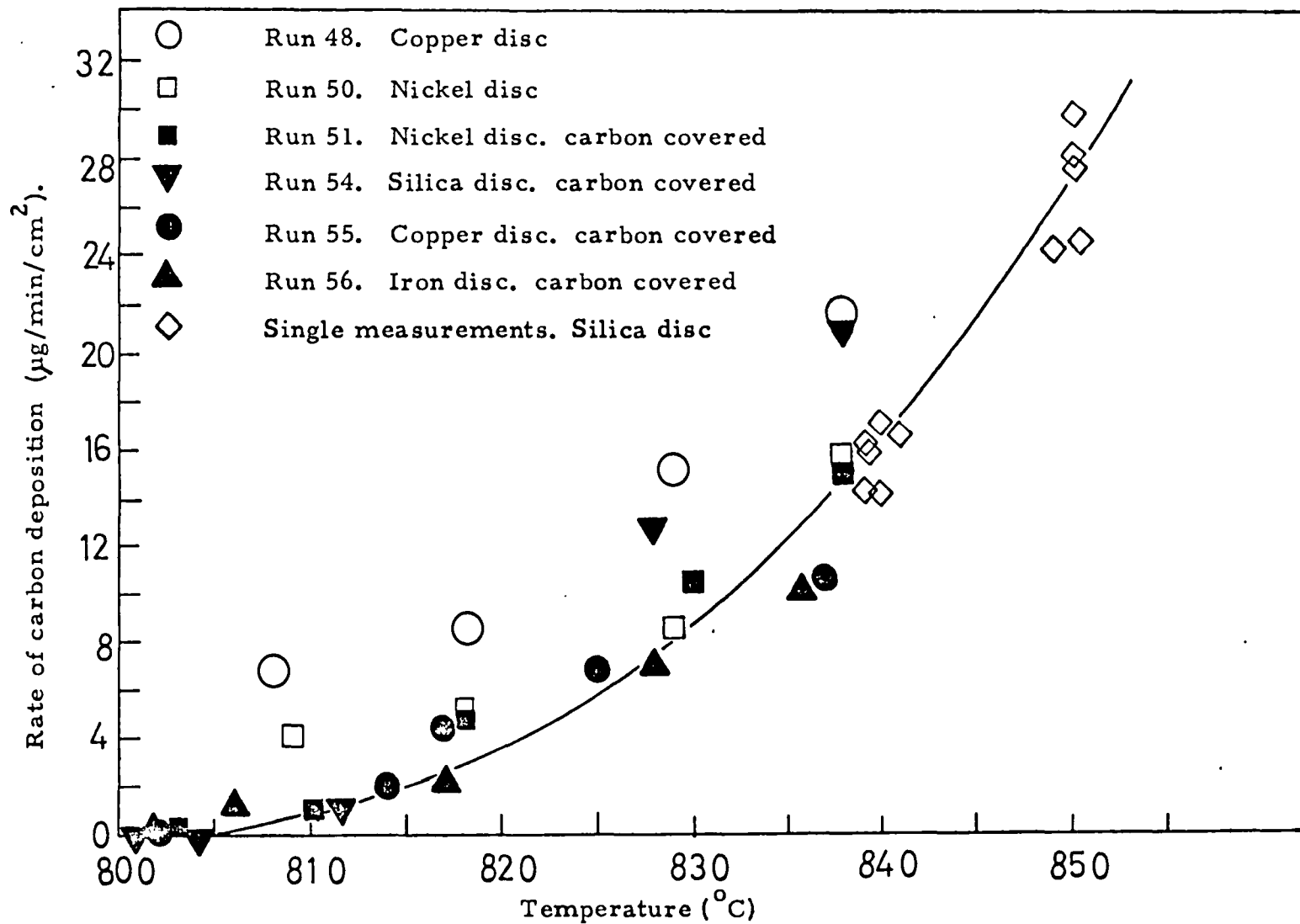
Graph 3.7. Iron disc 810°C .



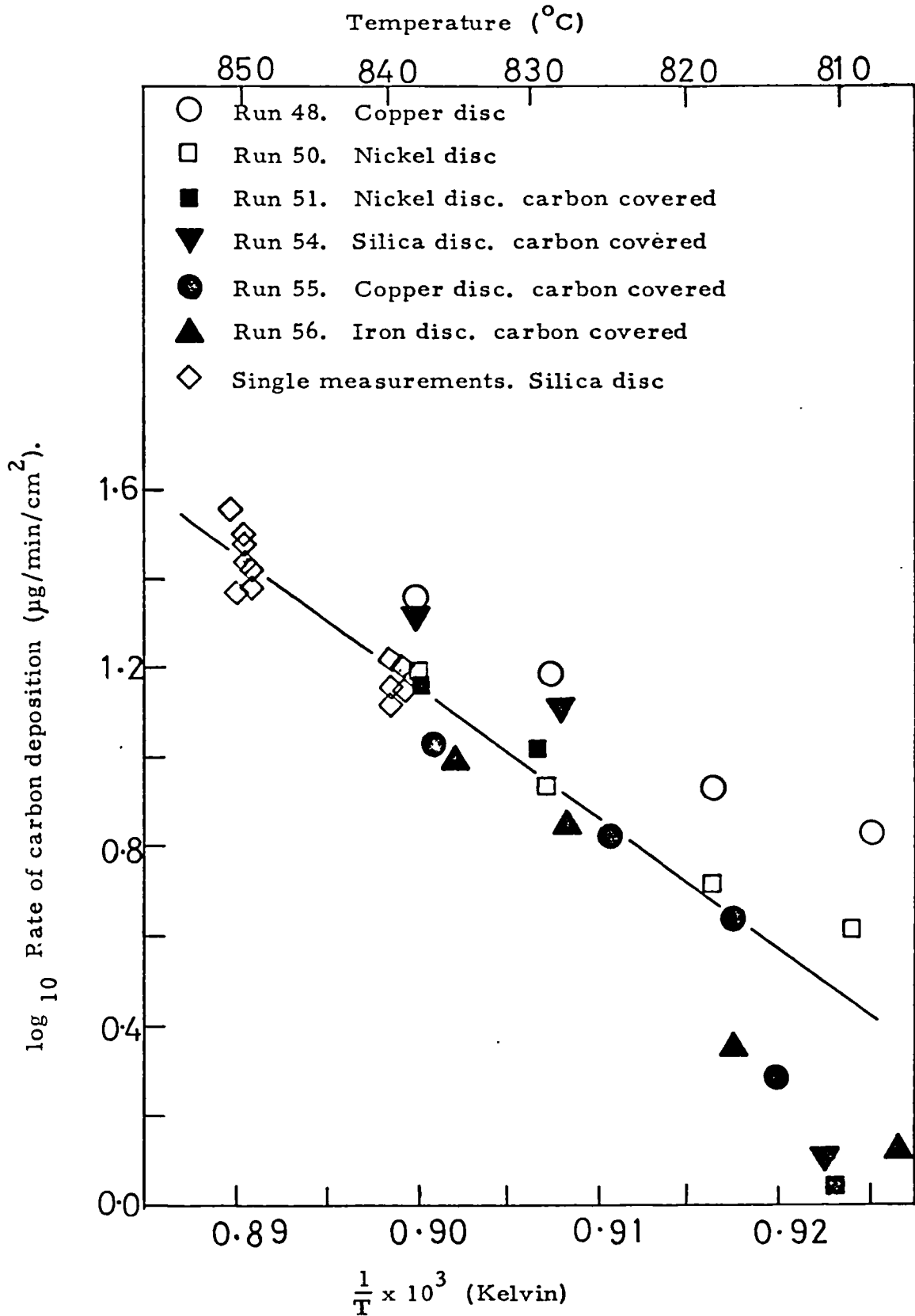
Graph 3.8. Stainless steel disc 810°C .



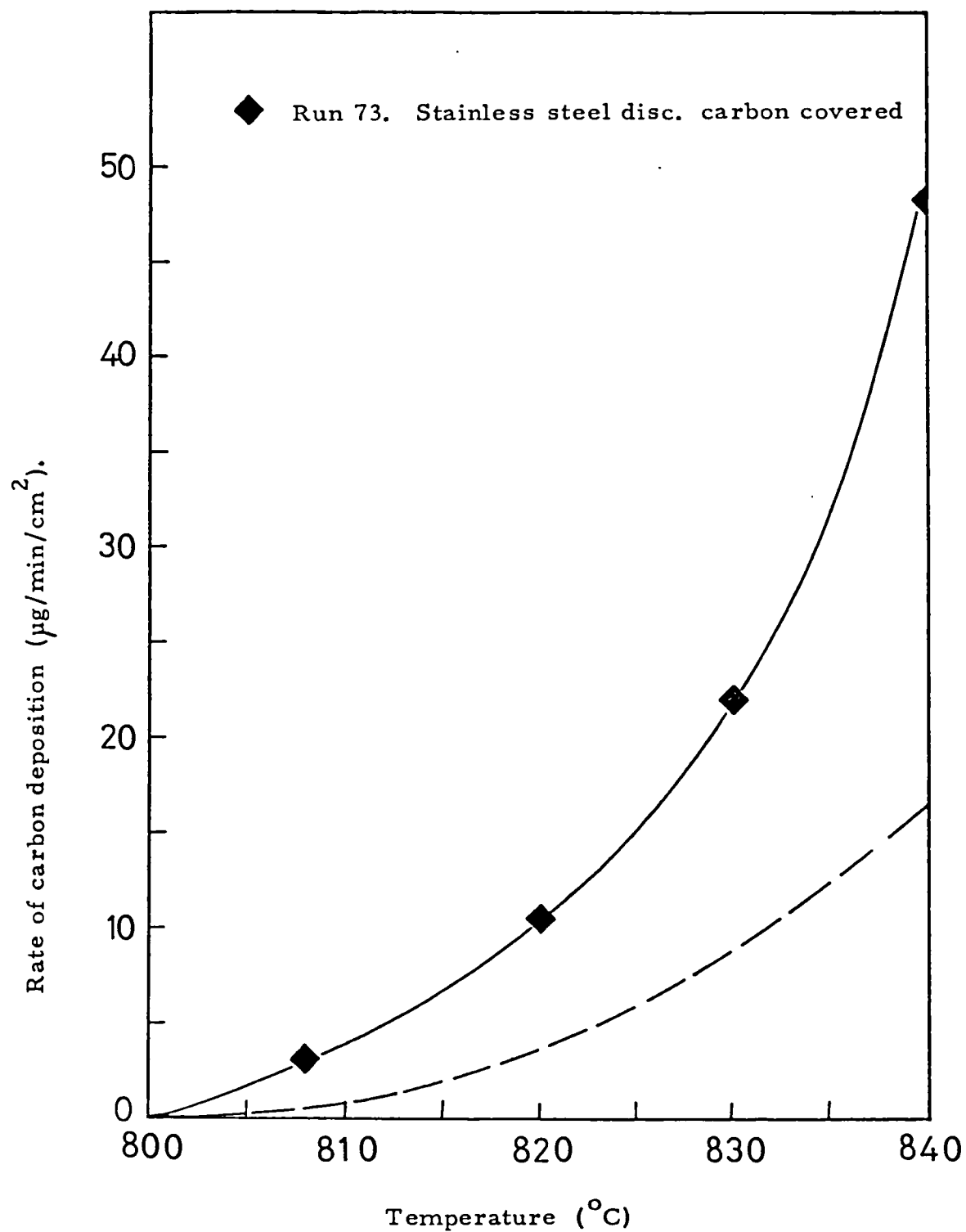
Graph 3.9. Iron disc 810°C .



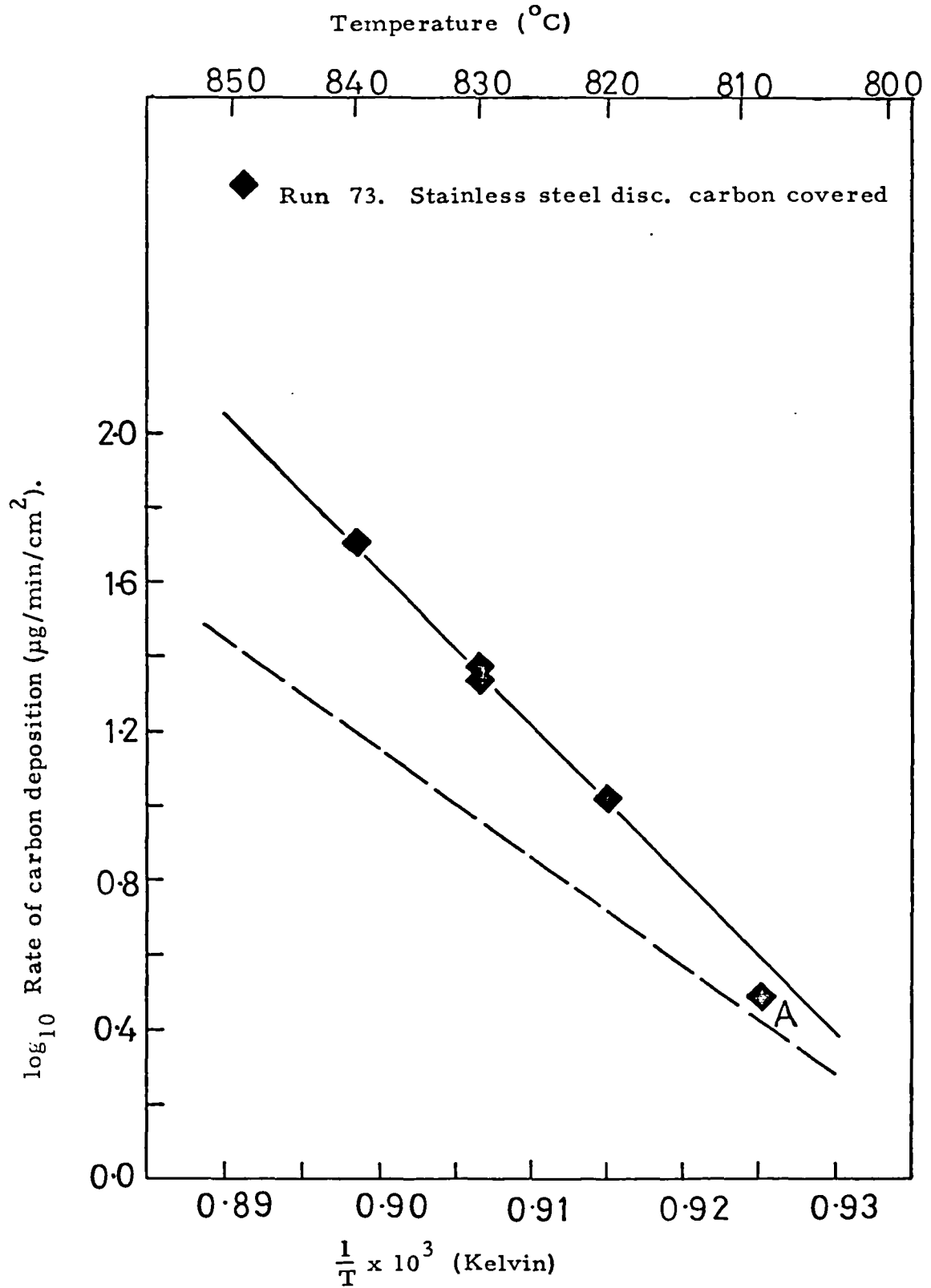
Graph 3.10. Inlet residence time = 2.0 secs.



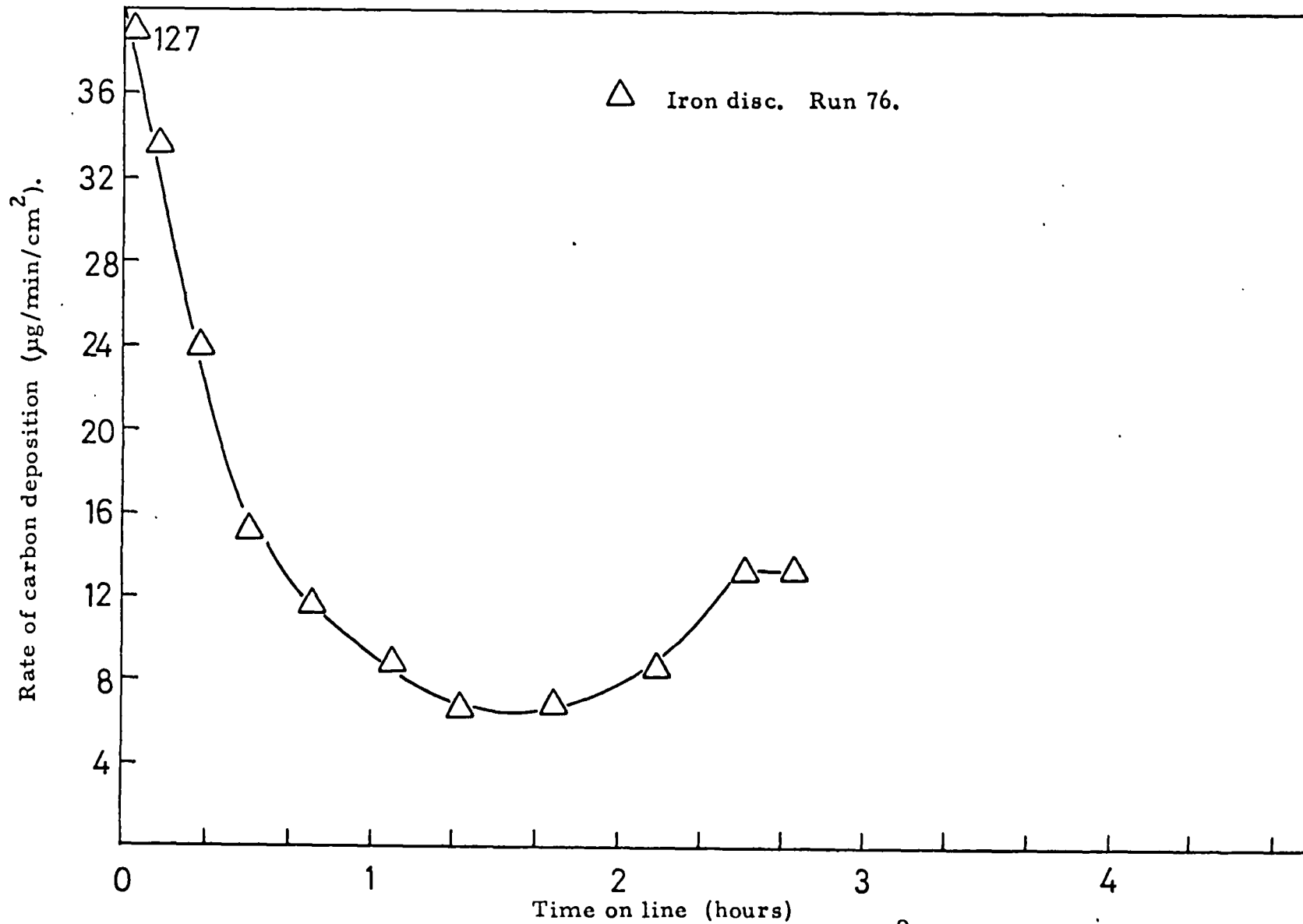
Graph 3.11. Inlet residence time = 2.0 secs.



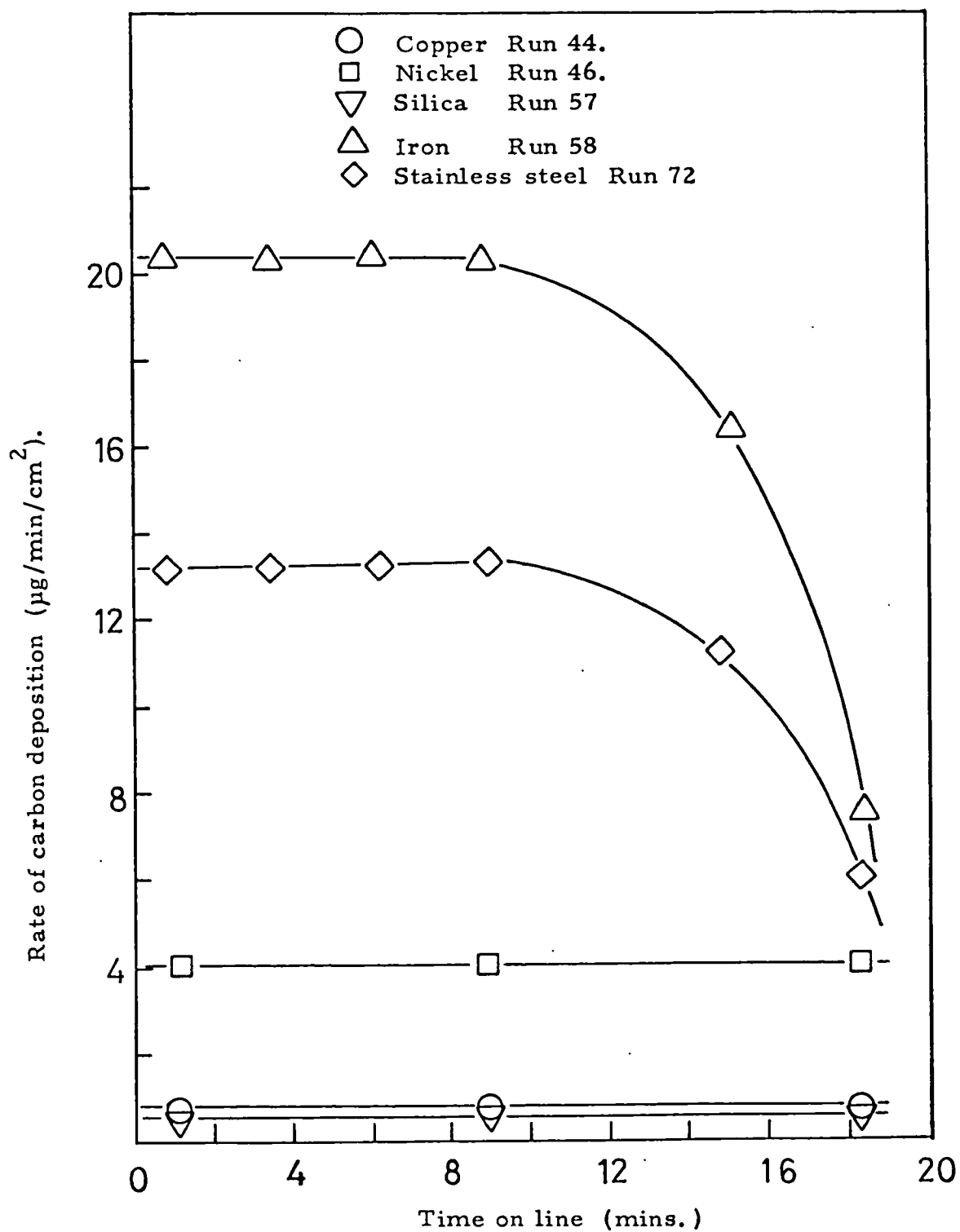
Graph 3.12. Inlet residence time = 2.0 secs.



Graph 3.13. Inlet residence time = 2.0 secs.

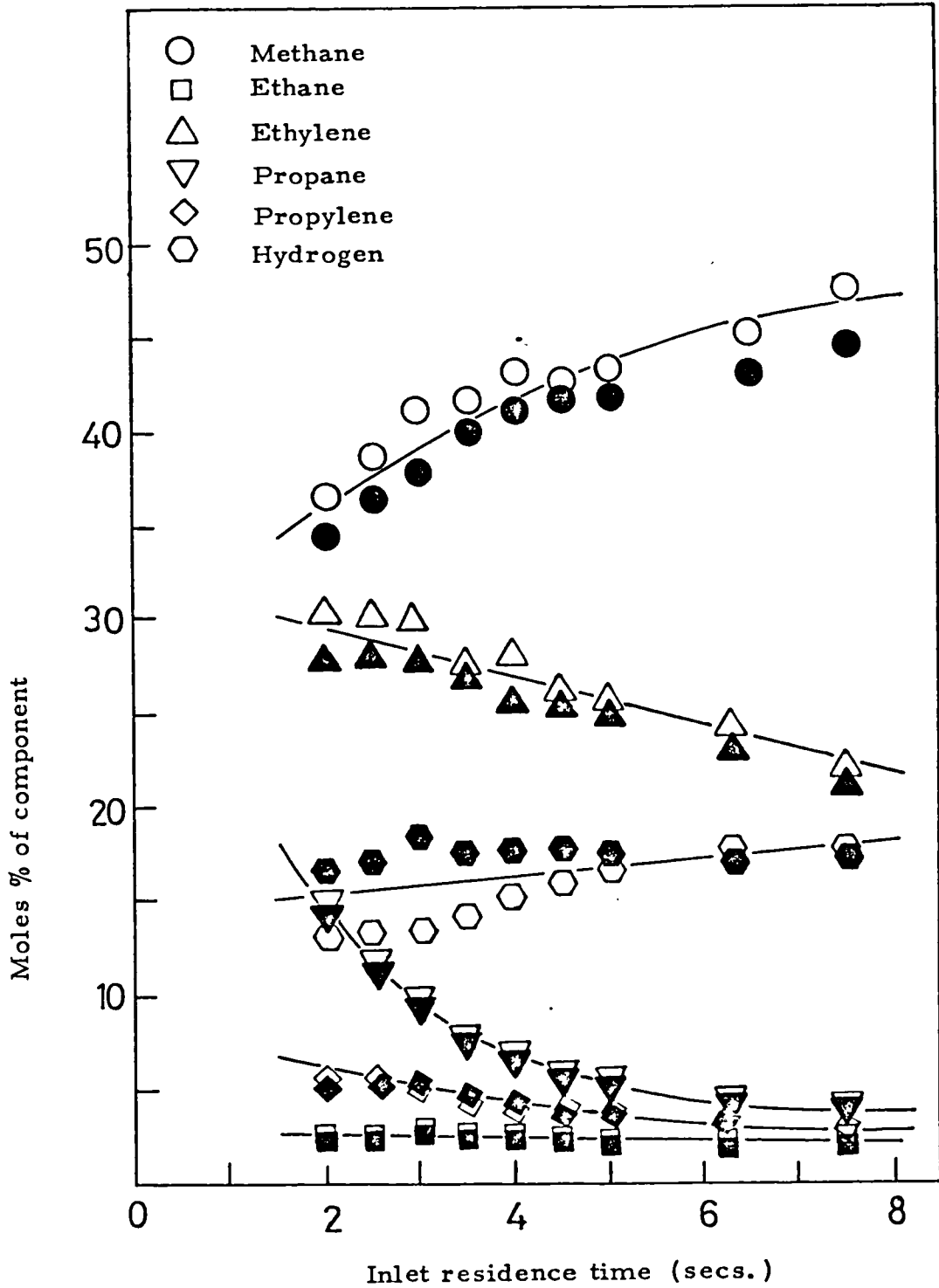


Graph 3.14. Inlet residence time = 2.0 secs. 765°C.



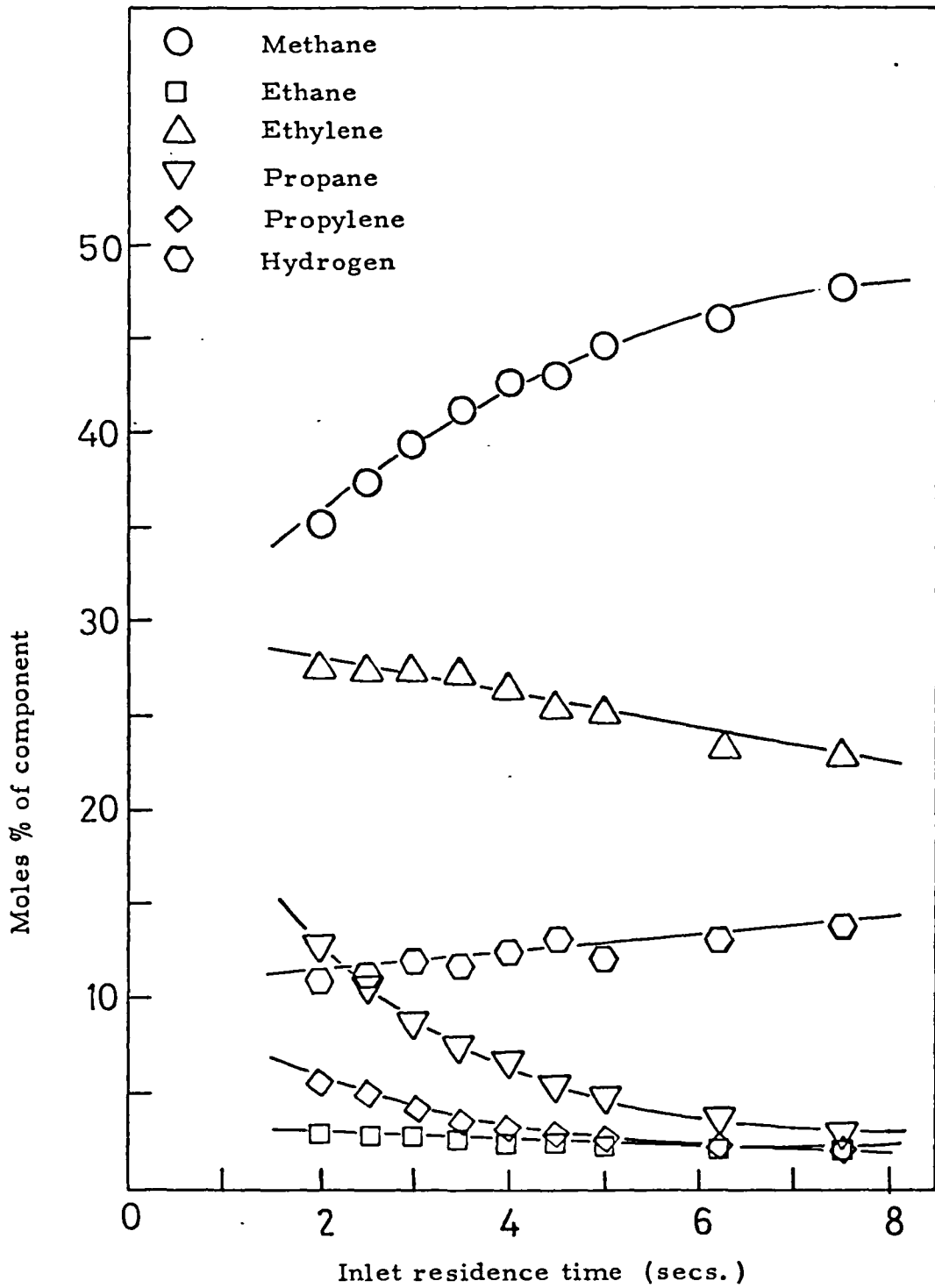
Graph 3.15. Inlet residence time = 2.0 secs. 810°C

Suspended metal discs. No liner

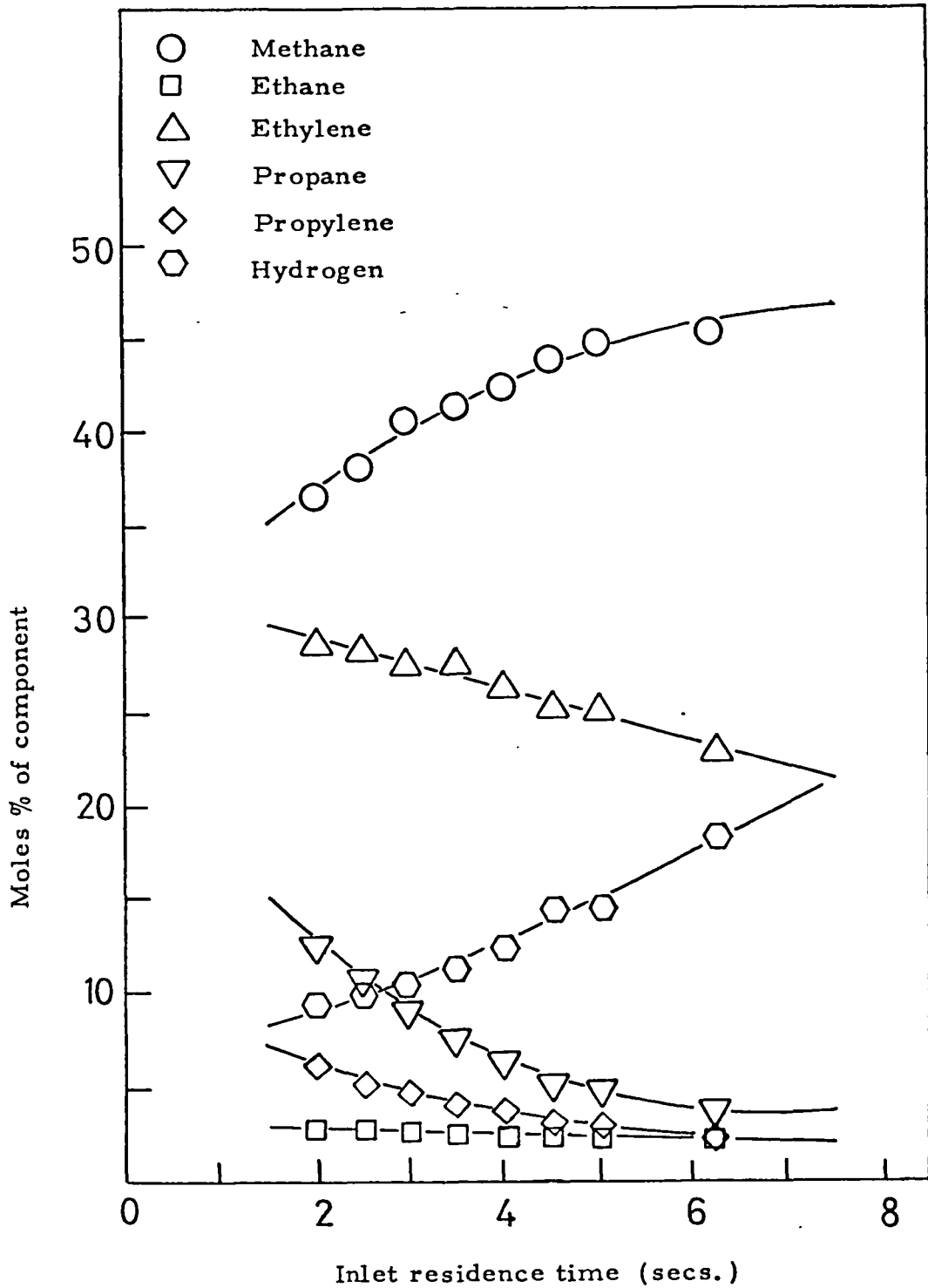


Graph 3.16. Silica disc. 810°C

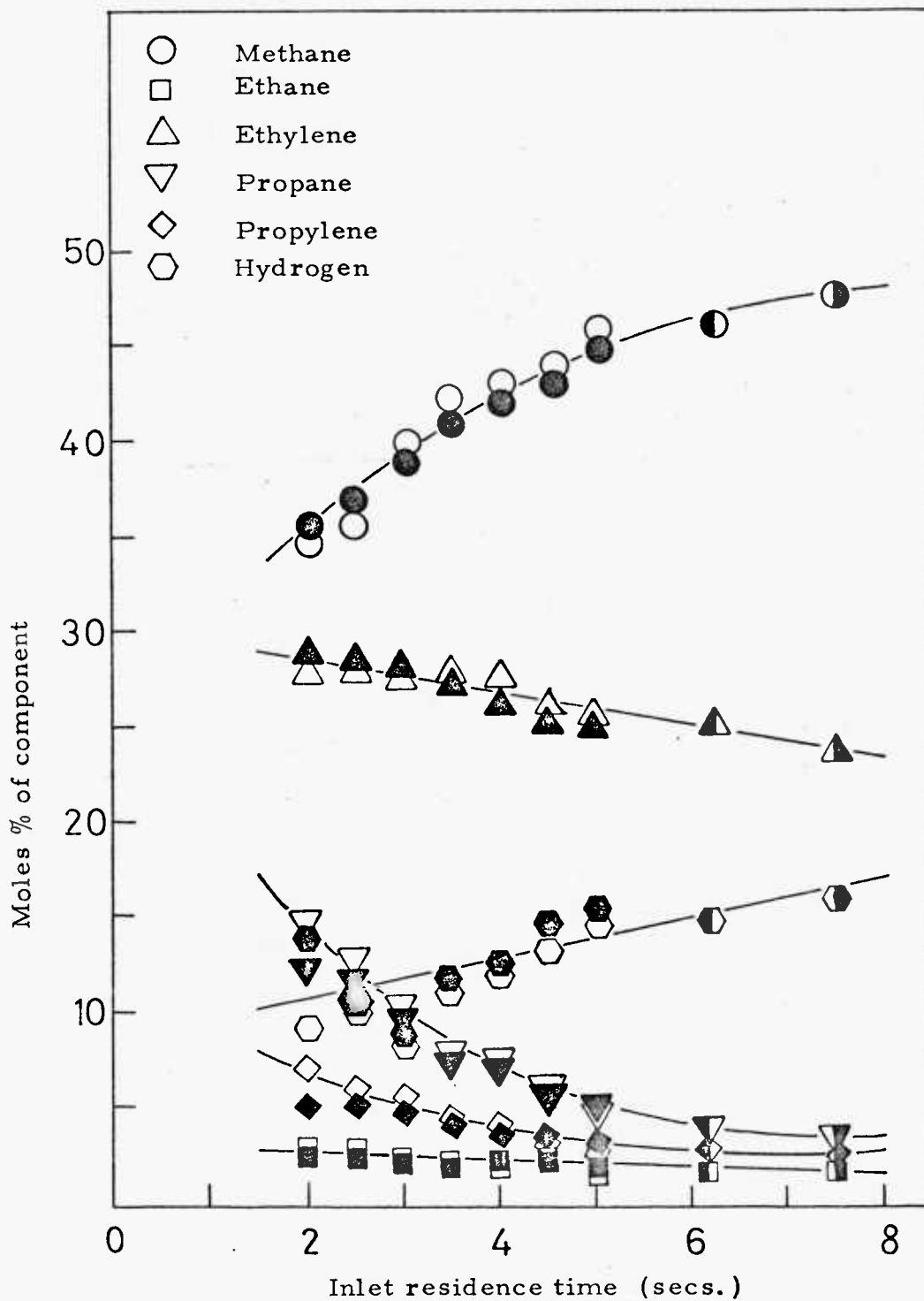
Open symbols, run 54; closed symbols, run 57.



Graph 3.17. Copper disc. 810°C. Run 55.



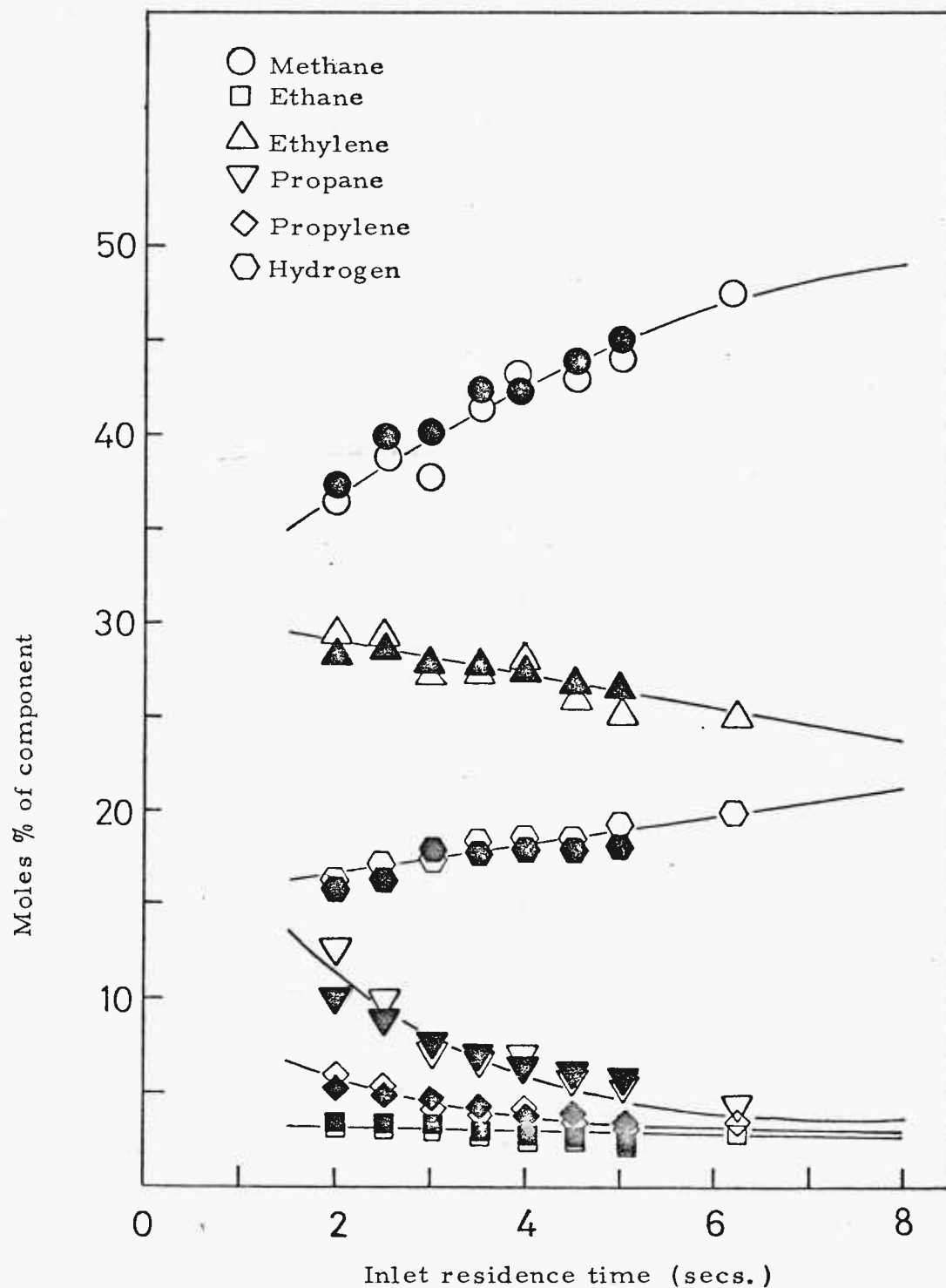
Graph 3.18. Nickel disc. 810°C. Run 51.



Graph 3.19. Iron disc. 810°C.

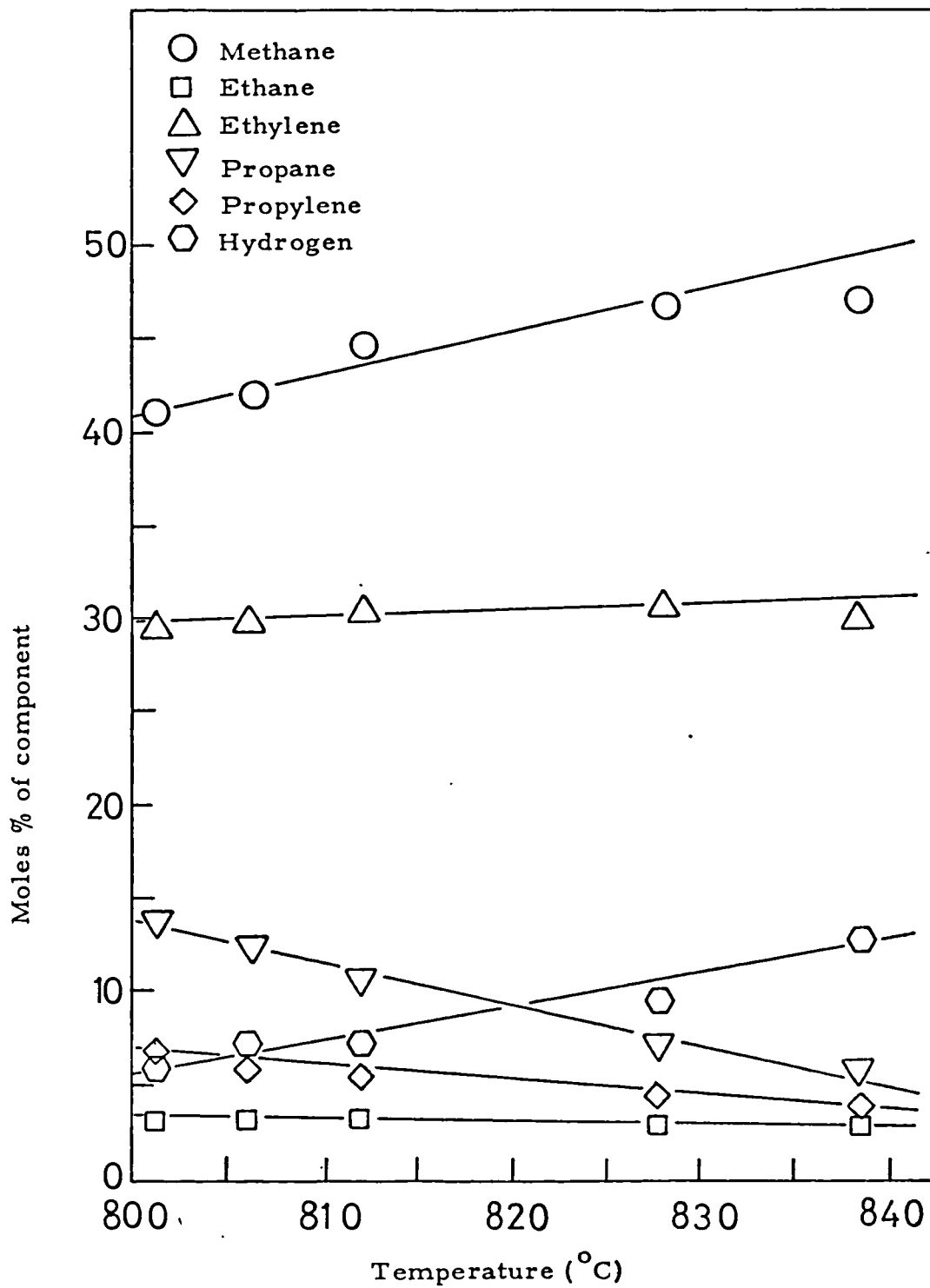
Open symbols, run 53; closed symbols, run 56

Left side closed, run 52; right side closed run 58



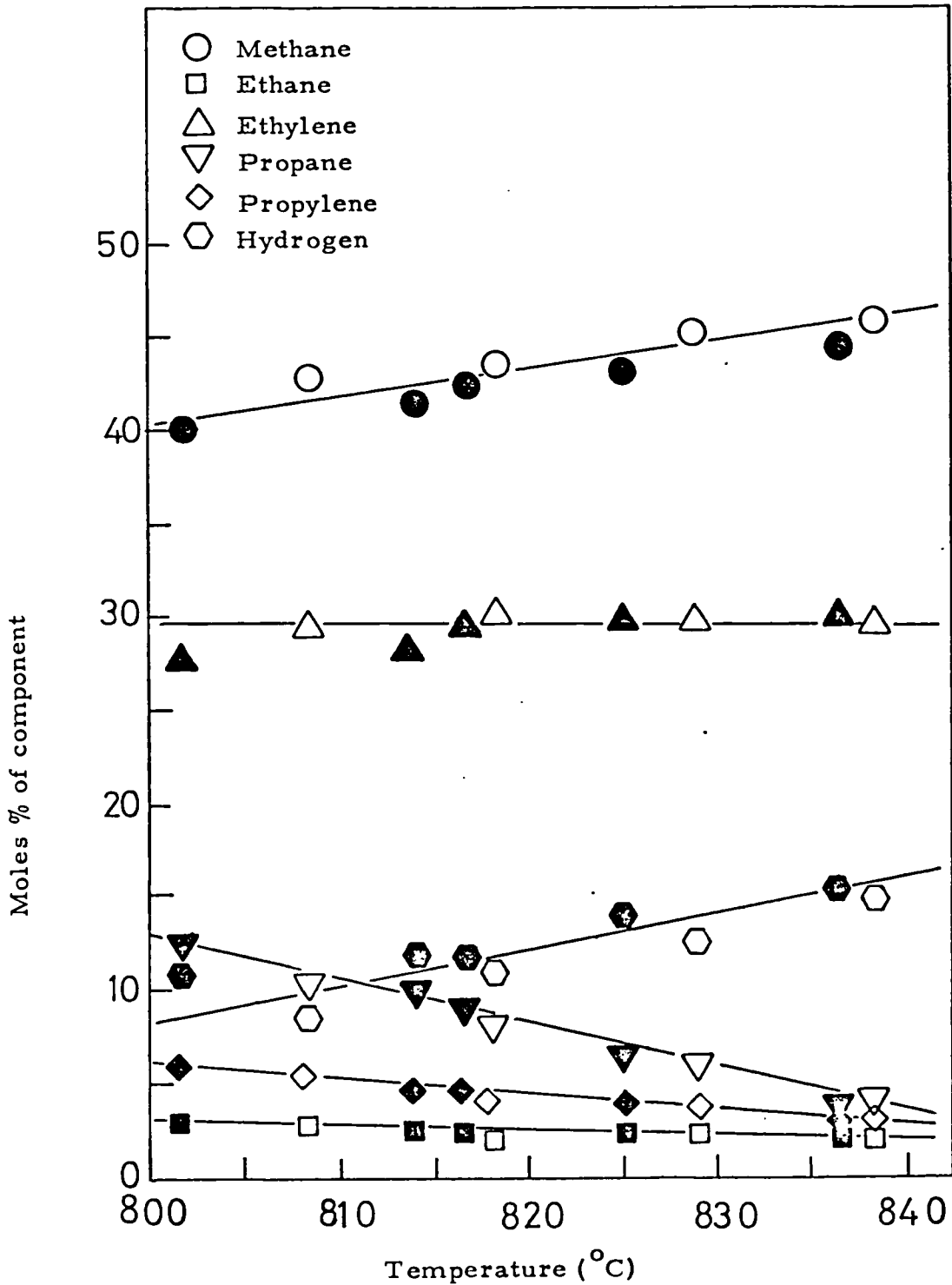
Graph 3.20. Stainless steel disc. 810°C

Open symbols, run 72; closed symbols, run 73.



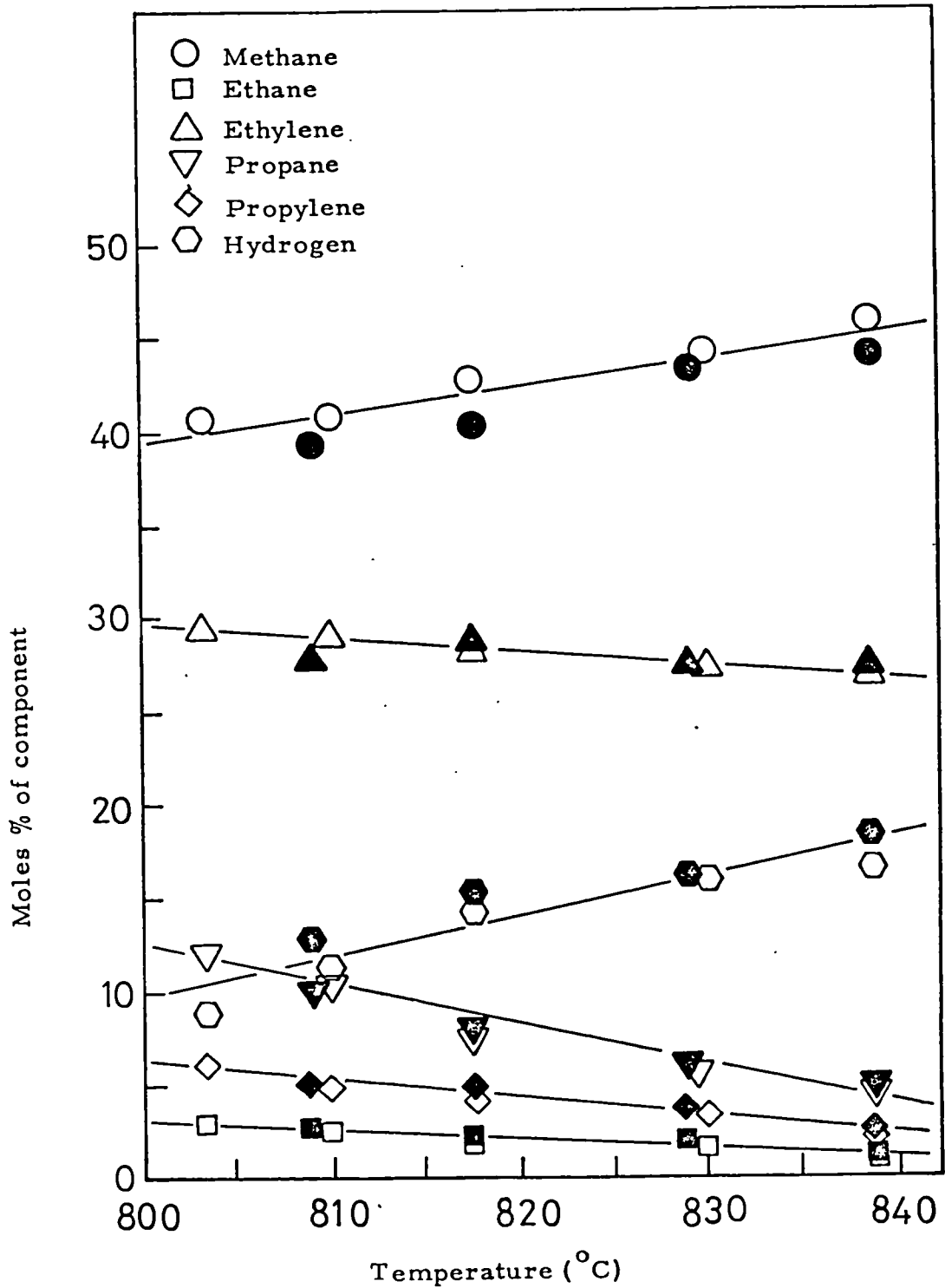
Graph 3.21. Silica disc. Run 54

Inlet residence time = 2.0 secs.



Graph 3.22. Copper disc. Open symbols, run 48
closed symbols, run 55

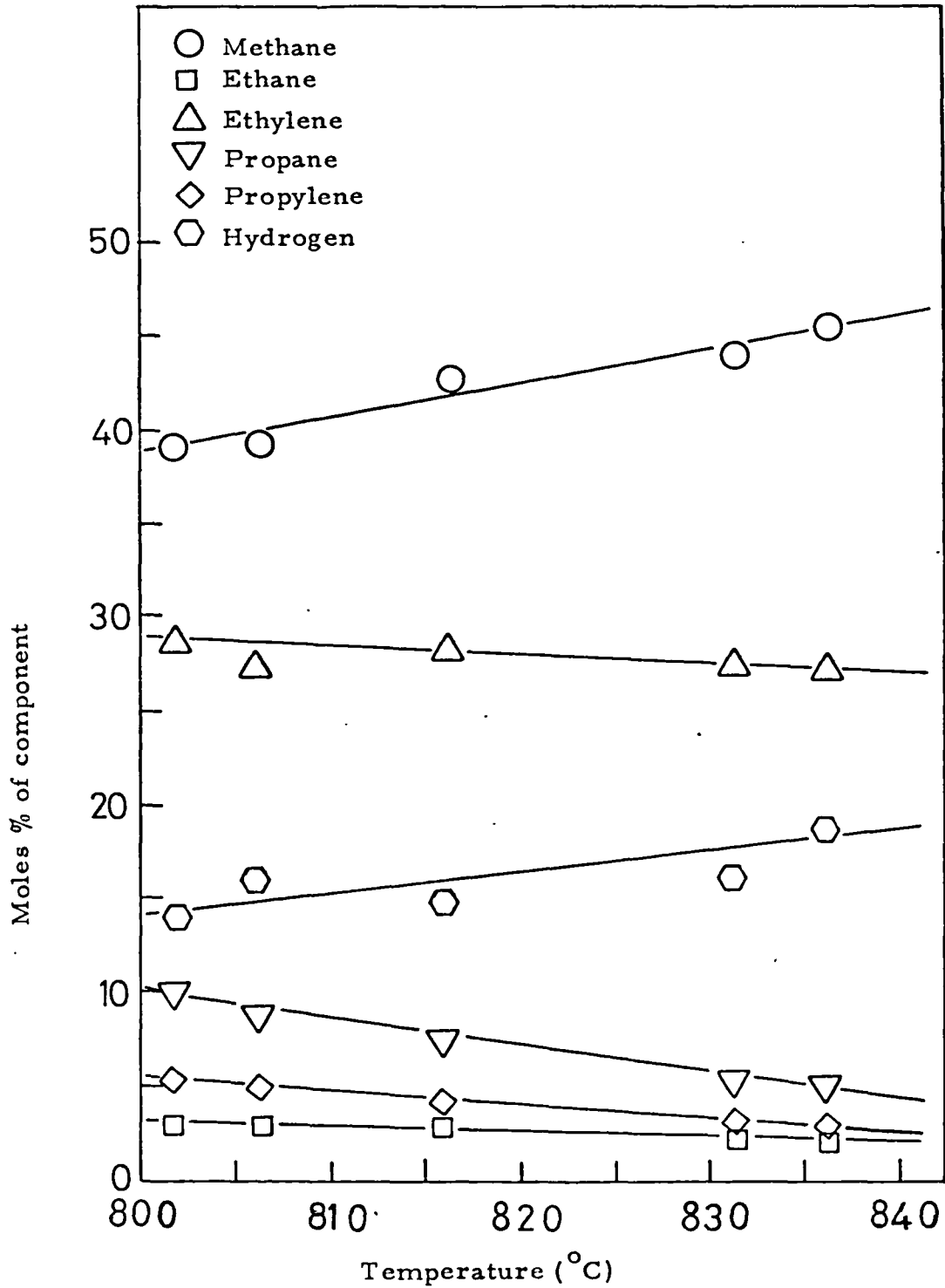
Inlet residence time = 2.0 secs.



Graph 3.23. Nickel disc. Open symbols, run 51

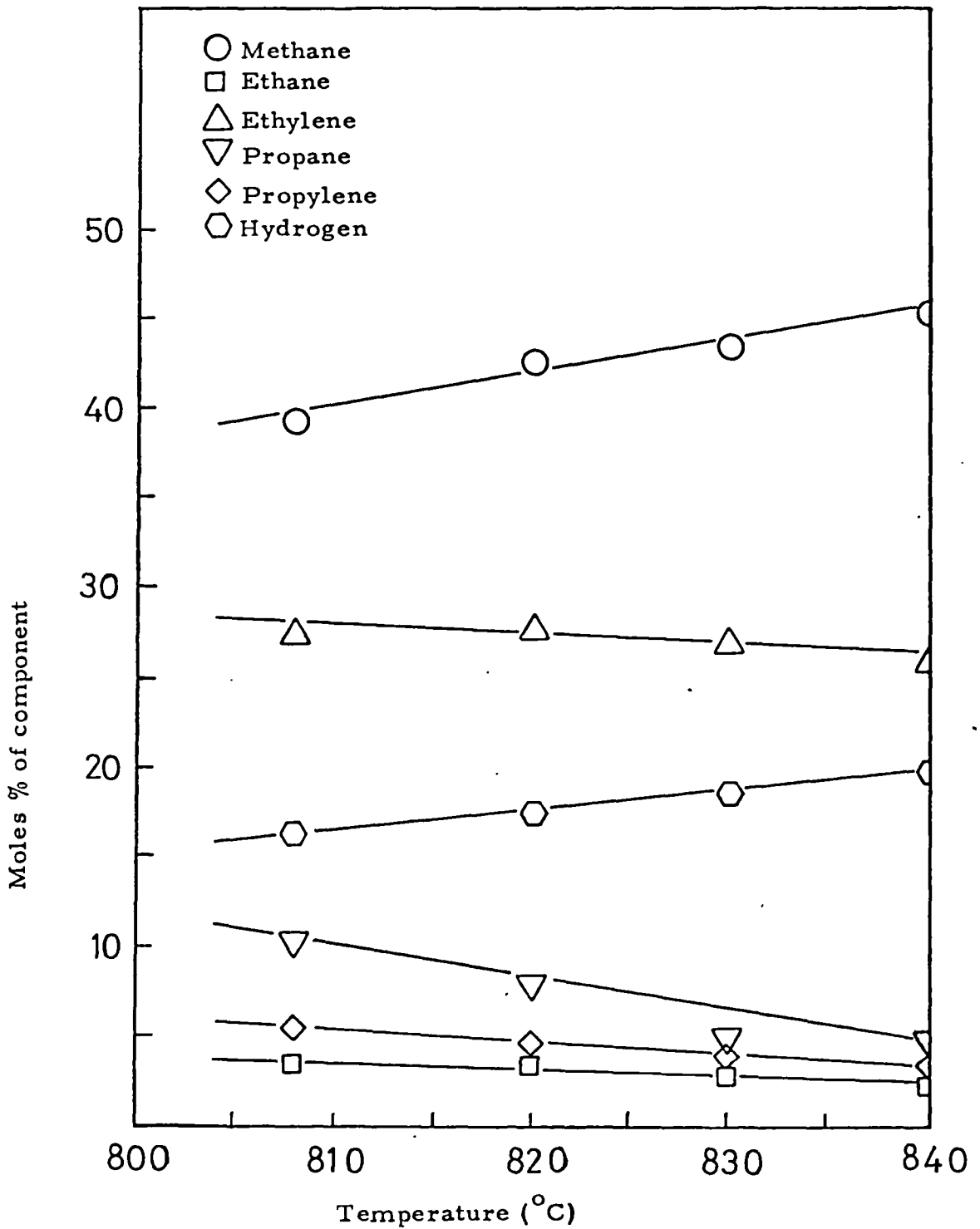
closed symbols, run 50

Inlet residence time = 2.0 secs.



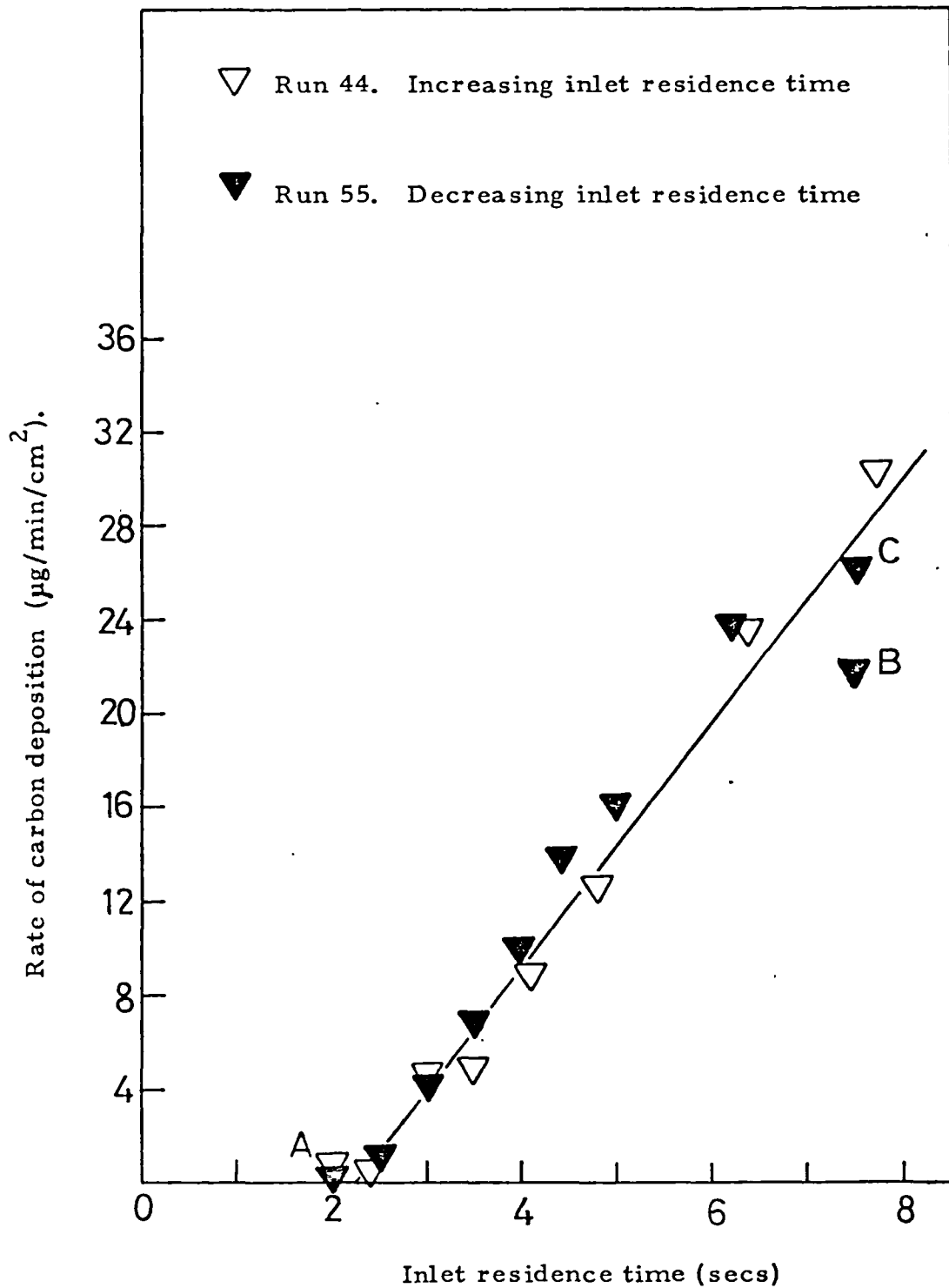
Graph 3.24. Iron disc. Run 56

Inlet residence time = 2.0 secs.

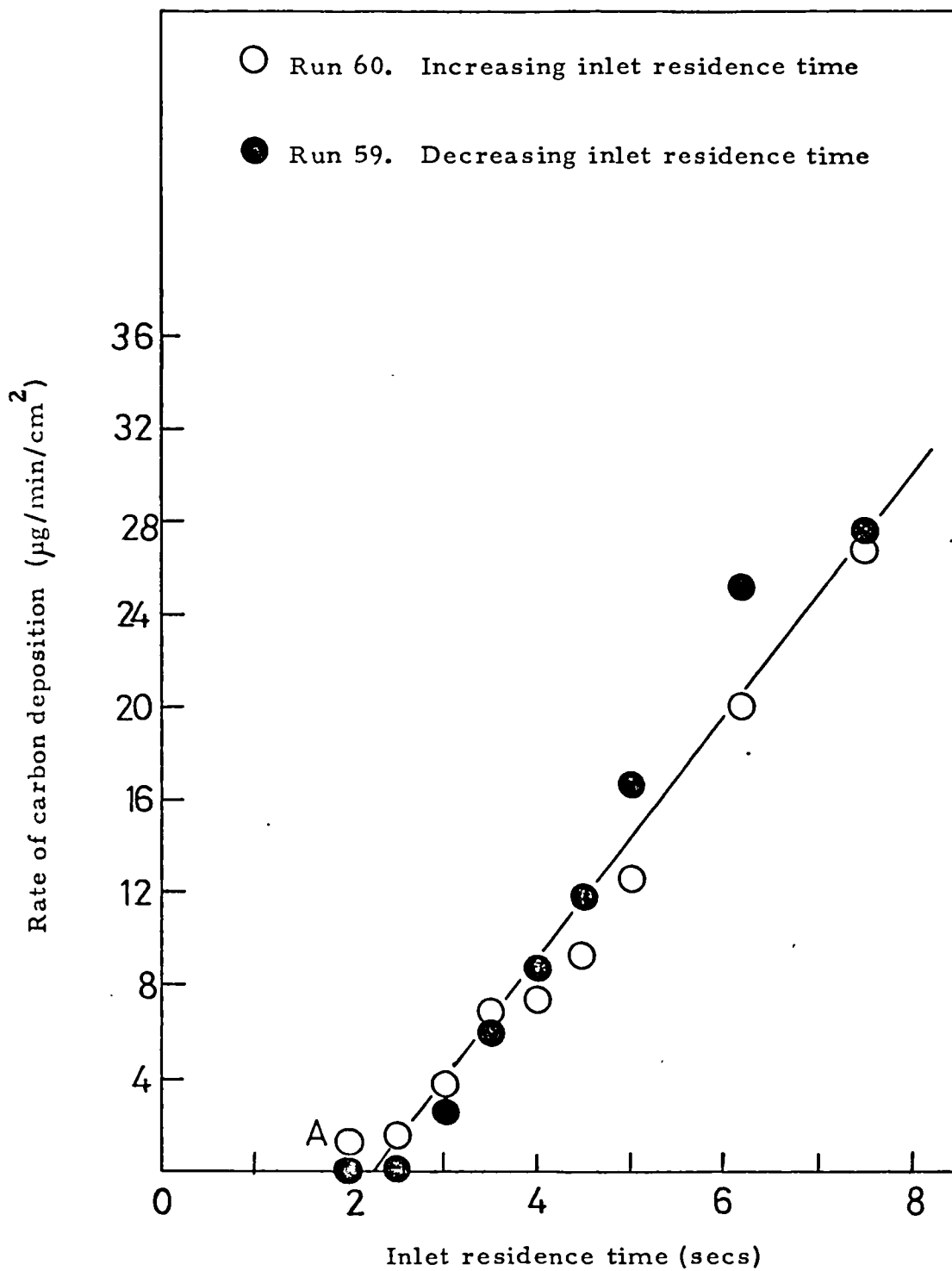


Graph 3.25. Stainless steel disc. Run 73

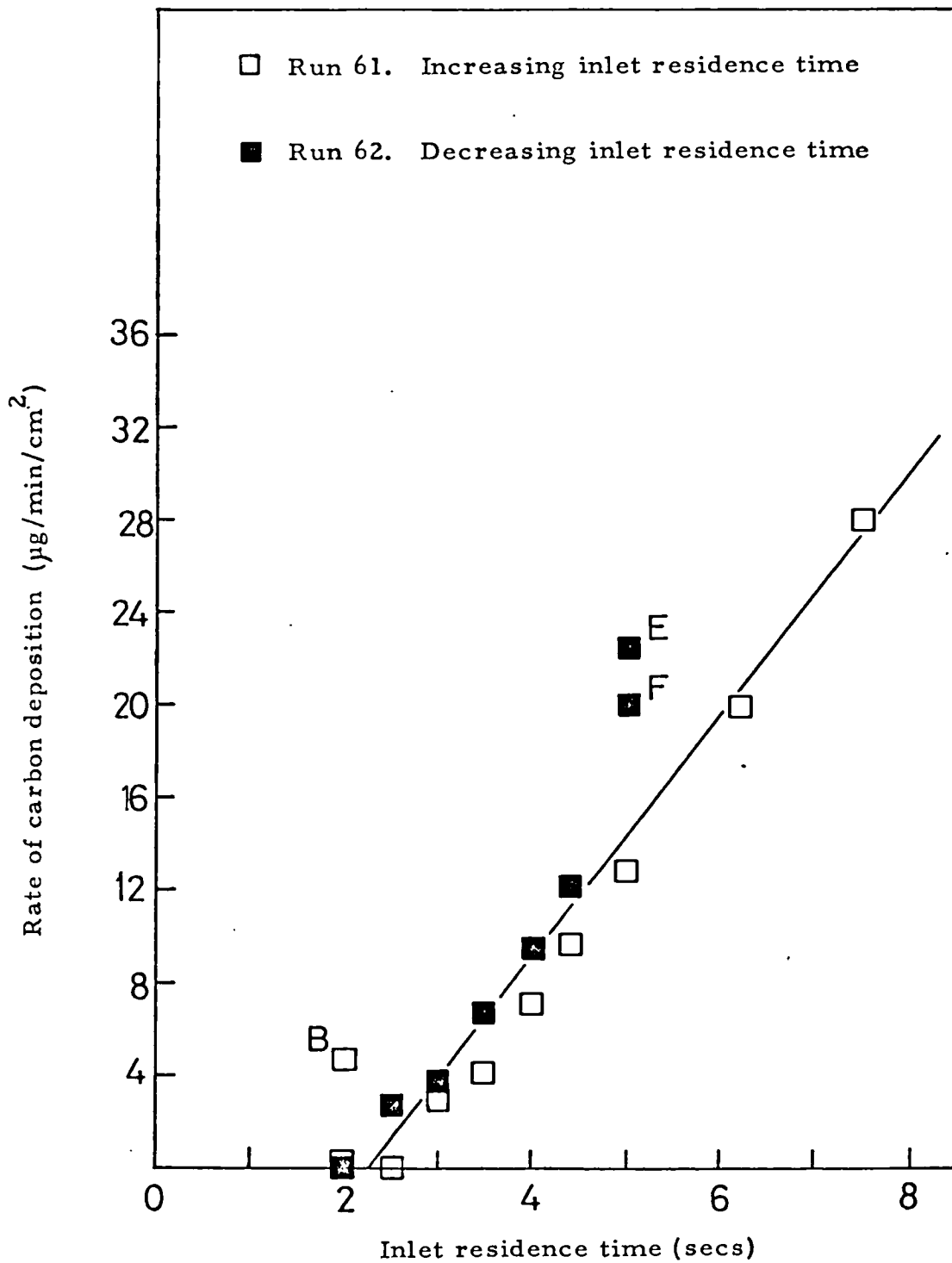
Inlet residence time = 2.0 secs.



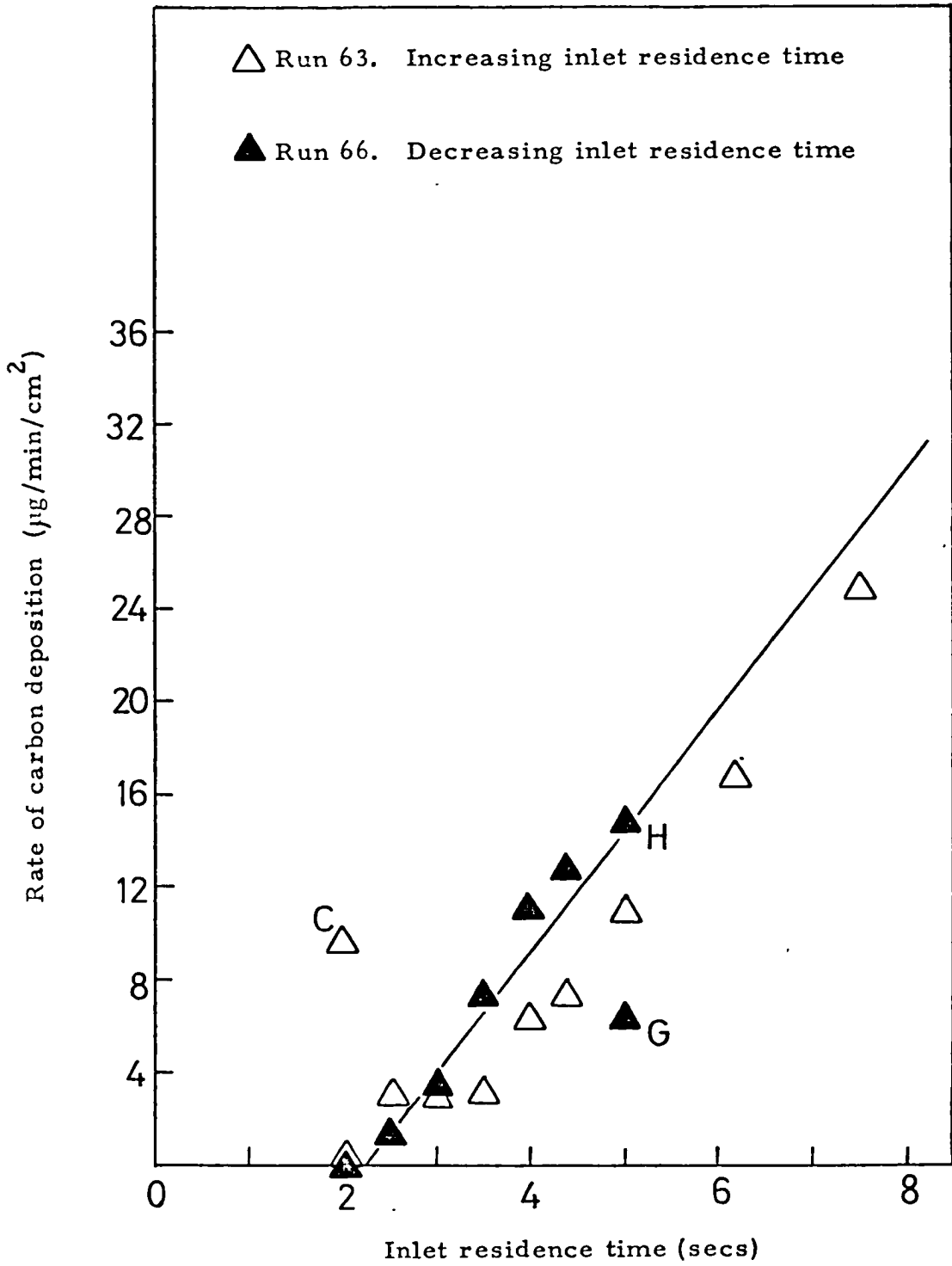
Graph 3.26. Silica "liner" with copper collector disc
810°C



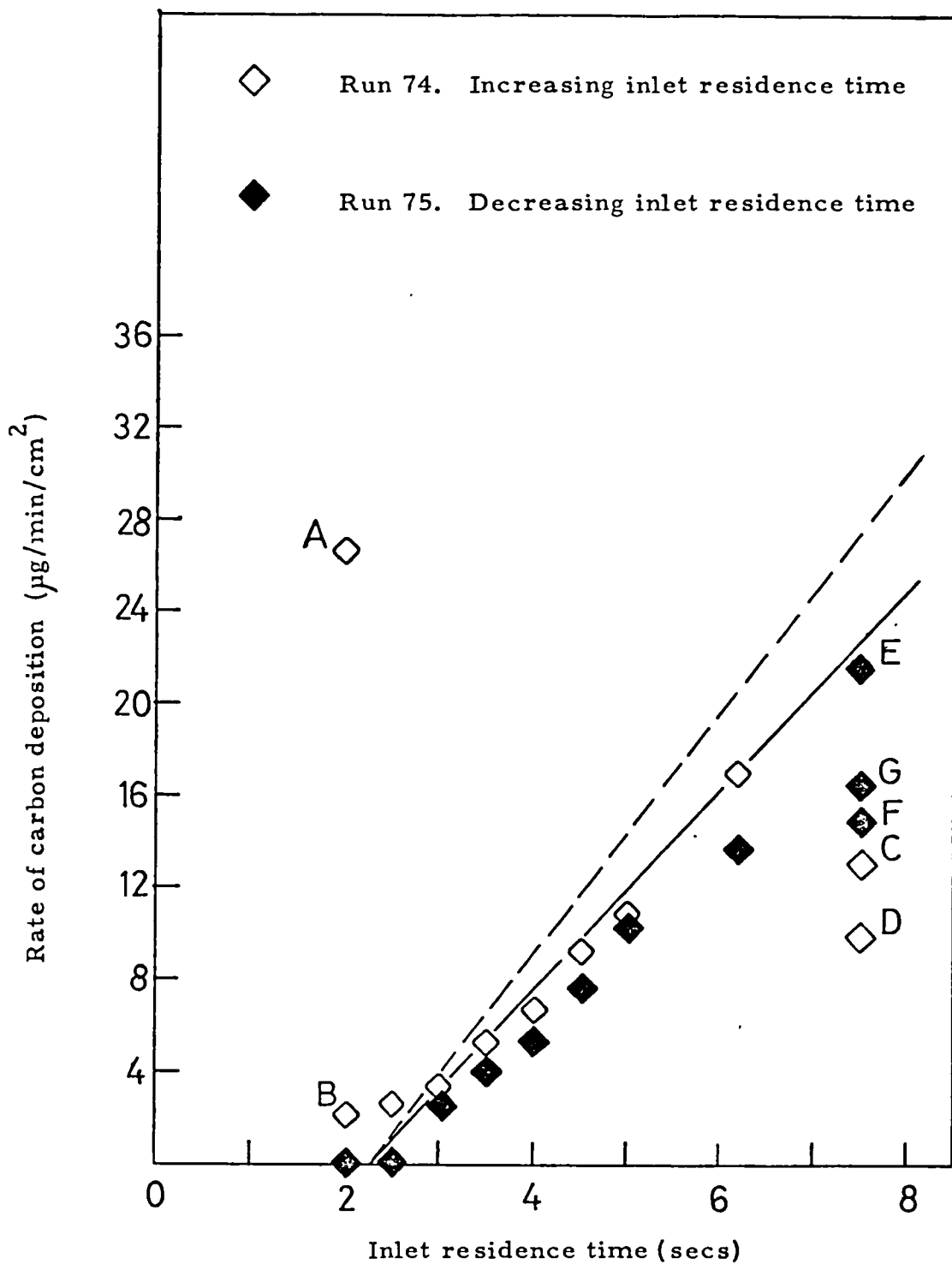
Graph 3.27. Copper liner with copper collector disc
810°C



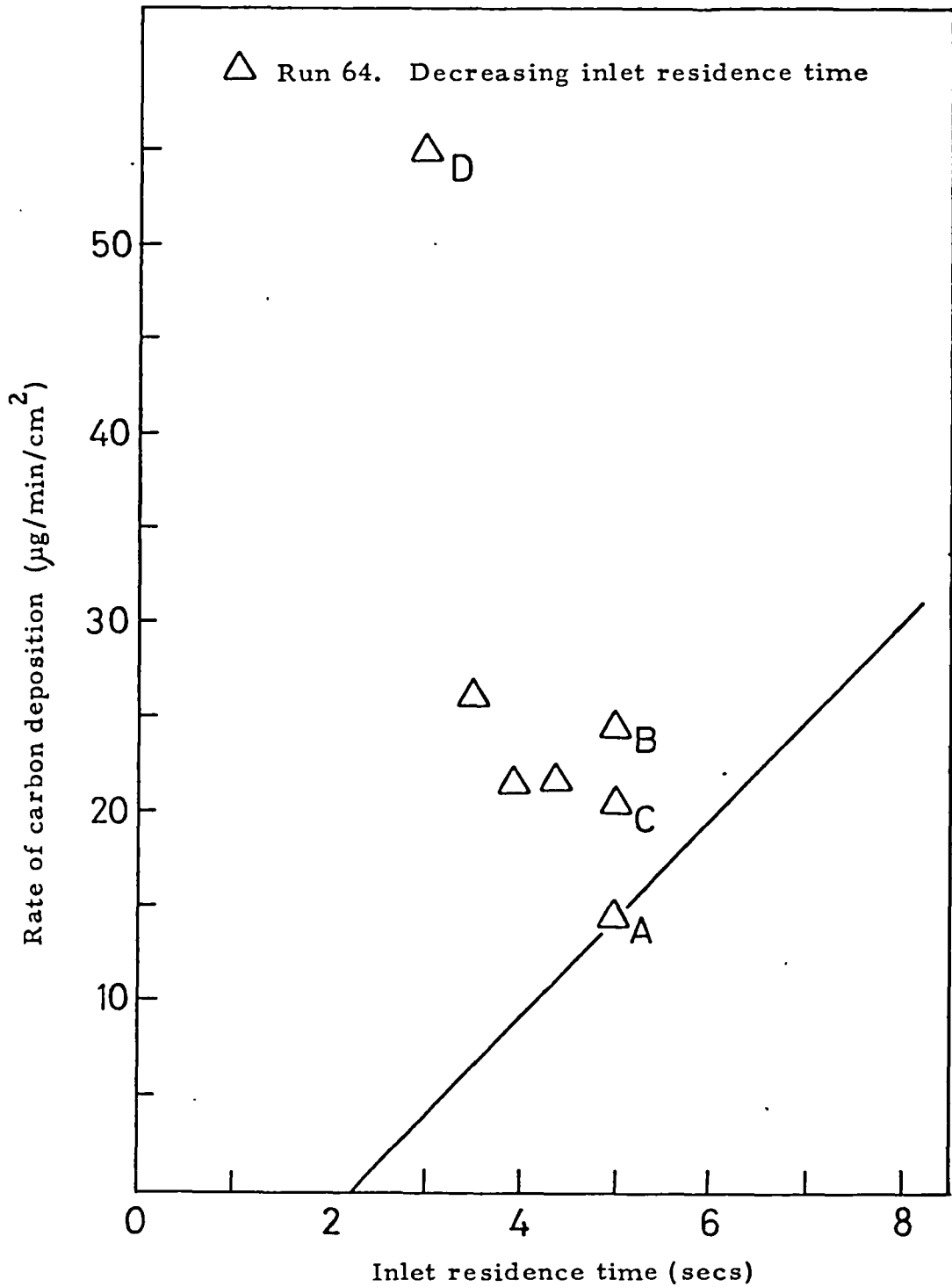
Graph 3.28. Nickel liner with copper collector disc
810°C



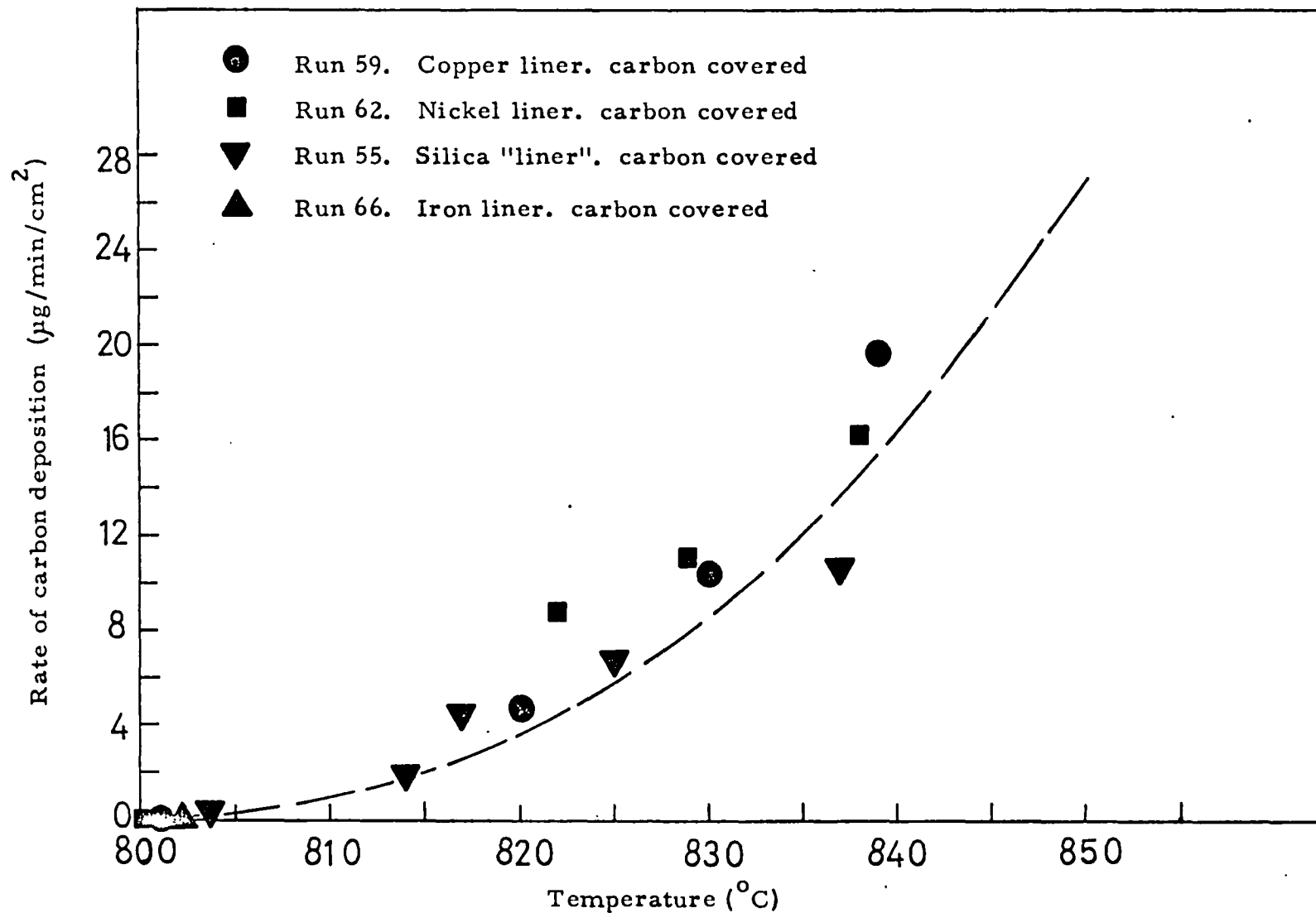
Graph 3.29. Iron liner with copper collector disc
810°C



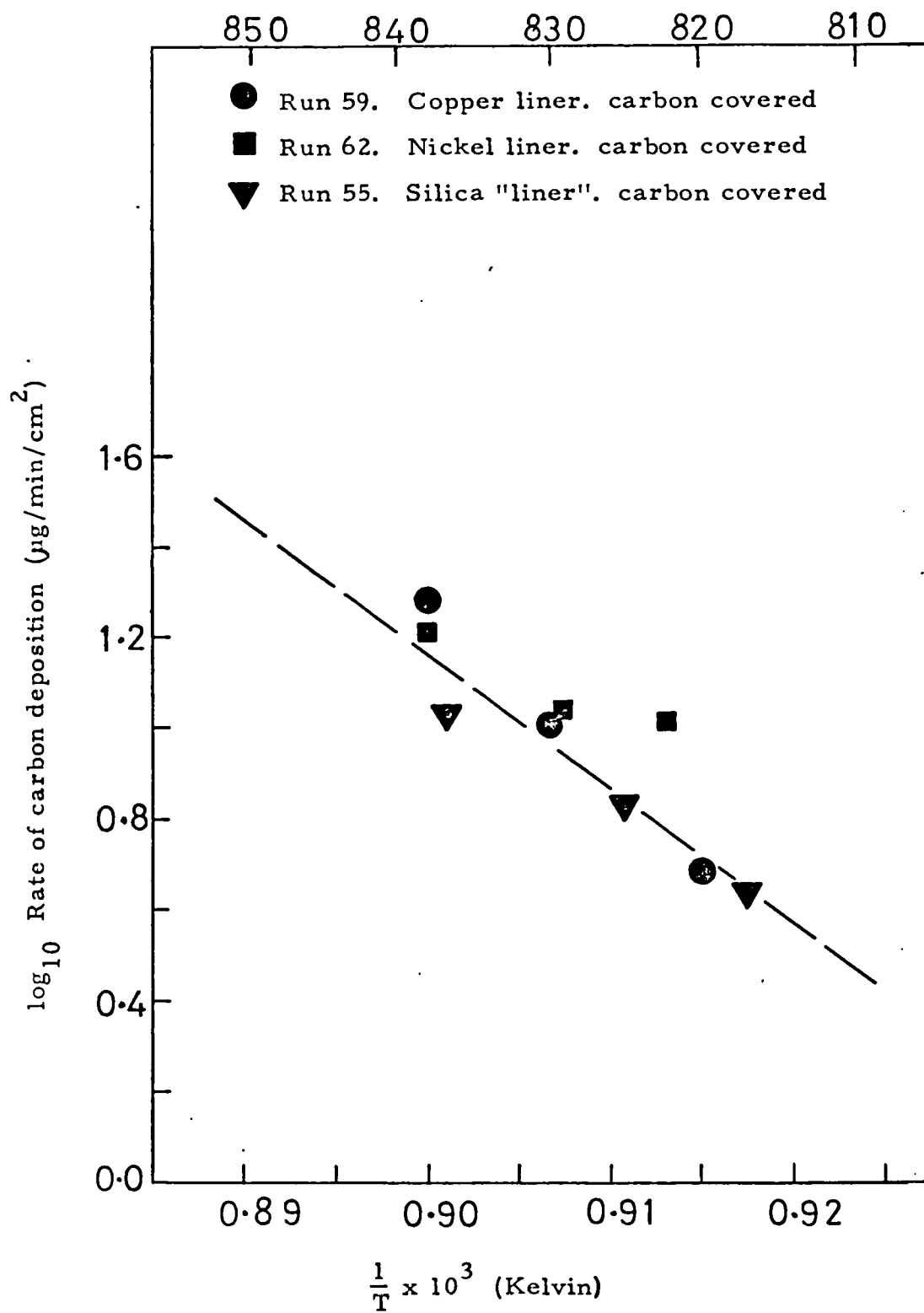
Graph 3.30. Stainless steel liner with copper collector disc
810°C



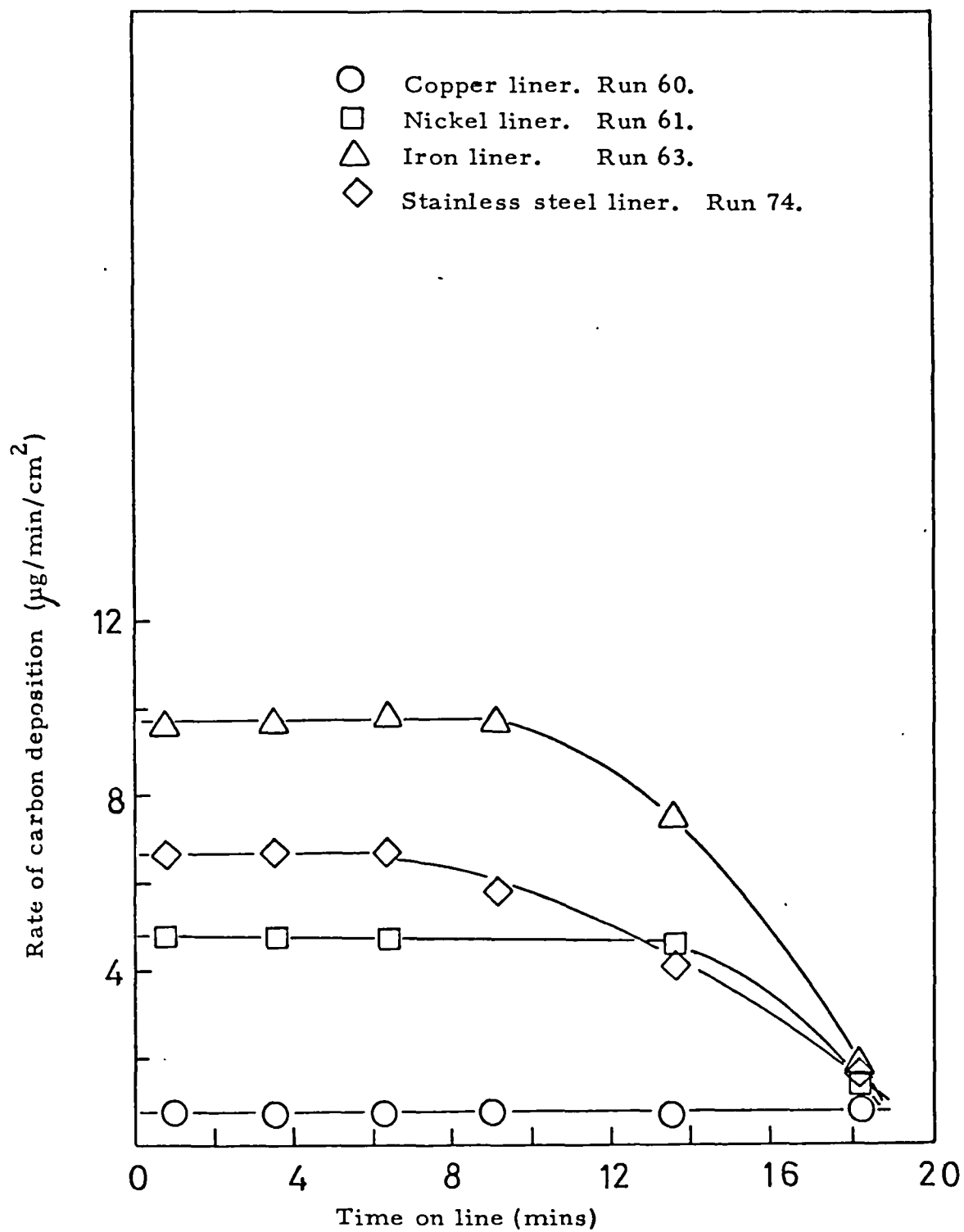
Graph 3. 31. Iron liner with copper collector disc
810°C



Graph 3.32. Inlet residence time = 2.0 secs.

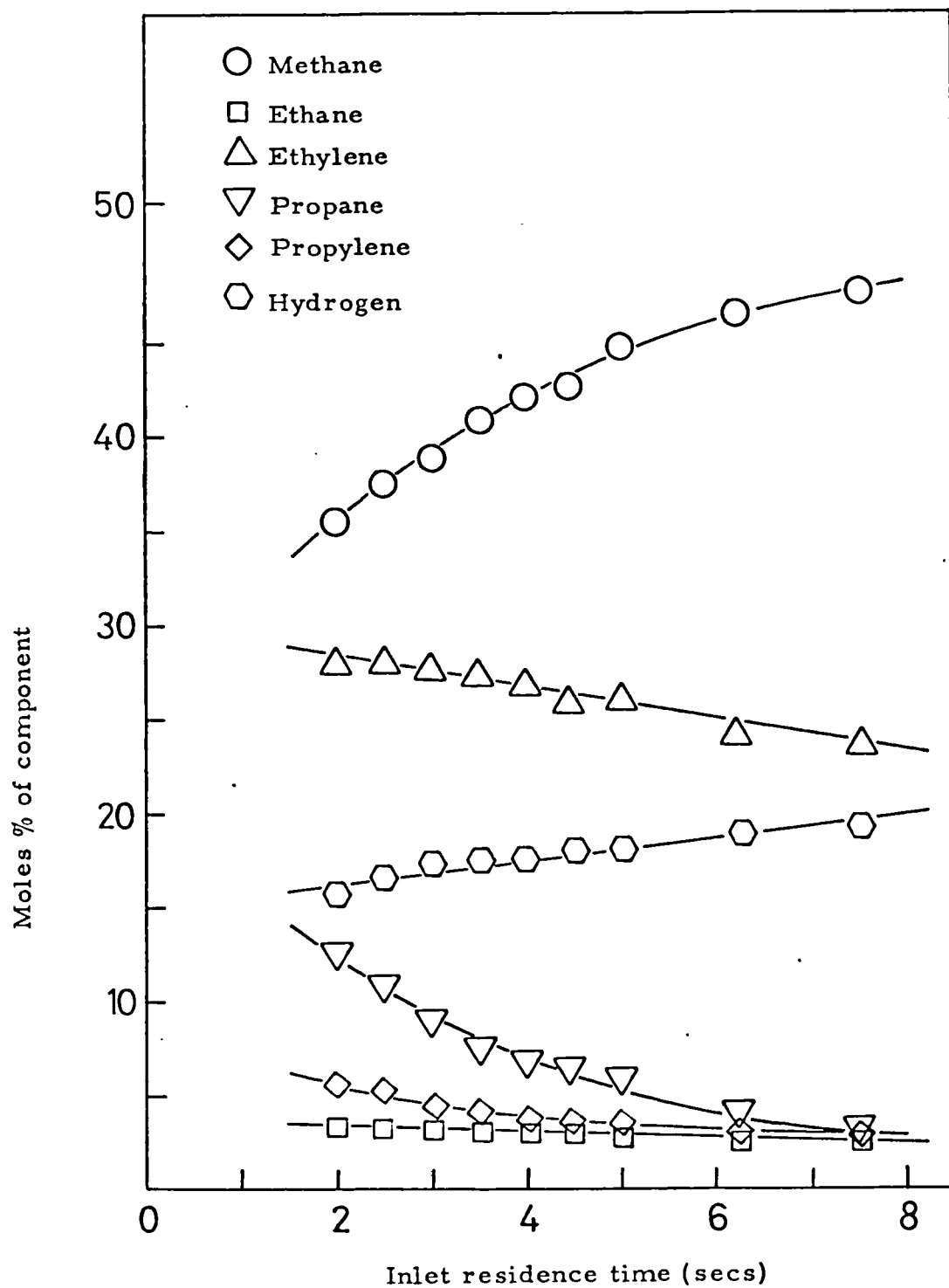


Graph 3.33. Inlet residence time = 2.0 secs.

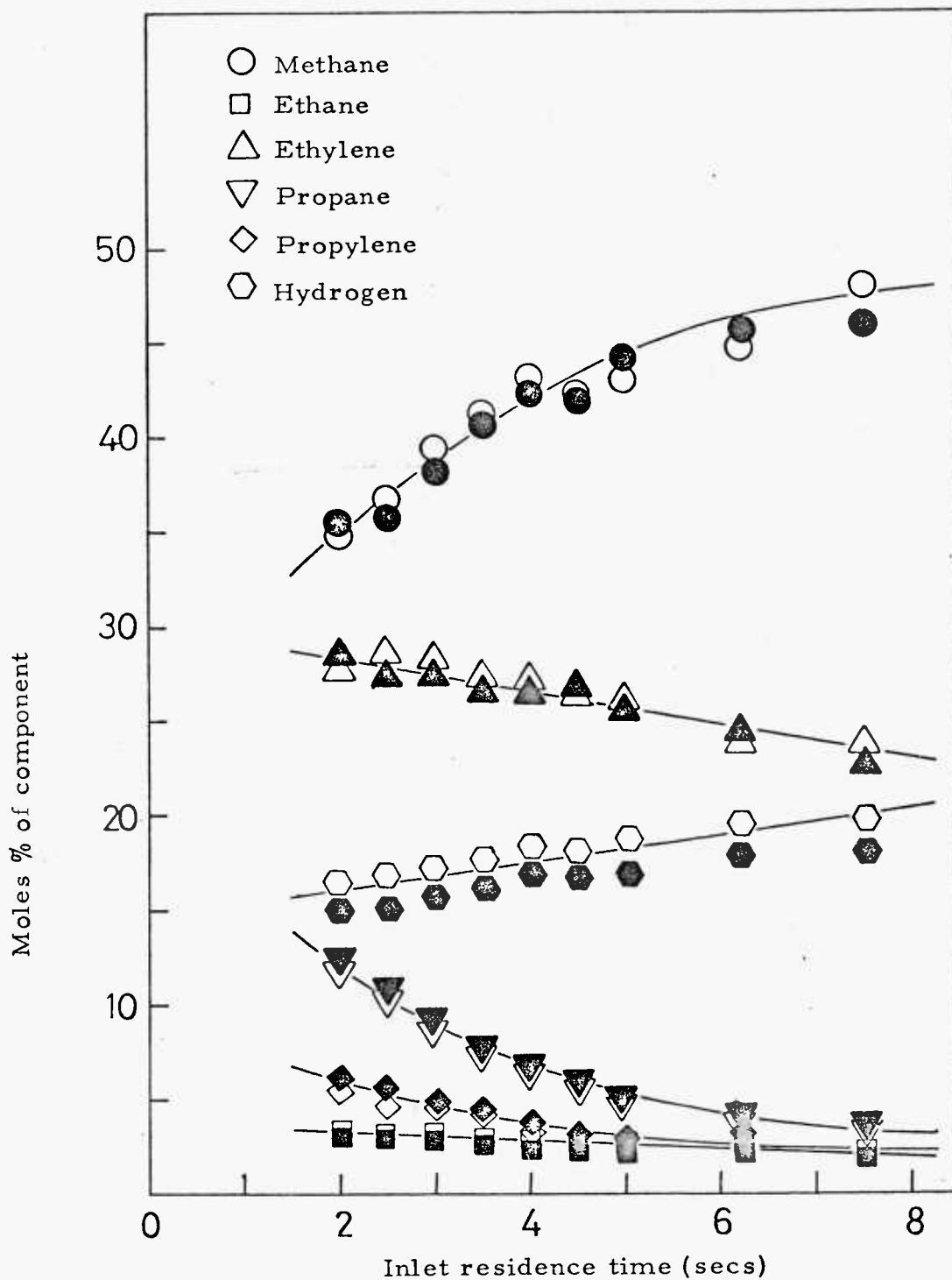


Graph 3. 34. Inlet residence time = 2.0 secs. 810°C

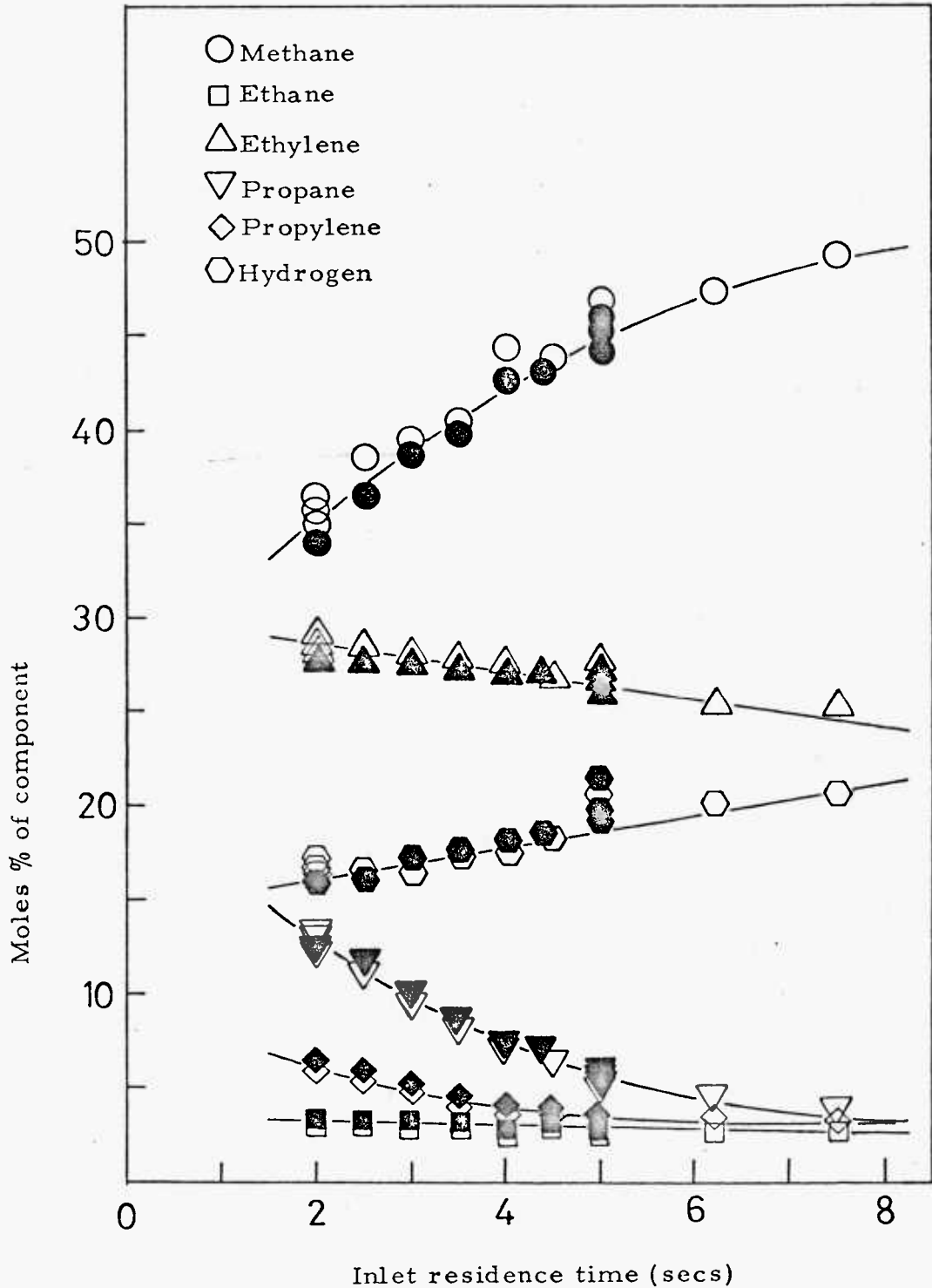
Suspended copper discs, various metal liners.



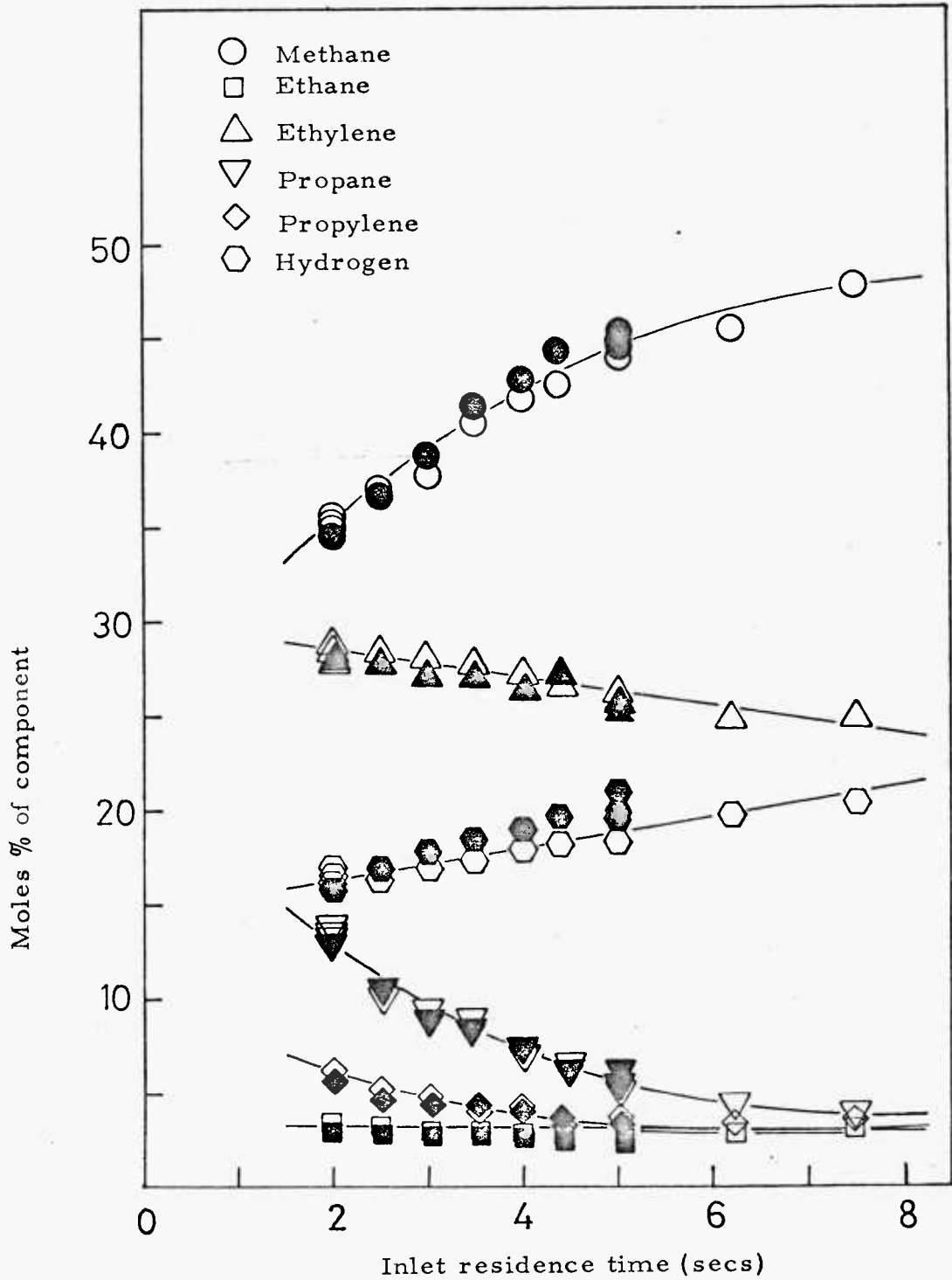
Graph 3.35. Silica "liner" with copper collector disc
Run 55. 810°C



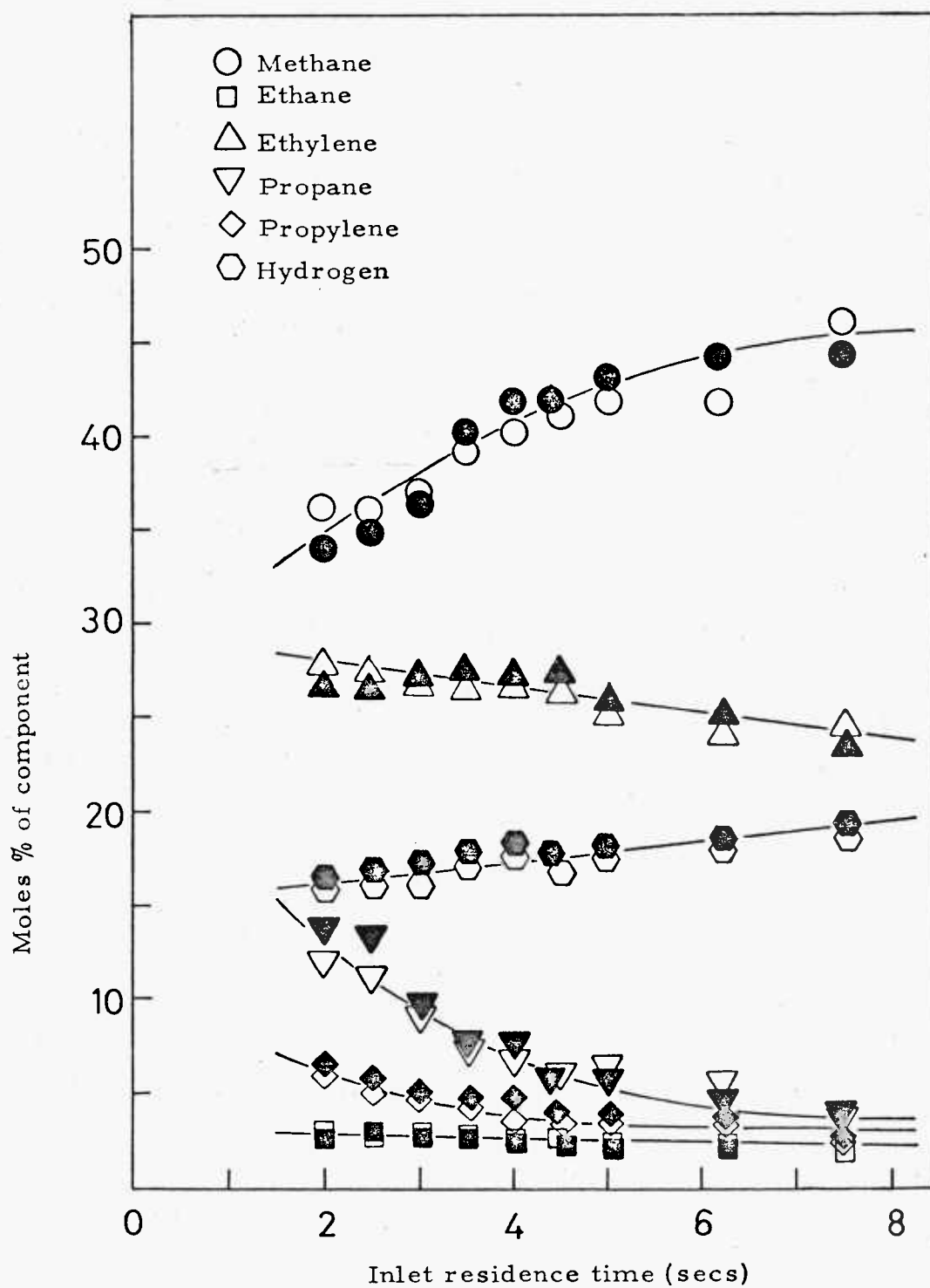
Graph 3.36. Copper liner with copper collector disc
 Open symbols, run 60; closed symbols, run 59, 810°C



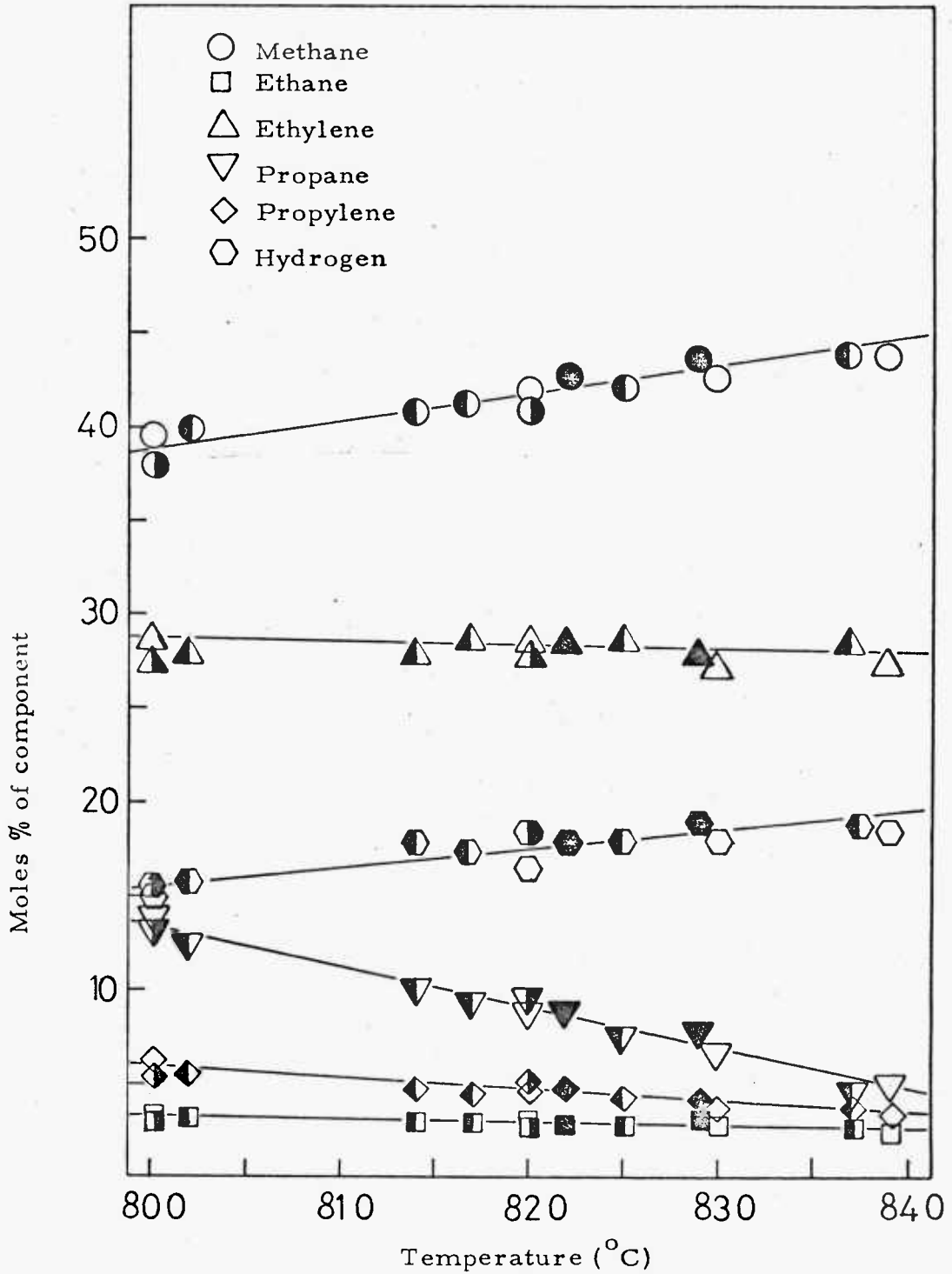
Graph 3.37. Nickel liner with copper collector disc
 Open symbols, run 61; closed symbols, run 62, 810°C



Graph 3.38. Iron liner with copper collector disc
Open symbols, run 63; closed symbols, run 66, 810°C



Graph 3.39. Stainless steel liner with copper collector disc
Open symbols, run 74; closed symbols, run 75, 810°C

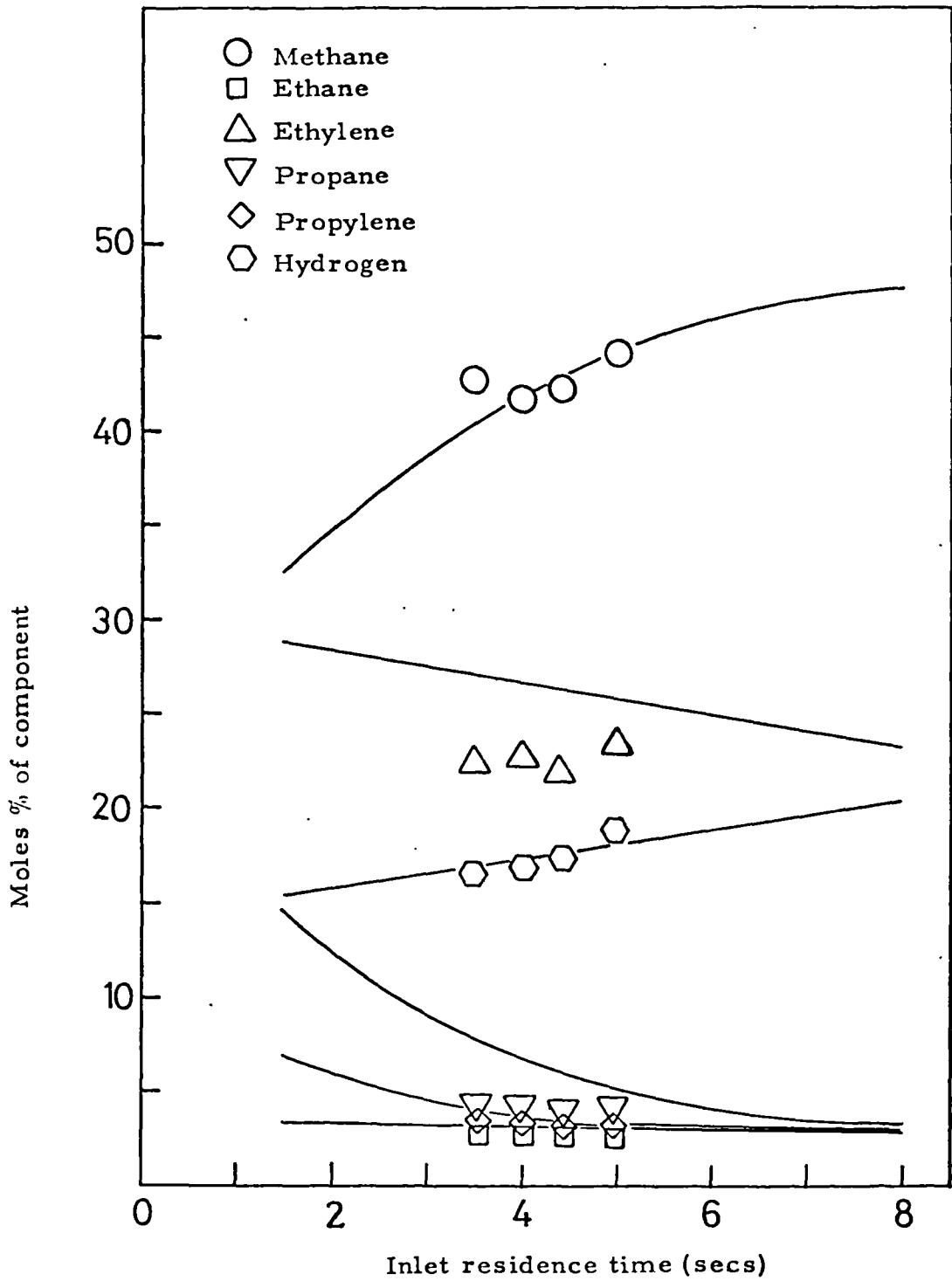


Graph 3.40. Various liners with copper collector disc

Open symbols, run 59 copper liner; closed symbols, run 62 Nickel liner

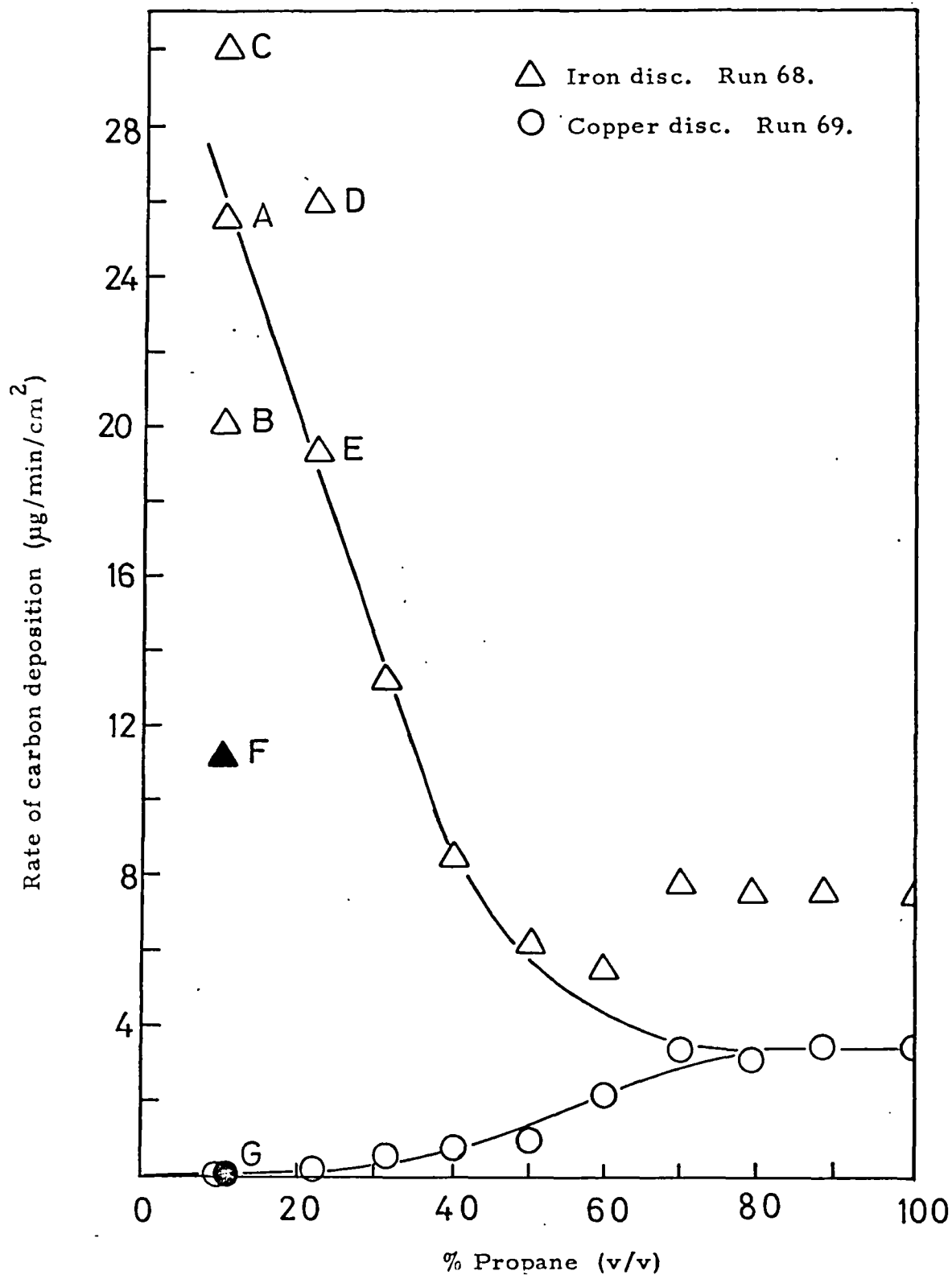
Left side closed, run 55, "silica" liner; right side closed, run 66, iron liner

Inlet residence time = 2.0 secs.



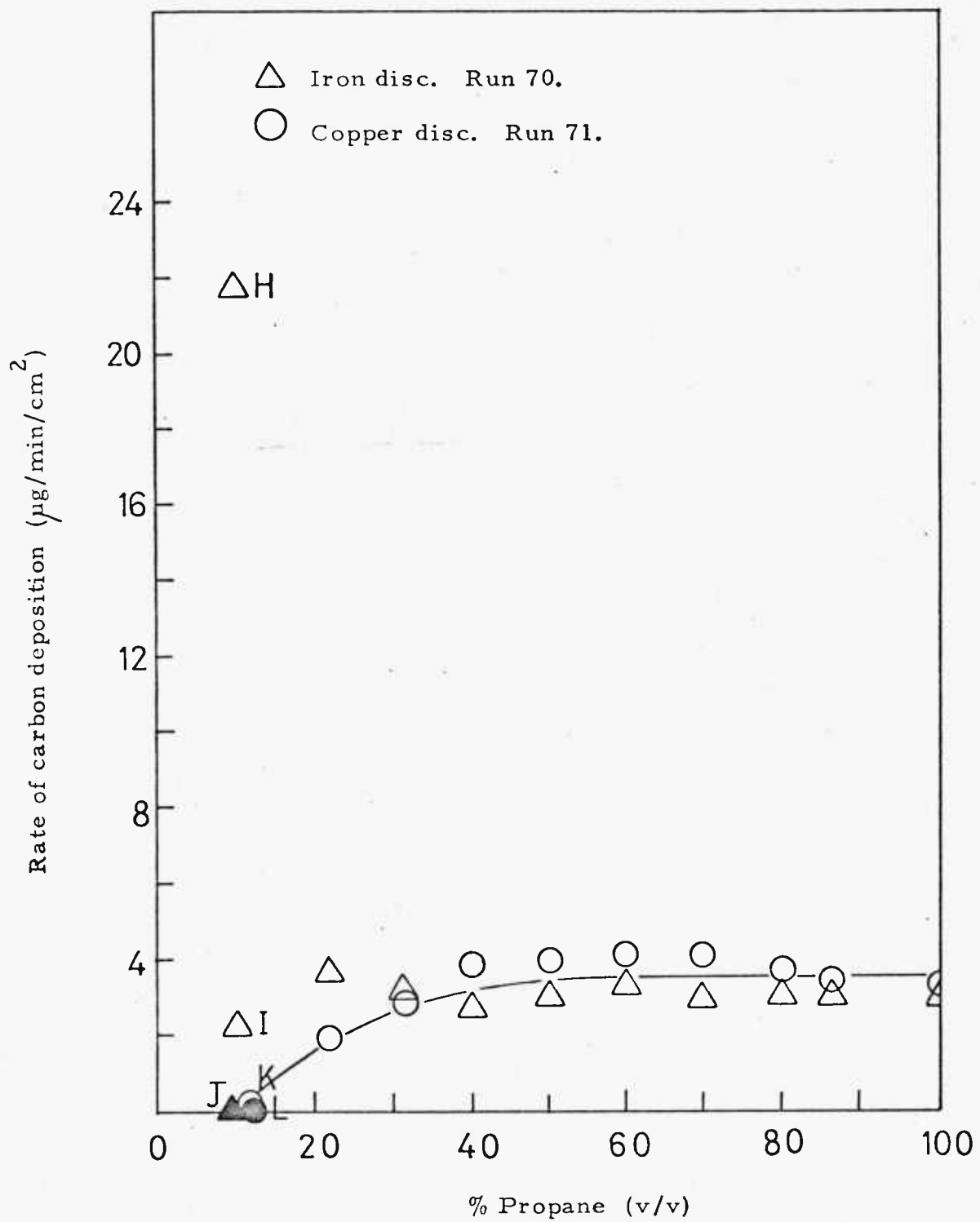
Graph 3.41. Iron liner with copper collector disc

Run 64. 810°C

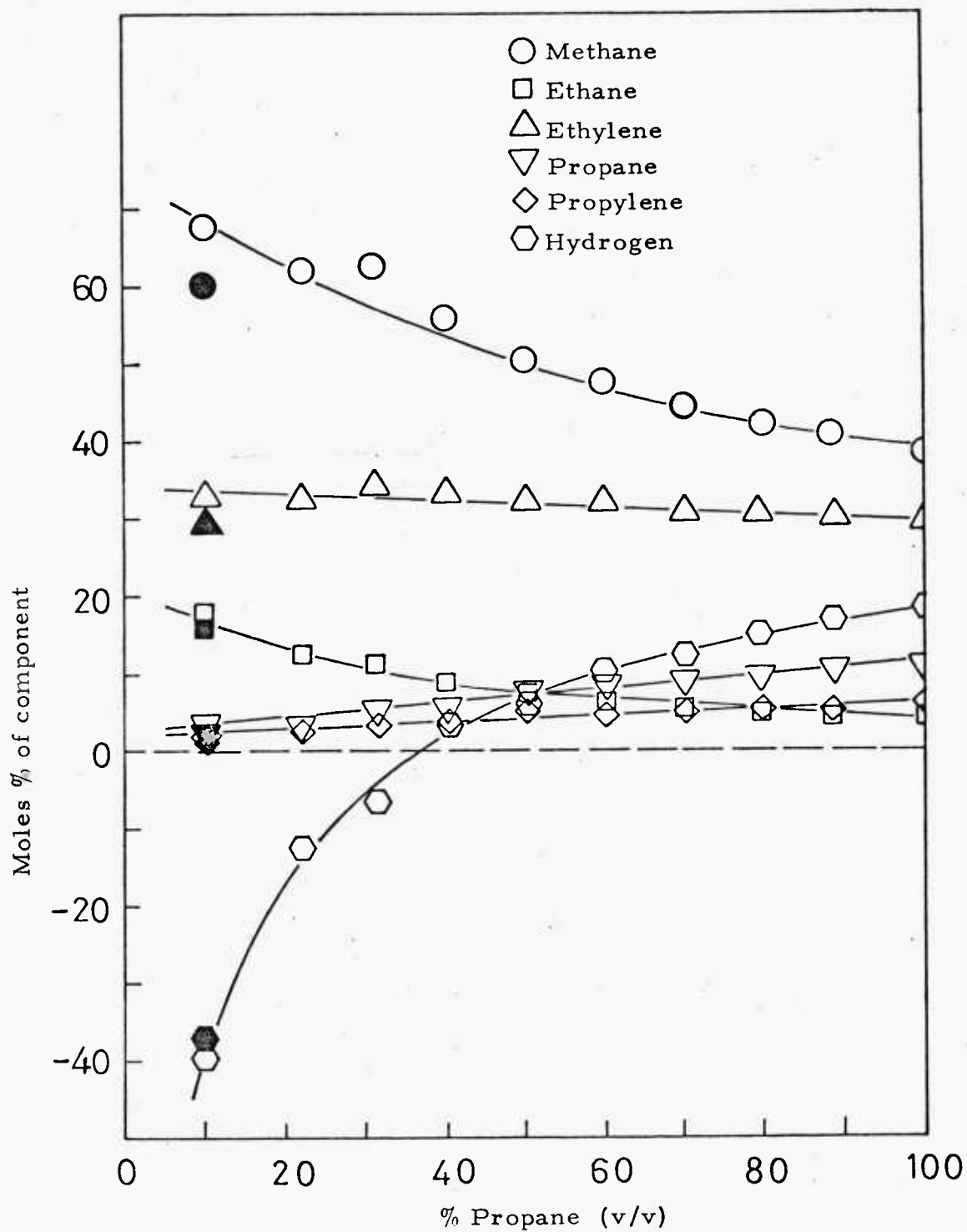


Graph 3.42. Hydrogen dilution. 806°C

Inlet residence time = 3.0 secs.

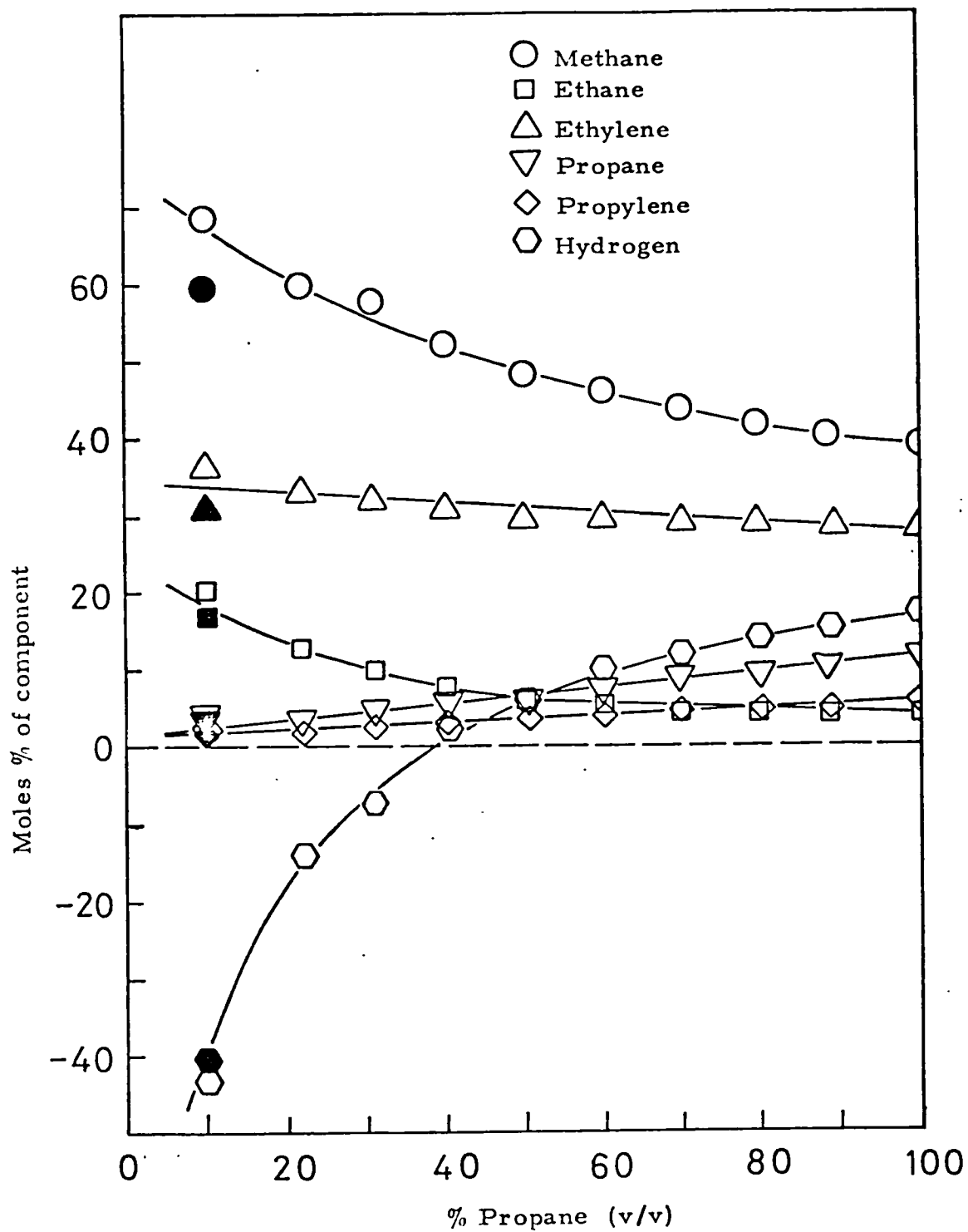


Graph 3.43. Helium dilution. 806°C
 Inlet residence time = 3.0 secs.



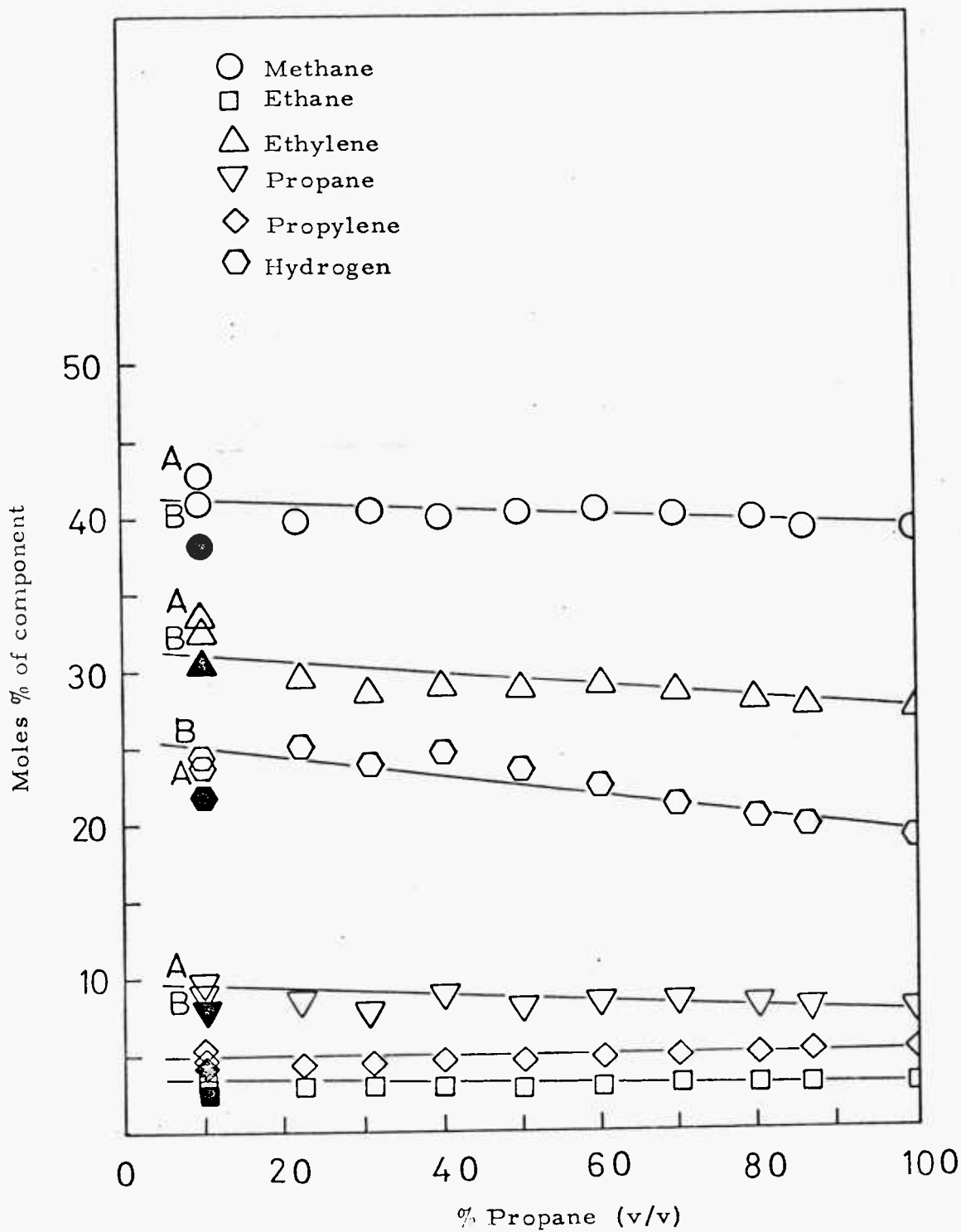
Graph 3.44. Hydrogen dilution. 806°C

Iron disc. Run 68. Inlet residence time = 3.0 secs.



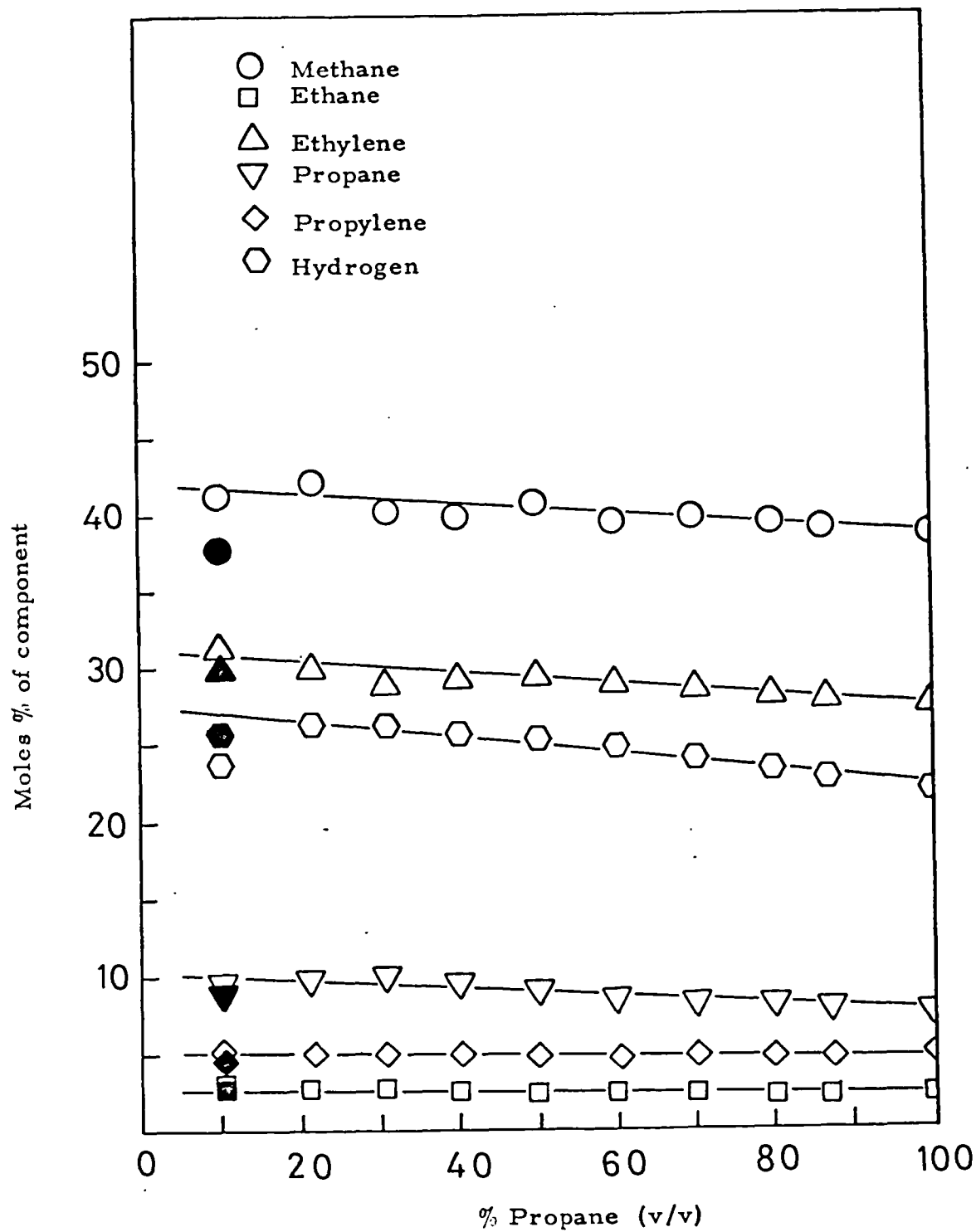
Graph 3.45. Hydrogen dilution. 806°C

Copper disc. Run 69. Inlet residence time = 3.0 secs.



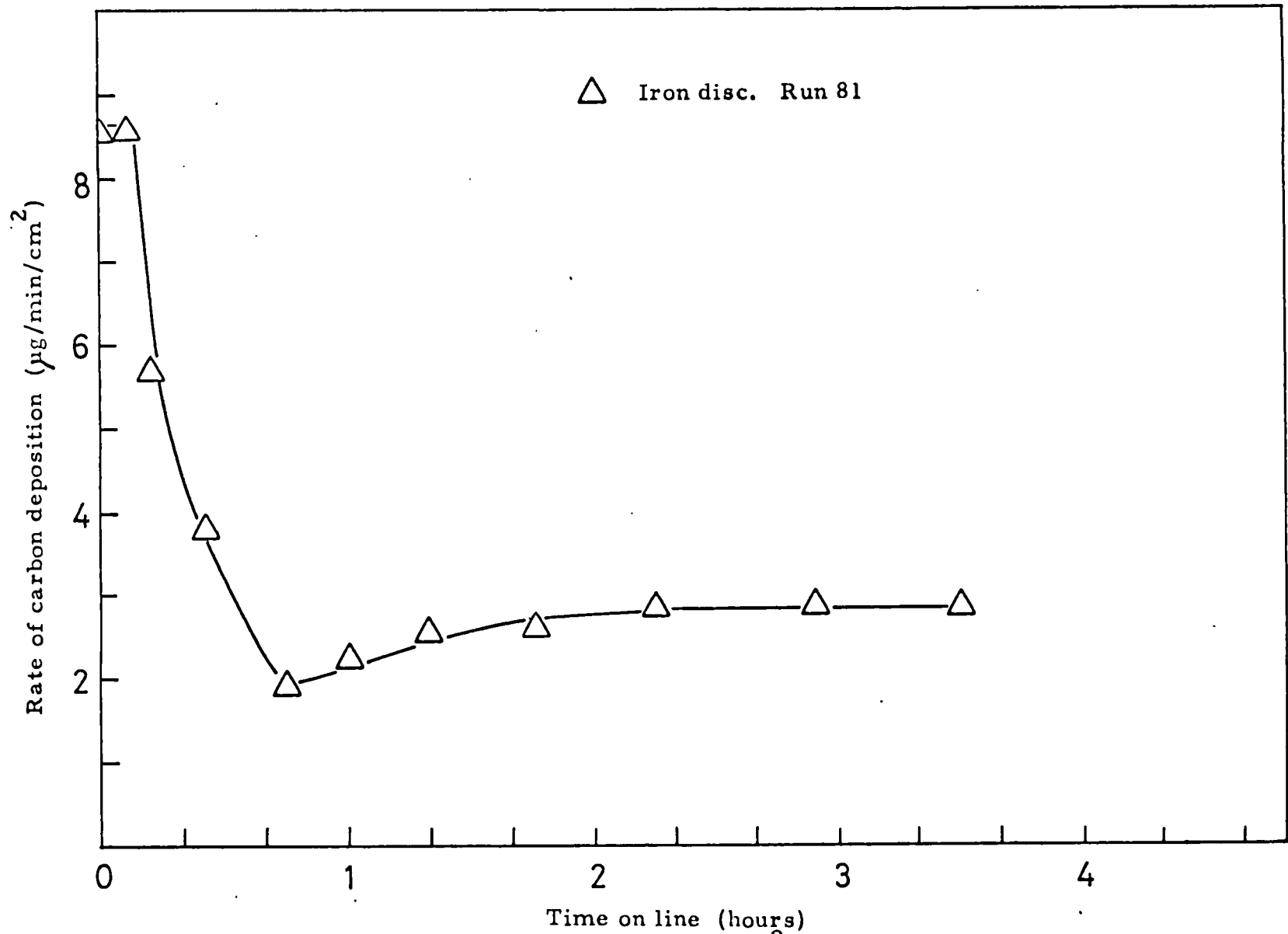
Graph 3.46. Helium dilution. 806°C

Iron disc. Run 70. Inlet residence time = 3.0 secs.

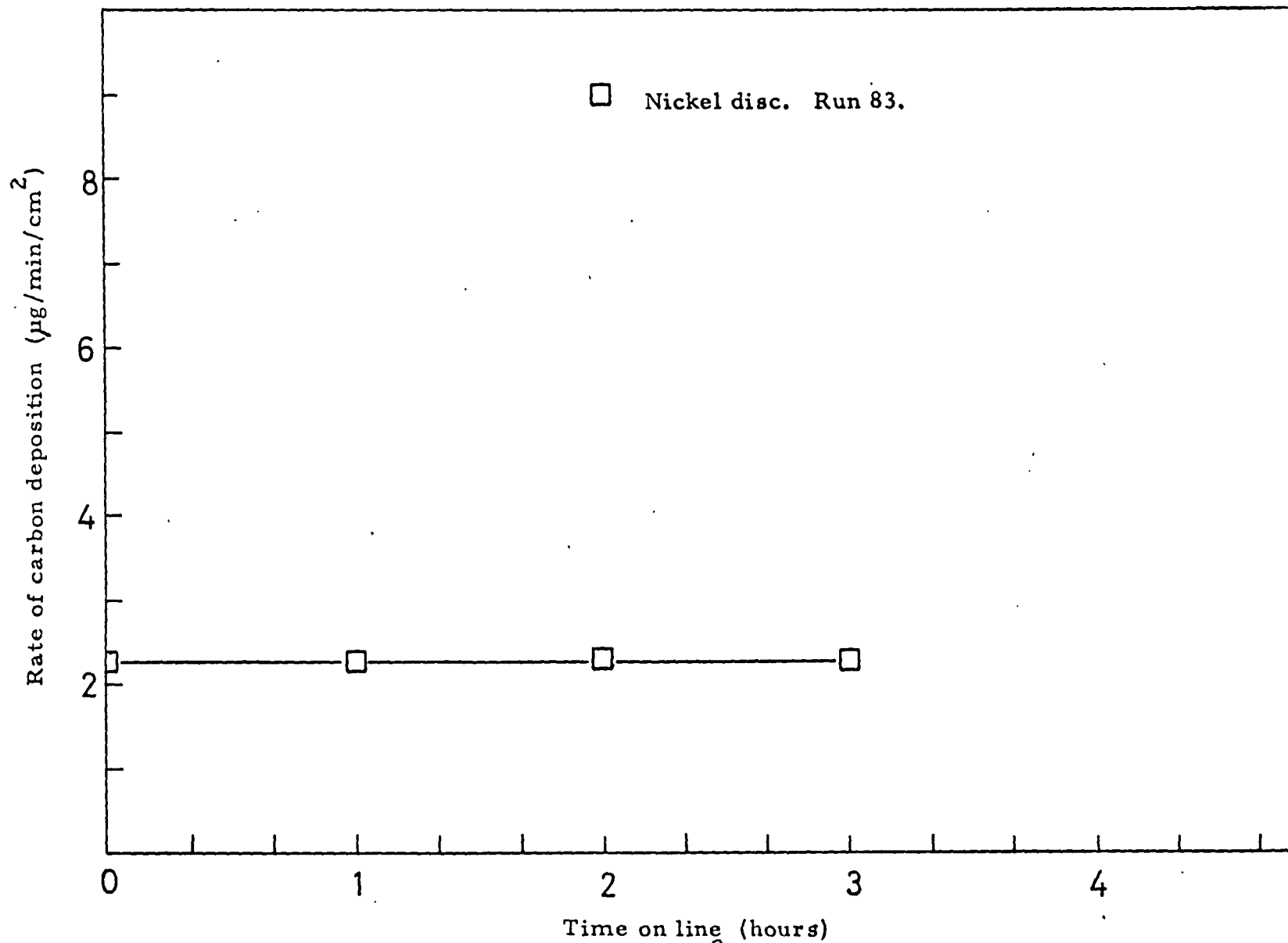


Graph 3.47. Helium dilution. 806°C

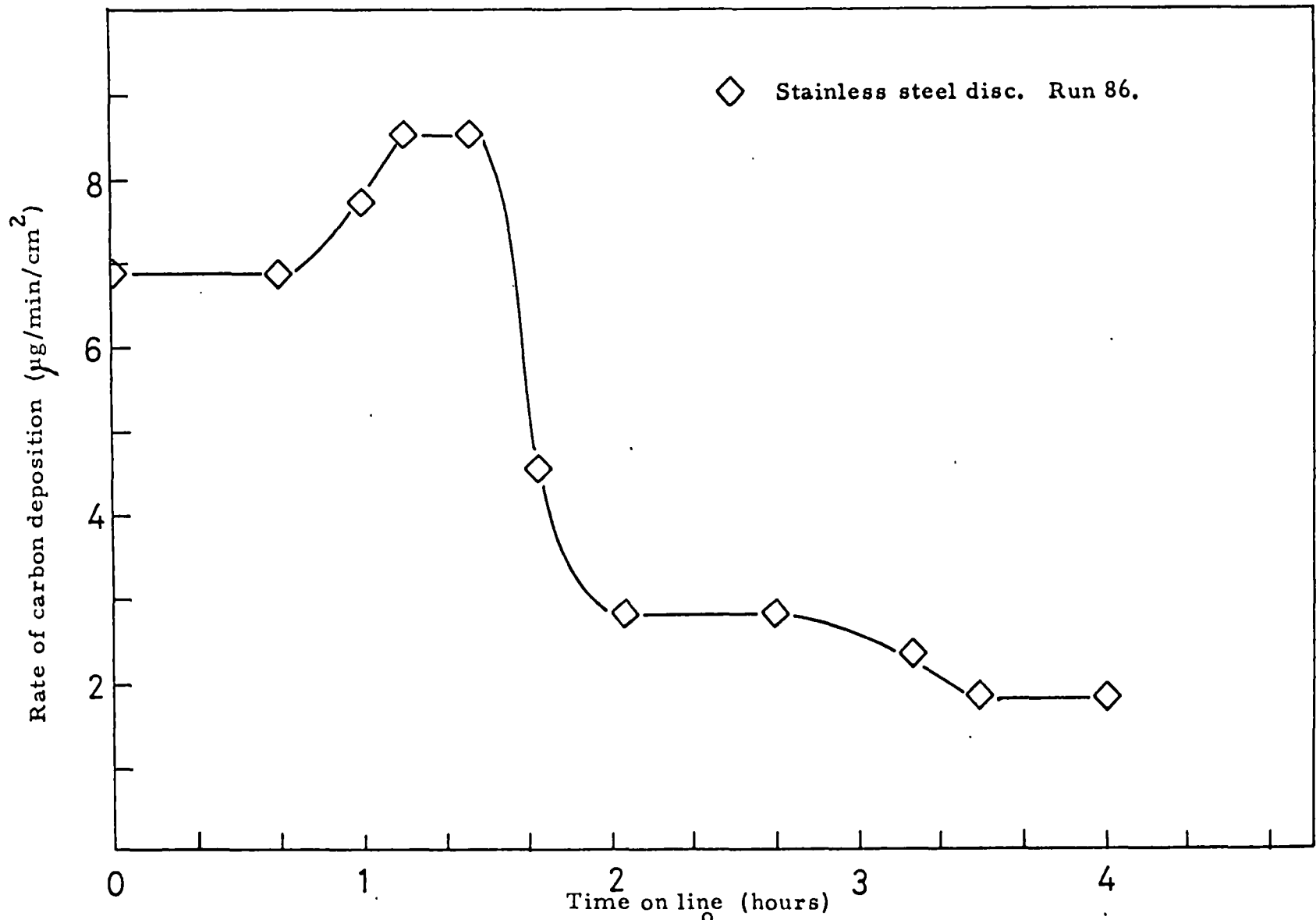
Copper disc. Run 71. Inlet residence time = 3.0 secs.



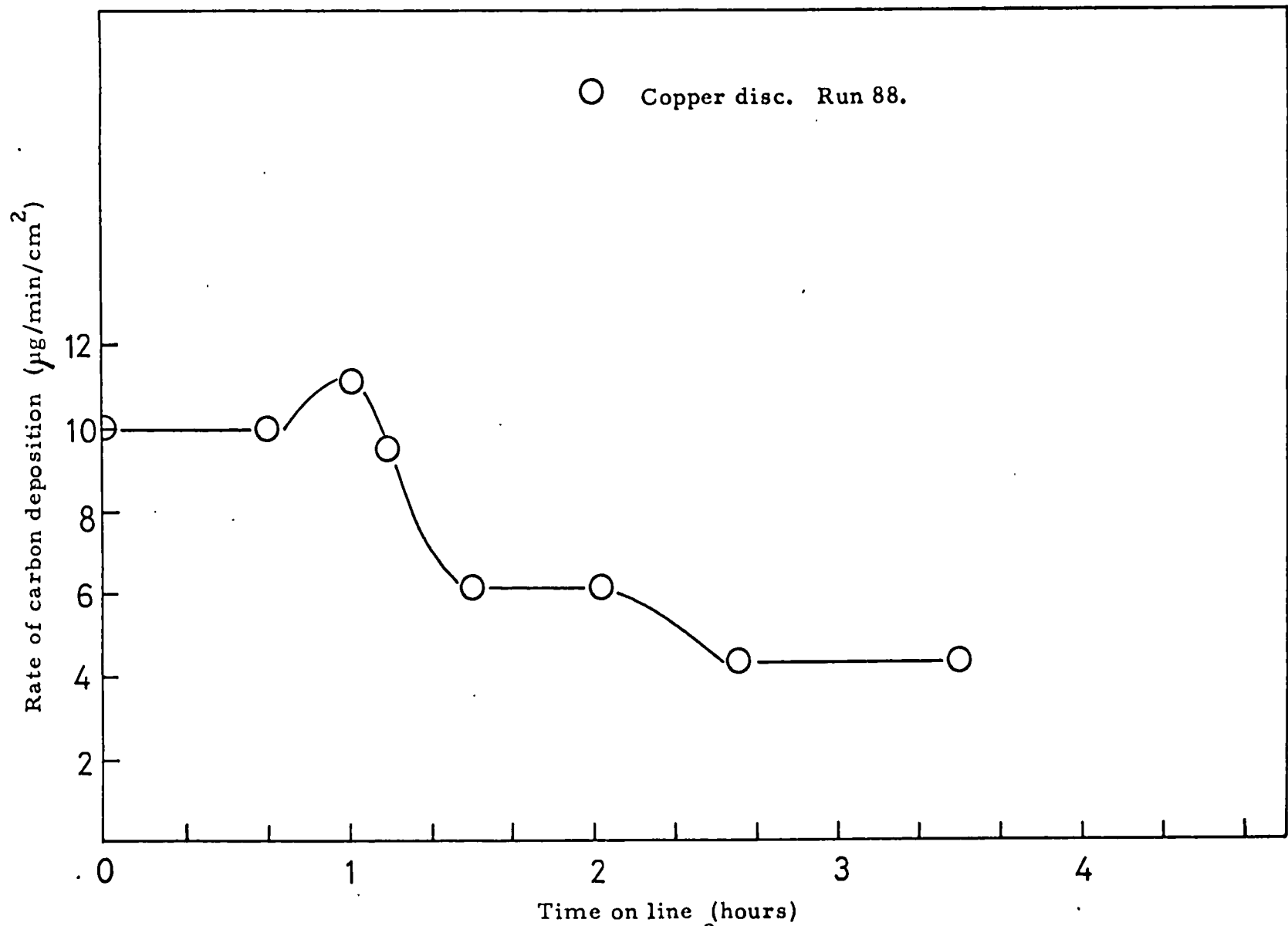
Graph 3.48. H_2S Pre-treatment. 805°C . Inlet residence time = 2.0 secs.



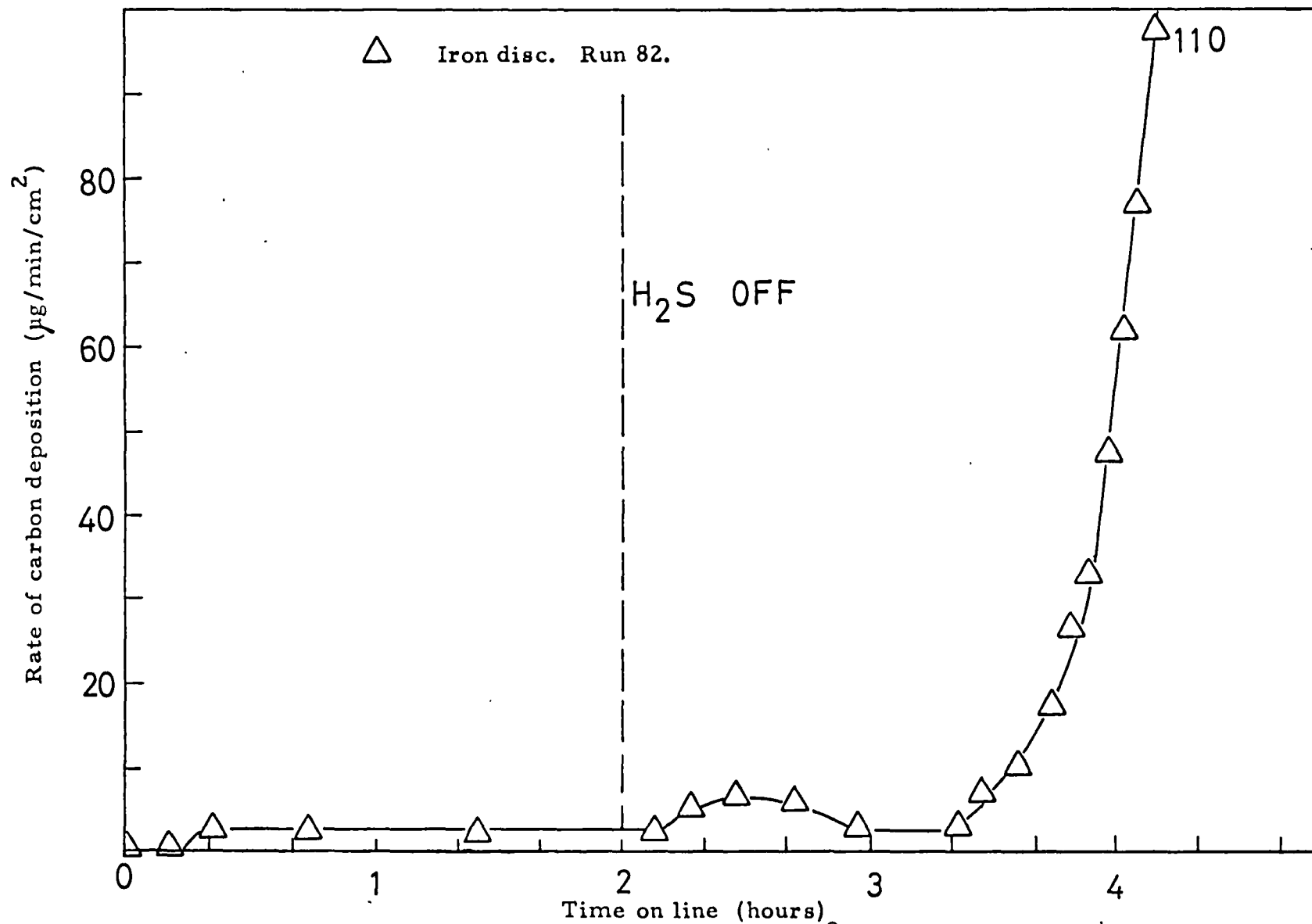
Graph 3.49. H_2S Pre-treatment. 805°C . Inlet residence time = 2.0 secs.



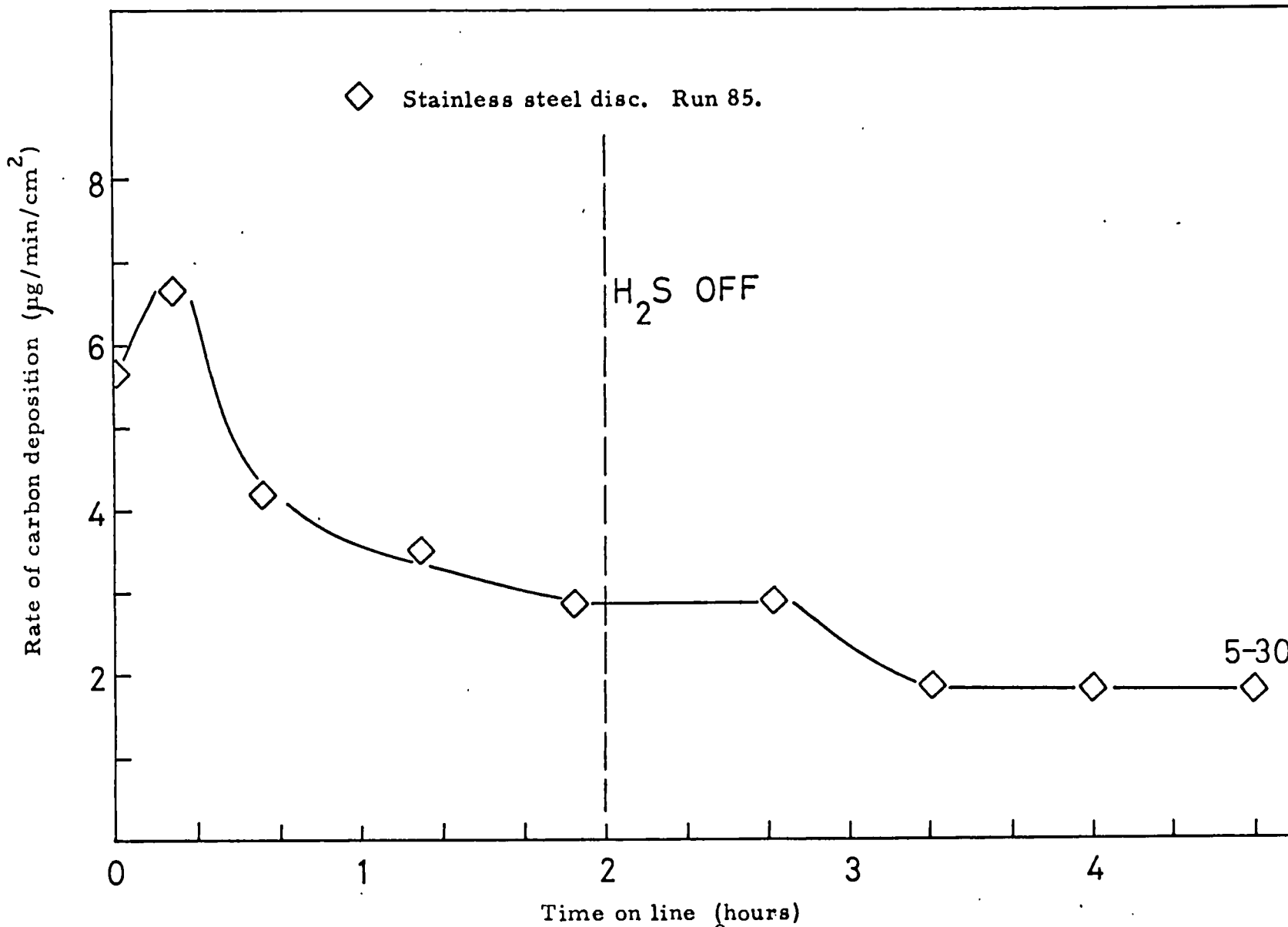
Graph 3.50. H_2S Pre-treatment. 805°C . Inlet residence time = 2.0 secs.



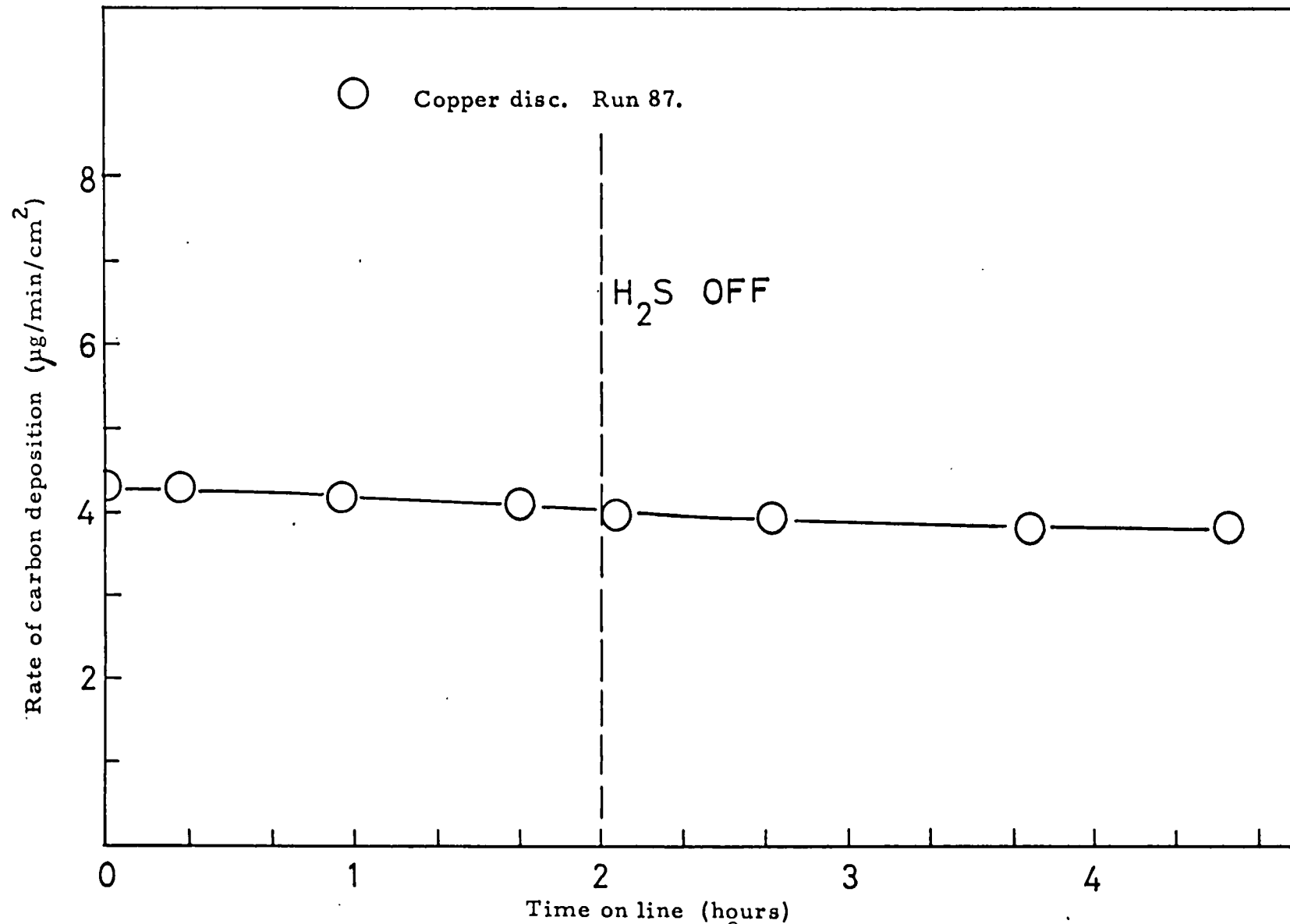
Graph 3.51. H_2S Pre-treatment. 805°C . Inlet residence time = 2.0 secs.



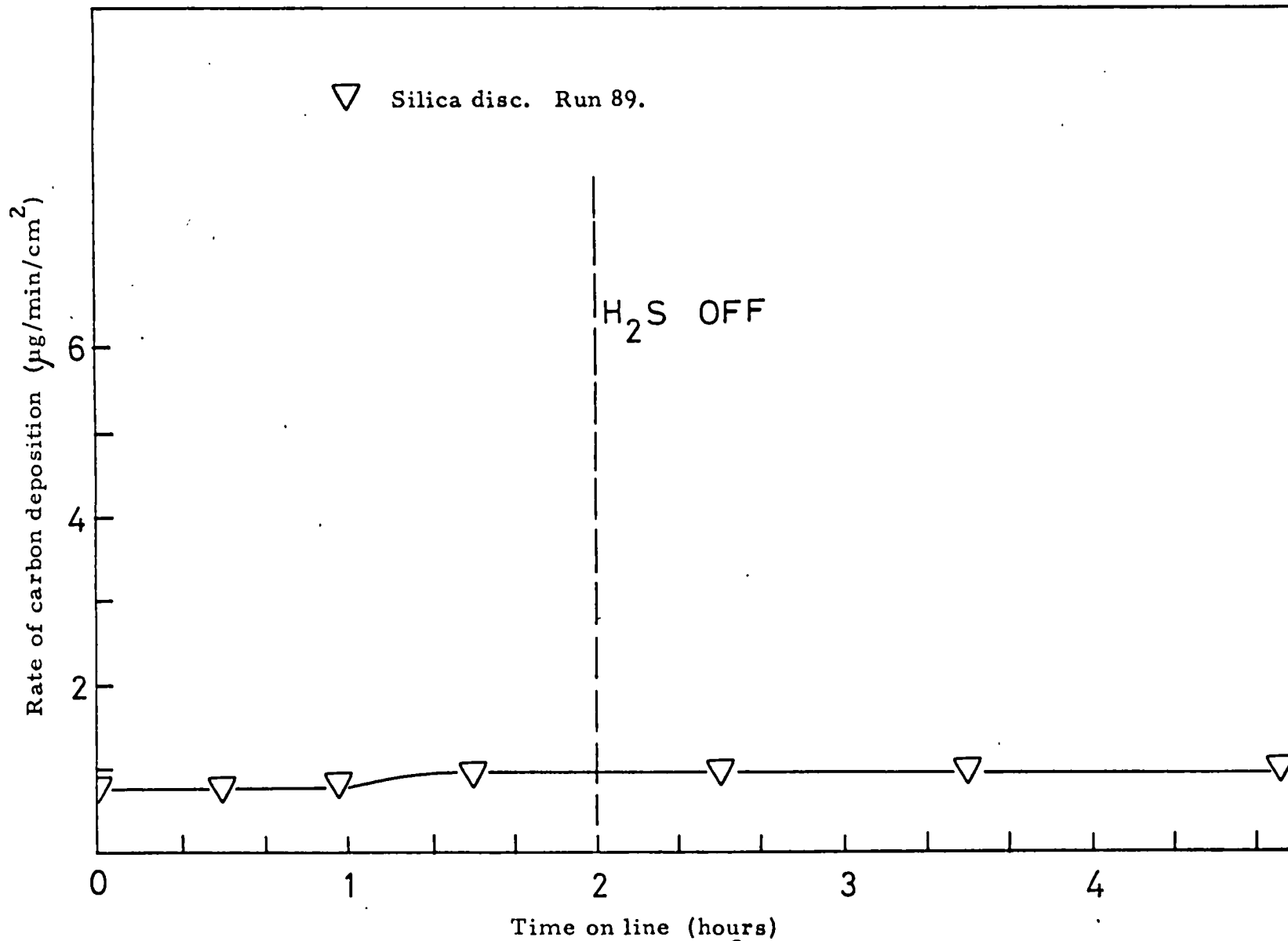
Graph 3.52. 1% H₂S in propane feed. 805°C. Inlet residence time = 2.0 secs.



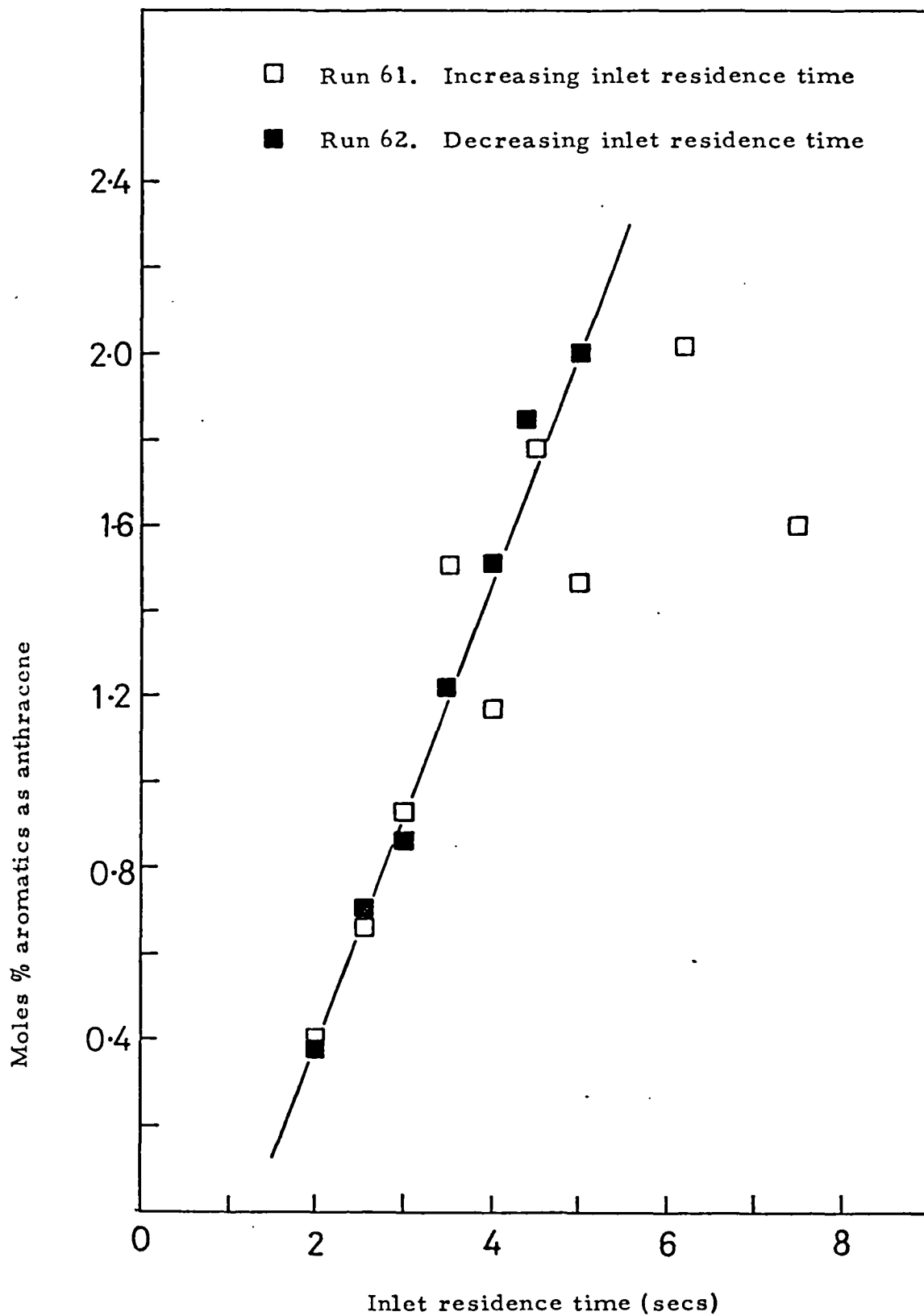
Graph 3.53. 1% H₂S in propane feed. 805°C. Inlet residence time = 2.0 secs.



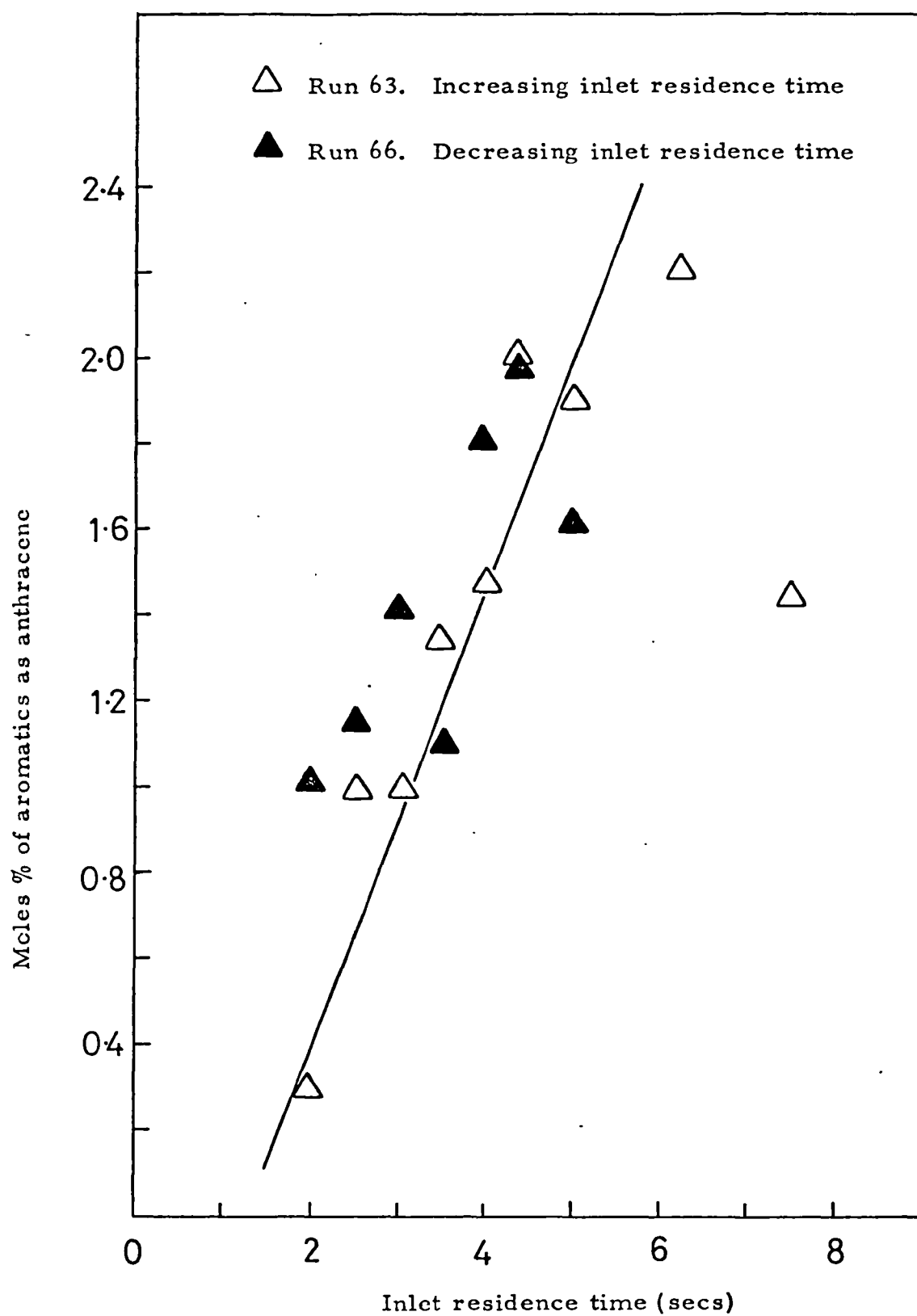
Graph 3.54. 1% H_2S in propane feed. 805°C . Inlet residence time = 2.0 secs.



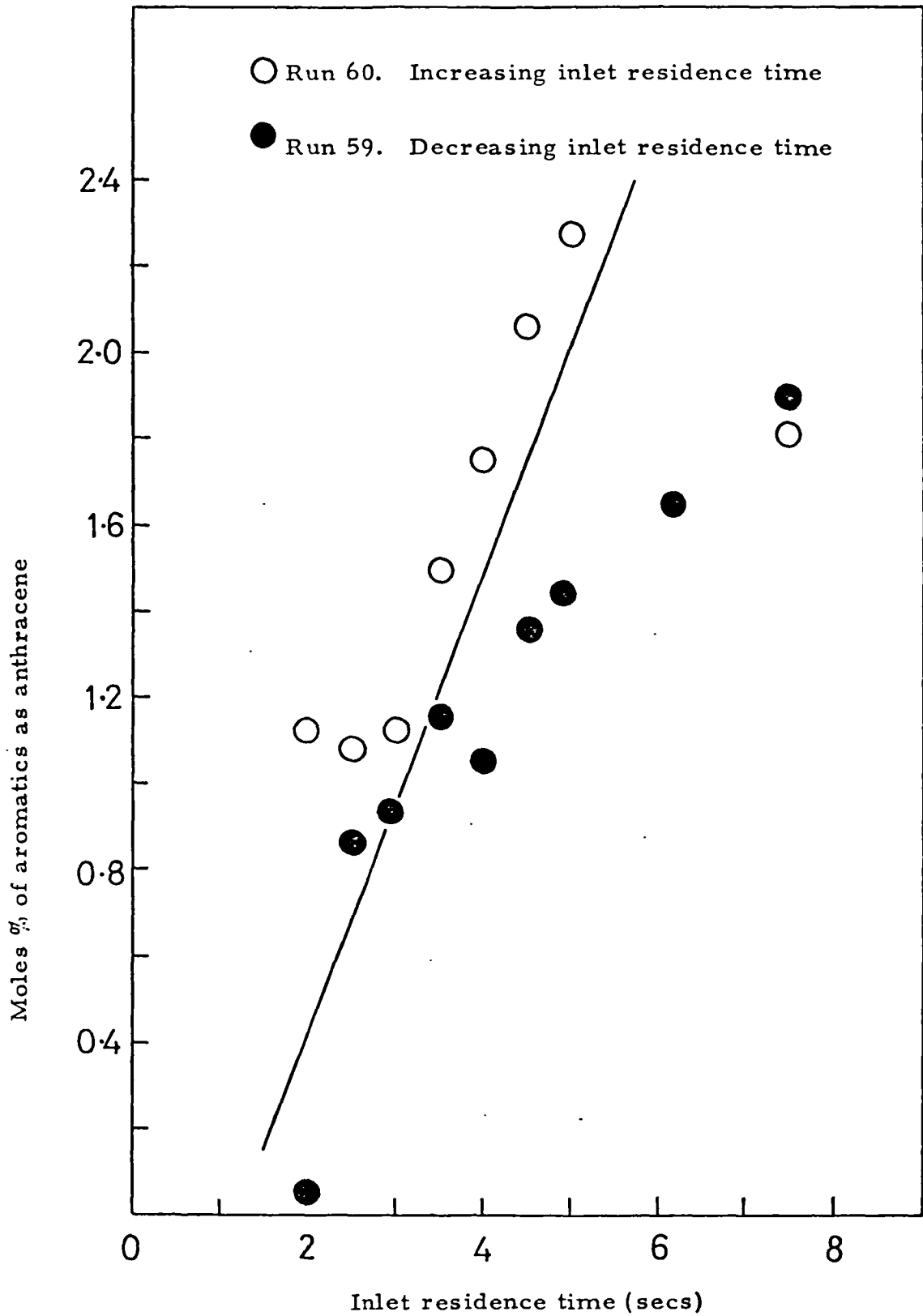
Graph 3.55. 1% H₂S in propane feed. 805°C. Inlet residence time = 2.0 secs.



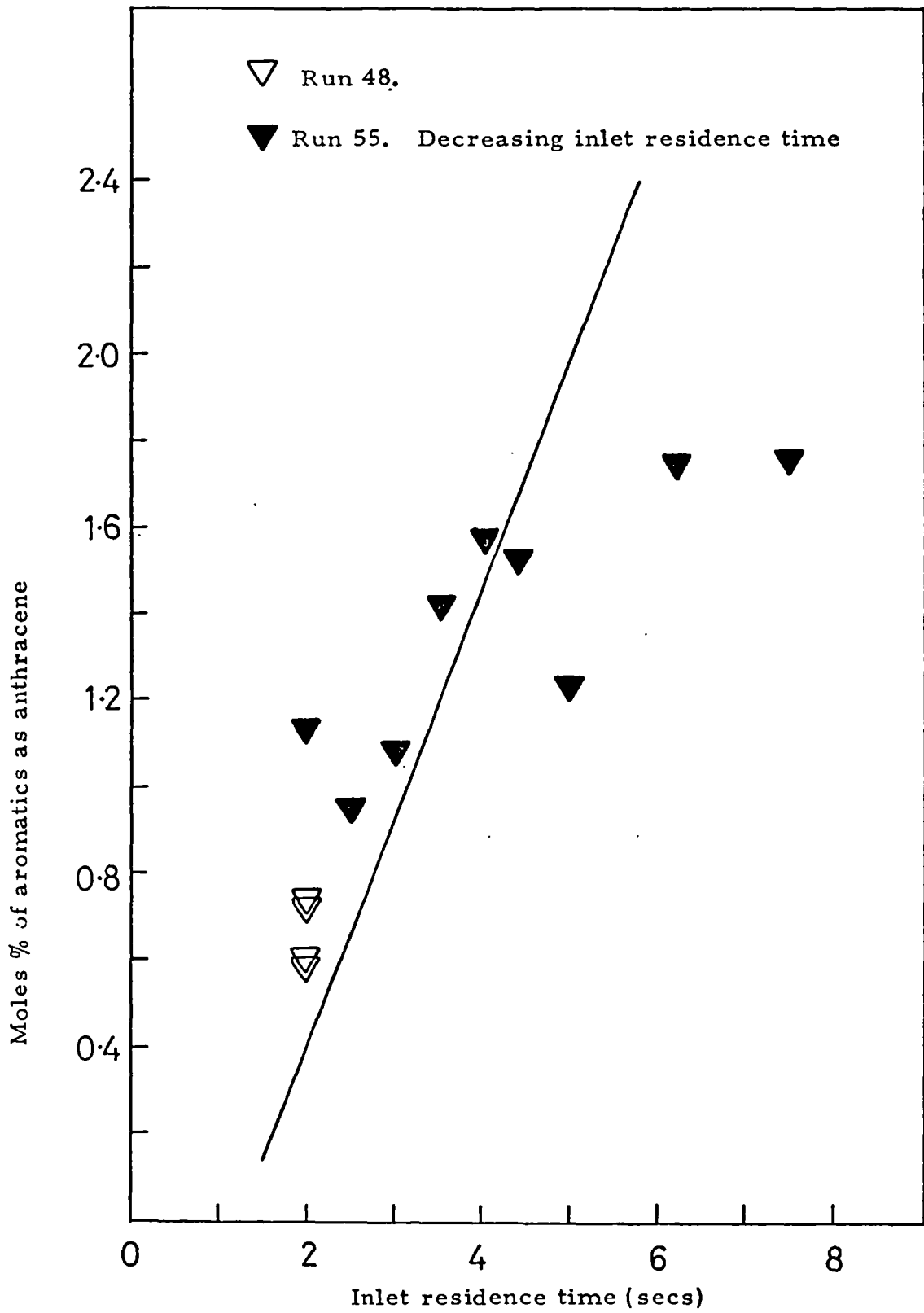
Graph 3.56. Nickel liner with copper collector disc. 810°C



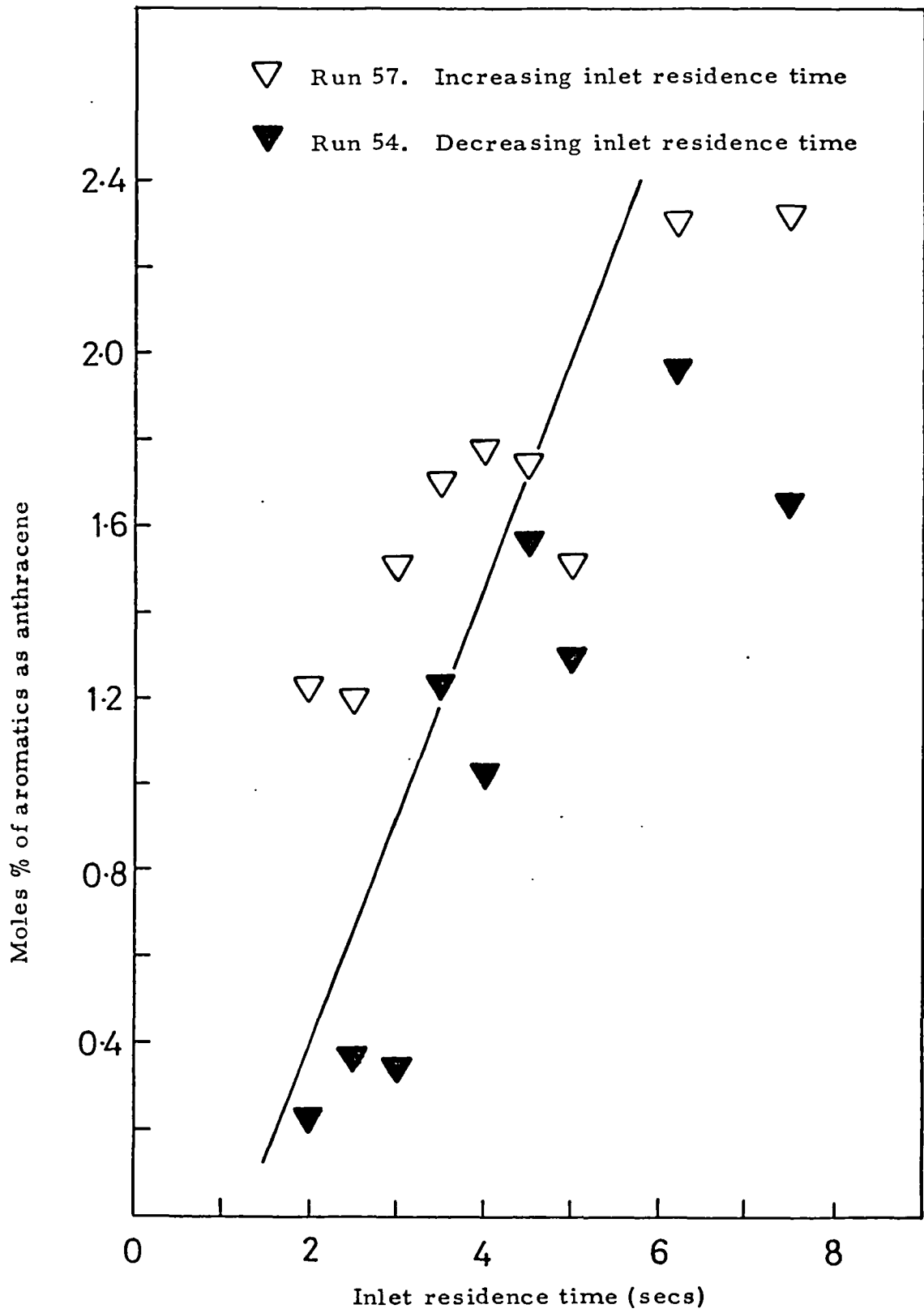
Graph 3.57. Iron liner with copper collector disc. 810°C



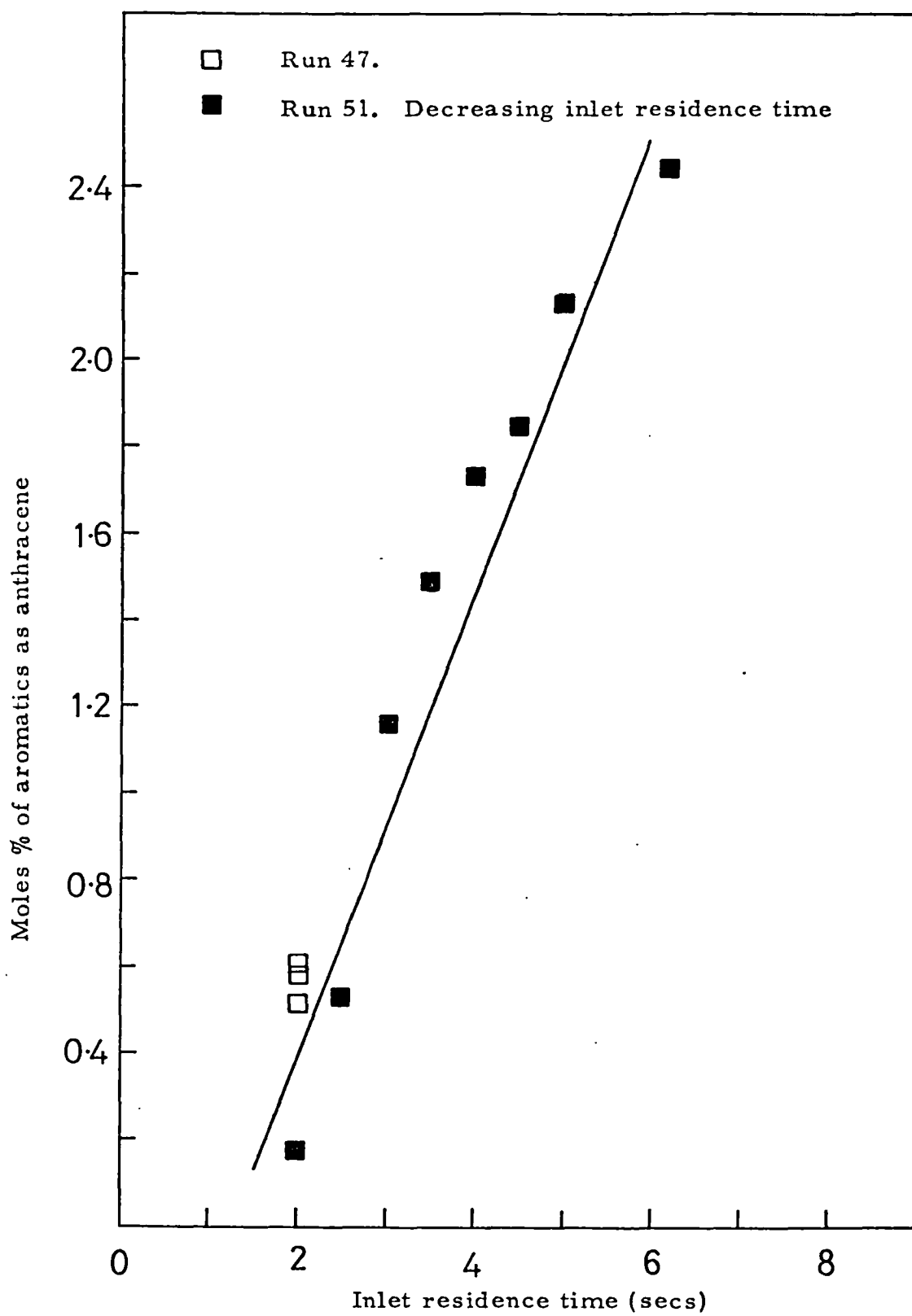
Graph 3.58. Copper liner with copper collector disc. 810°C



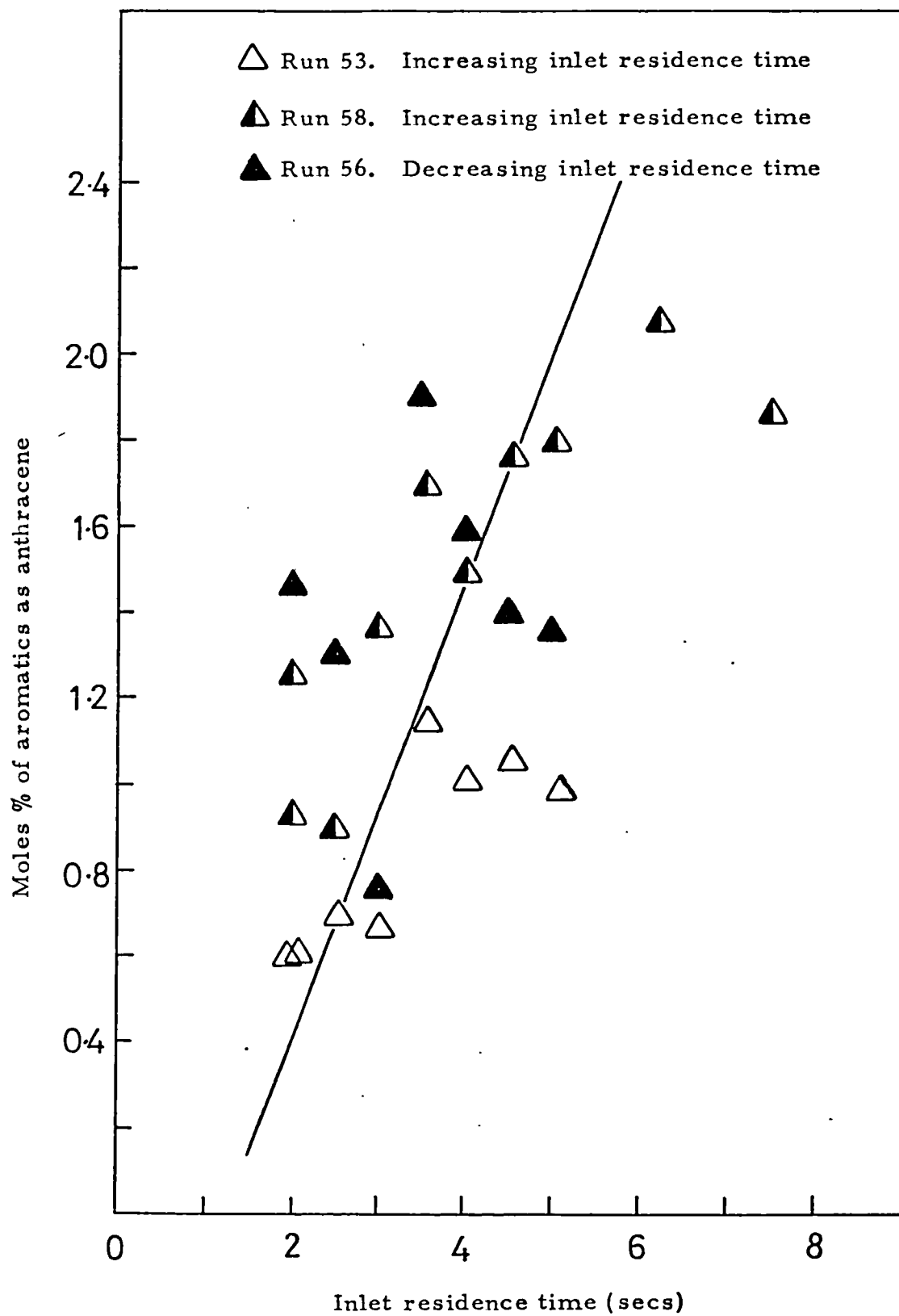
Graph 3.59. Silica "liner" with copper collector disc. 810°C



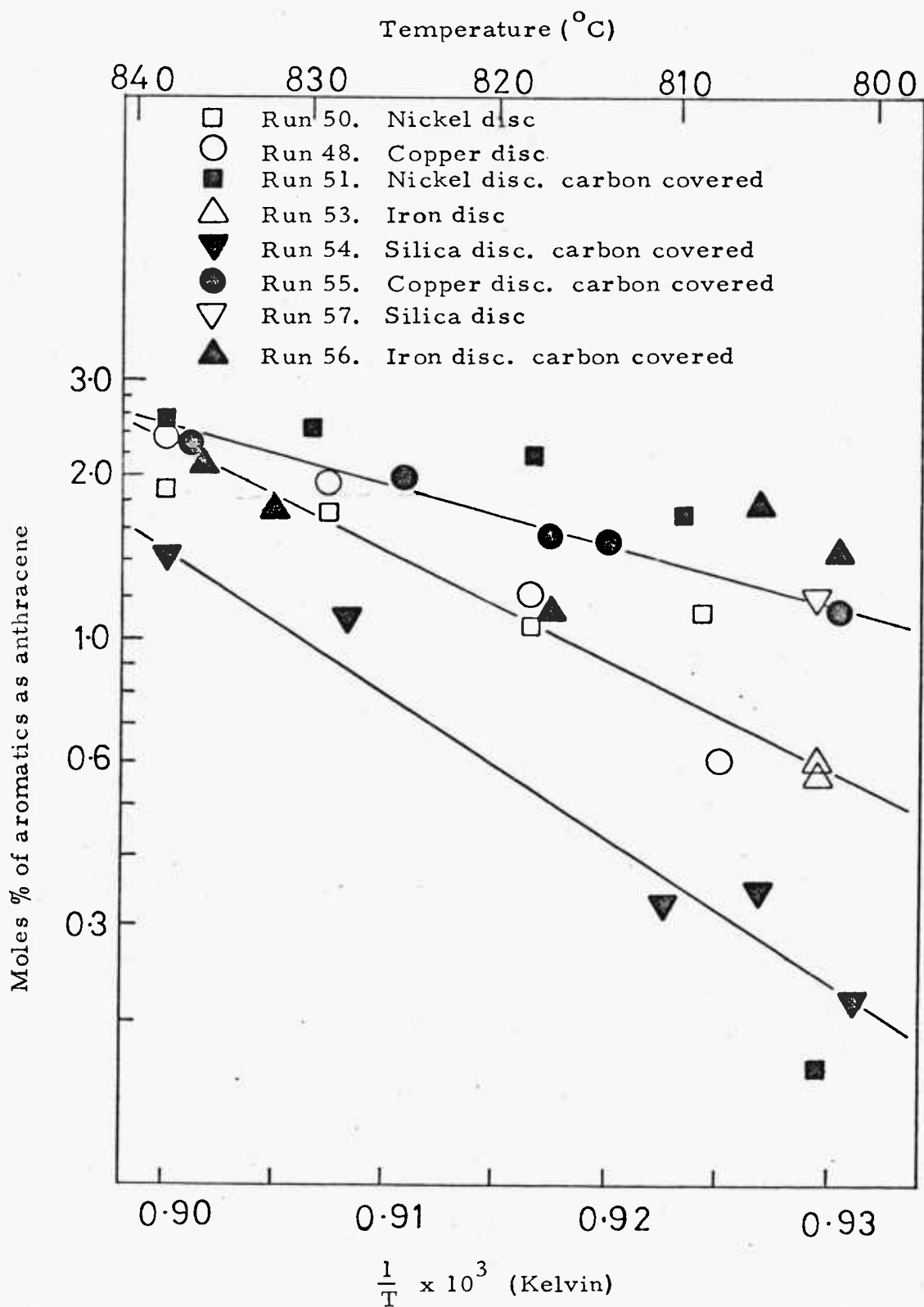
Graph 3.60. Silica disc. 810°C



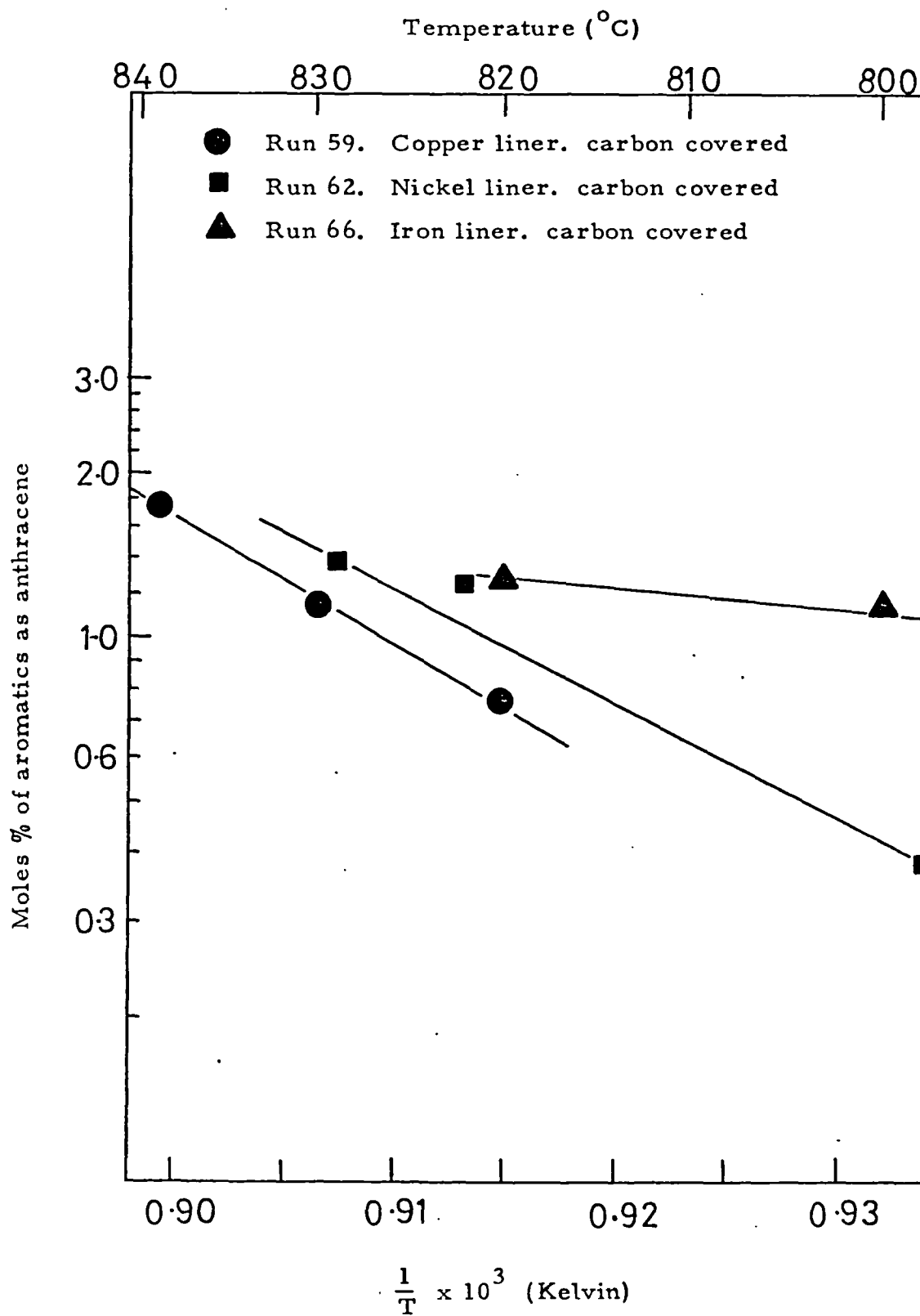
Graph 3.61. Nickel disc. 810°C



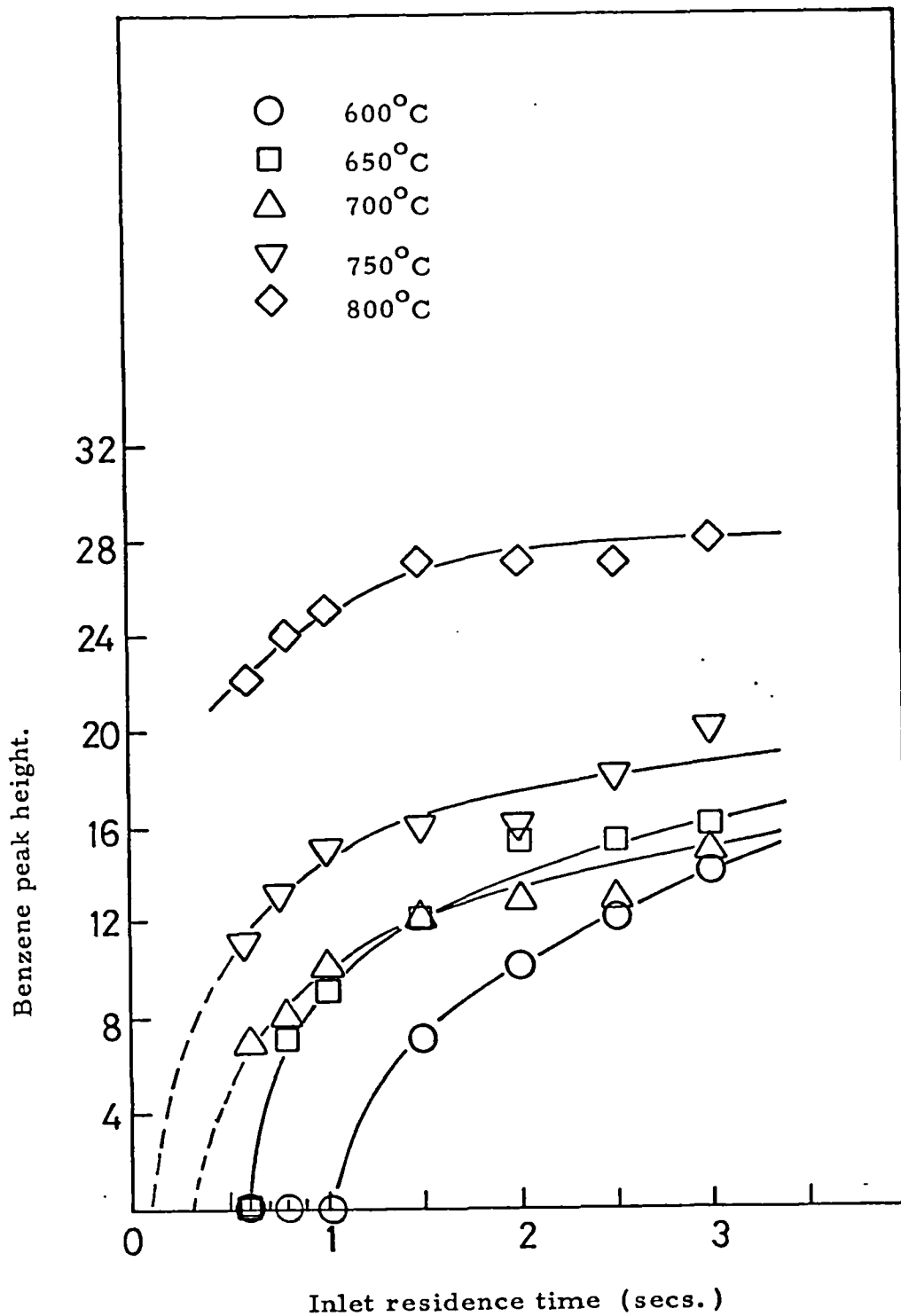
Graph 3.62. Iron disc. 810°C



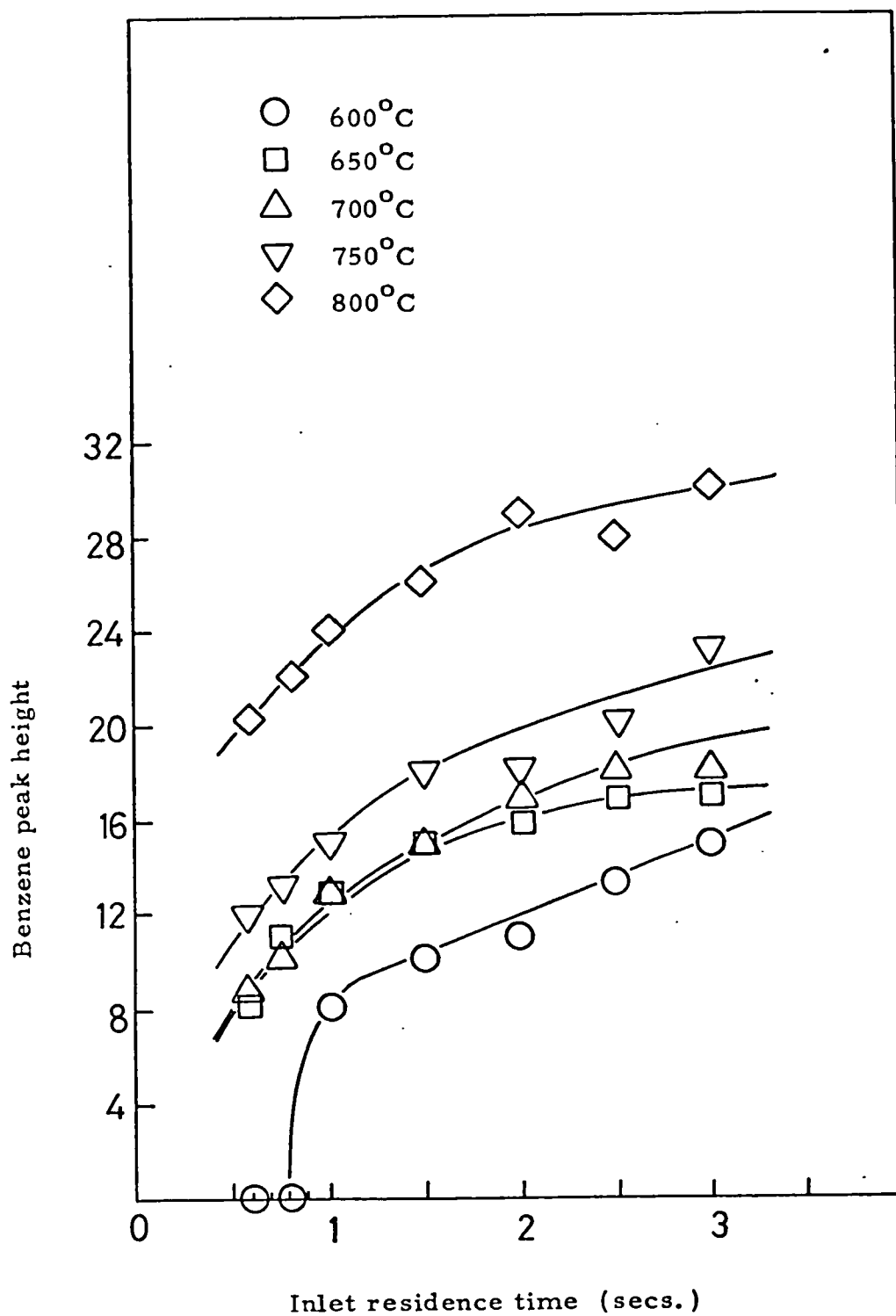
Graph 3.63. Inlet residence time = 2.0 secs.



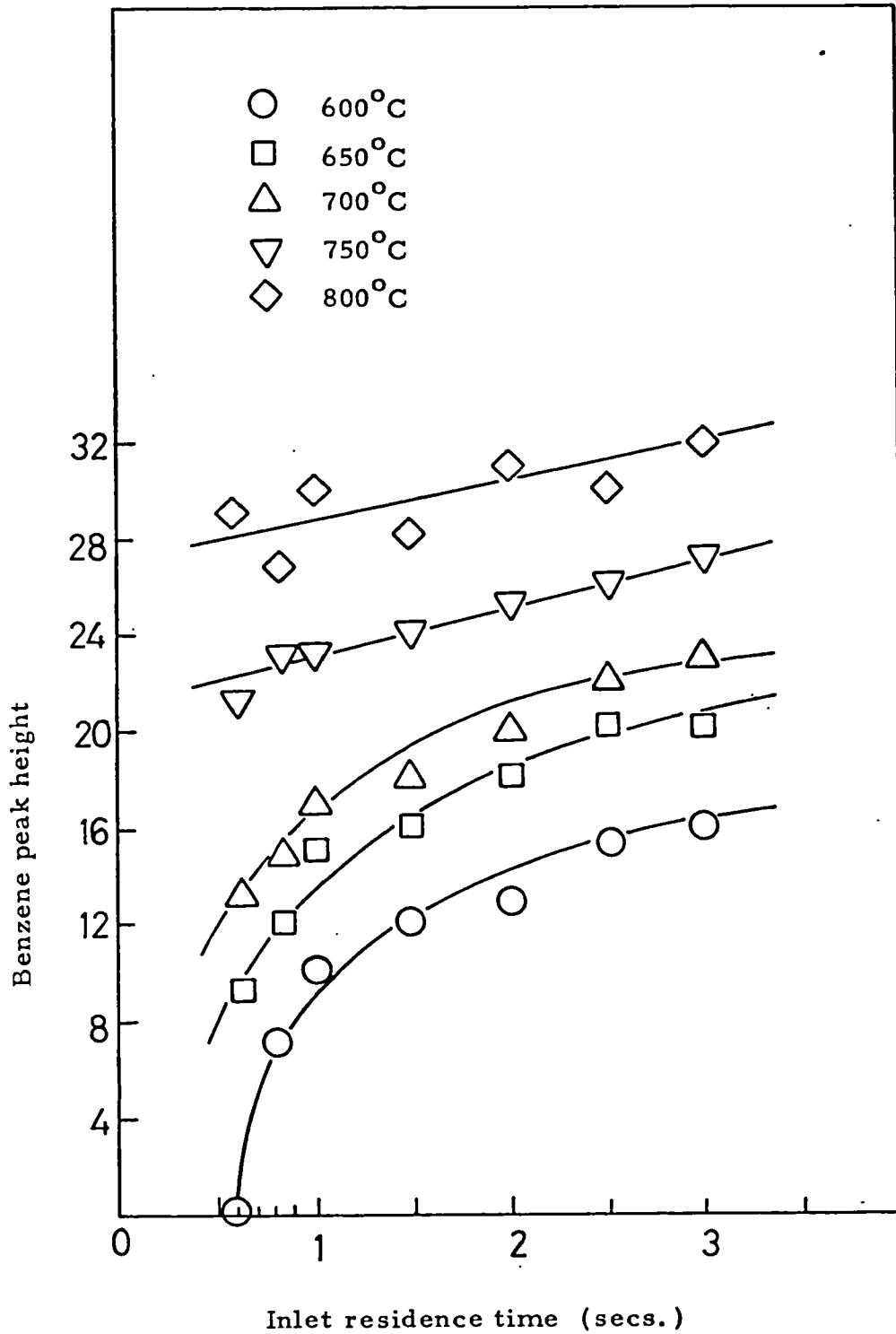
Graph 3.64. Inlet residence time = 2.0 secs.



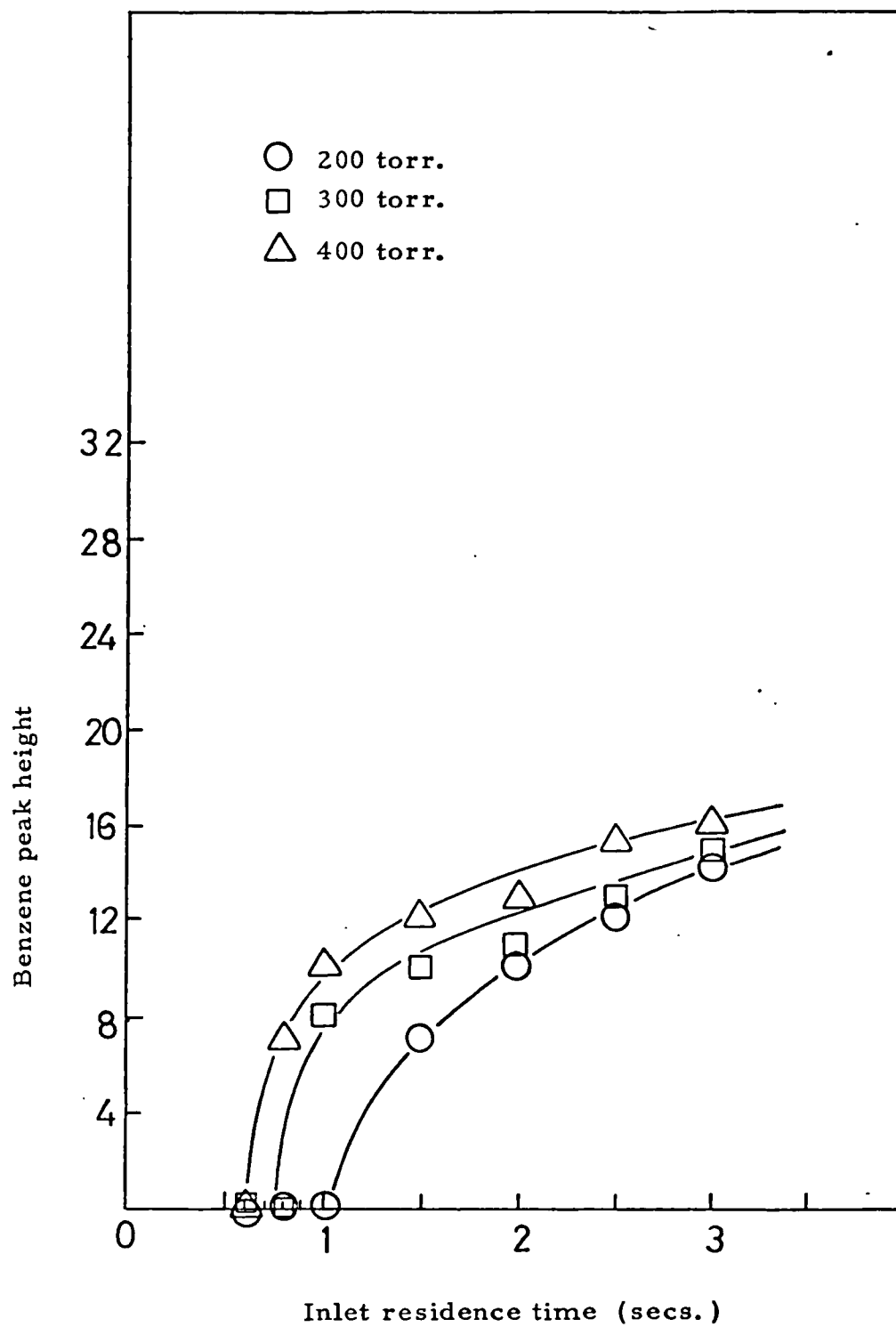
Graph 3.65. 200 torr



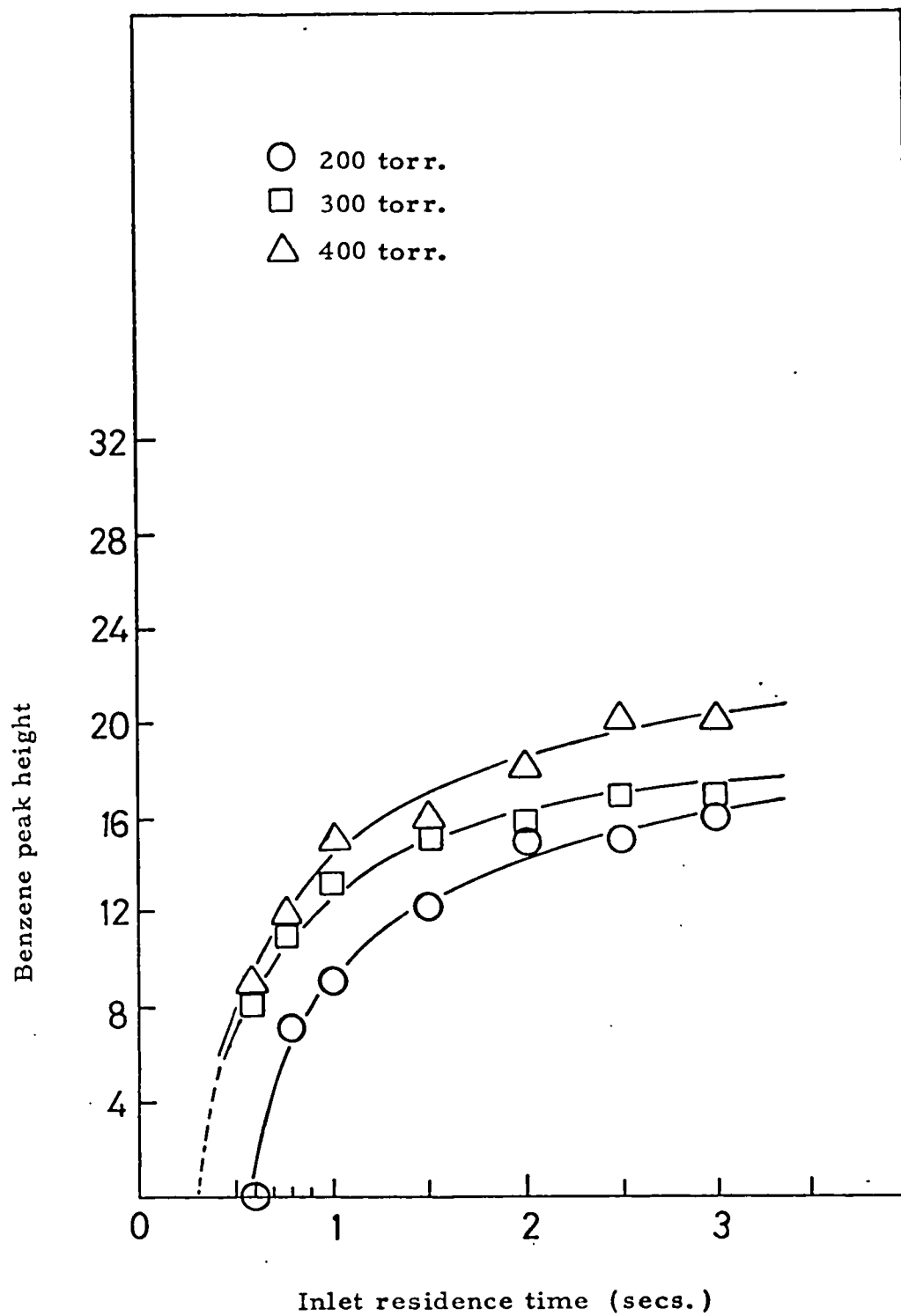
Graph 3.66. 300 torr.



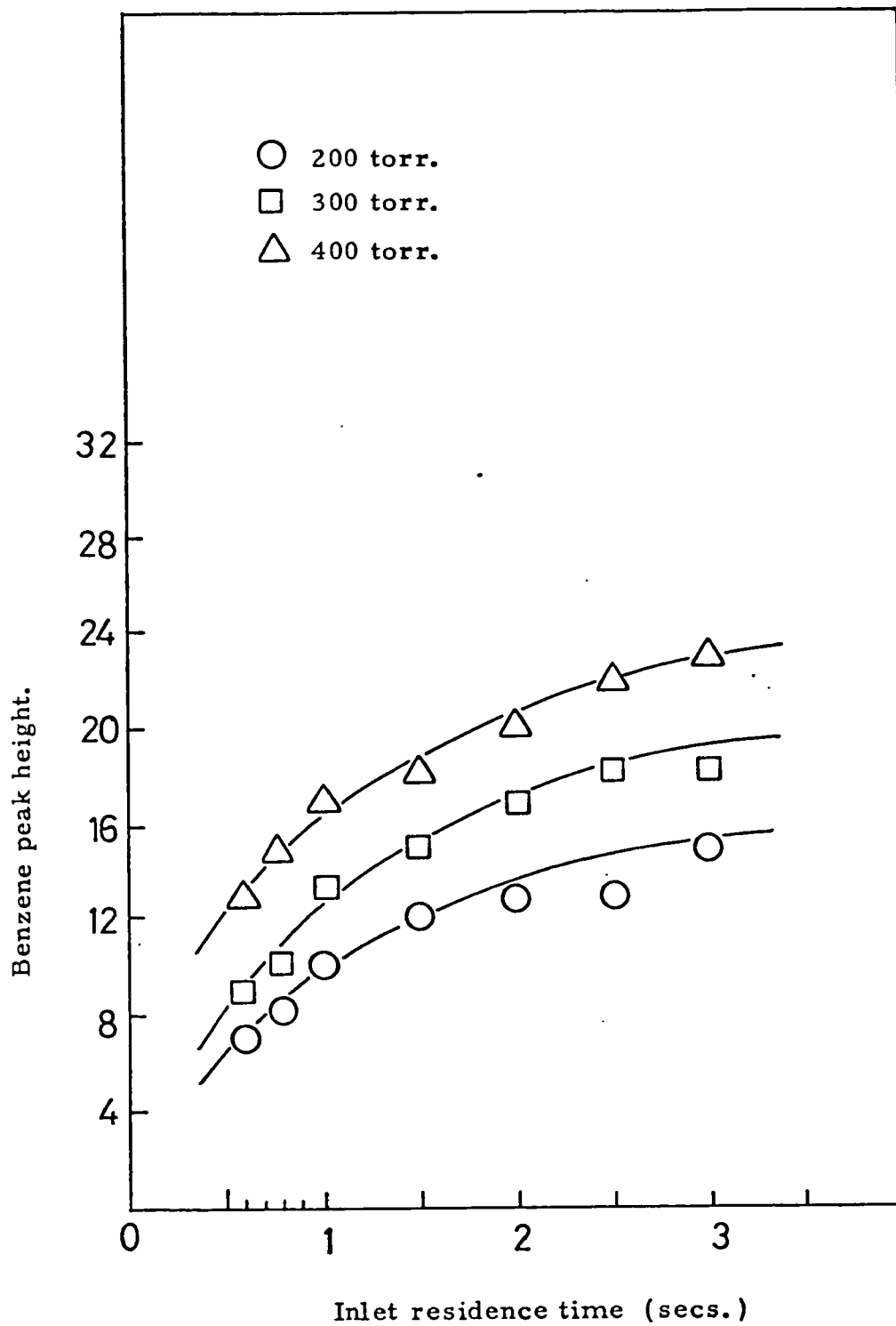
Graph 3.67. 400 torr.



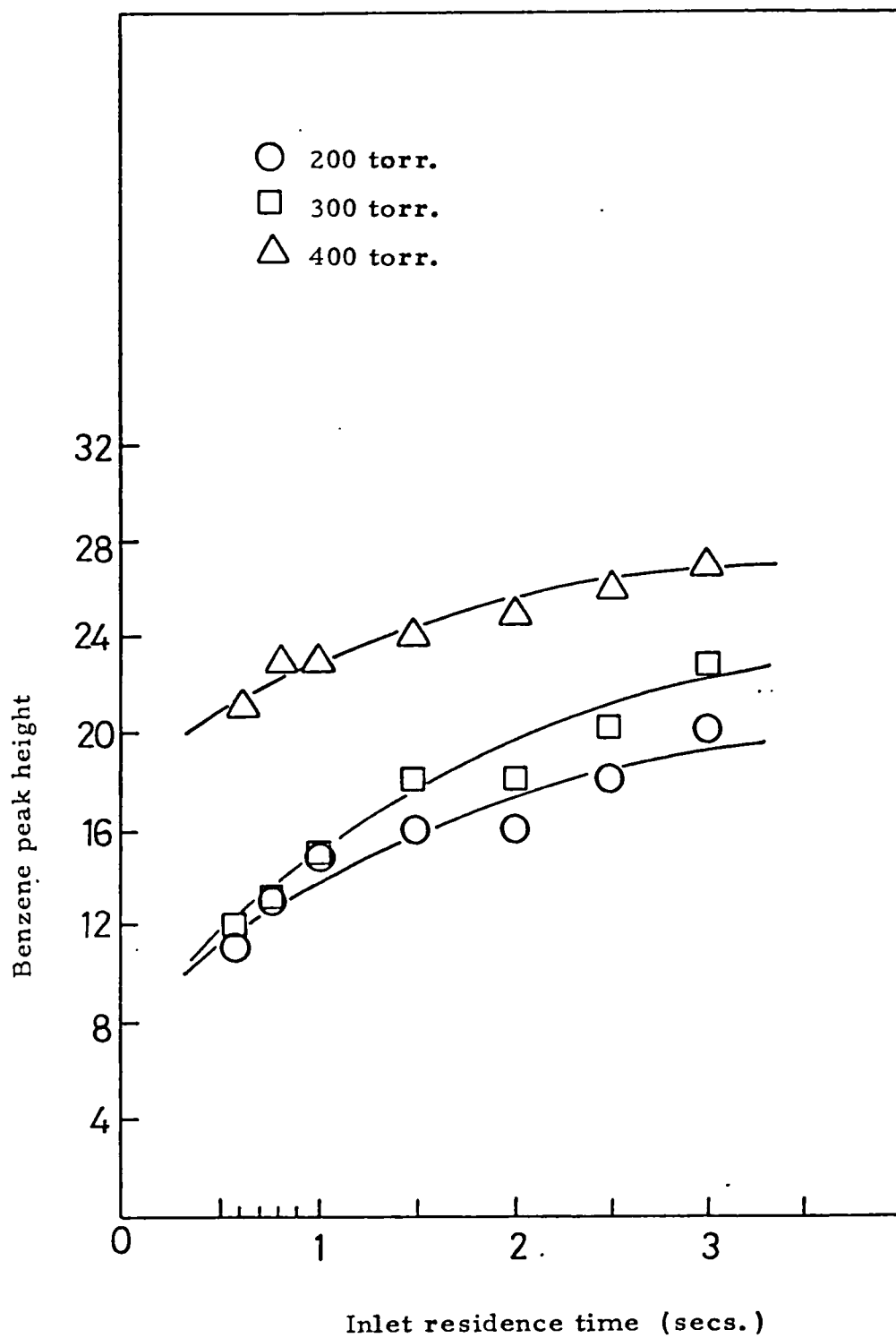
Graph 3.68. 600°C



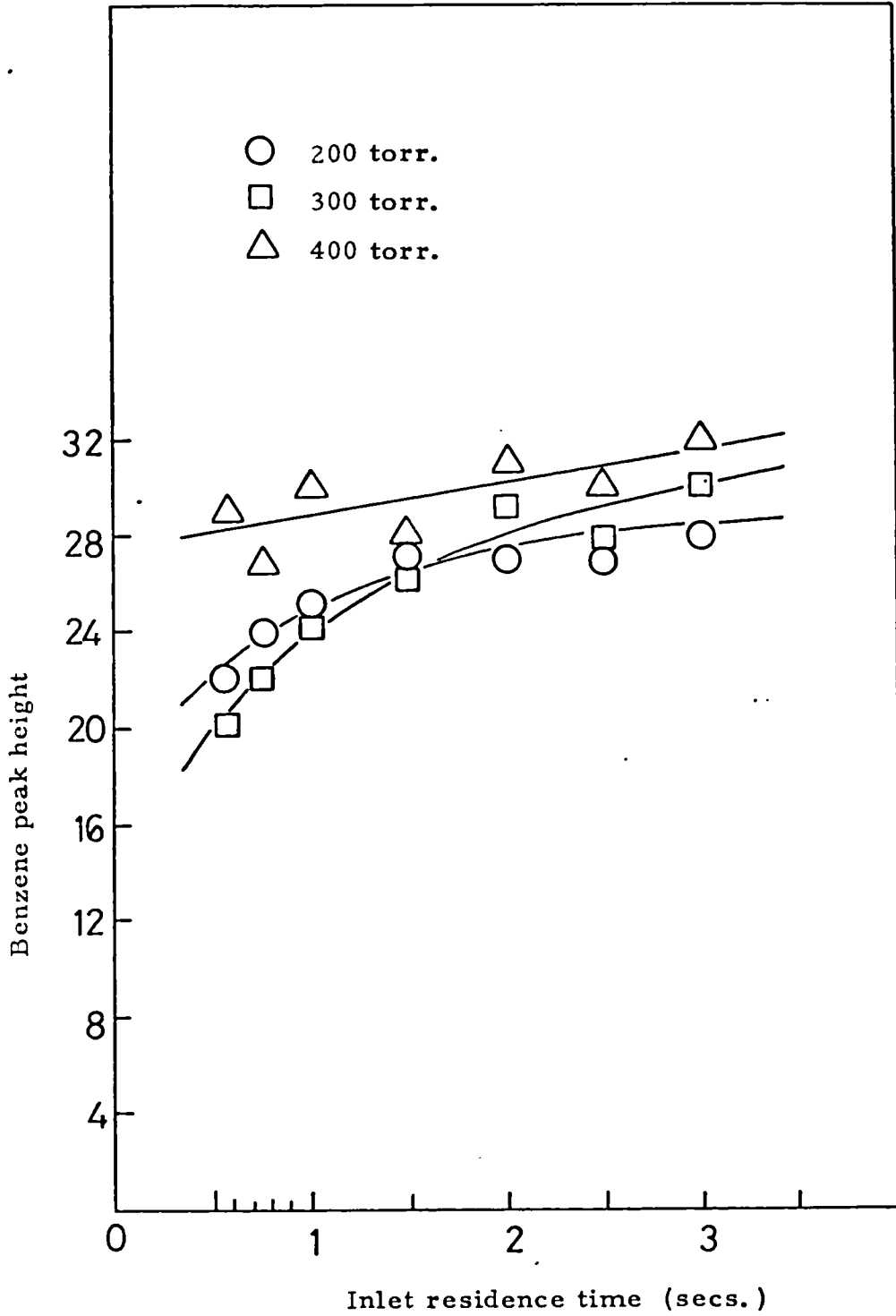
Graph 3.69. 650°C



Graph 3. 70. 700°C



Graph 3. 71. 750°C



Graph 3.72.

800°C

CHAPTER 4DISCUSSION

	Page
4. 1. <u>General</u>	210
4. 2. <u>Gas phase products</u>	212
4. 3. <u>Tars</u>	220
4. 4. <u>Carbon formation</u>	230
4. 4. 1. Heterogeneous-homogeneous effects	230
4. 4. 2. Heterogeneous effects	232
4. 4. 3. Deposition of carbon on "inert" surfaces	246
4. 5. <u>Summary</u>	248

4. 1. General

The process of hydrocarbon pyrolysis studied in the jet-stirred reactor resulted in the production, from a propane feed, of products of different physical natures. These can be classified either as gaseous, liquid phase aromatic and polynuclear aromatic compounds (referred to as tars), or carbons, found on the surface of the reactor or on a disc suspended inside the reactor. The formation of surface carbons can be further classified in terms of whether the surface on which deposition occurred exhibited catalytic activity for carbon formation or not (catalytic and non-catalytic carbon).

Analysis of the gaseous products by gas chromatography showed methane and ethylene to be the major products from propane pyrolysis. The conversion of propane was found to be dependent on the inlet residence time and the temperature. Greater conversions were obtained at longer inlet residence times and higher temperatures.

The liquid phase products were analysed by gas chromatography, which showed benzene to be the main component. Other aromatic and polynuclear aromatic compounds are formed in the pyrolysis process and were analysed by carbon balances and by mass spectrometry. The production of these products increases with increasing inlet residence time and increasing temperature.

The study of the formation of carbon on the surface of discs suspended inside the reactor identified a period during which the rate of carbon deposition is dependent on the disc material. After this period a steady-state rate of deposition was observed; further carbon being deposited on the carbon already deposited. The rate of carbon deposition increases with increasing inlet residence time and increasing temperature.

The temperature at which carbon deposition starts was found to be dependent on the metal present inside the reactor. A tendency was observed for the catalytic activity of the metal to change with time, as a result of encapsulation of the metal by carbon. Hydrogen was found to prevent this encapsulation.

It is useful to discuss the formation of gases, tars and carbons separately in some detail, and then to consider briefly, the combination of information obtained from each discussion.

4. 2. Gas phase products

The gas phase product distributions as described in the results summarised in section 3. 3. 2. , were found to be independent of the nature of the reactor wall. No differences could be observed in the product distribution when the nature of the wall was changed. Surface effects, Penninger (79)(80), would be expected to change the gas phase product distribution.

Calculations performed after the experiments showed, however, that any changes would be too small to identify using the analytical apparatus (section 3. 3. 2.). In view of the carbon results (sections 3. 2. 1. and 3. 3. 1.), a small change in the relative amounts of gases would be expected, were the analysis sufficiently sensitive.

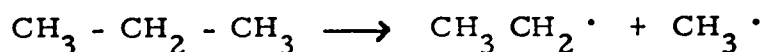
Pyrolysis of pure propane gave, in order of decreasing importance, methane, ethylene, hydrogen, propylene and ethane, for experiments carried out with pyrolysis at 810°C and 2-7.5 sec. inlet residence time (section 3. 2. 2.). Dilution of propane with helium had little effect on the relative magnitudes of these products (section 3. 4. 2. b.), but dilution with hydrogen influenced the distribution (section 3. 4. 2. a.). When less than 37% (v/v) propane was fed to the reactor, propane and measurable quantities of hydrogen were consumed, and the production of methane and ethane increased as the hydrogen consumption increased. Less propane was converted when hydrogen was consumed. The activation energy was measured for the product hydrocarbons, in the absence of added hydrogen, for pyrolysis between the temperature range 790°-850°C, at 2.0 secs. inlet residence time:

methane,	$E_a = + 11.2$	kcal/mole
ethylene,	$E_a = + 6.1$	kcal/mole (790-820°C).
	$E_a = - 7.8$	kcal/mole (820-850°C).
hydrogen,	$E_a = + 13.5$	kcal/mole
propylene,	$E_a = - 34.7$	kcal/mole
ethane,	$E_a = - 10.5$	kcal/mole

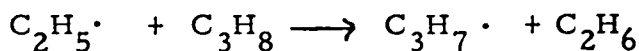
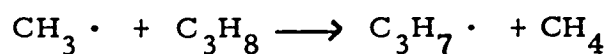
Thermodynamically, the observed products are not unexpected. Inspection of the free energy diagram for different

hydrocarbons given in figure 4.1., shows that at the operating temperatures of above 800°C (1073°K), all of the observed products could be expected.

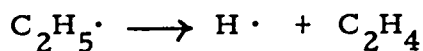
However, the pyrolysis of propane is known to be a free radical chain reaction, Laidler (115), and the individual reactions leading to products are more open to question. Thermal initiation of the reaction could involve C-H or C-C bond rupture, but the mean bond energies are such that initiation probably involves C-C bond rupture:



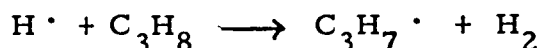
Subsequent propagation involves hydrogen abstraction from propane to give normal, or isopropyl radicals (less likely). Hinshelwood (116) found that at pyrolysis temperatures, the normal and isopropyl radicals are rapidly interconverted. The reaction scheme can be simplified by writing either radical as $\text{C}_3\text{H}_7\cdot$



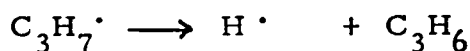
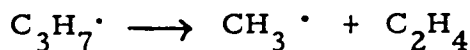
The ethyl radicals could also decompose:



to give a hydrogen atom which can complete the chain:



The propyl radicals will undergo some decomposition:



Termination of the chain is open to some question.

Conventionally, biradical termination



is considered the major termination reaction, but the basis for this rests on experiments carried out at sub-atmospheric pressures, Laidler (115). Only limited data is available at atmospheric pressure, where two possibilities exist. Either the concentration of radicals is high enough that biradical collision is favoured, or a radical could

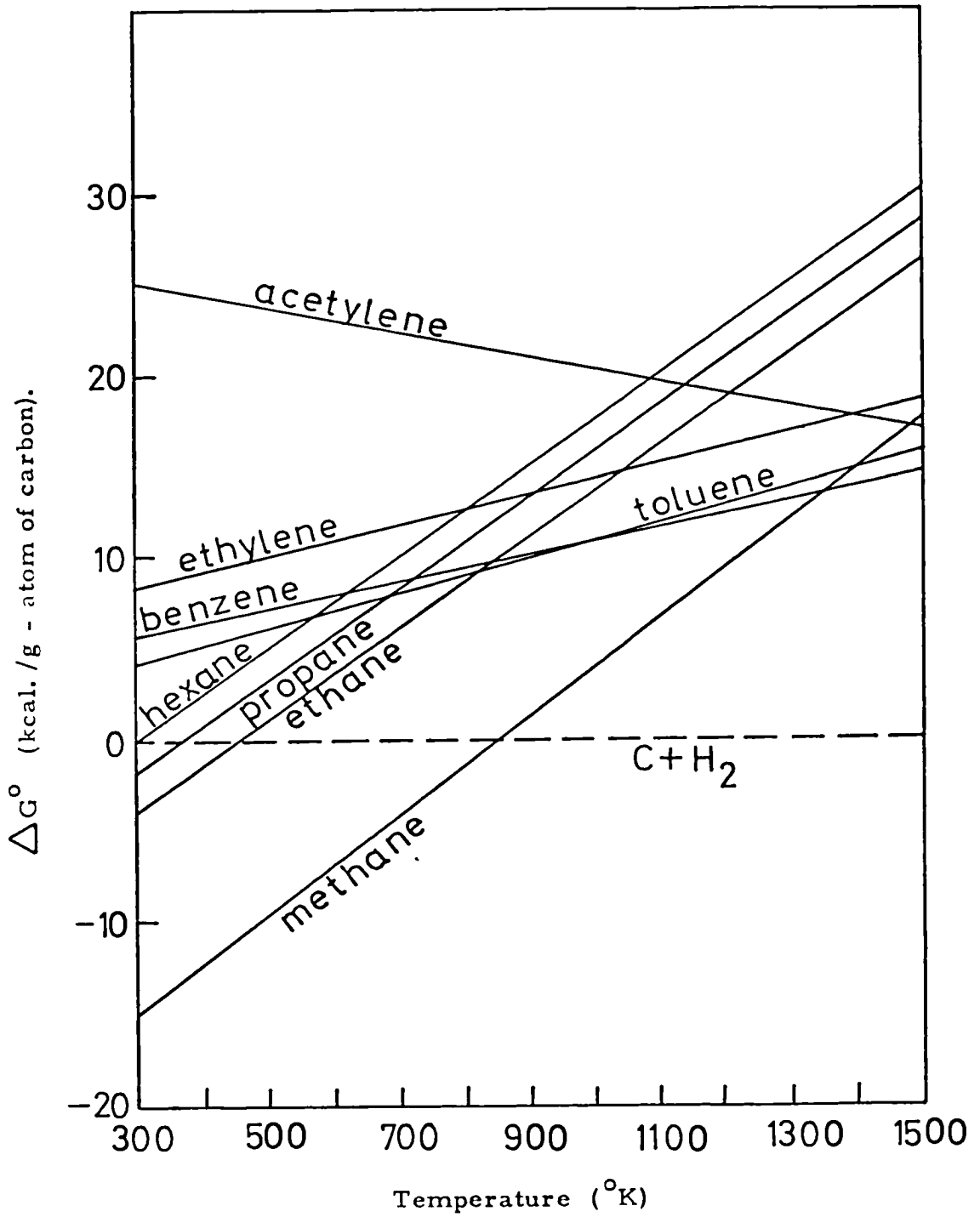


Fig. 4.1. Free energy of formation of hydrocarbons
(Germain (114)).

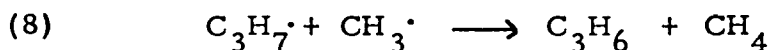
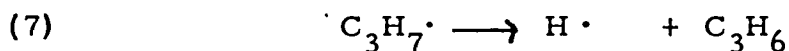
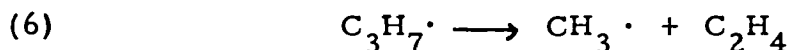
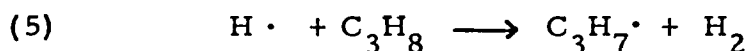
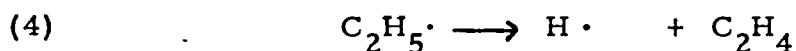
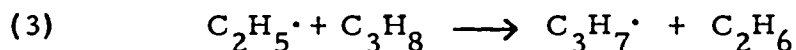
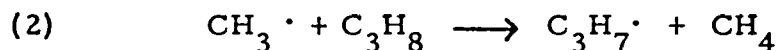
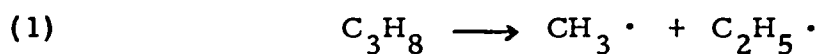
react with a third body and deactivate:



Atmospheric pressure will limit diffusion of radicals to the wall, but propane itself could have sufficiently high numbers of degrees of freedom to accept the excess energy without forming a radical i. e. to act as a third body. Inspection of the results (see, for example, graph 3.16.) shows that propane is consumed in the reaction, inferring that biradical termination is more likely. Following Herriott (117), the important termination reaction may be written



Then a possible reaction mechanism may be written:



Application of the steady-state approximation to this reaction scheme gives:

$$-\frac{d(C_3H_8)}{dt} = k_1(C_3H_8) + k_2(CH_3\cdot)(C_3H_8) + k_3(C_2H_5\cdot)(C_3H_8) + k_5(H\cdot)(C_3H_8) \quad (1)$$

and to the free radicals gives:

$$\frac{d(H\cdot)}{dt} = 0 = k_4(C_2H_5\cdot) - k_5(H\cdot)(C_3H_8) + k_7(C_3H_7\cdot) \quad (2)$$

$$(H\cdot) = \frac{k_4(C_2H_5\cdot) + k_7(C_3H_7\cdot)}{k_5(C_3H_8)} \quad (3)$$

$$\frac{d(CH_3\cdot)}{dt} = 0 = k_1(C_3H_8) - k_2(CH_3\cdot)(C_3H_8) + k_6(C_3H_7\cdot) - k_8(C_3H_7\cdot)(CH_3\cdot) \quad (4)$$

$$(\text{CH}_3\cdot) = \frac{k_1 (\text{C}_3\text{H}_8) + k_6 (\text{C}_3\text{H}_7\cdot)}{k_2 (\text{C}_3\text{H}_8) + k_8 (\text{C}_3\text{H}_7\cdot)} \quad (5)$$

$$\frac{d(\text{C}_2\text{H}_5\cdot)}{dt} = 0 = k_1 (\text{C}_3\text{H}_8) - k_3 (\text{C}_2\text{H}_5\cdot) (\text{C}_3\text{H}_8) - k_4 (\text{C}_2\text{H}_5\cdot) \quad (6)$$

$$(\text{C}_2\text{H}_5\cdot) = \frac{k_1 (\text{C}_3\text{H}_8)}{k_3 (\text{C}_3\text{H}_8) + k_4} \quad (7)$$

$$\frac{d(\text{C}_3\text{H}_7\cdot)}{dt} = 0 = k_2 (\text{CH}_3\cdot) (\text{C}_3\text{H}_8) + k_3 (\text{C}_2\text{H}_5\cdot) (\text{C}_3\text{H}_8) + k_5 (\text{H}\cdot) (\text{C}_3\text{H}_8) - k_6 (\text{C}_3\text{H}_7\cdot) - k_7 (\text{C}_3\text{H}_7\cdot) (\text{CH}_3\cdot) - k_8 (\text{C}_3\text{H}_7\cdot) (\text{CH}_3\cdot) \quad (8)$$

$$(\text{C}_3\text{H}_7\cdot) = \frac{k_2 (\text{CH}_3\cdot) (\text{C}_3\text{H}_8) + k_3 (\text{C}_2\text{H}_5\cdot) (\text{C}_3\text{H}_8) + k_5 (\text{H}\cdot) (\text{C}_3\text{H}_8)}{k_6 + k_7 + k_8 (\text{CH}_3\cdot)} \quad (9)$$

addition of these four free radical equations gives:

$$\begin{aligned} 0 &= k_4 (\text{C}_2\text{H}_5\cdot) - k_5 (\text{H}\cdot) (\text{C}_3\text{H}_8) + k_7 (\text{C}_3\text{H}_7\cdot) + k_1 (\text{C}_3\text{H}_8) - k_2 (\text{CH}_3\cdot) (\text{C}_3\text{H}_8) + k_6 (\text{C}_3\text{H}_7\cdot) \\ &\quad - k_8 (\text{C}_3\text{H}_7\cdot) (\text{CH}_3\cdot) + k_1 (\text{C}_3\text{H}_8) - k_3 (\text{C}_2\text{H}_5\cdot) (\text{C}_3\text{H}_8) - k_4 (\text{C}_2\text{H}_5\cdot) + k_2 (\text{CH}_3\cdot) (\text{C}_3\text{H}_8) \\ &\quad + k_3 (\text{C}_2\text{H}_5\cdot) (\text{C}_3\text{H}_8) + k_5 (\text{H}\cdot) (\text{C}_3\text{H}_8) - k_6 (\text{C}_3\text{H}_7\cdot) - k_7 (\text{C}_3\text{H}_7\cdot) (\text{CH}_3\cdot) - k_8 (\text{C}_3\text{H}_7\cdot) (\text{CH}_3\cdot) \\ 0 &= 2k_1 (\text{C}_3\text{H}_8) - 2k_8 (\text{C}_3\text{H}_7\cdot) (\text{CH}_3\cdot) \end{aligned}$$

$$\therefore k_1 (\text{C}_3\text{H}_8) = k_8 (\text{C}_3\text{H}_7\cdot) (\text{CH}_3\cdot) \quad (10)$$

Hence from equation (4) and equation (10)

$$\frac{d(\text{CH}_3\cdot)}{dt} = 0 = -k_2 (\text{CH}_3\cdot) (\text{C}_3\text{H}_8) + k_6 (\text{C}_3\text{H}_7\cdot) \quad (11)$$

$$\therefore (\text{C}_3\text{H}_7\cdot) = \frac{k_2 (\text{CH}_3\cdot) (\text{C}_3\text{H}_8)}{k_6} \quad (12)$$

Combining with equation (10), we obtain

$$\frac{k_2 (\text{CH}_3\cdot) (\text{C}_3\text{H}_8)}{k_6} = \frac{k_1 (\text{C}_3\text{H}_8)}{k_8 (\text{CH}_3\cdot)} \quad (13)$$

which, on rearrangement, gives

$$(\text{CH}_3\cdot)^2 = \frac{k_1 k_6}{k_2 k_8}$$

Now, substituting equations (3), (7), and (11) in equation (1), gives

$$\begin{aligned} \frac{-d(\text{C}_3\text{H}_8)}{dt} &= k_1 (\text{C}_3\text{H}_8) + \frac{k_2 (\text{C}_3\text{H}_8) k_6 (\text{C}_3\text{H}_7\cdot)}{k_2 (\text{C}_3\text{H}_8)} + \frac{k_3 (\text{C}_3\text{H}_8) k_1 (\text{C}_3\text{H}_8)}{k_4 + k_3 (\text{C}_3\text{H}_8)} \\ &\quad + k_5 (\text{C}_3\text{H}_8) \left[\frac{k_4 (\text{C}_2\text{H}_5\cdot) + k_7 (\text{C}_3\text{H}_7\cdot)}{k_5 (\text{C}_3\text{H}_8)} \right] \quad (14) \end{aligned}$$

$$= k_1(C_3H_8) + k_6(C_3H_7\cdot) + \frac{k_3(C_3H_8)k_1(C_3H_8)}{k_4 + k_3(C_3H_8)} + k_4(C_2H_5\cdot) + k_7(C_3H_7\cdot) \quad (15)$$

Substituting for $(C_2H_5\cdot)$ gives

$$= k_1(C_3H_8) + (k_6+k_7)(C_3H_7\cdot) + \frac{k_3(C_3H_8)k_1(C_3H_8)}{k_4 + k_3(C_3H_8)} + \frac{k_4 \cdot k_1(C_3H_8)}{k_4 + k_3(C_3H_8)} \quad (16)$$

$$= k_1(C_3H_8) + (k_6+k_7)(C_3H_7\cdot) + k_1(C_3H_8) \quad (17)$$

Now, from equations (12) and (13)

$$\frac{-d(C_3H_8)}{dt} = 2k_1(C_3H_8) + (k_6+k_7) \cdot \frac{k_2(C_3H_8)}{k_6} \cdot \left(\frac{k_1 k_6}{k_2 k_8}\right)^{\frac{1}{2}} \quad (18)$$

As a result, predictions based on steady-state approximation show that the disappearance of propane should be first order.

The predicted rates of other products can also be established.

Thus,

$$\begin{aligned} \frac{d(CH_4)}{dt} &= k_2(CH_3\cdot)(C_3H_8) + k_8(C_3H_7\cdot)(CH_3\cdot) \\ &= k_1(C_3H_8) + k_2(C_3H_8) \left(\frac{k_1 k_6}{k_2 k_8}\right)^{\frac{1}{2}} \end{aligned} \quad (19)$$

$$\begin{aligned} \frac{d(C_2H_4)}{dt} &= k_4(C_2H_5\cdot) + k_6(C_3H_7\cdot) \\ &= \frac{k_1 k_4(C_3H_8)}{k_4 + k_3(C_3H_8)} + k_2(C_3H_8) \left(\frac{k_1 k_6}{k_2 k_8}\right)^{\frac{1}{2}} \end{aligned} \quad (20)$$

$$\frac{d(C_2H_6)}{dt} = k_3(C_2H_5\cdot)(C_3H_8)$$

$$= \frac{k_1 k_3 (C_3H_8)^2}{k_4 + k_3 (C_3H_8)} \quad (21)$$

$$\frac{d(H_2)}{dt} = k_5 (H^\cdot) (C_3H_8) \\ = \frac{k_1 k_4 (C_3H_8)}{k_4 + k_3 (C_3H_8)} + \frac{k_2 k_7}{k_6} (C_3H_8) \left(\frac{k_1 k_6}{k_2 k_8} \right)^{\frac{1}{2}} \quad (22)$$

$$\frac{d(C_3H_6)}{dt} = k_7 (C_3H_7^\cdot) + k_8 (C_3H_7^\cdot) (CH_3^\cdot) \\ = k_1 (C_3H_8) + \frac{k_2 k_7}{k_6} (C_3H_8) \left(\frac{k_1 k_6}{k_2 k_8} \right)^{\frac{1}{2}} \quad (23)$$

Thus the production of all products will be first order in propane, with the exception of ethane, which will be first order when $k_3(C_3H_8) > k_4$ and second order when $k_4 > k_3(C_3H_8)$.

In addition, it is seen that, from equations (18), (19) and (23), that

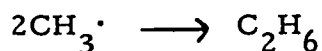
$$-\frac{d(C_3H_8)}{dt} = \frac{d(C_3H_6)}{dt} + \frac{d(CH_4)}{dt} \quad (24)$$

Examination of the experimental results shows that these predictions do give a reasonably accurate picture of experimental observations. Remembering that the experiments were carried out in a jet-stirred reactor, the dependence of propane disappearance and product formation is found to be first order in all cases, even for ethane: in view of the pressures used, it is very probable that $k_3(C_3H_8) \gg k_4$. In addition, adjusting for the fact that one propane can produce three methane molecules, the results are seen to be in agreement with equation (24).

Of course, this reaction scheme is somewhat simplified in that it ignores the possibility of product pyrolysis or of alternative termination reactions. However the agreement between prediction and experiment indicates that reactions (1) - (8) are a reasonable description of the overall pyrolysis.

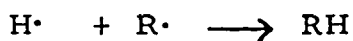
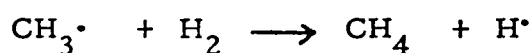
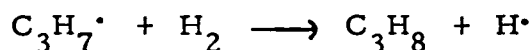
These results are also in reasonable agreement with other studies of propane pyrolysis. Thus, for example, Laidler (115) has shown that the overall order tends to three halves at lower pressures

and higher temperatures, and to unity at higher pressures and lower temperatures. This was explained in terms of the importance of the reaction



which could lead to an order of three halves. In the present system (graph 3.16.) ethane production is very low, and pressures are high inferring, as expected, first order dependencies.

In the presence of hydrogen, interference with the proposed chain can be expected via reactions of the type:



As a result, less propane would be expected to react, and the overall reaction should produce more methane and ethane. These effects were observed in the experiments (graph 3.44.).

Thus it can be seen that the gaseous products from the pyrolysis of propane are entirely consistent with a free radical chain reaction occurring completely in the gas phase. Quantitative predictions of experimental results can be made on the basis of a stationary state analysis of a proposed free radical chain mechanism.

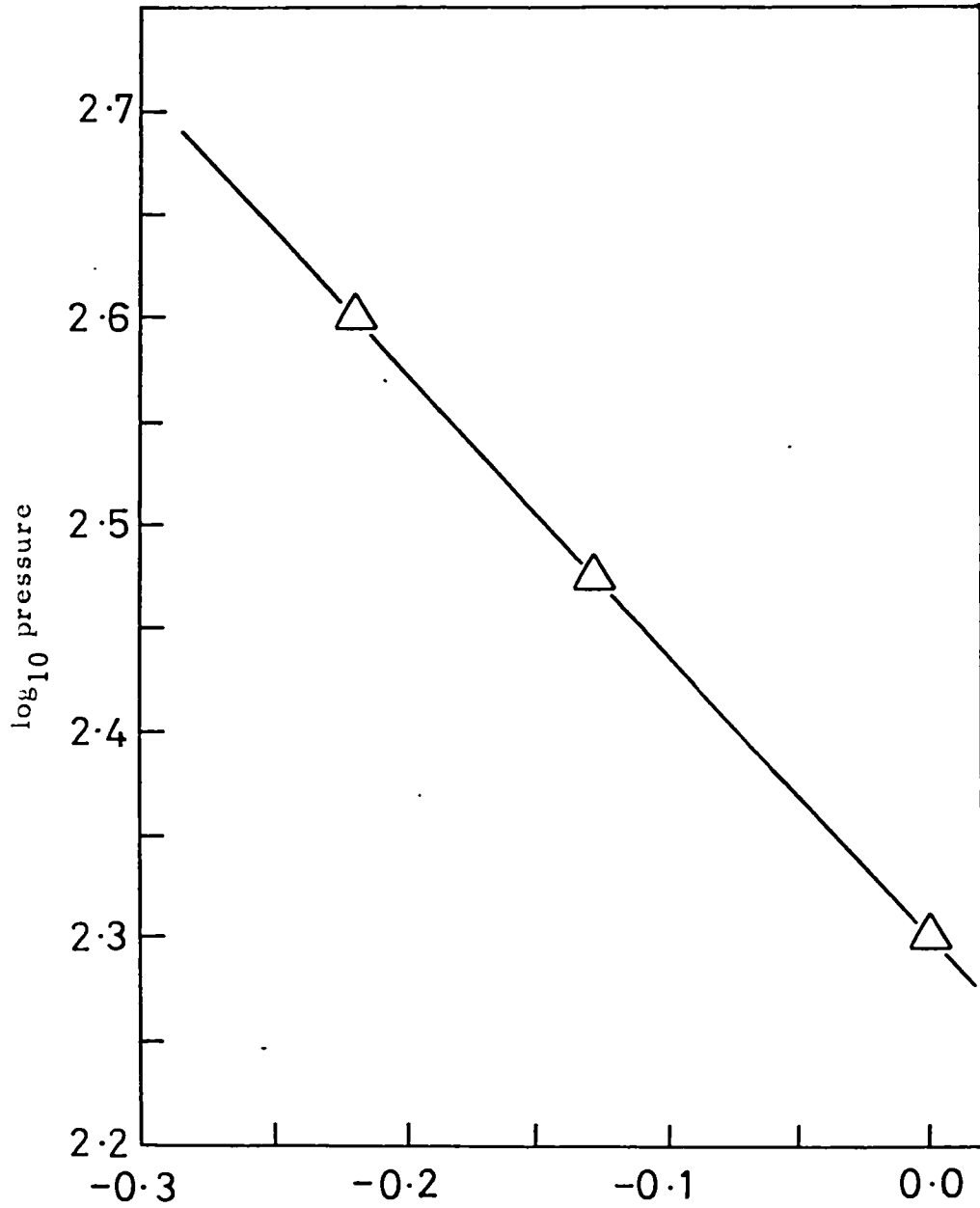
4. 3. Tars

One of the products of the pyrolysis of propane is a fraction called, collectively, tars. It consisted of material boiling above 70°C and, by the nature of the method of collection, condensing below 25°C. As shown in Table 3. 3. , the major component was benzene, but there was a range of polycyclic aromatic compounds present up to picene (5 aromatic rings), Table 3. 7. Had the mass spectrometer been able to analyse compounds of atomic molecular units higher than 290, there is little doubt that higher molecular weight compounds would have been observed. Thus, for example, Brooks (25) reports the probable presence of ovalene (8 rings) in a similar system.

Both the carbon balance studies and the mass spectroscopy results show that the amount of tars increases with increasing pressure, temperature and inlet residence time. Although the results reported in graphs 3. 65. - 3. 72 must be regarded as semiquantitative, they do yield some interesting trends. At low residence times, no tar appears to be formed, but the production then accelerates rapidly and finally settles down to a steady and lower rate of production (graphs 3. 65-3. 69.). Both the induction period (i. p.) and the initial rate of production of tars (r_i) appear to be functions of the pressure of propane and the temperature, (graphs 4. 1. -4. 6.) and give the following relationships (where semiquantitative measurement was possible):

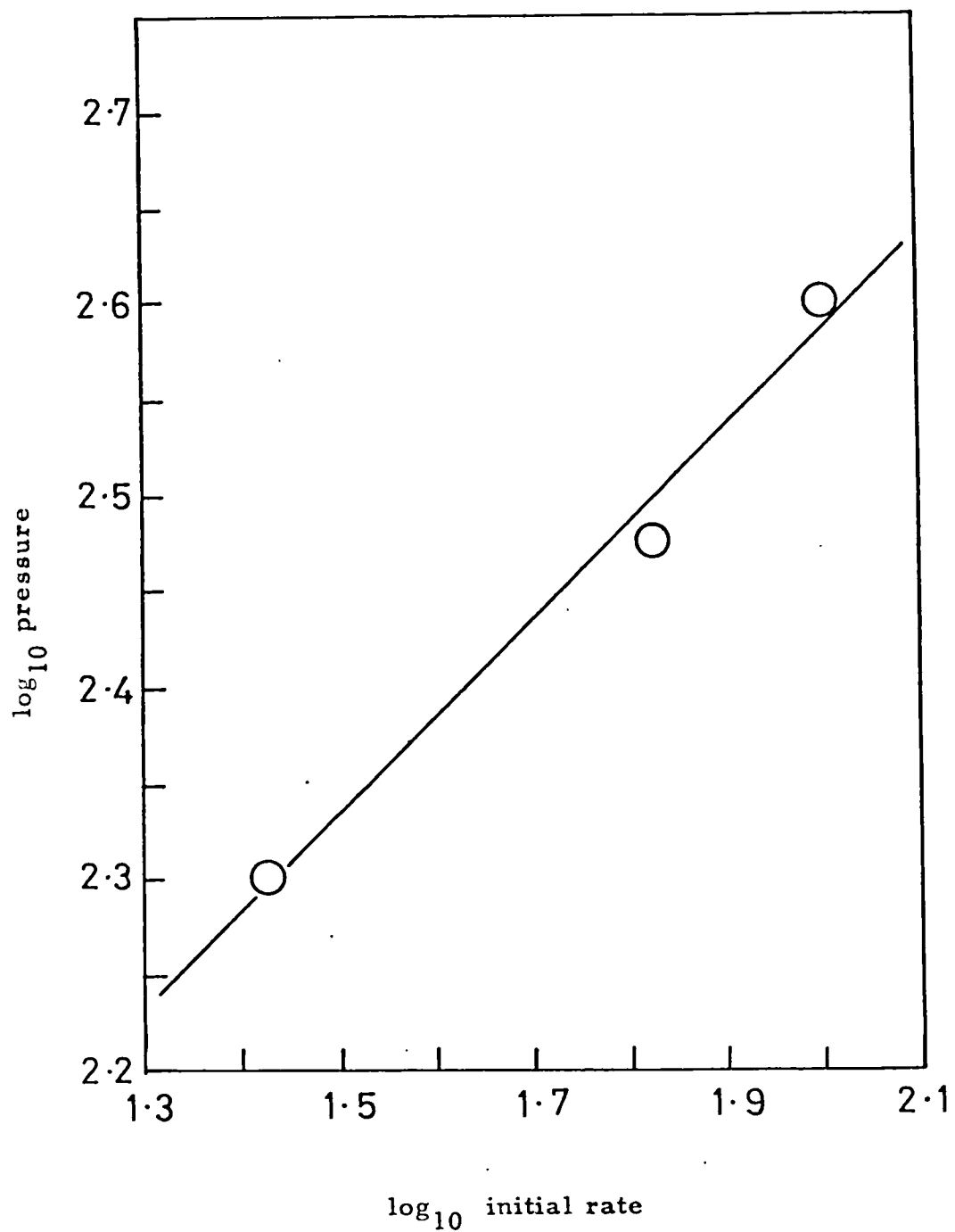
$$\begin{array}{ll}
 T = 600^{\circ}\text{C} & \text{induction period (i. p.)} \propto \text{pressure}^{-0.7} \quad (\text{graph 4. 1.}) \\
 & \text{initial rate } (r_i) \quad \propto \text{pressure}^{2.0} \quad (\text{graph 4. 2.}) \\
 T = 650^{\circ}\text{C} & \text{induction period (i. p.)} \propto \text{pressure}^{-1.7} \quad (\text{graph 4. 3.}) \\
 & \text{initial rate } (r_i) \quad \propto \text{pressure}^{2.3} \quad (\text{graph 4. 4.}) \\
 T = 600\text{-}750^{\circ}\text{C} & \text{induction period (i. p.)} \propto \exp\left(\frac{-E_a}{RT}\right) \\
 & \text{where } E_a = -27.4 \text{ kcal/mole} \quad (\text{graph 4. 5.}) \\
 & \text{initial rate } (r_i) \quad \propto \exp\left(\frac{-E_a}{RT}\right) \\
 & \text{where } E_a = +12.0 \text{ kcal/mole} \quad (\text{graph 4. 6.})
 \end{array}$$

The production of tars in a pyrolysis system is not unexpected, since thermodynamic considerations show that the decrease in free energy of the system resulting from the resonance energy of the



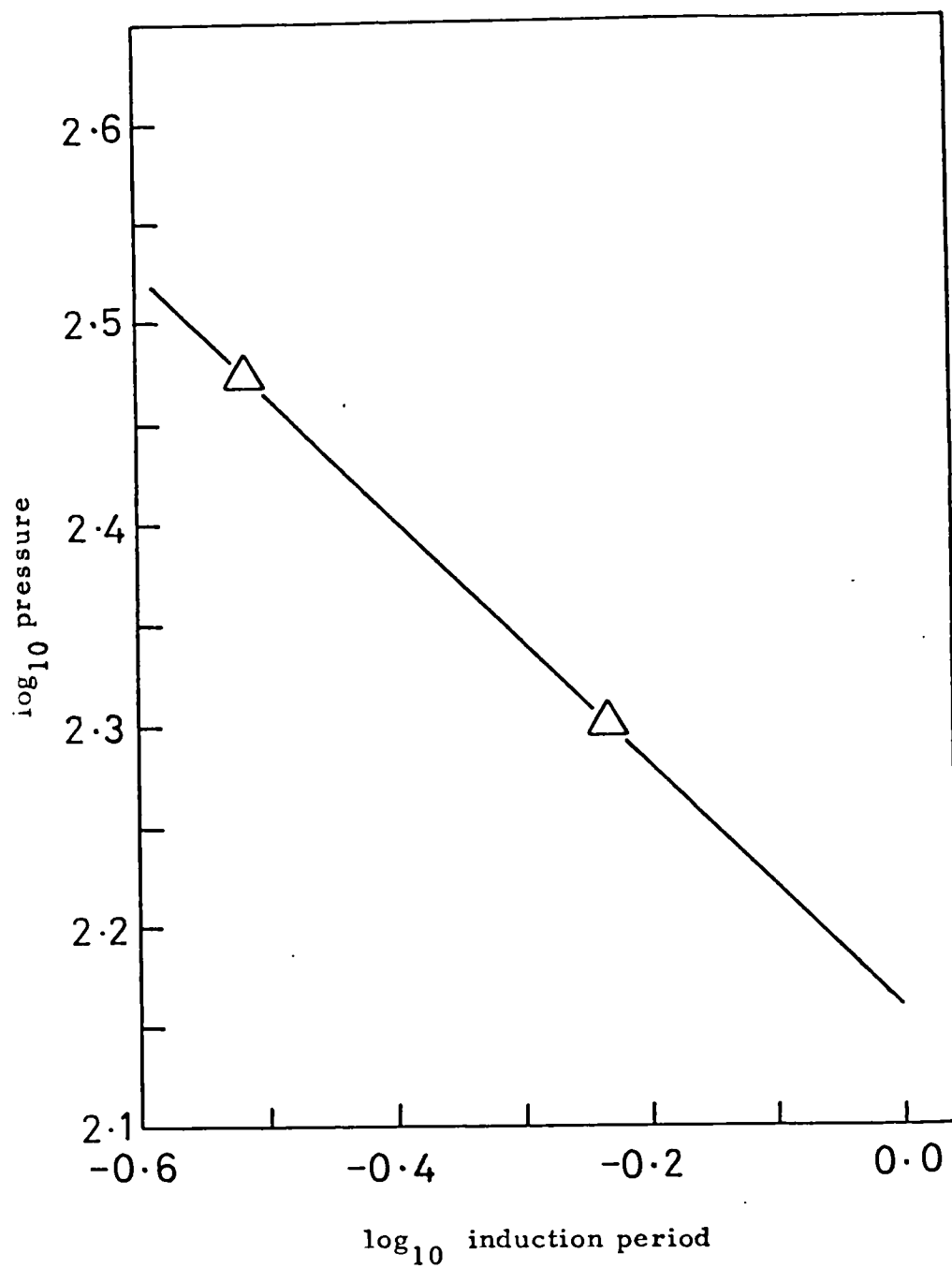
\log_{10} induction period

Graph 4. 1. 600°C

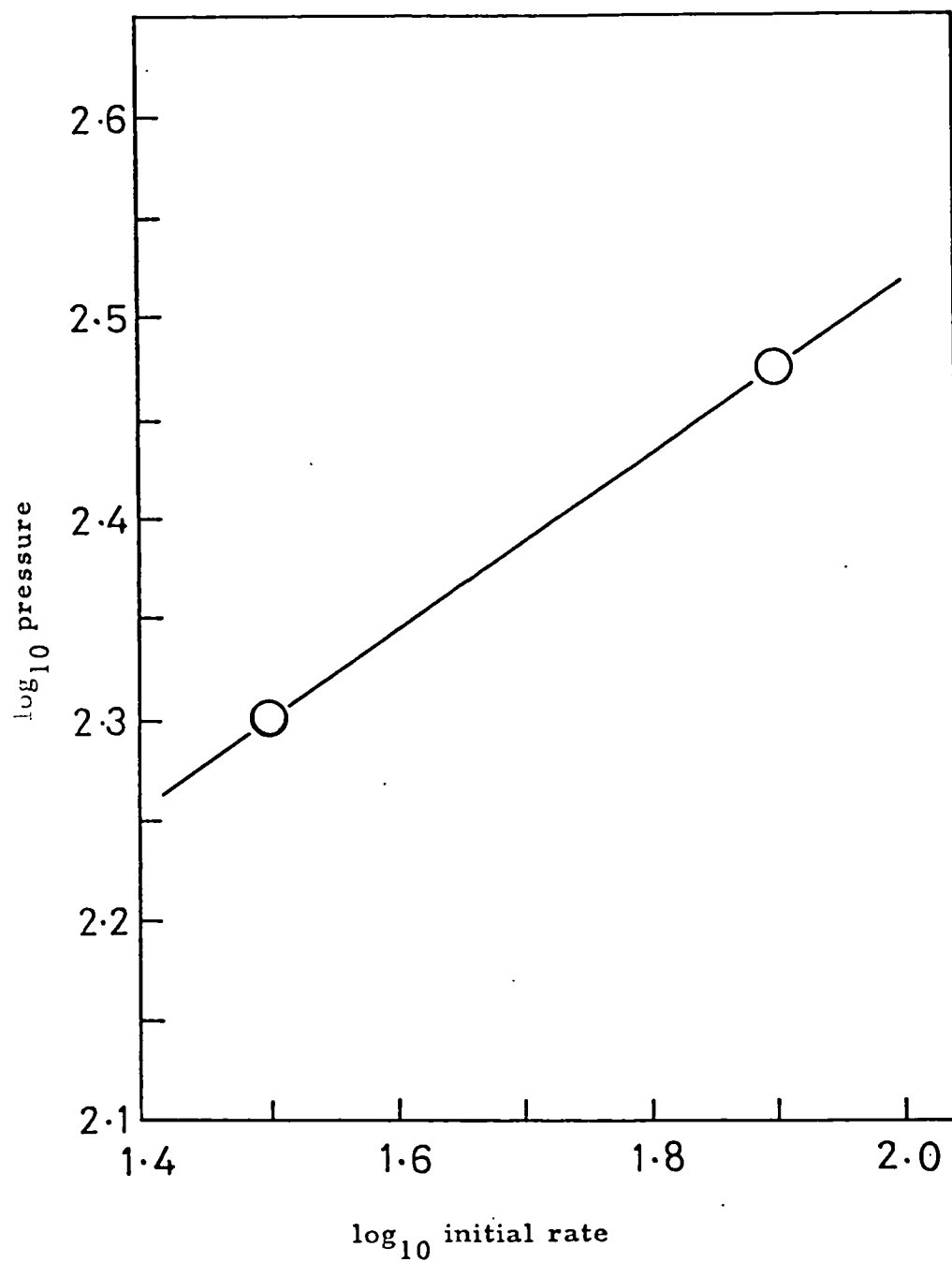


\log_{10} initial rate

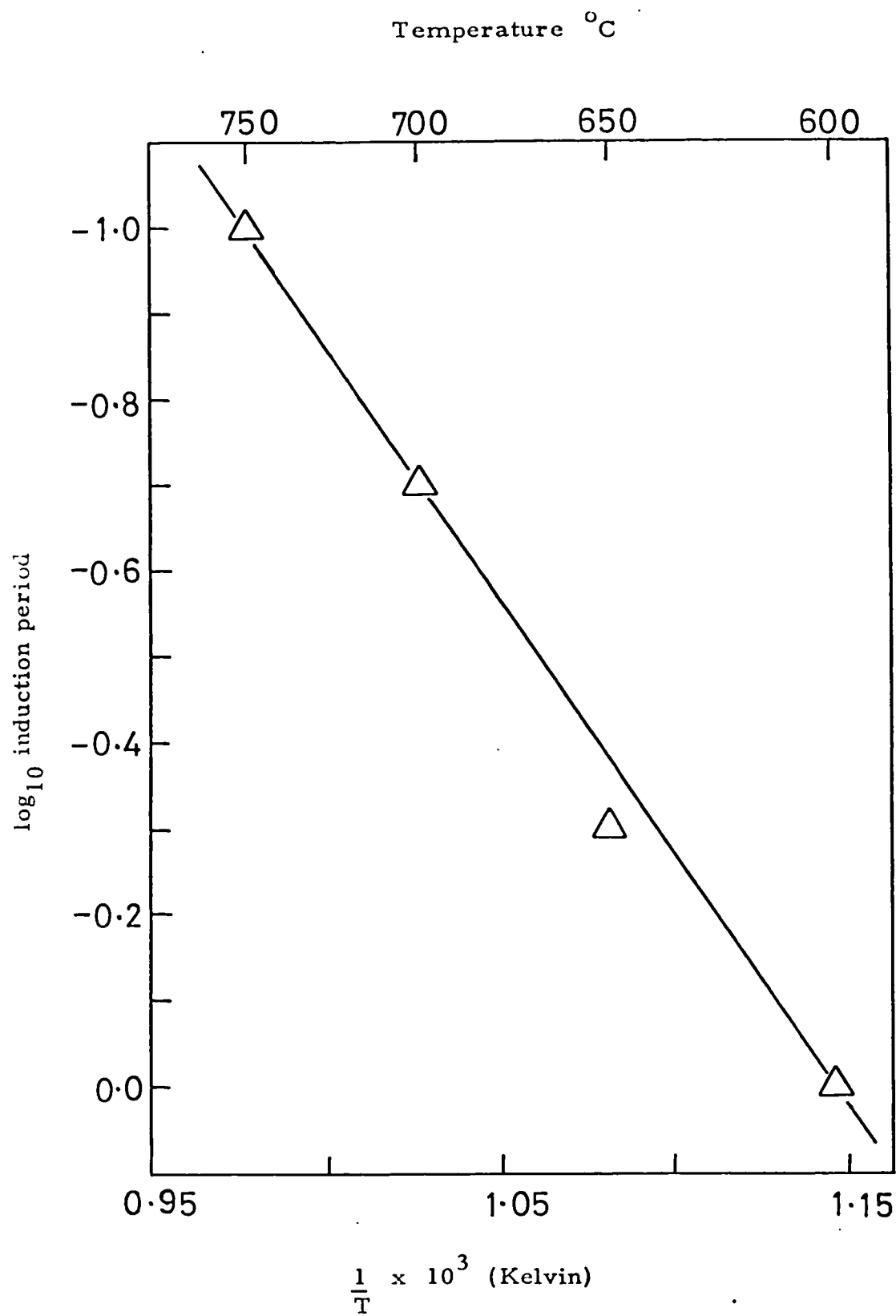
Graph 4.2. 600°C



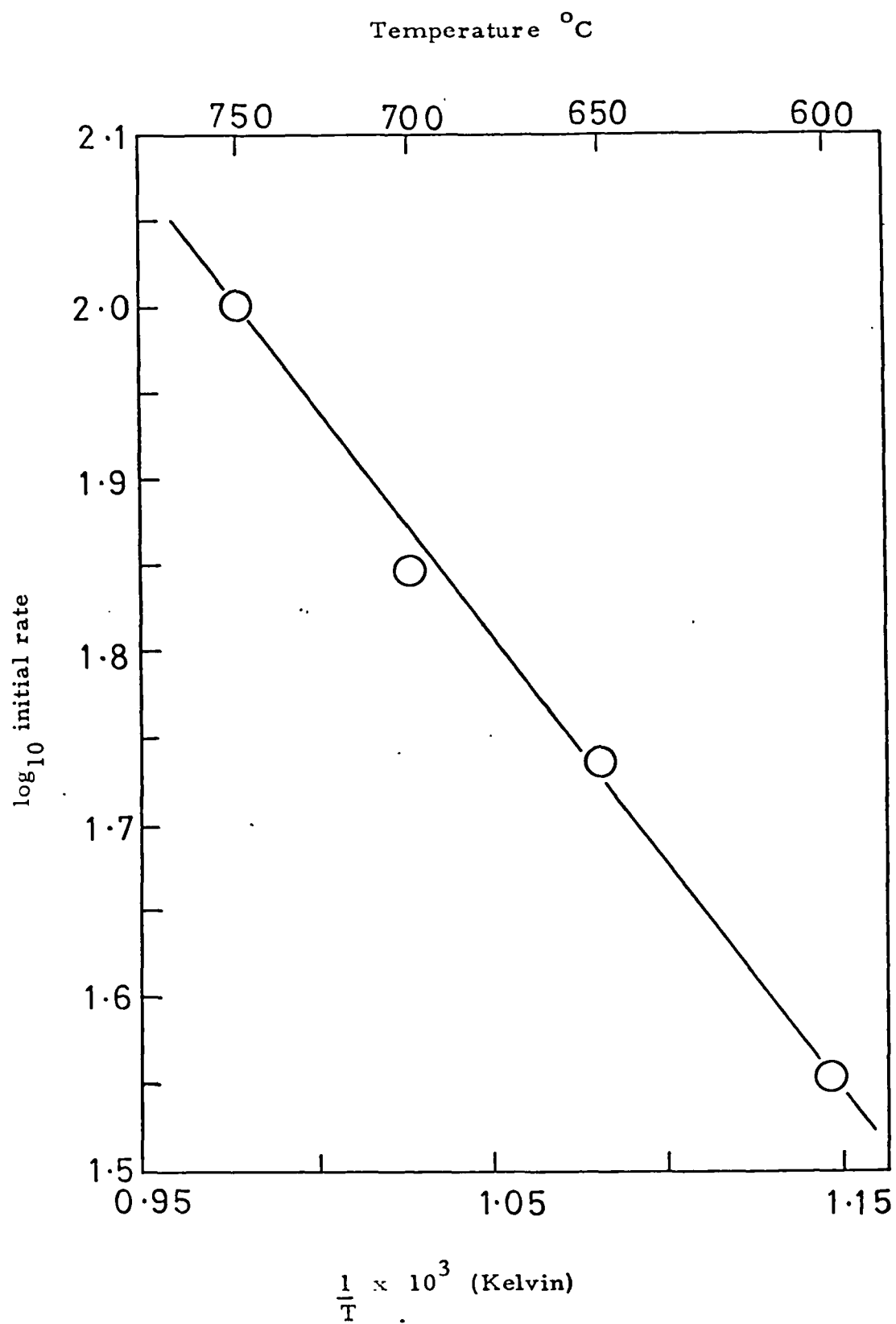
Graph 4.3. 650°C



Graph 4.4. 650°C



Graph 4.5. 200 torr



Graph 4.6. 200 torr

polycyclic aromatic molecules favours their production. From such calculations, several reactions can be expected

- (i) cracking of non-aromatic hydrocarbons to smaller molecules, together with dehydrogenation of the larger and smaller molecules
- (ii) cyclisation of hydrocarbons to give aromatics
- (iii) dealkylation of any aromatic groups with side chains
- (iv) condensation of aromatics to form polycyclic aromatics of increasing molecular weight
- (v) eventual formation of carbon

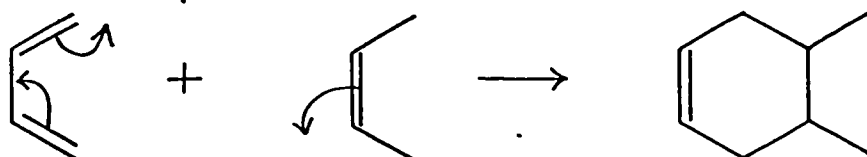
The relative importance of these reactions depends on reaction conditions. As the pyrolysis temperature is increased, C-H bond breakage becomes more important than C-C bond rupture but, at temperatures above 700°C , aromatisation is preferred.

The reactions occurring during pyrolysis are open to considerable doubt, both with respect to the gas phase (see section 4.2.) and to tar and carbon production. There is general agreement that the formation of higher molecular weight aromatic molecules is connected with the formation of carbon, and it is known that the former can be converted to the latter. However, it is not certain that carbon can only be formed in this way.

Considering the tar product spectrum (Table 3.7.), it is seen that reaction produces a range of substituted benzenes, relatively large amounts of polycyclic aromatics and relatively small amounts of diphenyl type compounds. Analysis of the gas phase products argues against the acetylene theory of tar and carbon production (22), where larger molecules are suggested to be built up from acetylenic fractions: under all conditions, acetylene is a very minor product.

The results are, however, consistent with a Diels-Alder type of condensation reaction to produce tars and carbon (23).

e. g.



However, this is probably too simple a picture since the concentration of C_4 molecules is low, and the kinetic results (see above) are more typical of a free radical type of condensation. Thus the existence of an induction period which depends on pressure of reactants and temperature, the autocatalytic nature of tar production (figures 3.65 - 3.72) and the eventual tail-off of rate to a steady value are all typical of free radical reactions (115).

The role of these polycyclic aromatic compounds in the formation of carbon is similarly open to some question. Lahaye (68) suggested that the partial pressure of polynuclear aromatic hydrocarbons increases with reaction time, until supersaturation is high enough to induce condensation droplet formation. The liquid droplets are pyrolysed into gas phase carbon. Graham (69) questioned the condensed droplet theory and suggested that initially, soot is formed directly from gas phase intermediates. The intermediates of the initial formation of soot were considered to be present in the gas phase and not the condensed phase. Growth may occur from the polynuclear aromatics in the gas phase and further growth may occur by the aggregation of soot particles.

The carbon balance figures for the total amount of tar, and the mass spectrometer analysis of the relative amounts of different molecules in the tar, indicate that the partial pressures of the individual compounds in the reactor do not approach the saturation vapour pressures at the temperature of reaction. Hence, the results tend to argue against the droplet condensation/carbonisation theory of Lahaye (68). However, comparison of the rates of tar production (Table 3.4.) and carbon production (section 3.2.1.) are revealing. Carbon formation shows an induction period similar to those for tar formation (graphs 3.65. - 3.72.), and the acceleration of rate is comparable. The steady-state concentration of tars in the reactor is accompanied by an enrichment in higher molecular weight polynuclear aromatic compounds which react to form carbon. The results are in general agreement with the concept that tars are formed as precursors to carbon formation and the kinetic results are in agreement with the theory of Graham (69) in which carbon is formed directly from gas phase intermediates.

No evidence was obtained that the production of tars was dependent on the nature of the reactor wall. As seen from section 3.7.4., changes in the nature of the liner or the foil appeared to have little effect on tar production, as calculated by carbon balance figures, even though these liners did have an effect on the rates of carbon formation (section 3.3.1.). Although not tested, the surface : volume ratio in the reactor would be expected to have a much larger effect on tar production.

4.4. Carbon formation

Two conclusions clearly emerge from the results; that the rate of carbon formation on a surface is dependent upon the chemical nature of that surface and that carbon formation on a surface may be affected by the nature of a second surface, physically separated from the first surface by a gap in which gas can react. These may be considered in turn, dealing first with heterogenous - homogeneous effects.

4.4.1. Heterogeneous-homogeneous effects

When the suspended material was kept constant, and the metal liner was changed, some surprising effects were noted at the start of an experiment (section 3.3.1.). Admission of the gaseous reagents at constant residence time caused an initial high rate of carbon deposition on the foil, but this gradually dropped away to a constant value (graph 3.34.). The initial rate and the rate of approach to a constant rate were found to depend upon the nature of the metal liner.

As before, this may be explained in the following terms. On admission of reactants, both the liner and the foil are clean, and carbon formation on the foil reflects two effects. Firstly, the nature of the foil itself will affect carbon formation (see below). Secondly, it would seem that a reaction occurs on the liner to produce gas phase products which are typical of the reactant and the catalyst (metal liner). These products pass through the gas phase, possibly reacting en route, to the foil where they react to form carbon. This occurs at a rate which is typical of the gas products themselves (which depends on the nature of the liner) and of the nature of the foil.

Considering the runs described in section 3.3.1., the original reactant (propane) and the nature of the foil (copper) remain constant, and any changes are due to changes in the nature of the liner. For the runs with a silica "liner" in section 3.2.1., the changes are due to changes in the foil, since the reactant and the silica "liner"

are kept constant. As would be expected from the relative magnitude of the foil and the liner, these changes are relatively small.

As the reaction proceeds, both the liner and the foil become covered in carbon and, unless metal can migrate through this carbon, the rate of carbon formation reduces to the rate expected from propane reacting on carbon liners to produce gaseous products which deposit carbon on a carbon foil. This is not to say that the nature of the liner and the foil do not influence the reaction, but to infer that, whatever the starting material, the actual surfaces seen by the gases are common (and are carbon). If, for any reason, the original material continues to be available to the gases, then the net rate of carbon formation will continue to reflect the nature of the original material.

These assumptions explain nearly all of the results observed. Considering first a silica "liner" with a variable foil (section 3.2.1.), it is seen that iron is a very active carbon former, followed by stainless steel, nickel, carbon and silica/copper (only slightly less than carbon). The particular activity of a foil tended to disappear after the deposition of 1.5-2.0 mg. of carbon on the foil, and this is equivalent to a layer 2.28 microns deep (about 7000 layers of carbon). This was so in all cases except stainless steel, where a rate significantly greater than the "carbon on carbon" rate was observed for long periods of time.

A similar order of activity was observed when the foil was constant (copper) and the nature of the liner was changed (section 3.3.1.). Iron gave considerably more carbon than nickel, while silica and copper gave slightly less than carbon. Stainless steel was again anomalous, in giving a rate significantly lower than that for a carbon liner. In these experiments, the rate fell to a "carbon on carbon" rate following the deposition of 0.2-0.3 mg. of carbon on the foil (a layer 0.34 microns thick, containing about 1000 layers of carbon).

Differences between copper, silica and carbon are thought to result primarily from a surface area effect. Carbon formation is

known to be affected by the ease of "trapping" of gaseous intermediates on a surface, Makarov (87), and this will be enhanced in the presence of a porous carbon surface as compared to a non-porous copper or silica surface. This is not to say that the surface has no effect, but to point to the surface acting as a chemically "inert" third body.

The complexity of the system is illustrated however, by considering stainless steel. Studying the variable liner experiments, it could be suggested that stainless steel produces less deposition on the foil than a carbon liner because it has a greater affinity for carbon. The primary reaction occurs on a stainless steel surface, and this could lead to carbon deposition on the steel and to the formation of gaseous products which deposit carbon on the copper. If the affinity for carbon is high (or the primary reaction goes further towards carbon), more carbon would be formed on the steel at the expense of gaseous products. The variable foil experiments tend to bear this out, in that higher rates of carbon formation are observed on steel even after carbon has been deposited sufficient to encapsulate an iron or nickel foil i. e. the carbon may well migrate into the body of the steel, leaving free metal surface.

Although these observations are new and important, in some ways they raise more questions than they solve. It is possible to assess the effect of foil and liner on carbon formation, and it is seen that the nature of the foil is less significant. However, the important questions now lie in the area of what are the gaseous products produced at the liner which are responsible for carbon formation on the foil, and what effect do the liner and the foil have on the product spectra. Although these have been attempted during the section on tars, most of these questions are still open.

4.4.2. Heterogeneous effects

From the above discussion, it has been established that the effect of a metal on the reactions leading to carbon depends markedly on the surface exposed to the reacting gases. It has been established that the activity for promoting carbon formation on a

second surface decreases in the order:

Iron > stainless steel > nickel > carbon > copper/silica.

Similar effects should be observed in considering the formation of carbon on the metal itself, and this is found to be the case. Thus, for example, studies of the temperature at which carbon formation becomes significant (section 3.6.) gave a similar order of activity with iron and stainless steel initiating carbon formation at significantly lower temperatures than other systems. The method of measuring the activity pattern is important, since deposition is measured on a clean foil.

As a result of the fact that iron catalysed carbon formation at a lower temperature than carbon, it was possible to make an interesting observation on this system. Operating at 40°C below the temperature at which the "carbon on carbon" system became important, iron discs were, in some cases, found to remain active for long periods of time (run 76: graph 3.14.).

Metallographic analysis (section 3.8.2.) of the iron foils from run 64, (graph 3.31., active, not encapsulated) and run 66, (graph 3.29., carbon encapsulated), showed that carbon had diffused through the foil thickness. The major structure was found to be coarse pearlite, 0.87% by weight of carbon. The carbon encapsulated foil had a layer of ferrite (α -iron), containing cementite (Fe_3C ; 6.67% by weight of carbon) at the carbon face, and the cementite "patches" were surrounded by ferrite. These 'patches' penetrated about $\frac{1}{5}$ th of the thickness of the metal foil. The non-encapsulated foil was coarse pearlite throughout, indicating an even uptake of carbon. However, for the carbon encapsulated foil, the carbon uptake appeared to have been irregularly distributed over the metal surface. Carbon had been adsorbed over the whole surface, but more intensely in some areas. It is this difference in carbon distribution which probably causes the unpredictable behaviour of the iron foils with regard to carbon deposition. Sometimes the foil is encapsulated with carbon, whilst in repeat experiments the iron foil remains active.

The foils were found to have absorbed an appreciable amount of carbon (0.87% by weight of carbon in pearlite). The carbon

encapsulated foil was found to have taken in more carbon, and formed a different layer at the carbon face. For both foils, iron was found to have entered the carbon layer. This iron transport system causes the active iron sites to remain present in the growing carbon layer and to act as nuclei for further carbon deposition.

Metallographic analysis of the stainless steel foil (run 75, graph 3. 30.) shows carbon to have been absorbed over the whole surface, but more rapidly at the metal grain boundaries. The absorption of carbon at the carbon face resulted in attack at the grain boundaries throughout the foil and carbon possibly entered the surface layer grains, (giving the extra etching seen after hydrochloric acid treatment). The diffusion zone only progressed $\frac{1}{4}$ to $\frac{1}{3}$ of the way through the thickness of the metal.

The steel used contained a little molybdenum, used as a stabiliser against intergranular "weld decay". This is likely to influence the effect of carbon considerably, particularly in the early stages. However, attack at the grain boundaries had occurred and x-ray diffraction confirmed the presence of an iron-carbon system in the carbon deposit. This included metal which could act as growth nuclei, as in the case of the iron foils.

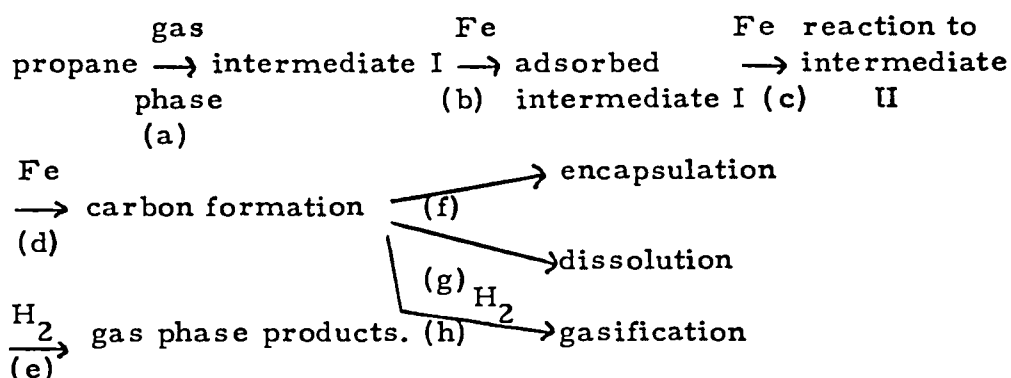
Hydrogen and helium were used as diluent gases to study the effect of dilution on the rate of carbon formation on iron (section 3. 4. 1.), a metal which showed high activity for carbon formation from propane. Hydrogen has a very pronounced effect on the period during which carbon formation is dependent on the nature of the disc material. The suspended iron disc exhibited high rates of deposition even after 2. 3 mg. of carbon had been deposited, as compared to undiluted propane, where carbon formation is dependent on the disc material only until 1. 5-2. 0 mg. of carbon have been deposited. The iron disc used in the hydrogen dilution study did not exhibit the "carbon on carbon" rate of deposition (graph 3. 42.).

This iron disc, in not exhibiting the "carbon on carbon" rate of deposition, together with very much higher rates of carbon deposition being observed at dilutions of 10% and 22% (v/v) propane,

indicates a behaviour similar to that of a non-encapsulated iron system. The metallographic analysis of such an iron system, showed the iron foil to have a structure of coarse pearlite throughout, indicating an even uptake of carbon with no concentrations of carbon at any part of the surface. Thus the effect of hydrogen in the dilution of propane has been to promote an even uptake of carbon into the iron disc, resulting in the high rates of carbon deposition which were observed.

In the helium dilution system, the suspended iron disc exhibited high rates of carbon deposition until 1 mg. of carbon was deposited. The "carbon on carbon" rate was then observed. This is consistent with an iron disc showing the initial high activity of iron and then becoming carbon covered. Hence helium, an inert gas, had no effect on the surface (heterogeneous) formation of carbon on the iron disc. Helium did not ensure an even uptake of carbon into the disc and the disc became carbon covered, exhibiting the "carbon on carbon" rate of deposition.

Thus it can be seen that hydrogen has a highly specific effect on carbon formation, but it is difficult to establish the nature of this effect. Considering the chain of events leading to carbon, it is reasonable to suggest a sequence:

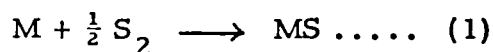


Hydrogen could affect reactions (a), (c), (d), (e), (g) and (h). Examination of reaction (a) by analysis of gas phase products does show that hydrogen influences the product distribution (section 3.4.2. and 4.2.), but it is difficult to establish a chain of events leading to carbon (see above discussion on gas phase products and tars). Hydrogen will certainly affect reaction (c), Lobo (42), and

is known to gasify potentially encapsulating intermediates or carbon (reactions (e) and (h)), Figueiredo (46). In addition, hydrogen is known to favour grain boundary attack, thereby increasing the probability of reaction (g), Moayeri (50). In view of the even-ness of carbon deposition, it seems likely that the gas has a strong influence on reactions (c), (e), (g), and (h), the deposition of carbon being enhanced to give an even distribution throughout the foil.

Since the effect of the surface in contact with the gas is seen to be so important, studies were made of surfaces modified by the addition of hydrogen sulphide to the reacting gases (section 3.5.). This additive, by forming metal sulphides, could be expected to have a significant effect on metals and a small effect on silica. Two types of experiment were carried out. In the first, the foils were pre-sulphided (section 3.5.1.), the hydrogen sulphide flushed out of the reactor and propane admitted. In the second, a 1% (v/v) stream of hydrogen sulphide was added to the propane feed on a continuous basis. The flow of hydrogen sulphide could be stopped at any time without affecting the propane feed. Before considering the results, it is useful to discuss the changes that may occur on the surface as a result of these sulphiding processes.

The process of sulphidation, confined to a theoretical consideration of the sulphidation behaviour of metals and alloys, has been reviewed by Strafford (100). For the formation of a metal sulphide, MS, from a divalent metal and sulphur vapour containing S₂ molecules, the driving force is the decrease in free energy (ΔG°) attending the reaction. Provided that ΔG° is negative, then it is reasonable to assume, on the basis of thermodynamic arguments, that the reaction will occur spontaneously.



Applying the van't Hoff Reaction Isotherm to reaction (1) gives,

$$\Delta G^\circ = -RT \ln K_p = RT \ln (pS_2)^{\frac{1}{2}}$$

where R is the gas constant, T the temperature ($^\circ K$), for the formation of the sulphide according to equation (1).

For the converse of reaction (1), the dissociation of the sulphide;

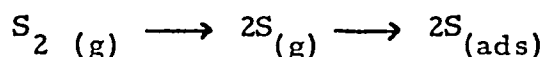
$$\Delta G^{\circ} = -RT \ln (pS_2)^{\frac{1}{2}}$$

the equilibrium dissociation pressure, pS_2 , may be calculated from ΔG° data for a given temperature, T °K. Sulphidation of a metal M according to reaction (1), will occur only if the partial pressure of the sulphur in the gaseous environment, is greater than the dissociation pressure of the bulk sulphide MS, at the given temperature T.

The thermodynamic properties of binary sulphides have been reviewed by Kubaschewski and Evans (101). The theory and use of free energy/temperature diagrams to conveniently summarise these thermodynamic data have been discussed by Ellingham (102), and by Richardson and Jeffes (103).

In practice, thermodynamic considerations of this type are of only limited use. The sulphide product either partially or completely covers the metal surface. The subsequent reaction is applicable to a study of the reaction kinetics and not thermodynamics. Kubaschewski and von Goldbeck (104) found that the volume of many sulphides produced is greater than the volume of metal consumed in producing that volume of sulphide, according to the principles established by Pilling and Bedworth (105). Hence, if it is assumed that the layer is compact, dense and pore-free, affording a protective covering to the underlying metal surface, then the rate of continued sulphide layer formation will be governed by one of several possible mechanisms, which together constitute the overall process.

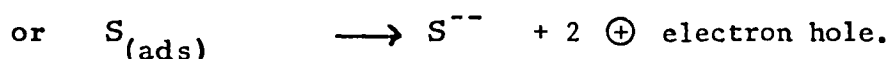
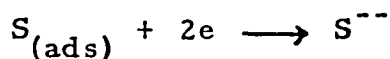
- (1) Adsorption and dissociation of sulphur molecules into atoms at the sulphide/sulphur interface.



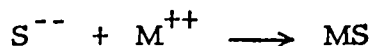
- (2) Ionisation of the metal atoms into ions and electrons at the metal/sulphide interface.



- (3) Flow of the electrons towards the sulphide/sulphur vapour interface, to allow production of sulphur ions.



(4) A diffusion either of cations, M^{++} , outwards through the sulphide lattice towards the sulphide/sulphur interface, or alternatively of anions, S^{--} , inwards through the lattice towards the metal /sulphide interface. Either process allows the formation of the sulphide, but at different interfaces.



Pilling and Bedworth (105), suggested that sulphide scale would be protective when the volume of sulphide produced, was greater than the volume of metal consumed in producing that volume of sulphide, if sulphide scale growth occurred by inward diffusion of anions. In practice, it has been found that sulphide scale, formed by the alternative mechanism, may also be protective. However, even when such a favourable potentially protective sulphide/metal volume relationship exists within a given reaction system, often the protective scale breaks down mechanically and develops porosity, leading to an enhanced reaction rate. This breakdown occurs because of the large stresses that are produced within the system by virtue of this large volume ratio.

Which of these two possible alternative diffusion mechanisms may actually be involved, is determined by the defect nature of the sulphide layer, which is commonly a semi-conductor. Many metal sulphides, e. g. NiS, FeS, contain a deficit of the metal component and diffusion transport of metal cations via these vacancies in the sulphide lattice is possible (p-type semi-conductor). The metal sulphide layer is presumed to thicken by the outward movement of cations and electrons from the metal, through the sulphide layer to the (outer) sulphide/sulphur interface. The metal ions then react with sulphur that has been ionised by the electrons. An alternative p-type defect model involving an interstitial excess of the negative component S^{--} is unlikely, because of the large ionic radius of the sulphur anion compared with the smaller cation.

In general, the defect models proposed for sulphides are not so well supported by experimental evidence as are those for metal oxides.

The possibility of the formation of fused sulphide scales, often leading to catastrophic non-protective kinetics, is illustrated by the sulphidation behaviour of nickel. Hancock (106), demonstrated that nickel, when exposed to hydrogen sulphide at 900°C, is very rapidly corroded following linear kinetics, as defined by the expression

$$\Delta m = k_1 t$$

where Δm is the increase in weight per unit area of sample due to sulphidation, t is the exposure time, k_1 the linear rate constant. X-ray and metallographic analysis of the corroded samples showed them to consist entirely of nickel and the sulphide Ni_3S_2 . These materials form a low-melting eutectic at 645°C and examination indicated that they had been molten at this temperature. NiS is reported to melt at 797°C (107).

The interaction between copper and sulphur has also been studied, (108), (109) and (110). These authors observed that, in the early stages of sulphidation, a time law prevails (linear), which is independent of the thickness of the Cu_2S layer. The transfer of copper ions through the Cu/Cu_2S phase boundary is rate-controlling.

Although kinetic effects may be more important, the thermodynamic parameters of sulphidation are available from published literature. The standard free energies of reaction, in the form,

$$\Delta G_T = A + BT \log T + CT$$

have been listed (101) for the various temperatures of T (°K). Free energy/temperature diagrams (102), (103), enable the determination of the H_2S/H_2 ratio above the metal/metal sulphide surface and the partial pressure of sulphur, pS_2 and the equilibrium constant, k , pertaining to the system at equilibrium at a given temperature.

Ingraham (111) has listed the equilibrium constants for both the NiS and the Ni_3S_2 systems at various temperatures. The equilibrium constant k is related to the partial pressure of sulphur, pS_2 .

$$\frac{1}{k} = pS_2$$

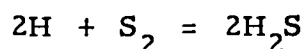
The figures for the metal/metal sulphide systems used in the propane pyrolysis experiments, calculated for 805°C, (1078°K), are tabulated in Table 4.1.

Table 4.1. Equilibrium data at 805°C. (1078°K)

Reaction	ΔG_T cal.	$\log_{10} k$	$p S_2$ atm.	$p S_2$ atm.
$2Ni + S_2 = 2NiS$	-32866 (A)	6.66 (C)	2.2×10^{-7} (C)	4×10^{-7} (B)
$3Ni + S_2 = Ni_3S_2$	-37187 (A)	7.53 (C)	3.0×10^{-8} (C)	4×10^{-8} (B)
$2Fe + S_2 = 2FeS$	-44741 (A)			1×10^{-9} (B)
$4Cu + S_2 = 2Cu_2S$	-48000 (B)			5×10^{-10} (B)

Source:- (A) Kubaschewski and Evans. reference (101).
 (B) Free energy diagrams.
 (C) Ingraham. reference (111).

For the reaction,



at 805°C , (1078°K), $\Delta G_T = -17820$ cal. (112). The free energy of formation of hydrogen sulphide does not become positive until temperatures in excess of 1560°C .

The results of propane pyrolysis experiments at 805°C and 2.0 secs. inlet residence time, indicate that the hydrogen concentration in the product gas stream is 15% (v/v), and a 1.9 times volume expansion of the propane feed occurs. Hence, for the experiments with 1% hydrogen sulphide (v/v) in the propane feed, the ratio of hydrogen sulphide to hydrogen is $\text{H}_2\text{S} : \text{H}_2 :: 1 : 28$. The free energy diagrams then enable the $\text{H}_2\text{S}/\text{H}_2$ ratio at 805°C to be converted to the partial pressure of sulphur, i. e. $p_{\text{S}_2} = 5 \times 10^{-7}$ atm. This is the partial pressure of sulphur (S_2) present inside the reactor. Thus metal sulphides will only exist if the equilibrium partial pressure of S_2 above the metal/metal sulphide surface is less than 5×10^{-7} atm. From Table 4.1., it is seen that the sulphur partial pressure inside the reactor is sufficient to form FeS and Cu_2S but probably insufficient to form NiS or Ni_3S_2 . The sulphur partial pressures required to form NiS and Ni_3S_2 are too close to the partial pressure of sulphur present to be the basis of a reliable prediction as to the formation of nickel sulphides. The electron probe micro-analysis of the nickel foil used in the 1% hydrogen sulphide in propane experiment, did not detect sulphur on the nickel surface.

In the experiments where the metal foils of known weight and surface area were pre-sulphided, the amount of sulphur deposited on the foil was weighed using the on-line microbalance. Thus, by knowing the weight of the metal foil, the total number of metal atoms can be calculated; knowing the weight uptake of sulphur, the number of sulphur atoms can be calculated; knowing the metal crystallite dimensions, the number of metal atoms in the metal surface can be calculated. These calculations (Table 4.2.) show that more sulphur has been deposited on the foils than that required to form a surface layer.

Table 4.2. Sulphur uptake by metal foils

metal foil	foil weight (mg.)	weight of S deposit(mg)	crystalite cell edge (Å) Ref(113)	total number of metal atoms
Nickel (Run 83)	120.4 mg.	43 mg.	3.52 Å	12.35×10^{20}
Iron (Run 81)	109.0	43	3.59	11.76×10^{20}
Copper (Run 88)	119.6	33	3.61	11.34×10^{20}

	total number of sulphur atoms	number of metal atoms in surface
Nickel	8.08×10^{20}	2.26×10^{15}
Iron	8.08×10^{20}	2.17×10^{15}
Copper	6.20×10^{20}	2.15×10^{15}

Table 4.3. The degree of sulphide formation

metal foil	sulphide formed	% of metal converted to sulphide
Nickel	Ni S	65%
Iron	Fe S	68%
Copper	Cu ₂ S	ALL

In addition, on the assumption that sulphides formed are approximately stoichiometric, then the degree of sulphide formation can be calculated (Table 4.3.).

These results are useful in discussing carbon formation on the foils. Pre-sulphiding of the iron disc (run 81) was found to reduce the initial activity of the iron. The "carbon on carbon" rate was observed after the deposition of only one quarter of the carbon required to reduce the initial activity of iron to the "carbon on carbon" system in the absence of sulphide. Carbon was found to be deposited on a layer of iron sulphide and the rate of deposition quickly fell to the "carbon on carbon" rate.

The presence of 1% hydrogen sulphide in the propane feed suppressed the iron activity (run 82) and a rate equivalent to the "carbon on carbon" rate was observed. A surface layer of FeS is probably present, which may thicken by transport of cations and electrons from the metal, through the sulphide layer to the (outer) sulphide/sulphur interface. When the hydrogen sulphide flow was discontinued and only propane passed into the reactor, the disc was observed to regain and exceed the full activity associated with a "clean" disc. This occurred 1 hr. 23 mins. after the hydrogen sulphide was turned off. It is likely that the FeS decomposed leaving a finely divided and disrupted iron surface, having high activity for carbon deposition. Metallographic analysis of carbon covered iron foils (run 64 and 66), showed that carbon had diffused through the foil thickness. The disruption of the surface caused by the decomposition of the FeS layer is likely to enhance carbon diffusion through the iron foil.

Pre-sulphiding of the nickel disc (run 83) resulted in a constant rate of deposition, equivalent to the "carbon on carbon" rate, throughout the experiment and the initial nickel activity was destroyed. Carbon was deposited on a layer of nickel sulphide. The temperature of the experiment, 805°C , is about 10°C above the melting point of NiS and Ni_3S_2 . However, the sulphur weight increase observed indicated that 65% of the nickel was converted to sulphide. Also, the "carbon on carbon" rate observed throughout the experiment indicates that

the loss of sulphur or nickel sulphide from the disc surface did not occur. Hence, it is reasonable to assume that carbon was deposited on nickel sulphide.

With a nickel disc, the presence of 1% hydrogen sulphide (run 84), resulted in a very fast rate of carbon deposition, which continued after the hydrogen sulphide was turned off. A very large amount of carbon was deposited. When hydrogen was introduced into the reactor, only a slight weight loss was observed, confirming that the deposit was carbon and not sulphur. On investigation, the very large amount of carbon deposited was found to be equally above and below the disc and the disc, shaken free of deposit, had lost weight. Examination of the foil disc and deposit did not detect sulphur near or at the foil surface (under 0.2 - 0.4%), but the carbon deposits were found to contain sulphur and nickel, and nickel was identified in the carbon surface layer on the foil.

Thermodynamic calculations indicate that the partial pressure of sulphur present in the reactor was too close to the partial pressure required to form nickel sulphides to be the basis of a reliable prediction as to their formation. It seems likely that slight fluctuations in the hydrogen sulphide flow caused repeated formation and decomposition of nickel sulphides and the B. E. I. photographs show the pitted surface of the foil consistent with this. This formation/decomposition process would result in the creation of finely divided nickel at the foil surface, becoming active sites for carbon deposition. Analysis confirmed that nickel nuclei were transported through the carbon deposit, and more nickel atoms than sulphur atoms are present in the carbon deposit, (Table 3.1.). This indicates that more nickel than nickel sulphide was present and these nickel nuclei are known to be active for further carbon deposition, Lobo (42).

The pre-sulphiding of a stainless steel disc (run 86), reduced the initial activity of the stainless steel. The amount of sulphur deposited on the disc is consistent with the formation of metal sulphides. The pre-sulphided disc exhibited the "carbon on carbon" rate of deposition: a "clean" stainless steel disc did not and, a significantly

higher rate was observed. Metallographic analysis of a stainless steel liner showed carbon to be absorbed over the whole stainless steel surface, but more rapidly at the metal grain boundaries. It is this grain boundary attack which probably results in the stainless steel foil exhibiting a higher rate of deposition than the "carbon on carbon" rate of a carbon encapsulated foil. The formation of metal sulphides probably blocked the activity of the grain boundary sites to carbon deposition and resulted in the "carbon on carbon" rate being observed.

The presence of 1% hydrogen sulphide (run 85) reduced the initial stainless steel activity and the "carbon on carbon" rate was later observed. A "clean" stainless steel disc does not exhibit the "carbon on carbon" rate but gives a significantly higher rate. Thermodynamic calculations indicate that the partial pressure of sulphur present was sufficient to form iron sulphide on the steel. The formation of sulphide probably blocks the activity of the grain boundary sites to carbon deposition and results in the "carbon on carbon" rate being observed. When the hydrogen sulphide flow was discontinued, the stainless steel disc did not regain the initial activity.

Pre-sulphiding of the copper disc (run 88) resulted in conversion of the copper to Cu_2S . The initial rate of carbon deposition on Cu_2S was significantly higher than that for a "clean" copper disc, which exhibits a rate equivalent to the "carbon on carbon" rate. On the Cu_2S disc, the "carbon on carbon" rate was not observed. It is likely that the formation of Cu_2S disrupted the foil surface, resulting in increased activity to carbon deposition. The non-encapsulation of the foil by carbon (indicated by the "carbon on carbon" rate not being observed) also suggests carbon deposition occurring on a disrupted surface.

The presence of 1% hydrogen sulphide (run 87) resulted in a rate of deposition on a copper disc which was slightly higher than that observed for a "clean" copper disc, which is considered to have minimal activity for carbon deposition and exhibits a rate of deposition less than or equal to the "carbon on carbon" rate. The thermodynamic calculations indicate that the partial pressure of sulphur present was

sufficient to form Cu_2S . Hence the higher rate of deposition observed may have included a contribution from the sulphide formation. However, when the hydrogen sulphide flow was discontinued, the rate of deposition observed was still a little above the "carbon on carbon" rate and the deposit could only be carbon. It is likely that the copper surface was disrupted by the sulphur, resulting in increased activity to carbon deposition.

The experiment with a silica disc, with 1% hydrogen sulphide in the propane feed, gave a rate of deposition equivalent to that for a "clean" silica disc. Unlike the copper experiment, the rate was not enhanced, and the surface was not disrupted. The silica disc in the sulphur experiment may be considered as a control disc. The rate of carbon deposition observed in the sulphur experiment was the same as that for a "clean" silica disc, indicating that sulphur does not affect the activity of silica.

4.4.3. Deposition of carbon on "inert" surfaces

The rates of carbon deposition observed on suspended copper and silica discs in the jet-stirred reactor were less than the rate observed when carbon was deposited on carbon already deposited, (the "carbon on carbon" system). Lower rates were also observed on a suspended copper disc when a copper liner was present inside the reactor.

It seems probable that copper, silica and carbon are acting essentially as "third body" materials, which are largely chemically inert but act to terminate free radicals from the gas phase and as collection centres for carbon or near-carbon intermediates formed in the gas phase. Considering first the possibility of a chemical interaction, all three surfaces show similar activities towards carbon formation (sections 3.2.1. and 3.3.1.) and, although the actual surface may be similar - for example, adsorbed - OH groups, - bulk effects, if they exist, would be expected to appear during carbon formation. The similarity of the three surfaces towards carbon formation indicates that the chemical nature of these materials is

not affecting carbon formation.

In addition to carbon formation on surfaces, carbon formation in the gas phase can be expected, Cullis (3). In outline terms, this will involve a series of free radical reactions leading, eventually, to the formation of homogeneous carbon (c. f. Chapter 1). A chemically inert body can either influence this process by trapping intermediate radicals to give chain termination, or by acting as a collection zone for carbon formed in the gas phase.

Hydrogen and helium were used as diluent gases to try to distinguish these possibilities, (section 3.4.). The copper disc used in the hydrogen dilution studies showed no initial activity, but, as the propane concentration was gradually increased, the rate of carbon deposition gradually increased to the "carbon on carbon" rate. No surface influence on carbon deposition was observed. When less than 37% (v/v) propane is present in the inlet mixture, hydrogen is consumed and the formation of saturated hydrocarbons is favoured. Higher concentrations of propane give rise to greater formation of unsaturated hydrocarbons, and to carbon deposits on the copper disc.

In the helium dilution study the copper disc showed no initial activity, the rate of deposition gradually increasing to the "carbon on carbon" rate as the propane concentration was increased. The gas product distribution was found to be the same over the dilution range studied, and very similar to that from the pyrolysis of undiluted propane at the same conditions of pyrolysis. The carbon deposition which was observed was formed in the absence of heterogeneous effects.

Comparison of these experiments shows that 0.5 mg. less of carbon is deposited in the hydrogen experiments than in the helium experiments, (0.85 mg. total with hydrogen, 1.35 mg. total with helium). Figueiredo (46) has shown that uncatalysed gasification of carbon by hydrogen is not significant below 850°C, and the conclusion emerges that hydrogen is interfering with the free radical chain leading to carbon. Although not proven, it would thus seem that the free radical chain processes are rate determining, and the role of the surface as a carbon collector is secondary.

4.5. Summary

A period exists during which the rate of carbon deposition occurring in the jet-stirred reactor is dependent on the materials present inside the reactor. After this period ceases, a steady-state deposition is observed, further carbon being deposited on the carbon already deposited. The rate of carbon deposition is dependent on the inlet residence time and the temperature. When the temperature is increased and the inlet residence time is lengthened, the conversion of propane increases. Higher concentrations of aromatic and polynuclear aromatic compounds are formed and the rate of carbon deposition increases. The temperature at which carbon deposition starts is dependent on the metal present inside the reactor. Iron, stainless steel and nickel impart a heterogeneous influence and carbon formation occurs on these metals at a lower temperature than on copper and silica, which impart no heterogeneous influence.

No change in the gas phase product distribution was detected when a metal surface influenced the rate of carbon deposition. Similarly, no change in the concentration of aromatic and polynuclear aromatic species was detected when such a heterogeneous influence was present. However, calculations showed that a change which may be associated with a significant change in the rate of carbon deposition when a heterogeneous influence is present is below the detection level of the gas chromatograph. Active metal liners did not exhibit a greater influence on aromatic and polynuclear aromatic production than carbon covered liners or those liners (copper and silica) with no heterogeneous activity. The absence of any influence suggests that heterogeneous interactions do not play a significant role in the gas phase production of aromatic species.

The activation energy values measured reflect the temperature dependence of the rate constants in equation (18) (section 4.2.). Predictions based on steady-state approximation show that the disappearance of propane should be first order and the experiments in the jet-stirred reactor demonstrated that this was the case.

In the presence of hydrogen, interference with the free

radical chain occurs with less propane being consumed and more methane and ethane being produced. The gaseous products formed in the pyrolysis of propane are produced via a free radical chain reaction occurring completely in the gas phase.

It has been shown that carbon formation on a surface is influenced by another separate surface in contact with the gas. This is explained in terms of a surface reaction producing carbon and gas phase products. The nature of those products is dependent upon reaction conditions and the chemical nature of the surface. Carbon formation on the second surface is typical of the nature of these products and of the second surface. The important intermediates could not be satisfactorily established.

The carbon deposition studies indicate that the order of activity for carbon deposition is:

Iron and stainless steel > nickel > carbon > copper/silica. Iron, stainless steel and nickel exhibit a heterogeneous influence on the rate of carbon deposition. Copper and silica do not exhibit such a heterogeneous influence.

The activity for promoting carbon formation on a second surface decreases in the order:

Iron > stainless steel > nickel > carbon > copper/silica. The effect of a metal on the reactions leading to carbon formation is dependent on the surface exposed to the reacting gases. Copper, silica and carbon act as essentially "third body" materials, which are largely chemically inert but act to terminate free radicals from the gas phase and as collection centres for carbon or near-carbon intermediates formed in the gas phase.

When a iron foil remains active and is not encapsulated by carbon (the "carbon on carbon" rate is not observed), the analysis of the foil shows it to be of different iron phases than a carbon encapsulated foil. The carbon encapsulated foil has a layer of ferrite (α -iron) containing cementite (Fe_3C) at the carbon face. The cementite "patches" are surrounded by ferrite and penetrate about $1/5^{\text{th}}$ of the thickness of the metal foil. The active foil is coarse pearlite (6.67% by weight of carbon) throughout. This indicates an

even uptake of carbon. It is this difference in carbon distribution which probably causes the unpredictable behaviour of iron foils with regard to the rate of carbon deposition observed. The carbon encapsulated foil formed a different layer at the carbon face.

Stainless steel absorbs carbon over the whole surface, but more rapidly at the metal grain boundaries, resulting in attack at the grain boundaries and carbon entering the surface layer and diffusing into the foil.

For both stainless steel and iron, iron enters the carbon layer and the transport of these active iron sites causes further carbon deposition. The iron present in the growing carbon layer acts as a nucleus for further carbon deposition.

The dilution of propane with hydrogen results in an iron disc remaining active at 10% and 22% (v/v) propane in hydrogen dilutions. Hydrogen promotes an even uptake of carbon into the iron disc and the heterogeneous influence of the iron disc remains. Helium does not have this effect and the activity of the iron disc was lowered to the "carbon on carbon" level.

Neither hydrogen nor helium dilutions induced heterogeneous activity in a copper disc. The rate of carbon deposition which was observed was that for a surface exhibiting no activity for carbon deposition. Less carbon was deposited in the hydrogen dilution experiments than in the helium dilution experiments and the conclusion was reached that hydrogen interfered with the free radical chain leading to carbon. The role of the surface as a carbon collector appears to be secondary to the free radical chain processes which appear to be rate determining.

At short residence times, propane is converted to hydrocarbon gases and hydrogen, but tars and carbon are not formed. As the residence time is increased tars start to form. A relationship between this induction period and the pressure of propane was established, and a relationship between the initial rate of production and the pressure was also demonstrated. At longer residence times the concentration of tars increases with an associated enrichment in the higher molecular weight species, which are the precursors to carbon formation. Hence,

at short residence times, only hydrocarbon gases and hydrogen are formed, and - as the residence time is increased - the production of tars also increases with a parallel increase in the production of carbon. The production of carbon is dependent on the formation of tars.

Pre-sulphiding iron and stainless steel discs reduces the initial activity for carbon deposition. For nickel, the rate is enhanced. The carbon deposition measurements were made on metal discs having a substantial sulphide layer, and no reversible change to an active metal deposition system was observed.

The presence of 1% hydrogen sulphide in the propane feed causes a reversible reduction in the iron activity for carbon deposition and an irreversible reduction for stainless steel. Initially, a layer of FeS is probably present which blocks the active iron sites and grain boundaries, preventing high rates of activity being observed. With the iron disc, the FeS decomposes leaving a finely divided and disrupted surface, having high activity for carbon deposition. For stainless steel, the dissociation of the FeS is accompanied by carbon encapsulation of the metal.

Nickel exhibits a very high activity when 1% hydrogen sulphide is present in the propane feed. This very high activity continues after the hydrogen sulphide flow is stopped. The carbon deposit contained both sulphur and nickel, with more nickel atoms than sulphur atoms present. The nickel atoms which were not converted to sulphides acted as active nuclei for further carbon deposition. It is likely that slight fluctuations in the hydrogen sulphide flow caused repeated formation and decomposition of nickel sulphides, resulting in the creation of finely divided nickel at the foil surface; these become active sites for carbon deposition.

For a copper disc, the presence of 1% hydrogen sulphide slightly enhances the rate of carbon deposition. Cu_2S is formed which disrupts the copper surface and results in an increased activity to carbon formation. For a silica disc, no surface disruption occurs and no subsequent enhancement of the activity to carbon formation is observed.

CONCLUSIONS

- (1) Changes in the gas phase product distribution caused by the nature of the reactor wall are too small to identify using the analytical gas chromatography system.
- (2) The carbon results indicate that small changes in the relative amounts of gases are expected, were the analysis sufficiently sensitive.
- (3) The gas phase products from the pyrolysis of pure propane at 810°C and 2 - 7.5 sec. inlet residence time are, in order of decreasing importance, methane, ethylene, hydrogen, propylene and ethane.
- (4) Increasing the pyrolysis temperature increases the propane conversion.
- (5) Lengthening the inlet residence time increases the propane conversion.
- (6) The pyrolysis of propane is a free radical chain reaction, initiation occurring via C-C bond rupture, and subsequent propagation involving hydrogen abstraction from propane.
- (7) Termination is likely to be a biradical termination process involving propyl and methyl radicals.
- (8) Predictions based on steady-state approximation show that the disappearance of propane should be first order, and the production of the gas phase products will be first order in propane.
- (9) These predictions give a reasonably accurate picture of the experimental observations, and indicate that the rate of the disappearance of propane is equal to the sum of the rate of formation of propylene and the rate of formation of methane.
- (10) The gaseous products from the pyrolysis of propane are entirely consistent with a free radical chain reaction occurring completely in the gas phase.
- (11) The dilution of propane with helium has little effect on the relative magnitudes of the gas phase products.

- (12) Dilution with hydrogen influences the product distribution. When less than 37% (v/v) propane is fed to the reactor, propane and measurable quantities of hydrogen were consumed, and the production of methane and ethane increases as the hydrogen consumption increases. Less propane was converted when hydrogen was consumed.
- (13) In the presence of hydrogen, interference with the chain occurs and less propane reacts and more methane and ethane are produced.
- (14) The amount of tars increases with increasing pressure, temperature and inlet residence time. At longer residence times an enrichment in higher molecular weight tars occurs and these are the precursors for carbon formation.
- (15) Both the induction period and the initial rate of production of tars appear to be functions of the pressure of propane and the temperature.
- (16) The existence of an induction period which depends on the pressure of the reactants and the temperature, the autocatalytic nature of tar production and the eventual tail-off of rate to a steady value are all typical of free radical reactions.
- (17) The rate of carbon formation on a surface is dependent upon the chemical nature of that surface. The order of activity for carbon formation is:
Iron and stainless steel > nickel > carbon > copper/silica.
- (18) Carbon formation on a surface may be affected by the nature of a second surface, physically separated from the first surface by a gap in which gas can react. The order of activity for promoting carbon formation on a second surface is:
Iron > stainless steel > nickel > carbon > copper/silica
- (19) Iron, stainless steel and nickel exhibit a heterogeneous influence on the rate of carbon deposition.
- (20) Copper, silica and carbon act as essentially "third body" materials, which are largely chemically inert but act to terminate free radicals from the gas phase and as collection centres for carbon or near-carbon intermediates formed in the gas phase.

- (21) Increasing the pyrolysis temperature increases the rate of carbon formation.
- (22) Lengthening the inlet residence time increases the rate of carbon formation.
- (23) Throughout the reaction the liner and the foil become progressively covered in carbon and, unless metal can migrate through this carbon, the rate of carbon formation reduces to the rate expected from propane reacting on a carbon surface to produce gaseous products which deposit carbon on a carbon surface.
- (24) If the original material continues to be available to the gases, then the net rate of carbon formation continues to reflect the nature of the original material.
- (25) Iron and stainless steel initiate carbon formation at significantly lower temperatures than nickel, copper, silica and carbon.
- (26) The carbon uptake of a carbon encapsulated iron foil is irregularly distributed over the metal surface. Carbon is absorbed over the whole surface, but more intensely in some areas.
- (27) The carbon uptake of a non-encapsulated iron foil is evenly distributed over the metal surface. This difference in carbon distribution probably causes the unpredictable behaviour of the iron foils with regard to carbon deposition.
- (28) For both carbon encapsulated and non-encapsulated iron foils, iron enters the carbon layer and acts as growth nuclei for further carbon deposition.
- (29) Carbon is absorbed over the whole surface of a stainless steel foil, but more rapidly at the metal grain boundaries, resulting in attack at the grain boundaries.
- (30) Iron particles enter the carbon layer on a stainless steel foil and acts as growth nuclei for further carbon deposition.
- (31) Hydrogen has a very pronounced effect on the period during which carbon formation is dependent on the nature of the disc material. An even uptake of carbon is promoted on an iron surface and high rates of carbon deposition occur.

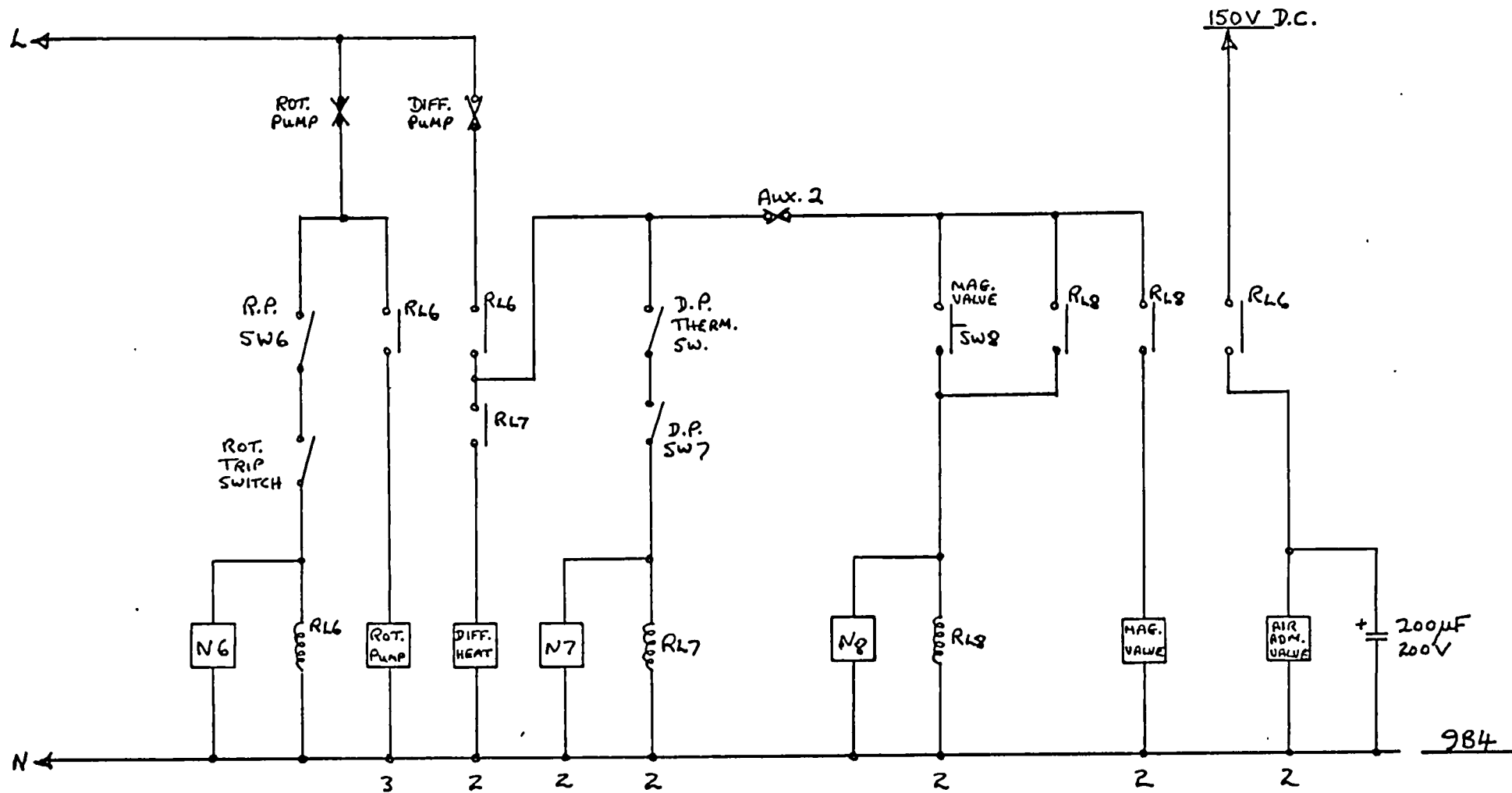
- (32) Hydrogen has a strong influence on the conversion of an adsorbed intermediate on an iron surface to a reaction intermediate; the formation of gas phase products; dissolution of carbon; and gasification of carbon.
- (33) Helium has no effect on the surface (heterogeneous) formation of carbon on an iron disc and does not ensure an even uptake of carbon into the disc; the disc becomes carbon covered.
- (34) With a copper disc, less carbon is deposited from hydrogen diluted propane than from helium diluted propane. Hydrogen interferes with the free radical chain leading to carbon.
- (35) Although not proven, it seems that the free radical chain processes are rate determining, and the role of the surface as a carbon collector is secondary.
- (36) Carbon deposition on a surface of iron sulphide and nickel sulphide is at a rate equivalent to carbon being deposited on a carbon surface. The presence of sulphur on the metal reduces the activity of the metal.
- (37) The formation of metal sulphides on stainless steel blocks the activity of the grain boundary sites to carbon deposition.
- (38) The presence of 1% H_2S in the propane feed suppresses the activity of iron, a surface layer of FeS probably being formed. Decomposition of the FeS caused by the discontinuation of the H_2S flow results in the formation of a finely divided and disrupted iron surface, which generates a high rate of carbon formation.
- (39) The presence of 1% H_2S in the propane feed suppresses the activity of stainless steel and the initial activity does not return after the H_2S flow is discontinued.
- (40) Thermodynamic calculations indicate that slight fluctuations in the H_2S flow when 1% H_2S in propane is passed over a nickel disc, results in repeated formation and decomposition of nickel sulphides. The finely divided nickel thus formed acts as very active sites for carbon deposition, a very high rate of carbon deposition results, and nickel nuclei are

transported through the "growing" carbon layer and act as sites for further carbon deposition.

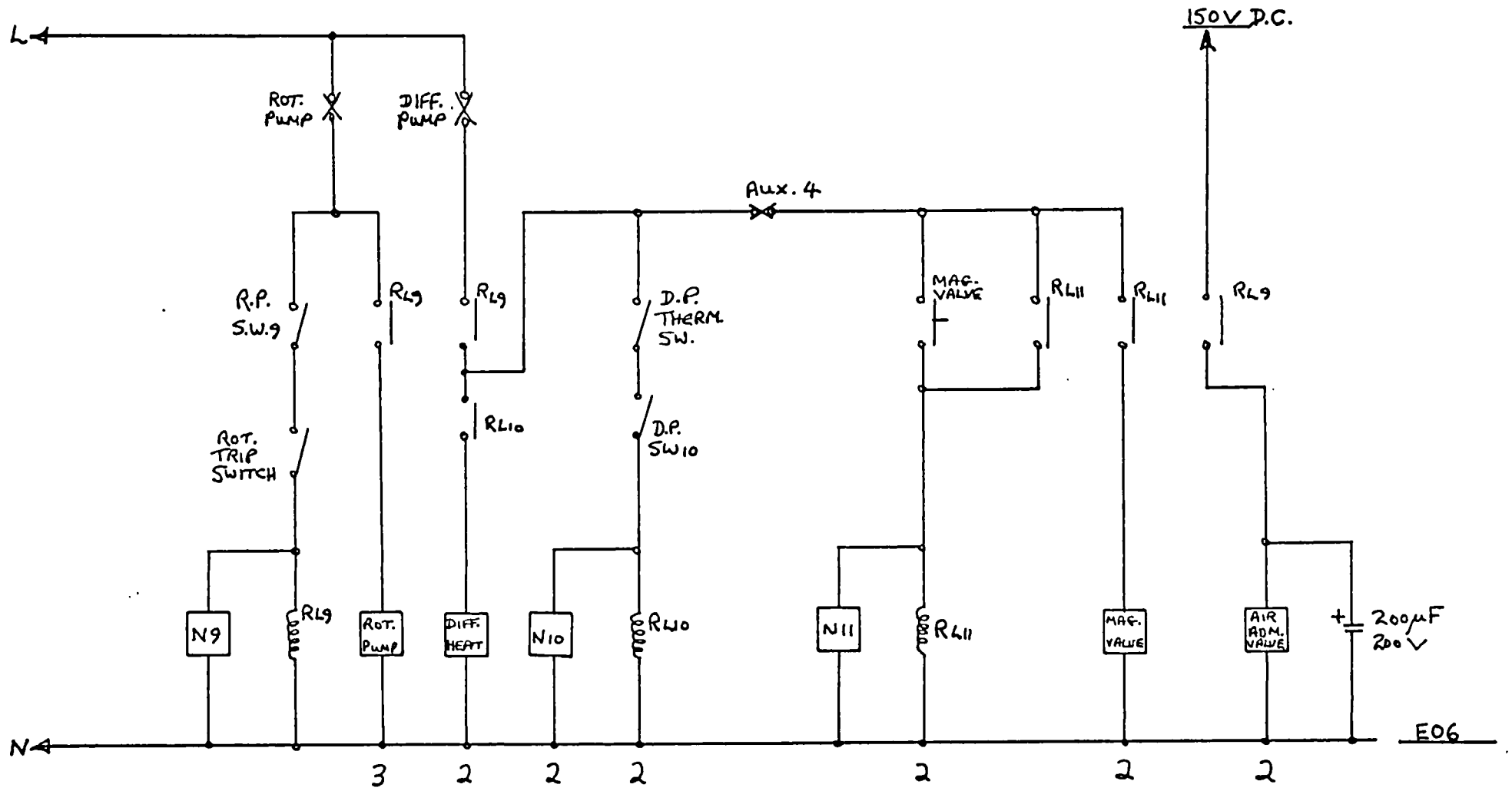
- (41) The rate of carbon formation on a surface of Cu_2S is greater than that on copper, activity being generated by the presence of sulphur which disrupts the copper surface.

Appendix

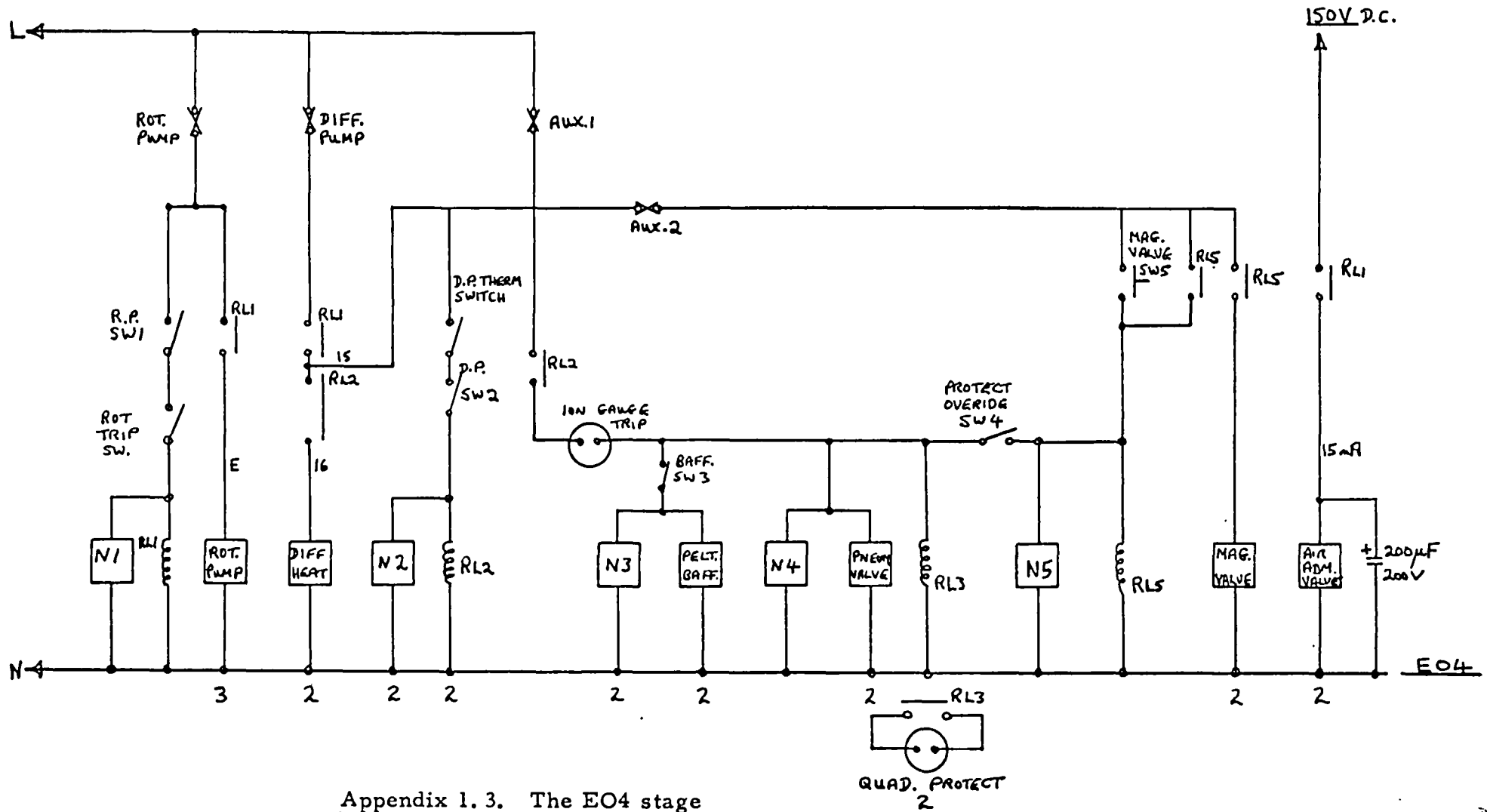
1. 1. The 9 B4 stage circuit diagram.
1. 2. The EO6 stage circuit diagram.
1. 3. The EO4 stage circuit diagram.
1. 4. The sweep generator circuit diagram.



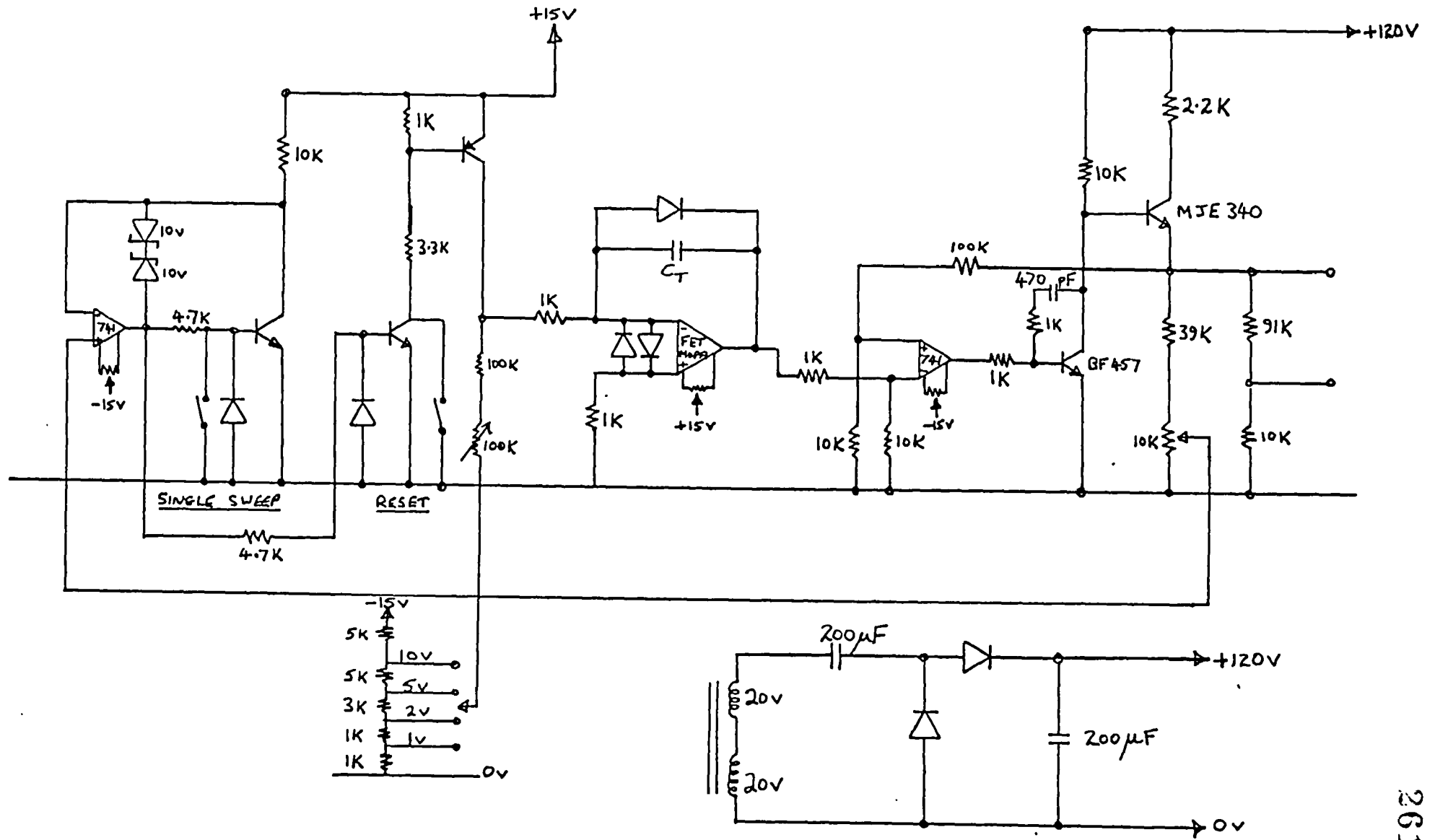
Appendix 1.1. The 9B4 stage



Appendix 1.2. The EO6 stage



Appendix 1.3. The EO4 stage



Appendix 1.4. The sweep generator

REFERENCES

1. Zdonik. S. B. , Green. E. J. and Hillee. L. P. , "Manufacturing Ethylene". , The Petroleum Publishing Co. Tulsa Oklahoma U.S.A. (1970).
2. Thompson. B. , Majumdar. B. and Conway. H. , J. Inst. Gas Eng. 6, 415 (1966)
3. Cullis. C.F. and Palmer. H. , Chemistry and Physics of Carbon. 1, 266 (1965). (P.L. Walker Jr. , Ed.).
4. Slotboom. H.W. and Penninger. J.H.M. , Ind. Eng. Chem. Process Des. Develop. 13, 296 (1974).
5. Leathard. D.A. and Purnell. J.H. , Ann. Rev. Phys. Chem. 21, 197 (1970).
6. Purnell. J.H. and Quinn. C. P. , Proc. Roy. Soc. London Ser.A. 270, 267 (1962).
7. Quinn. C. P. , Trans. Faraday Soc. 59, 2543 (1963).
8. Quinn. C. P. , Proc. Roy. Soc. London Ser.A. 275, 190 (1963).
9. Taiseki. K. , Tomoya. S. , Kazuhiko. S. and Yoichi. S. , Ind. Eng. Chem. Fund. 8, 374 (1969).
10. Nowak. S. , Bach. G. , Schroeder. J. , Leibnitz. E. , Lavrovskii. K. , Kalinenko. R. and Shevelkova. L. , Z. Phys. Chem. (Leipzig) 241, 249 (1969). , Chem. Abs. 71, 101191j (1969).
11. Ferrara. I. , Barbagallo. G. and Filia. U. , Chim. Ind. (Milan) 53, 1138 (1971). , Chem. Abs. 76, 47985j (1972).
12. Hirata. M. , Sekiyu Gakkai Shi. 11, 934 (1968). , Chem. Abs. 70, 96068 x (1969).
13. Benson. A. , Amer. Inst. Chem. Eng. J. 13, 903 (1967).
14. Friedmann. N. , Bovee. H. and Miller. S. , J. Org. Chem. 35, 3230 (1970).
15. Davis. R. and Williamson. K. , World Petrol. Congr. Proc. 5th N.Y. 4, 37 (1959).
16. Kallend. A. , Purnell. J. and Shurlock. B. , Proc. Roy. Soc. London Ser.A. 300, 128 (1967).
17. Niclause. M. , Bull. Soc. Chim. France. 4, 1599 (1968).
18. Garewal. D.S. , M. Sc. Thesis. University of London (1973).
19. La. Cava. A. , M. Sc. Thesis. University of London (1974).
20. Seinfeld. J.H. , Lapidus. L. and Hwang. M. , Ind. Eng. Chem. Fund. 9, 266 (1970).
21. Bush. S.F. , Trans. Inst. Chem. Eng. 47, T59 (1969).
22. Berthelot. From Badger. E. , Progress in Phys. Org. Chem. 3, 1 (1965).
23. Fitzer. E. , Mueller. K. and Schaefer. W. , Chemistry and Physics of Carbon. 7, 237 (1971).

24. Evans. S. and Marsh. H. , Carbon. 9, 733 (1971).
25. Brooks. C. T. and Thompson. B.H. , 165th American Chem. Soc. National Meeting, Dallas, U.S.A. (1973).
26. Akamatu. H. and Kuroda. H. , Fourth Carbon Conference. 355 (1961).
27. Kaye. G. , Carbon. 2, 413 (1965).
28. Conroy. J.S. , Proc. Third Carbon Conference. Pergamon Press, 395 (1959).
29. Diefendorf. R.J. , J. Chim. Phys. 57, 815 (1960).
30. Cullis. C. F. , Read. I.A. and Trimm. D. L. , Eleventh Symposium on Combustion. 391 (1967).
31. Thomas. A. , Combust. Flame. 6, 46 (1962).
32. Akamatu. H. and Sato. K. , Bull. Chem. Soc. Japan. 22, 127 (1949).
33. Banerjee. B.C. , Nature. 192, 450 (1961).
34. Karu. A.E. and Beer. M. , J. App. Phys. 37, 2179 (1966).
35. Robertson. S.D. , Carbon. 8 365 (1970).
36. Tamai. Y. , Nishiyama. Y. and Takahashi. M. , Carbon 6, 593 (1968).
37. Tamai. Y. , Nishiyama. Y. and Takahashi. M. , Carbon. 7 , 209 (1969).
38. Presland. A.E.B. and Walker. P. L. , Carbon. 7, 1 (1969).
39. Blau. G. and Presland. A.E.B. , Third Conference on Industrial Carbon and Graphite, Soc. Chem. Ind. , London (1970).
40. Moayeri. M. , M. Sc. Thesis. University of London (1970).
41. Renshaw. G. D. , Roscoe. C. and Walker. P.L. Jr. , J. Catal. 18, 164 (1970).
42. Lobo. L.F.G. , Ph. D. Thesis. University of London (1971).
43. Saito. T. and Gejyo. T. , Carbon. 9, 93 (1971).
44. Tomita. A. , Yoshida. K. , Nishiyama. Y. and Tamai. Y. , Carbon. 10, 601 (1972).
45. Derbyshire. F.J. , Ph. D. Thesis. University of London (1974).
46. Figueiredo. J.L. , Ph. D. Thesis. University of London (1975).
47. Renshaw. G.D. , Roscoe. C. and Walker. P.L. Jr. , J. Catal. 22, 394 (1971).
48. Gwathmey. A. T. and Cunningham. R.E. , Advances in Catalysis. 10, 57 (1958).
49. Wagner. J. B. and Gwathmey. A. T. , J. Am. Chem. Soc. 76, 390 (1954).

50. Moayeri. M. , Ph. D. Thesis. University of London (1974).
51. Lobo. L.F.G. and Trimm. D.L. , J. Catal. 29, 15 (1973).
52. Nishiyama. Y. and Tamai. Y. , J. Catal. 33, 98 (1974).
53. Walker. P.L. Jr. , Rakszswaki. J. and Imperial. G. , J. Phys. Chem. 63, 140 (1959).
54. Rostrup-Nielsen. J.R. , J. Catal. 27, 343 (1972).
55. Baird. T. , Freyer. J. and Grant. B. , Nature. 233, 329 (1971).
56. Baker. R. , Barber. M. , Harris. P. , Feates. F. and Waite. R. , J. Catal. 26, 51 (1972).
57. Tesner. P. , Robinovich. E. , Rafalkes. I. and Arefieva. E. , Carbon 8, 435 (1970).
58. Hofer. L. , Sterling. E. and McCartney. J. , J. Phys. Chem. 59, 1153 (1955).
59. Ruston. W. , Warzee. M. , Hennaut. J. and Waty. J. , Carbon. 7, 47 (1969).
60. Lobo. L. and Trimm. D.L. , Nature. 234, 15 (1971).
61. Haas. L. , Khalafalla. S. and Weston. P. , U.S. Bureau of Mines, Report 7064 (1968).
62. Lafitau. H. and Jacque. L. , Bull. Soc. Chim. France. 4779 (1968).
63. Lobo. L. , Trimm. D.L. and Figueiredo. J. , 5th. Int. Congr. Catalysis. Palm-Beach. (1972).
64. Cimino. A. and Parravano. G. , J. Phys. Chem. 56, 706 (1952).
65. Escoubes. M. , Quinson. J. and Eyraud. C. , Bull. Soc. Chim. France. 2435 (1967).
66. Nagakura. S. , J. Phys. Soc. Japan. 12, 482 (1957).
67. Baker. R. , Harris. P. , Thomas. R. and Waite. R. , J. Catal. 30, 86 (1973).
68. Lahaye. J. , Prado. G. and Donnet. J. , Carbon. 12, 27 (1974).
69. Graham. S. , Homer. J. and Rosenfeld. J. , 2nd European Combustion Symposium, Orleans, France (1975).
70. Kehrer. V. and Leidheiser. H. , J. Phys. Chem. 58, 550 (1954).
71. Cunningham. R. and Gwathmey. A. , Advances in Catalysis 9, 25 (1957).
72. Robertson. S. , Ph. D. Thesis. University of Glasgow (1968).
73. Baird. T. , Freyer. J. and Grant. B. , Carbon Symposium, University of Glasgow (1972).
74. Baker. R. , Barber, M. , Harris. P. , Feates. F. and Waite. R. , Carbon. 10, 93 (1972).
75. Starshov. I. and Syrmolaeva. G. , Neftepererabotka i Neftekljum, Nauchn-Tekhn. Sb. 2, 26 (1964). , Chem. Abs. 61, 5429a (1964).

76. Milosavljevic. L. , Technika (Belgrade). 22, 1246 (1967)
Chem. Abs. 69, 60359h (1968).
77. Anisonyan. A. , Dokl. Akad. Nank. Arm. (U.S.S.R.). 51,
101 (1970). , Chem. Abs. 74, 24038x (1971).
78. Crynes. B. and Albright. L. , Ind. Eng. Chem. Process Des.
Develop. 8, 25 (1969).
79. Penninger. J. and Slotboom. H. , Recl. Trav. Chim. Pays-Bas.
92, 513 (1973), Chem. Abs. 79, 65476K (1973).
80. Penninger. J. and Slotboom. H. , Erdoel Kohle, 26, 445 (1973). ,
Chem. Abs. 79, 136271c (1973).
81. Cramers. C. , Dissertation, Eindhoven University of Technology,
The Netherlands (1967).
82. Holbrook. K. , Walker. R. and Watson. W. , J. Chem. Soc. B.
10, 1089 (1968).
83. Gordon. A. , Chem. Inst. Can. Symp, Ottawa, Canada (1964).
84. Marshall. R. and Quinn. C. , Trans. Faraday Soc. 61, 2671
(1965).
85. Lin. M. and Back. M. , Can. J. Chem. 45, 3165 (1967).
86. Purnell. J. and Quinn. C. , Photochemistry and Reaction
Kinetics, Cambridge Univ. Press. 330 (1966).
87. Makarov. K. and Pechik. V. , Carbon. 7, 279 (1969).
88. Eltenton. G.C. , J. Chem. Phys. 15, 455 (1947).
89. Ramsey. N.F. , Molecular Beams, Clarendon Press, Oxford (1956).
90. Kantrowitz. A. and Grey. J. , Rev. Sci. Instr. 22, 328 (1951).
91. Zapata. R. , Bodine. J. and Parker. H. , Rar. Gas Dyn. ,
Academic Press, N.Y. (1961).
92. Deckers. J. and Fenn. J. , Rev. Sci. Instr. 34, 96 (1962).
93. Anderson. J. , Andres. R. and Fenn. J. , Adv. Chem. Phys.
10, Interscience (1965).
94. Fenn. J. and Deckers. J. , Rar. Gas Dyn. 3rd Int. Symp.
497 (1963).
95. Schugerl. K. , Rar. Gas Dyn. 6th Int. Symp. 909 (1969).
96. Scott. J. and Drewry. J. , Rar. Gas Dyn. 3rd Int. Symp.
516 (1963).
97. Milne. T. , Greene. F. and Brewer. J. , J. Chem. Phys.
40, 1488 (1964).
98. Kaiser. R. , Gas Phase Chromatography. 3, 101 (1963).
99. Tristram. M. , Ph. D. Thesis. University of London (1975).
100. Strafford. K. N. , Metallurgical Review 138 in Metals and
Materials. 3, 153 (1969).

101. Kubaschewski. O. and Evans. E. , Metallurgical Thermochemistry, Pergamon Press, London (1958).
102. Ellingham. H.J.T. , J. Soc. Chem. Ind. 63, 125 (1944).
103. Richardson. F.D. and Jeffes. J.H.E. , J. Iron Steel Inst. 171, 165 (1952).
104. Kubaschewski. O. and Von Goldbeck. O. , Metalloberfläche (A). 8, 33 (1954).
105. Pilling and Bedworth. , J. Inst. Metals. 29, 529 (1923).
106. Hancock. P. , First International Conference on Metallic Corrosion. London. Pub. Butterworth. 193 (1962).
107. Roberts. O.C. , Robertson. D.E.C. and Jenkins. A.E. , Trans. Metal. Soc. AIME. 245, 2413 (1969).
108. Rickert. H. , Z. Physikal Chem. 23, 355 (1960).
109. Rickert. H. and O'Brianin. C.D. , Z. Physikal Chem. 31, 71 (1962).
110. Czerski. L. , Mrowec. S. , Wallisch. K. and Werber. T. , Arch. Hutn. 3, 149 (1958).
111. Ingraham. , Trans. AIME. 236, 1064 (1966).
112. Elliott. J.F. and Gleiser. M. , Thermochemistry for Steelmaking, 1, Pub. Amer. Iron and Steel Inst.
113. Wyckoff. R.W. , Crystal Structures. 1, Pub. Interscience. 2nd Edition. (1965).
114. Germain. J.E. , Catalytic Conversion of Hydrocarbons Pub. Academic Press. 2 (1969).
115. Laidler. K.J. and Loucks. L.F. , Comprehensive Chemical Kinetics. , Pub. Elsevier, Ed. Bamford. C. and Tipper. C. , 5, 1 (1972).
116. Hinshelwood. C.N. , Danby. C.J. and Frey. H.M. , Proc. Roy. Soc. London Ser. A. 234, 301 (1956)
117. Herriott. G.E. , Eckert. R.E. and Albright. L.F. , A.I. Ch. E. Journal. 18, 84 (1972).